Technische Universität München

TUM School of Natural Sciences

Mechanistic insight into electrocatalytic carbonyl hydrogenation and C–C coupling on Cu

Hongwen Chen

Vollständiger Abdruck von der TUM School of Natural Sciences der Technischen Universität München zur Erlangung des akademischen Grades eines

Doktors der Naturwissenschaften (Dr. rer. nat.)

genehmigten Dissertation.

Vorsitz:	Prof. Dr. Jennifer Strunk
Prüfer der Dissertation:	1. Prof. Dr. Johannes A. Lercher
	2. Prof. Dr. Klaus Köhler

Die Dissertation wurde am 12.07.2024 bei der Technischen Universität München eingereicht und durch die TUM School of Natural Sciences am 29.08.2024 angenommen.

Die Ziellose erleidet sein Schicksal, der Zielbewusste gestaltet es.

—— *Markus Tullius Cicero*

Affirmation

I hereby assure that I have written the submitted thesis independently and have not used any sources and tools other than those indicated.

_____

Place, Date, Signature

Man merkt nie, was schon getan wurde, man sieht immer nur, was noch zu tun bleibt

Marie Skłodowska Curie

Acknowledgements

Foremost, I would like to express my sincere gratitude to Prof. Dr. Johannes A. Lercher for allowing me to join his group at the chair of Technical Chemistry II. It has been a great privilege and joy to study under his guidance and supervision. Furthermore, I am honored to benefit from his personality and diligence, which I will treasure my whole life.

I would also like to give my heartfelt thanks to my supervisors, Dr. Yue Liu, Prof. Dr. Andreas Jentys, and especially Dr. Rachit Khare. Yue, although we only worked together for several months at TUM, your suggestions and encouragement have given me much insight into my studies. You also help me a lot in my daily life in Munich. Thank you so much! Andreas, I am really grateful for your patience and suggestions on my research work. Then, I would express my grateful appreciation to Rachit. I am so lucky to find you to have a deep discussion for my research work in the second year when I was losing my direction. Every time, you can give me precious suggestions for the following projects. Thank you for the time and effort you spent coaching me.

Next, I would like to thank my former and current colleagues in my group, Dr. Ruixue Zhao, Dr. Yue Ma, Dr. Fuli Deng, Dr. Phillip Fischer, Dr. Guanhua Chen, Dr. Xi Chen, Dr. Kaming Yu, Dr. Wei Zhang, Dr. Yong Wang, Dr. Ling li Ni, Dr. Lei Tao, Dr. Aimen Shahpal, Dr. Roland Weindl, Simon Krebs, Yifan Feng, Chuanlei Li, Huidong Xu, Xiaomai Chen, Siyuan Huang, Lennart Wahl, Christoph Gross, Florian Zahn, and Mirjam Wenig. It is really a good time to work together with you.

Furthermore, I would like to thank the following colleagues in my group, Martin Neukamm, Andreas Marx and Iqbal Muhammad, thank you so much for your precious technical supports. Stefanie Seibold and Bettina Federmann, thank a lot for your administrative helps. Everything goes well with your help and support.

Last but not least, I would like to give my heartfelt thanks to my parents, for your endless love and care for me. Whatever I need and wherever I go, you are always there supporting me without any requirement in return. I thank my loving family and family is where I can forever turn. Also many thanks to my friends for being trusted, dedicated and supportive.

Hongwen Chen

September 2024

Abstract

The impact of reaction conditions on the reaction activity and product selectivity in electrocatalytic hydrogenation (ECH) of benzaldehyde on Cu/C has been explored. The mechanism of electrocatalytic H_2 evolution, carbonyl hydrogenation and carbon-carbon (C–C) coupling has been clarified in both acidic and alkaline conditions. The mechanistic requirements that facilitate the C–C coupling between aldehydes on Cu has also been elucidated. The MoS_2 has been selected as a co-catalyst to alter product selectivity during benzaldehyde ECH on Cu/C+MoS_2 electrode. The mechanistic insight into how MoS_2 affects product selectivity during benzaldehyde ECH on Cu/C+MoS_2 electrode has been studied.

Kurzzusammenfassung

Der Einfluss der Reaktionsbedingungen auf die Reaktionsaktivität und Produktselektivität bei der elektrokatalytischen Hydrierung (ECH) von Benzaldehyd auf Cu/C wurde untersucht. Der Mechanismus der elektrokatalytischen H_2-Entwicklung, Carbonylhydrierung und Kohlenstoff-Kohlenstoff-Kopplung (C–C) wurde sowohl unter sauren als auch unter alkalischen Bedingungen aufgeklärt. Die mechanistischen Voraussetzungen, die die C–C-Kopplung zwischen Aldehyden auf Cu ermöglichen, wurden ebenfalls aufgeklärt. MoS_2 wurde als Cokatalysator ausgewählt, um die Produktselektivität während der Benzaldehyd-ECH auf einer Cu/C+MoS_2-Elektrode zu verändern. Die mechanistischen Erkenntnisse darüber, wie MoS_2 die Produktselektivität während der Benzaldehyd-ECH auf einer Cu/C+MoS_2-Elektrode beeinflusst, wurden untersucht.

List of Abbreviations

ECH……Electrocatalytic Hydrogenation

HER……Hydrogen Evolution Reaction

LSV……Linear Sweep Voltammetry

CV…… Cyclic Voltammetry

e.g. ……. exempli gratia

FE……Faradaic Efficiency

GC……Gas Chromatography

ABS……Acetate Buffer Solution

i.e. …… id est

Eq. ……Equation

Fig. ……...Figure

MS……Mass Spectrometry

OER……Oxygen Evolution Reaction

PCET……...Proton Coupled Electron Transfer

LH……Langmuir-Hinshelwood

ER……Eley-Rideal

RE…… Reference Electrode

WE……Working Electrode

CE…… Counter Electrode

CF……Carbon Felt

RHE……Reversible Hydrogen Electrode

SHE…… Standard Hydrogen Electrode

TCH……Thermo-Chemical Hydrogenation

SI……..Supporting Information

Rxn……Reaction

XRD……X Ray Diffraction

TEM……Transmission Electron Microscopy

BET…… Brunauer Emmett Teller

ATR……Attenuated Total Reflection

XANES……. . . X-ray Absorption Near Edge Structure

FT-EXAFS……..…Fourier-Transformed Extended X-ray Absorption Fine Structure

C-C ……..……Carbon-Carbon

et al. ……..…… et alia

RDS……..……rate determining step

KIE……Kinetic isotopic effect

BZ……..…….Benzaldehyde

BA……..……Benzyl alcohol

HB……..……Hydrobenzoin

PA……..…..……..Pentanal

HCA……..Hydrocinnamaldehyde

CA……..Cinnamaldehyde

FAL……..Furfural

DMAB……..……p-dimethylaminobenzaldehyde

CO_2…….……..….Carbon dioxide

CO_2RR……..…Carbon dioxide electroreduction reaction

HDO……Hydrodeoxygenation

DFT……Density Functional Theory

Table of Contents

Chapter 1

Introduction

1.1 General background

Energy consumption has been increasing since the industrial revolution due to the development of the world's economies. Using energy resources allowed for the unprecedented development of civilization and improved living conditions.[1] **Figure 1-1** shows the total global primary energy consumption by source between 1800 and 2023.[2] As can be seen, the total consumption is systematically increasing. This is mainly due to population growth, which leads to increasing energy needs. We can also see that although the dominating energy supply is always fossil fuels (coal, natural gas, and oil), the share of renewable resources is rising.

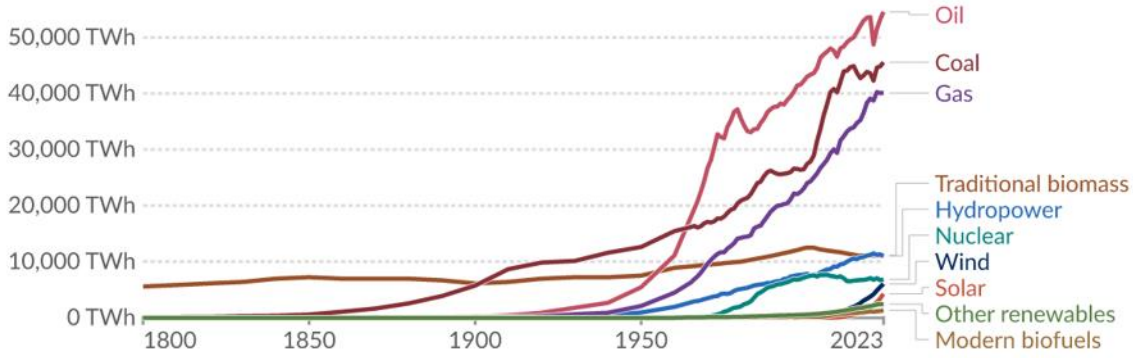

Figure 1-1. Total global primary energy consumption by source. (Data source: Energy institute – Statistical Review of World Energy (2024); Smil (2017)).

Although using traditional fossil fuels can lead to high-speed economic growth, the excessive utilization of non-renewable resources causes the over-emission of carbon dioxide (CO_2) and the severe greenhouse effect.[3,4] On the other hand, renewable energy sources (e.g. solar, wind, hydro, wave, and biomass) are environmentally friendly resources. Renewable sources in electricity/heat generation do not pollute the environment with greenhouse gas emissions.[5-7] So, increasing investment in renewable energy sources is essential for environmental protection and human development. **Figure 1-2** shows the global investments in renewable energy between 2004 and 2022.[8] The good news is that the total global investment in renewable energy is increasing, and solar and wind power dominate renewable energy resources. On the other hand, biofuels from biomass upgrading are also essential renewable energy components that need more investment in the future.

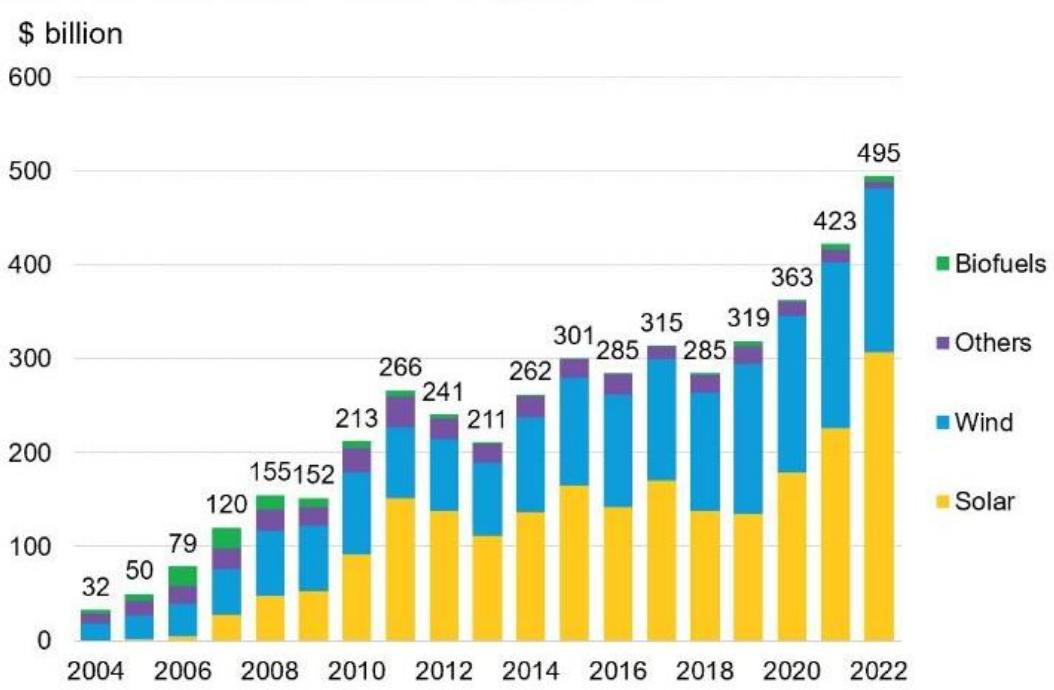

Figure 1-2. Global investments in renewable energy 2004–2022. (Reprinted with permission from reference 8. Copyright © 2023, Elsevier.)

Biomass stores energy and carbon dioxide naturally and is a promising alternative to compensate for the fluctuating availability of wind and solar power, which can also release the world's energy problems.[9-10] The second generation biofuels are considered to be a promising renewable alternative to the traditional fossil fuels.[11] **Figure 1-3** shows an industrial-scale thermochemical conversion of lignocellulosic biomass into biofuel, electricity, and heat.[12] The industrial process chain includes biomass collection, decentralized conversion effect (chipping, drying, and pyrolysis) for biomass, intermediate biosyncrude product transportation, and centralized biomass conversion effect (gasification, synthesis, and CHP). Finally, we can get the fuels for transportation and electricity generation for living.

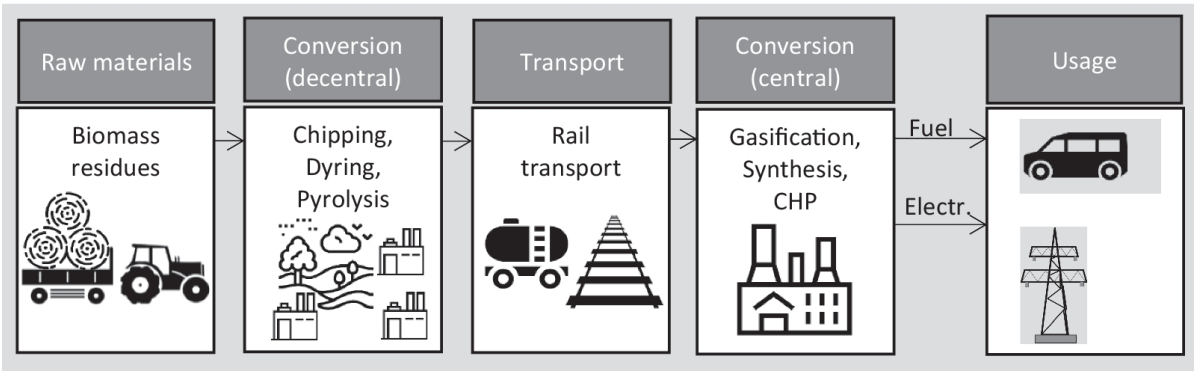

Figure 1-3. The industrial scale thermochemical conversion of lignocellulosic biomass. (Reprinted with permission from reference 12. Copyright © 2022, Springer Berlin Heidelberg.)

1.2 Biomass upgrading

Biomass is highly oxygenated and highly functionalized.[13] On the one side, the high oxygen content of biomass platform molecules (compared to petroleum feedstocks) suggests that removing oxygen and thus increasing the energy density is essential if the bio-fuel is the target product from biomass.[14,15] On the other side, we also need to reduce biomass reactivity by decreasing the functional group content in biomass when producing some high value-added chemicals and products at high yields.[16] So, upgrading biomass is needed in order to use it efficiently.

Several strategies and technologies can be applied to upgrade biomass to biofuels or value-added chemicals and products. The most important and wildly used technologies for biomass conversion are thermal conversion[17-19] and electrocatalytic conversion.[20,21]

1.2.1 Thermal conversion

Biomass can be converted to high value-added products with increased energy density by thermal technology. Such technology is widely used for reducing greenhouse gas emissions and addressing problems related to climate change nowadays. Thermal technology can be used to produce gas or liquid fuels, and it can also be used for the direct production of heat and electricity.[17,22,23] Biomass thermochemical conversion is an active and fast-growing field of research. There are many thermal conversion processes for biomass upgrading in industry, such as combustion,[24] gasification,[25] and pyrolysis.[26] **Figure1-4** illustrates products from these three main thermal processes available for converting biomass into useful energy.[23]

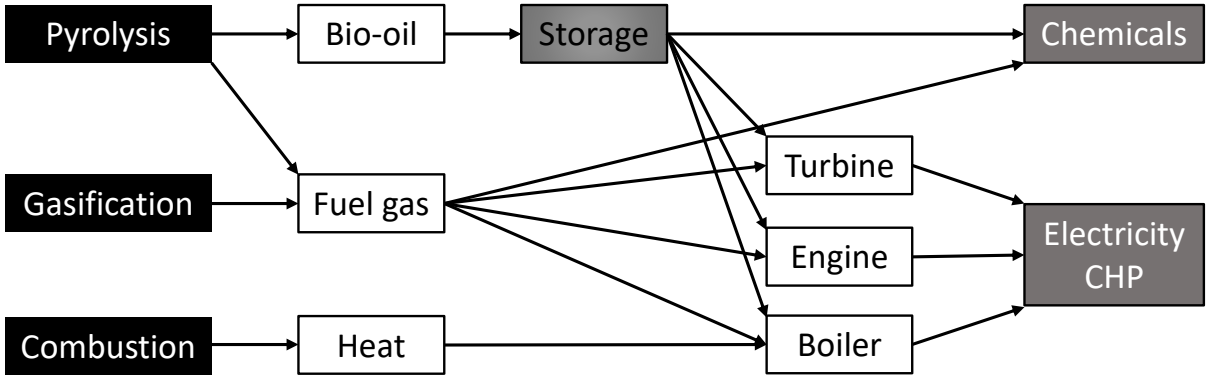

Figure 1-4. Products from thermal biomass conversion. (Reprinted with permission from reference 23. Copyright © 2003, Elsevier.)

Biomass combustion is arguably the oldest known and most widely used controllable energy source on earth. In recent years, rising costs of fossil fuels and the development of advanced equipment have made biomass combustion an economical, efficient, and practical energy source. In the combustion process, two ingredients (biomass and oxygen) are combined in a high temperature environment (900-1500 °C) to form carbon dioxide, water vapor, and heat.[24,27] For biomass combustion to be efficient and clean, the ingredients must be well-mixed at the correct temperatures for a right amount of time. [28]

Gasification for biomass conversion is an efficient and environmentally friendly method to produce chemicals and products. Typically, the low-value lignocellulosic biomass can be converted to syngas, liquid fuels, and hydrogen by gasification. Many chemical reactions happen during the gasification process under a high temperature range of 800–1300 °C.[25,29] Compared with the gasification for coal, biomass gasification is more suitable and promising because of the low sulfur content and less reactive character. Biomass fuels are suitable for highly energy-efficient power generation cycles based on gasification technology.

Pyrolysis is a thermal process that converts biomass in the absence of air/O_2 at temperatures ranging from around 400–800 °C to liquid (bio-oil), gaseous (syngas), and solid fractions (charcoal).[30] Some factors significantly affect product yield, including the reaction temperature, residence time, and pyrolysis rates. When it is necessary to maximize the yield of liquid products like bio-oil, the lower half of the applied temperature range is needed.[31]

1.2.2 Electrocatalytic conversion

Biomass upgrading by electrocatalytic conversion has been a research hotpot in the last several decades.[32] Compared with the traditional thermal biomass conversion technology (thermalcatalysis) that are normally conducted under extremely high temperature and pressure, electrocatalytic biomass conversion is a technology that uses electricity as driving force for chemical reactions in the presence of electrocatalysts under mild environment (ambient temperature and air pressure).[33] It is more energy-efficient and environmentally friendly due to less emission of the pollutants.[34]

By inducing an external potential, the reduction reaction of the substrate happens at the cathode and at the same time the oxidation reaction happens at the anode during electrocatalytic

process. By using electrons instead of hydrogen as the reductant, electrocatalytic technology can also get high reaction activity at relevant mild temperatures and pressures.

In order to produce defined hydrocarbon products that can be used as fuels, biomass feedstocks with high oxygen content and low energy density need to be refined for increased hydrogen content, low oxygen content and high energy density. **Figure 1-5** illustrates a schematic pathway of local chemical and fuel production by electrocatalytic biomass conversion technology.[20] Firstly, biomass with carbonyl functional group (e.g. aldehydes and ketones…) can be converted to stable oxygenates for further refinery operation by electrocatalytic hydrogenation. These primary alcohol products need further hydrodeoxygenation process to remove oxygen content by combining electrochemical reduction and acid catalysis. The obtained alkane mixtures finally undergo alkylation treatment to adjust molecular size to get high quality fuel that can be used further.

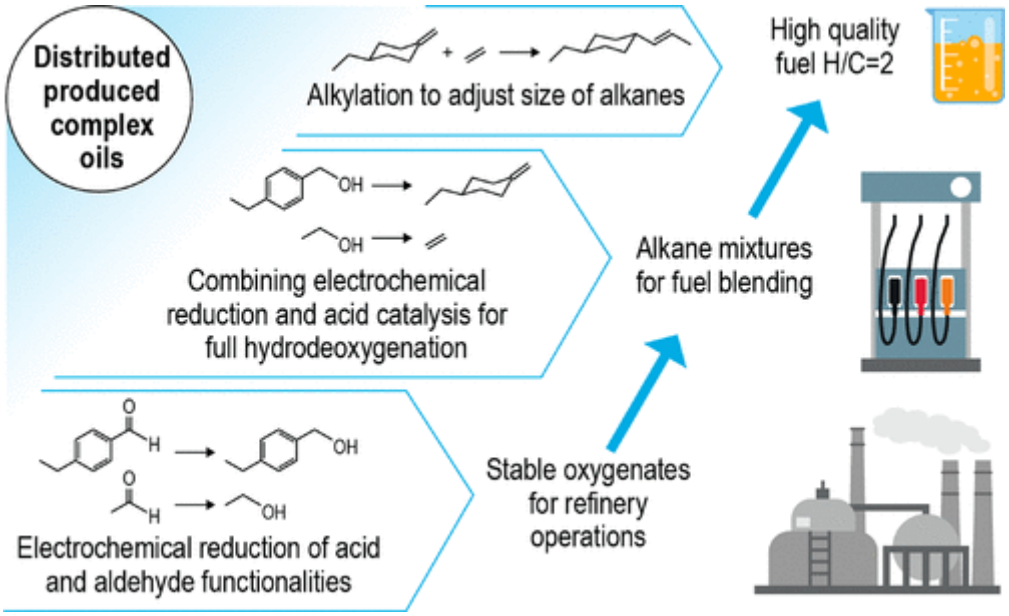

Figure 1-5. Electrochemical pathway to local chemical and fuel production. (Reprinted with permission from reference 20. Copyright © 2020, American Chemical Society.)

Except upgrading biomass to valued-added fuels, electrocatalytic technology can also be used to treat effluent containing phenols and other organic substrates, heavy metals, organic dyes, biodiesel, and ethylenedia-minetetraacetic acid (EDTA).[35] The technology has been used to reduce biomass derived liquids which contain oxygen functional group and unsaturated carbon bonds.

1.3 Electrochemical reactions

An electrochemical reaction uses an electric field between the cathode and anode to drive electron transfer between two substances— a solid (electrode) and a liquid (electrolyte solution). The external applied potentials provide the driving force to conduct electrochemical reduction/oxidation reactions in an electrochemical cell.[36]

Electrochemical reactions offer several advantages over other approaches. The electrochemical process is typically conducted under ambient or low temperature and air pressure, making the reaction conditions easier to control. Electrochemical reactions generally require no auxiliary chemicals and do not produce waste (environmental compatibility), since the main species involved in the oxidation process are electrons and oxidant agents produced in situ. Furthermore, it is easy and convenient to integrate with renewable harvesting (supply electricity) and combine with other technologies.[37]

1.3.1 Electrocatalytic hydrogenation

Hydrogenation is a common and the most important reaction in organic chemistry and plays a critical role in synthesizing value-added products within the chemical industry. Many studies have extensively investigated the hydrogenation reactions, both experimentally and computationally.[38-40] Traditional hydrogenation reactions are conducted at high temperatures and hydrogen pressure to get a high reaction conversion rate. However, such extreme conditions will lead to fast catalyst deactivation and high operating costs (by heating and the H_2 price). Aqueous phase electrocatalytic hydrogenation is one of the promising strategies that can be an alternative to traditional thermocatalytic hydrogenation reactions.

Unlike thermocatalytic hydrogenation reactions requiring external H_2 as a proton source, electrocatalytic hydrogenation generates hydrogen in situ from an aqueous electrolyte under an external electric potential, typically leading to high equilibrium pressures. Rather than forming H_2 (hydrogen evolution reactions), the formed surface hydrogen atoms (H*) can also react with (the biomass-derived) organic substrates under mild reaction conditions. With water as the proton source, electrochemical hydrogenation provides an environmentally friendly approach to the selective reduction of some multifunctional organic molecules.[20,41]

Electrocatalytic hydrogenation has several advantages over catalytic hydrogenation. Hydrogen sources from water solutions eliminate the problems related to H_2 gas storage and transport and reduce costs. Mild operating reaction conditions (ambient temperature and air pressure) can also reduce the additional cost and keep the catalytic activity longer. Electricity can be supplied by renewable energy (solar, wind, and hydro), and electrocatalytic equipment can easily integrate with renewable power harvesting. Lastly, controlling the hydrogenation rate by potential or current density adjustments is very easy.[20]

Figure 1-6 shows an electrocatalytic hydrogenation cell that can conduct hydrogenation reactions.[20] Typically, a catalyst deposited on a carbon felt was used as the working electrode. A double-junction Ag/AgCl and a Pt wire were used as the reference electrode and counter electrode, respectively. The anode and cathode compartments were separated by the Nafion membrane.

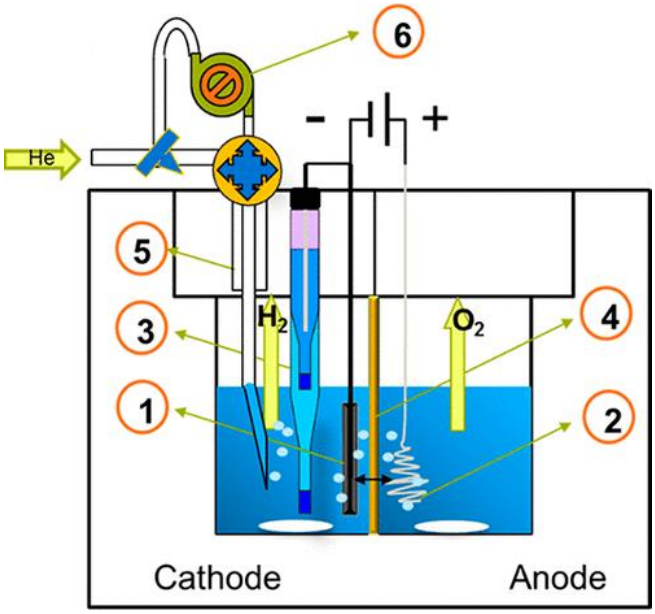

Figure 1-6. Schematic diagram of the ECH cell. Working electrode (ACF) (1); counter electrode (Pt wire) (2); reference electrode (Ag/AgCl) (3); proton exchange membrane (Nafion 117) (4); inert gasinlet (5); recycling pump connected in selected experiments (6). (Reprinted with permission from reference 20. Copyright © 2020, American Chemical Society.)

During electrocatalytic hydrogenation process, the generated hydrogen species (H*) can combine with organic or inorganic substrates, including CO_2, alkynes, aldehydes, inorganic nitrogen compounds (e.g. N_2, nitrates, nitrites), and organic nitrogen compounds, which contain unsaturated bonds such as C=C, C=O, C≡N, N≡N, and N=O, with electrons to form a range of hydrogenation products.[42-44]

Electrocatalysts play an essential role in efficient electrocatalytic hydrogenation reactions. Several features determine electrocatalysts, including activity, selectivity, and durability. Noble metal-based materials (e.g., Pt, Pd, and Rh) have been widely used and researched as high-efficiency catalysts for electrocatalytic hydrogenation reactions.[45,46] However, the scarcity and prohibitive cost impede the large-scale application of noble metal-based electrocatalysts. On the other hand, the base metal materials (e.g., Cu and Ni) with abundant presence, low cost, and high catalytic activity attract people's attention.[47,48] Up to now, lots of researchers have devoted themselves to developing noble metals, base metals, and alloying electrocatalysts for biomass conversion.

1.3.2 Electroreductive carbon-carbon coupling reaction

Like hydrogenation reactions, carbon-carbon formation (C–C coupling) reactions are also useful and widely researched reactions to highly value-added products in organic (for biomass upgrading) and inorganic (primarily for CO_2 conversion) chemistry.[49,50] The C–C coupling strategy has been applied to synthesize many complex organic compounds in organic synthesis. C-C coupling was also used in biomass conversion to increase the molecular weight and stabilize the molecular structure for biomass upgrading. In inorganic chemistry, the C–C coupling reaction mostly happens during the CO_2 conversion process leading to C_{2+} products. The Nobel Prize in Chemistry in 2010 was awarded to three pioneers who developed cross-coupling reactions using organozinc reagents (E. Negishi),[51] organoboron reagents (A. Suzuki),[52] and alkenes (R.F. Heck).[53] The coupling methods, which they and others originated, are appropriately considered to be the cornerstones in organic synthesis.

The electroreductive method is a promising strategy for C–C coupling reactions. The carbon dioxide electroreduction reaction (CO_2RR), an emerging electrocatalysis reaction, is promising for converting CO_2 into value-added fuels or chemicals. Besides, electroreductive C–C coupling or cross C–C coupling reactions have also been widely used for converting biomass molecules (e.g., benzaldehyde, furfural) into high-quality fuels or value-added chemicals.

1.3.2.1 The carbon dioxide electroreduction reaction

The carbon dioxide utilization offers routes to address climate change concerns and displaces the conventional manufacturing processes intensively relying on fossil fuels with a cost-

effective and environmentally friendly approach. The carbon dioxide electroreduction reaction (CO_2RR) driven by electricity is an emerging electrocatalytic reaction and the hottest research area nowadays. This reaction aims to convert CO_2 into high-energy-density and economically valuable fuels or chemicals with almost net-zero emissions.[54]

The reason why CO_2RR is a hot issue in the scientific area, on the one hand, is that CO_2RR can bring many benefits, like solving CO_2 problems for climate change and generating value-added fuels and products. On the other hand, the CO_2RR reaction still faces many issues and tough challenges even though scientists have researched it for many years. One issue we mostly face is the poor selectivity for converting CO_2 to C_2 or C_{2+} products. Another challenge we must address is that CO_2RR has a low current density, low CO_2 conversion, and dismal energy efficiency, significantly limiting its practical implementations.[55]

Enormous efforts have been devoted to developing the carbon dioxide electroreduction reaction, including (1) design unique electrocatalysts for high selective catalytic CO_2 conversion to C_2 or C_{2+} products,[56] (2) design rational electrode structures for fast mass transport or for more exposed active sites for CO_2 conversion,[57] (3) change electrolyte for maintaining the microenvironment (including pH, absorbed anionic and cationic species) of CO_2RR and for weakening HER to enhance the selectivity toward the target products.[58] Among these effects, electrocatalysts still occupy the most significant concern nowadays.

For CO_2RR reactions, the production of C_2 and C_{2+} products mainly depends on Cu-based catalysts at present.[59-61] Cu has a near-ideal binding affinity toward CO_2 conversion, thus intensely activating the CO_2 molecules. More importantly, Cu-based catalysts can promote C–C coupling formation, which is necessary for CO_2RR to get C_2 and C_{2+} products. Cu-based materials with different sizes, structures, morphologies, and compositions have been extensively applied in CO_2RR.

1.3.2.2 Electroreductive carbon-carbon coupling of biomass

Besides CO_2, carbon-carbon coupling is also a common phenomenon during biomass upgrading.[49,62,63] C-C bond formation serves as a versatile and important synthetic strategy in organic chemistry. Among different kinds of C–C coupling reactions, C–C bond formation among carbonyl functional groups (C=O) shows attractiveness in producing chemicals and

fuels that find widespread applications in medicines, pharmaceuticals and transportations. The carbonyl functional groups that are abundantly present in bio-oils, predominantly as aromatic aldehydes and ketones (e.g., furfural, 5-hydroxymethylfurfural, and benzaldehyde), can be utilized as the biomass feedstocks for C–C coupling.[63,64]

Mechanically, C–C coupling during the biomass upgrading process occurs primarily via the Langmuir-Hinshelwood mechanism involving the reaction of two surface ketyl intermediates. The ability of an electrocatalyst to form and stabilize the ketyl intermediate has been proposed as a key descriptor of its ability to promote C–C coupling.[63] The performance of the electrocatalyst for the coupling of aldehydes is determined by simultaneously generating and dimerizing the ketyl intermediate.

Except for the homo-dimer coupling, the C–C coupling of two different reactant molecules, referred to as cross C–C coupling, has recently caught people's attention.[49,65] Cross-coupling reactions are powerful tools for C–C bond formation and have been widely utilized for synthesizing various molecules. Copper, an electrocatalyst, is emerging as a viable catalytic metal for cross-coupling reactions to construct C–C bonds. Lanny et al.[66] revealed the unique attributes of the copper-catalyzed, aerobic reaction system applied to the formation of ketones by coupling thiol esters with boronic acids at neutral pH. Xu et al.[49] also found that Cu shows a higher selectivity toward the cross-coupling species in benzaldehyde and furfural co-reactants system.

1.3.3 Electrocatalytic oxidation

Oxidation reactions are also very important in organic chemistry and play a critical role in synthesizing value-added products within the chemical industry (e.g., for manufacturing polymers, pharmaceuticals, fragrances, fuels.).[67,68] As shown in **Figure 1-7a**, typically, biomass is high oxygen-contained feedstock (15 – 30 wt% of oxygen in lignin, 10 – 40 wt% of oxygen in hemicellulose, and 40 – 60 wt% of oxygen in cellulose). The highly oxygen-functionalized structure of biomass and its derivatives enables the energy-efficient and atom-economic production of organic oxygenates compared to that produced from petroleum feedstock without oxygen.[69]

Electrocatalytic oxidation of biomass platform chemicals instead of a petroleum source offers a sustainable and atom-economic avenue toward organic oxygenates, with additional benefits when coupled with renewable electricity-driven processes. Compared with traditional chemical conversion technology, electrocatalytic oxidation provides an efficient pathway toward oxidative transformations.[70-71] With sufficient potential bias, a lot of biomass feedstocks can lose electrons on the surface of the anode electrode, producing highly reactive surface intermediates for oxygenation, dehydrogenation, and coupling.[69] **Figure 1-7b** also shows some typical carbonyl compounds, such as 2,5-furandicarboxylic acid (FDCA), adipic acid, glucaric acid, formic acid, acetic acid, lactic acid, and the precursor of gasoline, which can be obtained from biomass by electrocatalytic oxidation reactions.

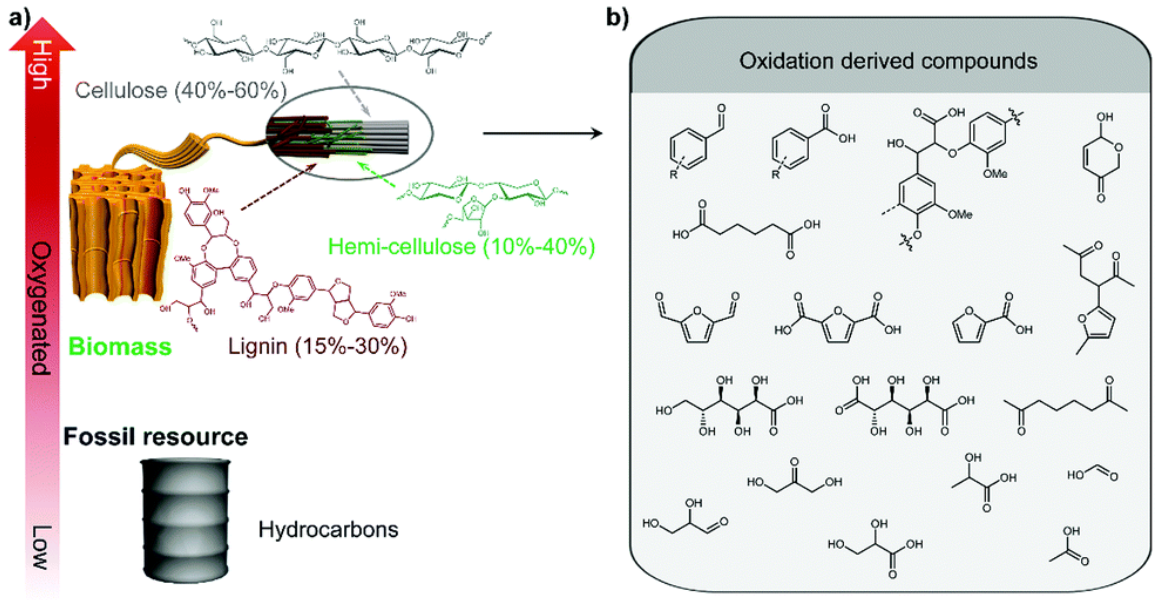

Figure 1-7. Oxygenates originating from biomass. (a) Representative structure of lignocellulosic biomass. (b) Typical compounds from biomass electrocatalytic oxidation. (Reprinted with permission from reference 69. Copyright © 2021, Royal Society of Chemistry.)

1.4 Benzaldehyde upgrading

Benzaldehyde compounds are the crucial class of platform substances from lignin, which are mainly used as raw materials for producing flavors and fragrances or as intermediates for producing fine chemicals.[73] As the simplest aromatic aldehyde, benzaldehyde (an aromatic ring connecting a C=O functional group) can be selectively hydrogenated to benzyl alcohol or reduced to hydrobenzoin (1,2-diphenyl-1,2-ethanediol) by C-C coupling reaction,[63] as shown in **Figure 1-8**.

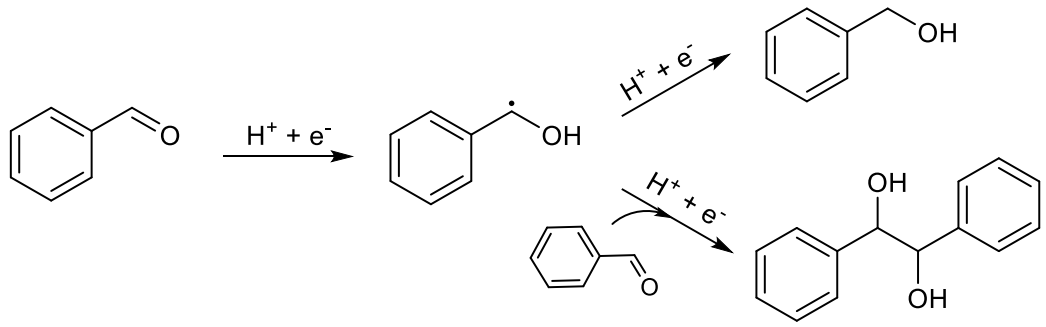

Figure 1-8. Hydrogenation of benzaldehyde to benzyl alcohol and hydrobenzoin.

Both value-added products are beneficial and essential to our society. Benzyl alcohol is an important industrial chemical generally used as a solvent for paints, lacquers, and inks. It is also an effective precursor for preparing esters in the cosmetics and flavoring industries. Hydrobenzoin is a structural motif in antiepileptic drugs (e.g., Phenytoin Sodium) and photo-initiators. At the same time, owing to the rigid chiral structure of the diphenylethylene group, multifunctional diol groups, and excellent availability, hydrobenzoin and the derivatives have recently been applied to various areas of chiral chemistry and further broadened application area to synthetic chemistry.[63,74] So, selective hydrogenation of unsaturated benzaldehyde molecules to different aimed products has recently received a growing interest.

1.4.1 Thermal catalytic hydrogenation of benzaldehyde

Thermal catalytic hydrogenation of benzaldehyde typically involves the reaction between H_2 and benzaldehyde feedstock under a relatively high temperature in the presence of relevant catalysts. Considerable research efforts have been made to explore both gaseous- and solution-phase thermal catalytic hydrogenation of benzaldehyde.[75-77]

A. Saadi et al. have reported that the structural support significantly impacts gaseous thermal catalytic benzaldehyde hydrogenation.[78] They investigated the benzaldehyde over Cu catalysts supported on different supports (Al_2O_3, SiO_2, TiO_2, CeO_2, and ZrO_2) at atmospheric pressure and the temperature range from 100 to 350◦C. The activity and product selectivity (benzyl alcohol, toluene, and benzene) depend on the nature of the support and reaction temperature. The varying activity can be attributed to metal and acid–base surface properties. They further revealed that the relative selectivity of toluene and benzyl alcohol was attributed to the OH functional group's adsorption strength on the catalyst surface. High selectivity to benzene was

attributed to the easiness of the catalyst to break the C–H aldehydic bond and the stability of the surface organic entity formed.

Studies have reported that the activity and product selectivity of liquid-phase thermal catalytic benzaldehyde hydrogenation depends strongly on the nature of the solvent. Cheng, G. et al. have recently investigated the impact of four solvents (methanol, water, dioxane, and tetrahydrofuran) on the reduction of benzaldehyde on carbon-supported palladium (Pd/C) using kinetic methods including isotope labelling and kinetic effects.[77] They showed that the activity of thermal catalytic benzaldehyde hydrogenation on palladium differs by up to one order of magnitude in different solvents (dioxane < tetrahydrofuran < water < methanol). They found that the solvents greatly influence the adsorbed reactants' chemical potential and the transition state. The reaction rates of benzaldehyde hydrogenation were mediated by the differences in the stabilization of the binding of hydrogen to the palladium surface. Weaker hydrogen binding to the surface (higher relative excess potentials) leads to higher reaction rates, that is, reactions in methanol and water are much more reactive than those in aprotic THF and dioxane. The dependence of reaction rate for benzaldehyde hydrogenation and strength of hydrogen adsorption on Pd in different solvents was shown in **Figure 1-9**.

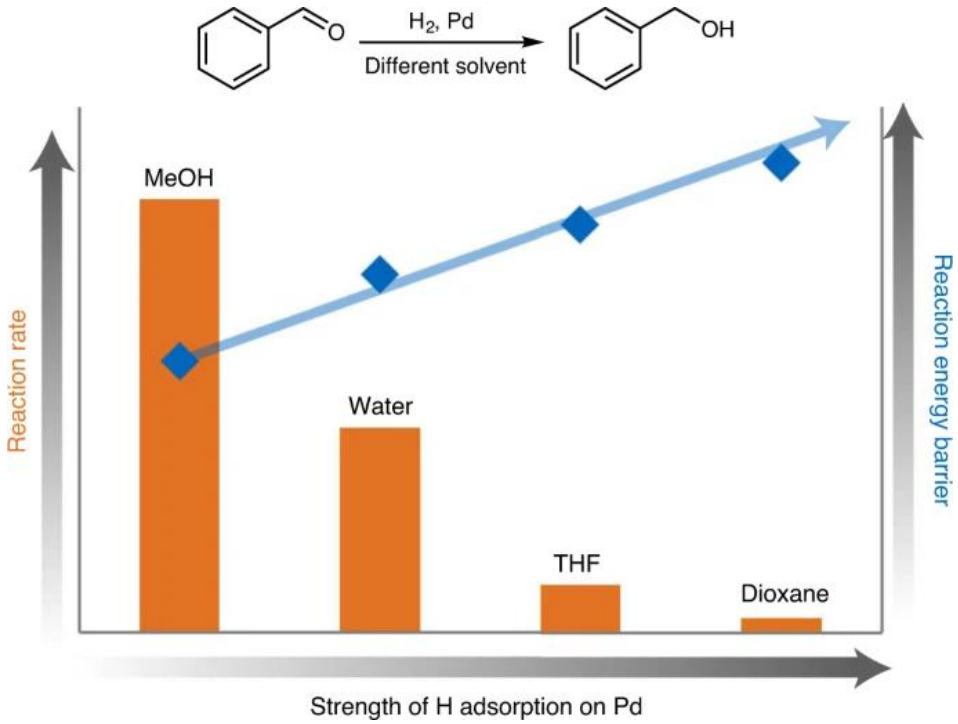

Figure 1-9. The dependence of reaction rate for benzaldehyde hydrogenation and strength of hydrogen adsorption on Pd in different solvent. (Reprinted with permission from reference 77. Copyright © 2021, Springer Nature.)

Besides experimental evidence for thermal catalytic hydrogenation of benzaldehyde in both gaseous and liquid solution, molecular calculation also provides evidence for discovering the reaction mechanism. Simuck F. Yuk et al. have studied the hydrogenation reaction of benzaldehyde over the Pt(111) and Pd(111) surfaces based on a Langmuir-Hinshelwood (LH) mechanism.[79] They revealed that the fcc adsorption site on the surface of Pd(111) was dominantly occupied by the H atom while the mixture of the H adsorption site is presented on the Pt(111). In the presence of water solvent, the benzaldehyde adsorption mode changed from titled on a neutral Pd surface to flat on a charged Pd surface. Apart from the benzaldehyde adsorption mode, the stability reaction intermediates, and the activation barrier between hydrogenation steps also changed in the presence of water solvent and charged Pd(111) surface. The solvent can stabilize reaction intermediates when charge transfer occurs. This can increase the surface coverage, decrease energy barriers, and thus enhance the reaction rate. On the other hand, applied potential can enhance the charge transfer and, therefore, also enhance rates. The calculated result is shown in **Figure 1-10**.

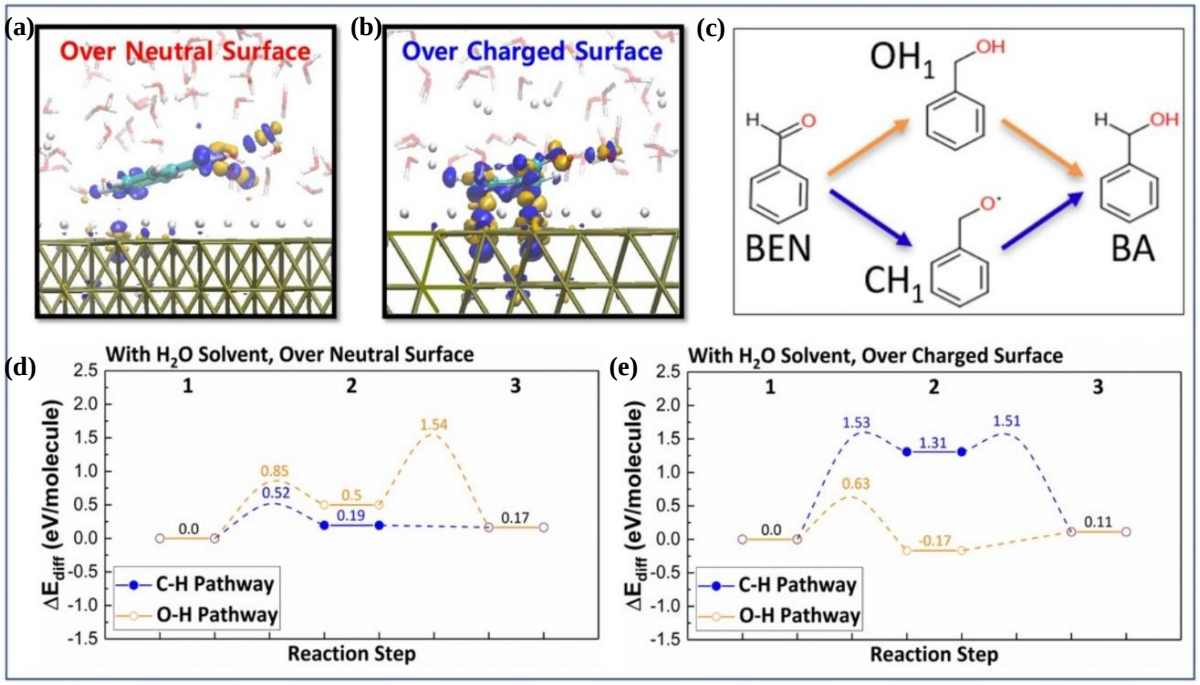

Figure 1-10. Atomic density profile and differential charge profile of adsorbed benzaldehyde, along with surface-bound H atoms and H_2 molecules on (a) neutral and (b) charged Pd(111). (c) Proposed Langmuir-Hinshelwood mechanism for benzaldehyde hydrogenation to benzyl alcohol over Pd(111) surface. DFT-based reaction pathways of benzaldehyde hydrogenation with the presence of water solvent over neutral surface (d) and with the presence of water solvent over charged surface (e). (Reprinted with permission from reference 79. Copyright © 2022, Elsevier.)

1.4.2 Electrocatalytic hydrogenation of benzaldehyde

Upgrading biomass present in the organic stream is commonly done by thermal catalytic hydrogenation at high temperatures and pressures. On the other hand, electrocatalytic hydrogenation (ECH) is a promising alternative wherein hydrogen is generated in situ from an aqueous electrolyte under an external electric potential. The produced surface hydride species can subsequently react with the biomass organic substrates under milder reaction conditions.

H_2 gas is the hydrogen source, and heat is the driving force for thermalcatalytic hydrogenation. In contrast, hydrogen is generated from an aqueous electrolyte for an ECH reaction driven by electric potential. So, catalytic performance for benzaldehyde ECH strongly depends on electrolyte and external potential. Lopez-Ruiz JA et al. systematically studied the effect of several alcohols (methanol, ethanol, and isopropanol) as co-solvents in the catholyte on the performance of Pd/C during the electrocatalytic reduction of benzaldehyde.[80] They found that increasing alcohol concentrations decreases ECH rates, while HER (the competitive reaction) rates remained constant when operating at constant external potential. Increasing potentials increases ECH rates and enhances HER rates to a greater extent. A first-order kinetic analysis following the Eley–Rideal (ER) – type mechanism shows that changes in ECH and HER rates as a function of external potentials are due to changes in benzaldehyde and H surface coverages.

Carbon is a widely used catalyst support, and metal supported on carbon materials is the most widely used electrocatalyst for benzaldehyde hydrogenation, such as palladium on carbon (Pd/C) and platinum on carbon (Pt/C). Reports revealed that the modified carbon materials impact catalytic reactions through electronic and acid–base-induced interactions with supported metal nanoparticles.[81,82] K. Koh et al. studied Pd nanoparticles (NPs) supported on various modified carbons in benzaldehyde's selective electrocatalytic hydrogenation to benzyl alcohol.[83] They applied three approaches to modify carbon supports' chemical and physical properties (acid treatment, carbonization of N- and O-precursors, and O_2 plasma treatment). They revealed that the functionalization of carbon supports with acid groups enhances the reaction rate for benzaldehyde ECH, as shown in **Figure 1-11a**. The enhancement also shows direct correlations with the concentration of Brønsted-acid sites of the modified felts and Pd catalysts in **Figure 1-11b**. They concluded that the enhancement of electrocatalytic reduction

is realized by the participation of support-generated hydronium ions in the proximity of the metal particles via a proton-coupled electron transfer (PCET) mechanism.

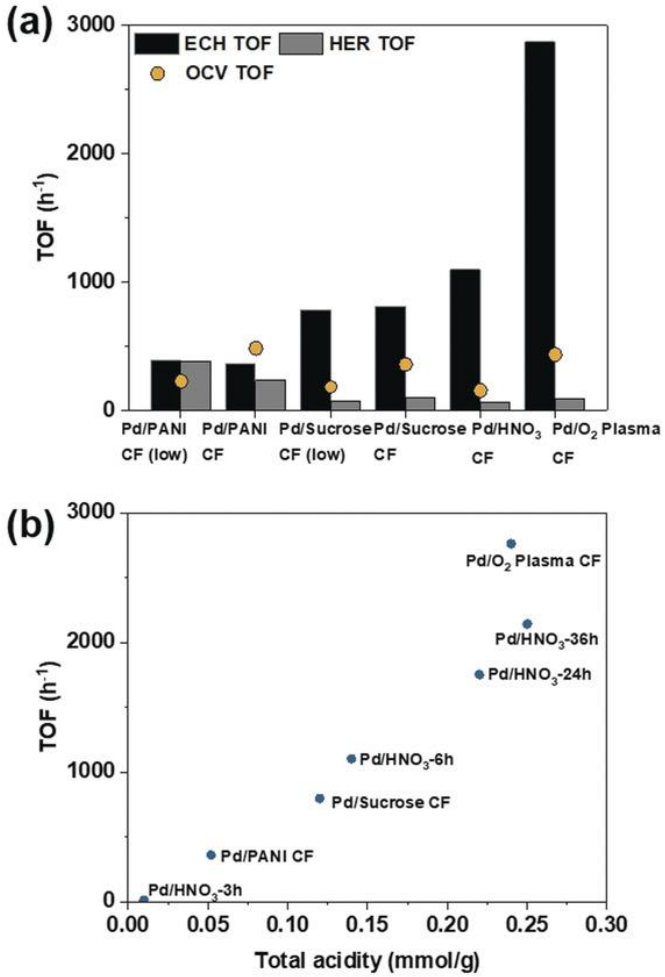

Figure 1-11. (a) Turnover frequency (TOF) of the electrocatalytic hydrogenation (ECH), open-circuit voltage (OCV) reactions, and H_2 evolution (HER) observed during the ECH of benzaldehyde on Pd supported on functionalized felts. (b) TOFs of the ECH of benzaldehyde vs. the concentration of acid sites in the Pd catalysts. (Reprinted with permission from reference 83. Copyright © 2020, John Wiley and Sons Ltd.)

Recently, the metal−organic framework (MOF) structures were applied to study the electrochemical hydrogenation of benzaldehyde. L. Gong et al. proposed a high-performance electrocatalyst (Pd nanoparticles supported on an oxygen-rich nickel-MOF, Pd@Ni-MOF) for benzaldehyde to benzyl alcohol hydrogenation reaction.[84] Pd@Ni-MOF electrocatalyst showed excellent activity toward the benzaldehyde ECH. They concluded that these outstanding performances can be attributed to the Ni-MOF support for promoting H-bond formation, facilitating water desorption, and inducing favorable tilted benzaldehyde adsorption

configuration on the surface of the Pd nanoparticles by conducting density functional theory calculations.

1.4.3 Electroreductive C-C coupling of benzaldehyde

Besides carbonyl hydrogenation to generate benzyl alcohol, benzaldehyde will undergo C-C coupling to form hydrobenzoin during the electrocatalytic hydrogenation. It is a parallel reaction pathway because both benzyl alcohol and hydrobenzoin are the primary products during benzaldehyde ECH. Unlike benzyl alcohol, which is always observed as a product for benzaldehyde ECH, hydrobenzoin has been observed as a product only on a few catalysts.[63,85] Most studies that reported the hydrobenzoin formation during benzaldehyde ECH are related to Cu or Cu-based catalysts.[63,74,85]

J. Yu et al. designed bimetallic Pd/Cu electrocatalysts with tunable surface coverage of Pd for benzaldehyde ECH.[63] The Pd/Cu catalyst with an optimized Pd coverage exhibits the highest coupling selectivity for hydrobenzoin formation with a Faradic efficiency of 63.2% and a yield of 85.3%. In situ benzaldehyde adsorption experiments revealed that the Pd sites are responsible for activating the ketyl intermediate, and Cu provides sites for the subsequent dimerization reaction, as shown in **Figure 1-12**. The balance between the formation and dimerization sites for ketyl intermediate on bimetallic Pd/Cu catalysts contributes to the enhanced Faradic efficiency and formation rate for hydrobenzoin. So, their study highlighted the role of Pd in providing a site for the formation of ketyl intermediate. However, Jacob Anibal et al. concluded that the formation of hydrobenzoin during benzaldehyde ECH is directly related to the ability of the Cu catalyst to stabilize a ketyl intermediate.[85] These studies revealed that the ability of a catalyst to form and stabilize the ketyl intermediate is a key descriptor of its ability to promote C-C coupling for hydrobenzoin formation during benzaldehyde ECH.

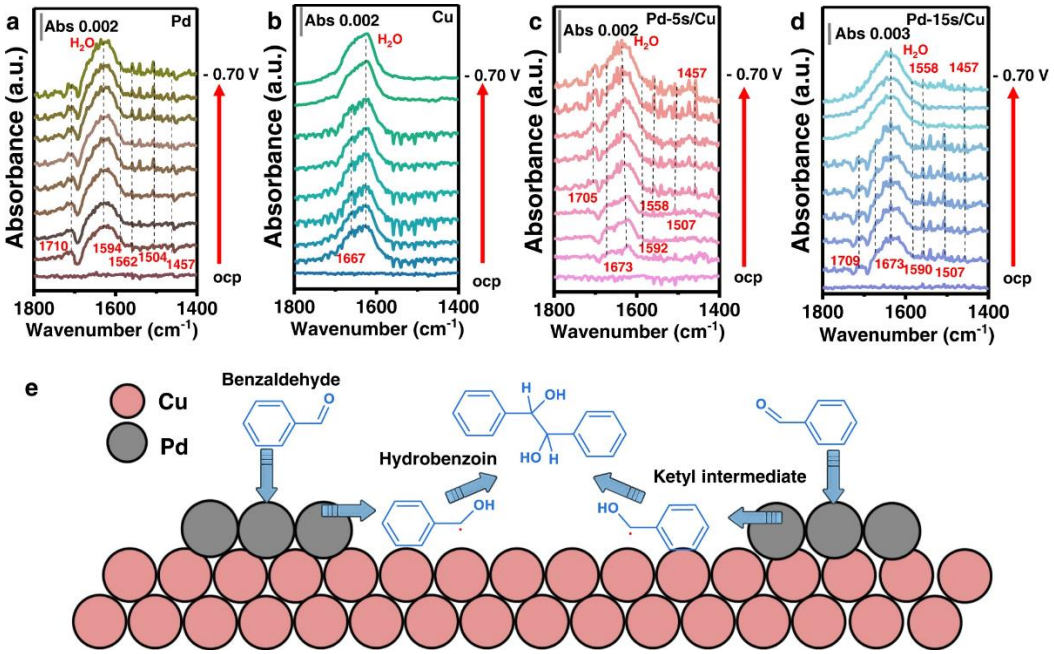

Figure 1-12. (a–d) In situ ATR-SEIRAS spectra of Pd (a), Cu (b), Pd-5s/Cu (c), and Pd-15s/Cu (d). (e) Proposed reaction mechanism for the electroreductive coupling of benzaldehyde to hydrobenzoin. (Reprinted with permission from reference 63. Copyright © 2022, Springer Nature.)

1.5 Electrolyte pH effect

Since hydrogen is generated in situ from an aqueous electrolyte under an external electric potential, the electrolyte pH has a significant impact on the electrocatalytic hydrogenation of biomass feedstock for providing the H source for the reaction. Besides, the properties of electrolytes, such as polarity, acidity, density, hydrogen-bond donating ability, and hydrogen-bond accepting ability, are critical in the catalytic performance concerning the reaction rate, product selectivity, reaction pathway, and reaction mechanism.[86-88] The potential reasons that electrolytes pH can significantly affect catalytic performance during aqueous-solid ECH reaction can be attributed to the mass transfer, dissolution, and the interaction of the electrolyte with reactant, intermediate, transition complex, and products.[89-91]

The hydrogen binding energy (HBE) can be significantly affected by electrolyte pH. In the aqueous phase, the hydrogenation rates of aromatic substrates such as phenol on Pt/C and Rh/C are influenced by varying activity of hydronium ions.[92] The metal surface's HBE would weaken at lower pH electrolyte. The lower HBE decreases the activation energy for the addition of

adsorbed H from the metal to the adsorbed organic. A less negative H binding energy with decreasing pH raises the total energy of adsorbed phenol, as shown in **Figure 1-13**.[92]

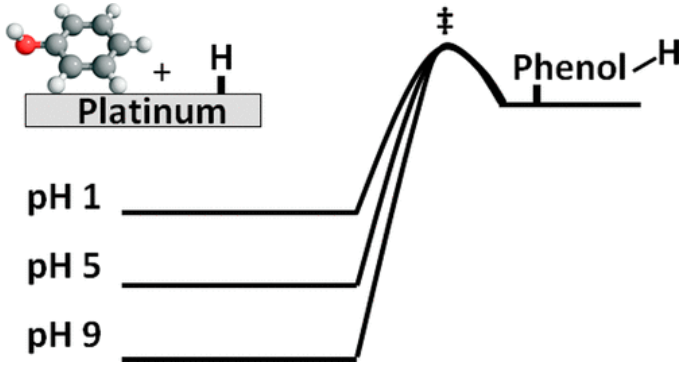

Figure 1-13. Diagram of a hydrogenation step at different pH values. (Reprinted with permission from reference 92. Copyright © 2019, American Chemical Society.)

Up to now, most of the ECH works have been conducted under acidic electrolytes, seldom focusing on the ECH reaction in alkaline electrolytes. A primary reason for this is that the acidic electrolyte was entirely composed of hydronium ions, which play a crucial role in H addition. Meanwhile, acidic media is an excellent conductor to eliminate or decrease the mass transfer effect.[93] However, the hydronium ion concentration in alkaline is negligible, water molecule is the only H source for ECH reactions. Zhao et al. confirmed H_2O was the hydrogen source during electrocatalytic hydrogenation of nitroarenes in alkaline media by conducting D_2O-labeling experiments.[94] The dissociation of H_2O needs additional energy supply which make the ECH reactions difficultly happen in alkaline compared with acidic media. However, alkaline media has its own advantage. Electroreduction of organics in alkaline media with high faradic efficiency has been researched recently due to the suppressed competing HER (lack of hydronium ions in alkaline media).[95,96]

Electrolyte pH or the reaction environment (acidic or alkaline) has been confirmed to greatly affect product selectivity. An electrolytic environment significantly affects product selectivity for furfural ECH on a Cu electrode.[97] The Faradic selectivity can reach ~70% for the selective formation of 2-methylfuran in a strong acid electrolyte during furfural ECH. Oppositely, the selective formation of another product, furfuryl alcohol, reached a much higher level (~90%) in an alkaline electrolyte. Under an acidic electrolyte, the O atom dissociated directly from hydrogenated furfural-derived alkoxyl intermediates, followed by stepwise hydrogenation until H_2O formation via a thermodynamically favorable proton-coupled electron transfer process,

thereby inducing a high proportion of the hydrogenolysis product (2-methylfuran). However, under partial alkaline conditions, furfural could be directly hydrogenated to furfuryl alcohol due to the high-energy barrier of the deoxidation process via a surface hydride transfer.[97]

1.6 Mechanistic studies

Recently, G.H. Cheng et,al. have suggested two possible reaction pathways for thermal catalytic hydrogenation of benzaldehyde to benzyl alcohol on palladium.[77] As shown in **Figure 1-14**, H_2 will dissociate and adsorb on a palladium site pair, forming two adsorbed hydrogen adatoms (H*) (step a). Meanwhile, benzaldehyde adsorbs on an ensemble of vacant palladium (*) sites as chemisorbed benzaldehyde (ArCHO*) (step b). The C=O bond hydrogenation requires two successive hydrogen addition steps, that is, step c and step d, in the two plausible pathways, namely the alkoxy pathway (c-I and d-I) and the hydroxy pathway (c-II and d-II), depending on the hydrogen addition sequence. In the hydroxy pathway, the carbonyl O of the adsorbed benzaldehyde (ArCHO*) is hydrogenated first to form a surface hydroxy intermediate (ArCHOH*), followed by a second H addition to the α-C to form benzyl alcohol. In the alkoxy pathway, on the other hand, the carbonyl C atom is first hydrogenated to form an alkoxy intermediate ($ArCH_2O$*), followed by hydrogenation of the O to form benzyl alcohol.

Isotope labelling studies can be used to distinguish between the alkoxy and the hydroxy pathways for benzyl alcohol formation.[77] During benzaldehyde hydrogenation (on Pd/C), adding D to the carbonyl C via the alkoxy pathway forms ArCHDO*. It would inevitably result in the formation of some deuterated benzaldehyde (ArCDO*) due to the reversibility of this step. On the other hand, adding D to the carbonyl O via the hydroxy pathway forms ArCHOD*. In this case, the reverse reaction would only form non-deuterated benzaldehyde (ArCHO*). Therefore, deuterated benzaldehyde in the electrolyte solution can be used to distinguish between the two pathways.

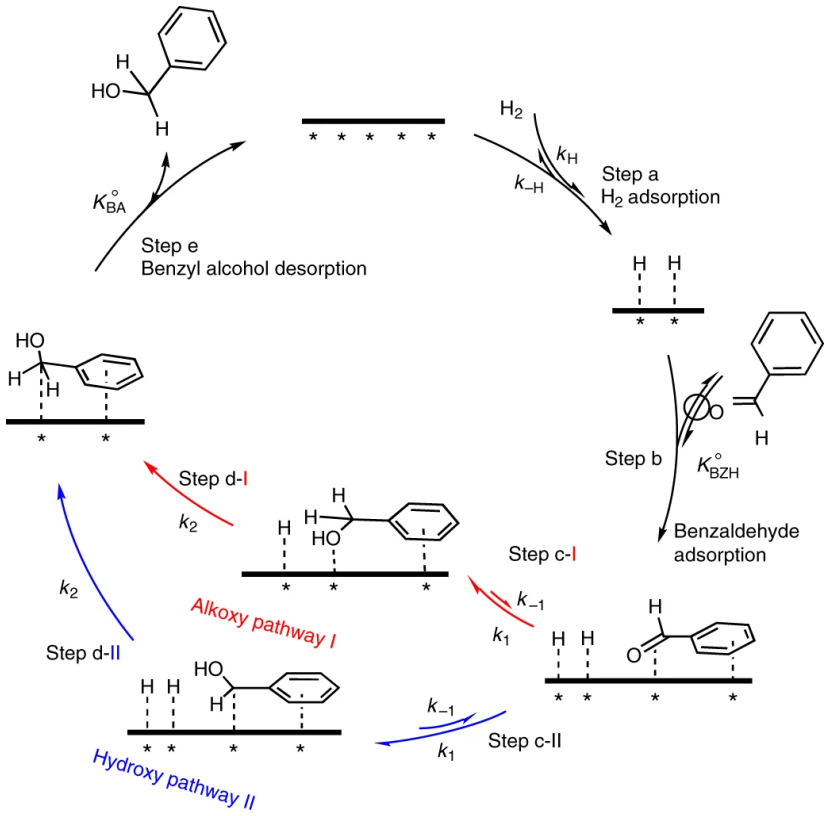

Figure 1-14. Benzaldehyde can be hydrogenated via either the alkoxy (red) or hydroxy (blue) pathways. (Reprinted with permission from reference 77. Copyright © 2021, Springer Nature.)

On the other hand, the pathway for C-C coupling formation has mainly been described in terms of the surface combination of two radical intermediates.[63,74,85] The formation of radical intermediates has been observed on Cu using infrared spectroscopy. Specifically, Jacob Anibal et al. illustrated that Cu uniquely mediates the C–C coupling of benzaldehyde to hydrobenzoin formation.[85] In their study, they conducted complementary in situ spectroscopic investigations, and the result suggested that the facilitation of C–C coupling is directly related to the ability of the Cu catalyst to stabilize a key reaction intermediate (ketyl radical). Spectroscopic features of the ketyl radical are observed on Cu surfaces at benzaldehyde reduction potentials but not on Pd and Pt. In **Figure 1-15a** and **Figure 1-15b**, the small and sharp peak around 1673 cm^{-1} corresponds to the ν(C–O) mode of the ketyl radical. On the Pd and Pt surfaces, CO formation is observed from dissociative adsorption and decarbonylation upon benzaldehyde introduction, suggesting surface adsorbate instability under reducing conditions. From the combined reactivity and spectroscopic evidence, they propose that the ability of a catalyst to produce and stabilize the ketyl radical intermediate is a key descriptor in its ability to mediate the C–C coupling chemistry of aldehydes and ketones.

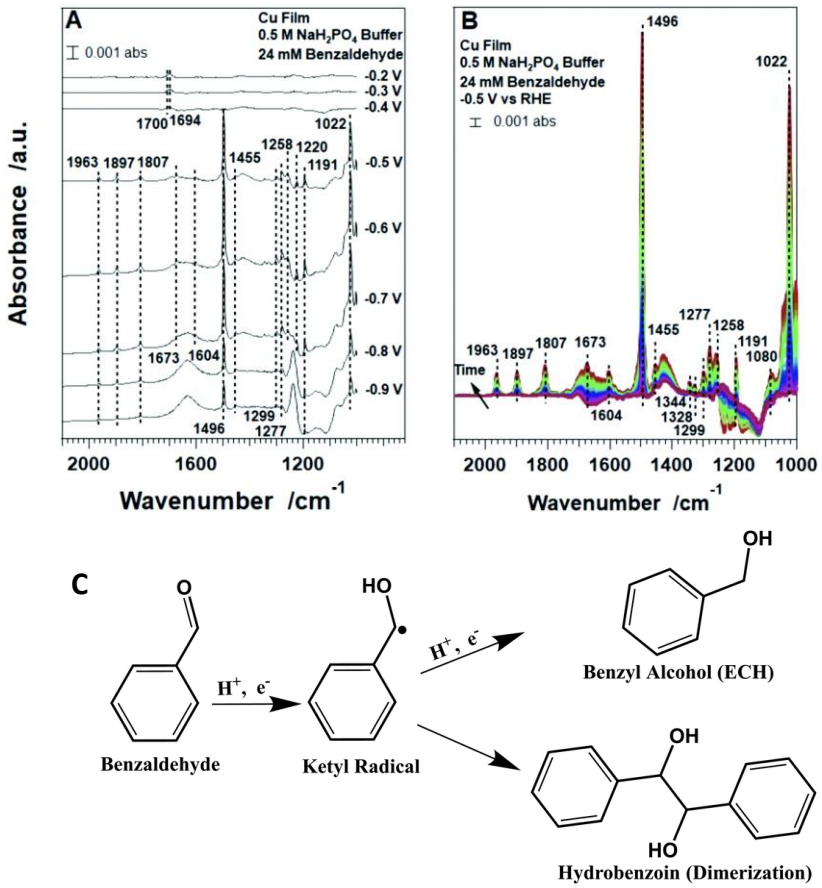

Figure 1-15. (a) ATR-SEIRAS spectra collected during cathodic potential steps on Cu. Each trace represents the final spectrum collected at the stated potential. (b) Time evolution spectra for the Cu surface upon stepping to −0.5 V. Spectra were collected ~3 min apart. (c) Electrochemical benzaldehyde reduction pathways. (Reprinted with permission from reference 85. Copyright © 2020, Royal Society of Chemistry.)

Except for the reaction pathways for two products during the benzaldehyde hydrogenation reaction, the H addition mechanism is also essential for distinguishing the behavior of benzaldehyde hydrogenation. The H addition has been proposed to proceed via two distinct mechanisms: (i) direct hydrogenation of adsorbed organic substrate by a surface hydride species (typically proceeding via Langmuir-Hinshelwood (LH) kinetics and often referred to as the LH mechanism),[76] or (ii) proton-coupled electron-transfer (PCET) mechanism.[83] Koh et al. proposed a PCET mechanism for benzaldehyde hydrogenation on Pd.[83] They ruled out the role of the support acidity effect for the rate of the ECH of benzaldehyde on Pd. The positive impact of the activity of benzaldehyde ECH on Pd with acidic support would imply that the rate-determining step of the catalyzed reaction is related to a PCET mechanism. They concluded

that the functional group acts as a channel for the proton transferred from the hydronium ions in the double layer (**Figure 1-16**).

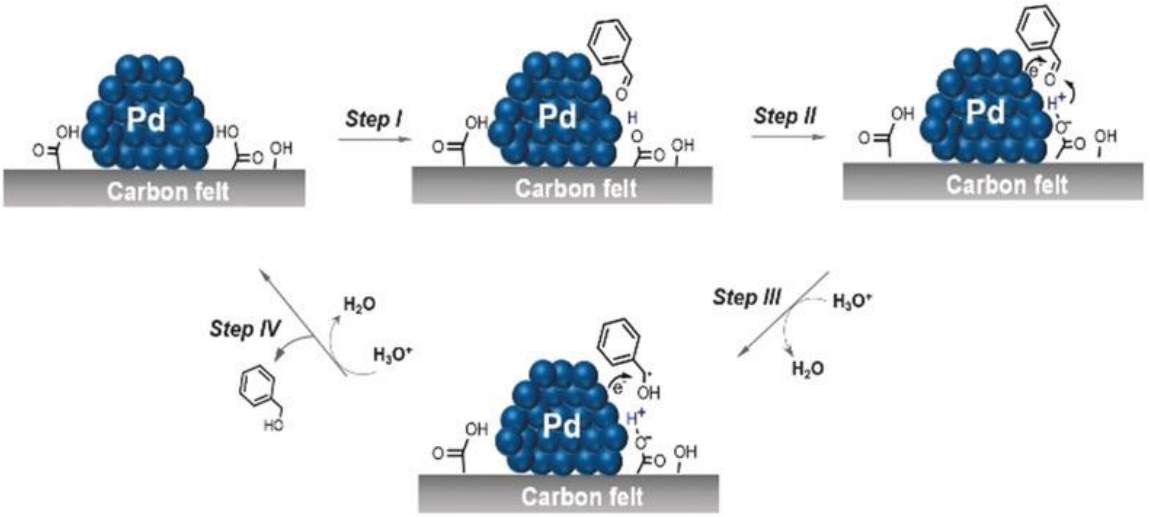

Figure 1-16. Hydrogenation cycle of benzaldehyde on an acid-functionalized support with the hydrogenation steps depicted as proton-coupled electron additions. (Reprinted with permission from reference 83. Copyright © 2020, John Wiley and Sons Ltd.)

Singh et al., on the other hand, investigated aqueous phase hydrogenation of benzaldehyde on Pt group metals and proposed the LH mechanism for H addition.[76] They concluded that the dependences of the reaction rates on reactant concentrations and temperature for all cases of both ECH and TCH for benzaldehyde on Pt/C, Pd/C and Rh/C in aqueous-phase can be described successfully by a Langmuir-Hinshelwood model where the rate-determining step is the addition of an adsorbed H from the surface to the adsorbed organic molecule, which competes for sites with H.

1.7 Scope of this thesis

The object of this research is to develop a deeper understanding of the mechanism for electrocatalytic hydrogenation of benzaldehyde under a wide range of reaction conditions. Cu nanoparticles supported on activated carbon were used as the catalyst due to their unique property of promoting aldehyde hydrogenation to benzyl alcohol and C-C coupling to hydrobenzoin during electrocatalytic hydrogenation process. Acidic media (acetate buffer solution, pH ~4.6) was first chosen as an electrolyte because the mechanism for C-C coupling was only speculatively addressed in acidic media. Alkaline media (Sodium hydroxide/sodium

chloride, pH ~11.3) was also used firstly for comparison with acidic media and secondly for the reason that rare work focused attention on the mechanism for benzaldehyde ECH in alkaline media. Finally, we investigated the co-catalyst effect for tuning product selectivity during benzaldehyde ECH on Cu. MoS_2 was chosen as the co-catalyst due to the high H activity on its surface and insignificant activity for benzaldehyde hydrogenation; adding MoS_2 was expected to change the H addition activity for benzaldehyde ECH on Cu.

For the mechanism in this research, we analyzed the H addition mechanism, the reaction pathways, and the rate-determining step for products (benzyl alcohol, hydrobenzoin, and H_2) in both acidic and alkaline media. The reaction mechanisms were confirmed based on kinetic measurements (e.g., reaction order and the H/D exchange experiment) and the first-principle periodic DFT molecular simulations. Besides, we further discussed the mechanistic reasons that facilitate self or cross C-C bond formation on Cu in the co-reactants system between different aldehydes (e.g., benzaldehyde, furfural, pentanal and cyclohexanal).

In **Chapter 2**, we present the reaction mechanism for benzaldehyde ECH on Cu in aqueous acidic media and the hydrogen evolution reaction (HER) in the presence or absence of benzaldehyde. By conducting the LSV test, calculating the corresponding Tafel slope (30 mV dec^{-1}), and using kinetic measurement (HER rate showed almost no dependence on hydronium ion concentration), we found that, in the absence of benzaldehyde, the HER on Cu/C follows the Volmer-Tafel(rds) pathway. Under benzaldehyde ECH reaction conditions, we found that the surface of Cu is predominantly covered with the organic substrate, and the coverage of H* is low based on the zero-order for benzyl alcohol formation and the inactive HER in the presence of benzaldehyde. By using the kinetic measurements (e.g., first-order reaction kinetics for hydrobenzoin formation, strong KIE for benzyl alcohol formation, and weak KIE for hydrobenzoin formation), assisted by first-principle periodic DFT molecular simulations, we proposed the detailed mechanism for benzaldehyde ECH. The adsorbed benzaldehyde undergoes a fast (equilibrated) first PCET H addition on the carbonyl O to form a hydroxy intermediate. The hydroxy intermediate then undergoes a second (rate-determining) PCET H addition on its α-C to form benzyl alcohol. In a parallel reaction, the electrophilic carbonyl C of a physisorbed benzaldehyde molecule is attacked by the radical α-C of the hydroxy intermediate to form the C-C bond. The C-C coupling is followed by a fast barrier-less second

PCET H addition to the radical O of the formed intermediate to form hydrobenzoin. The C-C coupling is the rate-determining step for hydrobenzoin formation.

In **Chapter 3**, we investigated the mechanism for benzaldehyde ECH under a totally different solution environment (the alkaline media). Compared with the mechanism in acidic media (illustrated in **Chapter 2**), the benzaldehyde ECH mechanism in alkaline media changed significantly in terms of the H addition mechanism, the reaction pathway, and the rate determining step for hydrobenzoin formation. In detail, in alkaline media, a water molecule is the proton donor and joins in the H addition step; the rate-determining for hydrobenzoin formation turns to the first H addition (for hydroxy intermediate formation). These conclusions were supported by various kinetic measurements (e.g., zero-order for hydrobenzoin formation, strong kinetic isotope effect for both benzyl alcohol and hydrobenzoin formation during H_2O/D_2O experiment and the first-principle periodic DFT molecular simulations). We also found that electrolyte pH and concentration of Na^+ cations notably affect the activity of benzaldehyde ECH on Cu/C. Increasing electrolyte pH indirectly enhances the hydrogenation rates by increasing the near-surface Na^+ concentration, which in turn increase the product formation rates by favoring the dissociation of H_2O.

In **Chapter 4**, we investigated the ECH of various aliphatic, cyclic, and aromatic aldehydes on several base (Cu and Ni) and noble metal (Pt, Pd, Ru, and Rh) catalysts in aqueous acidic media. We show that Cu uniquely catalyzes C–C coupling during the ECH of aldehydes. We also show that C–C coupling on Cu was only observed during the ECH of conjugated aromatic aldehydes like benzaldehyde, and furfural. Conversely, C–C coupling was not observed during the ECH of aliphatic aldehydes like butanal or ECH of non-conjugated cyclic aldehydes like cyclohexanal. We ruled the mechanistic requirements that facilitate the C–C coupling on Cu by conducting kinetic measurements and calorimetry measurements for aqueous-phase heat of the adsorption of the organic substrates and the first-principle periodic DFT molecular simulations. We found that the conjugated aldehydes like benzaldehyde and furfural are planar and adsorb strongly on the surface of Cu (evidenced by their high heat of adsorption). The strong binding of the aromatic aldehyde with Cu and the conjugated carbonyl group facilitate C-C coupling. Furthermore, the flat orientation allows (sterically) an ER-type attack by the physisorbed

aldehyde molecule. Conversely, weak adsorption of non-conjugated aldehydes, preferential first H addition to the carbonyl C, or a fast second H addition inhibits C-C coupling.

In **Chapter 5**, we introduced co-catalyst MoS_2 to Cu/C catalyst. We found that MoS_2 has higher H adsorption ability and hydrogen evolution activity compared with Cu/C by comparing LSV curves between MoS_2 and Cu/C electrode. We also found that MoS_2 can significantly increase benzyl alcohol selectivity on Cu/C+MoS_2 electrodes during benzaldehyde ECH in acidic media but oppositely increase C-C coupling selectivity on Cu/C+MoS_2 electrodes in alkaline media. By analyzing the mechanism for benzaldehyde ECH on Cu in acidic media (**Chapter 2**) and in alkaline media (**Chapter 3**), we illustrated that MoS_2 with high H adsorption ability can accelerate the second H addition step for benzyl alcohol formation, thus increasing hydrogenation of the hydroxyl intermediate to alcohol product on Cu in acidic media. However, MoS_2 can accelerate the first H addition step (rate-determining step for hydrobenzoin in alkaline media) during hydroxyl intermediate formation in alkaline media. The accumulated hydroxyl intermediate is more likely to follow the lower energy barrier pathway toward C-C bond formation. Thus MoS_2 increase C-C coupling selectivity on Cu/C+MoS_2 electrodes in alkaline media.

At the end, summary, conclusions and outlook are provided in **Chapter 6**.

1.8 References

1. Stern, David I., et al. "The role of energy in the industrial revolution and modern economic growth." The Energy Journal 33.3 (2012): 125-152.
2. Strielkowski, Wadim, et al. "Renewable energy in the sustainable development of electrical power sector: A review." Energies 14.24 (2021): 8240.
3. Rafiee, Ahmad, et al. "Trends in CO_2 conversion and utilization: A review from process systems perspective." Journal of environmental chemical engineering 6.5 (2018): 5771-5794.
4. Jamil, Khalid, et al. "Do remittance and renewable energy affect CO_2 emissions? An empirical evidence from selected G-20 countries." Energy & Environment 33.5 (2022): 916-932.

5. Ellabban, Omar., et al. "Renewable energy resources: Current status, future prospects and their enabling technology." Renewable and sustainable energy reviews 39 (2014): 748-764.
6. Rahman, Abidur., et al. "Environmental impact of renewable energy source based electrical power plants: Solar, wind, hydroelectric, biomass, geothermal, tidal, ocean, and osmotic." Renewable and Sustainable Energy Reviews 161 (2022): 112279.
7. Amponsah, Nana Yaw, et al. "Greenhouse gas emissions from renewable energy sources: A review of lifecycle considerations." Renewable and Sustainable Energy Reviews 39 (2014): 461-475.
8. Ma, Xavier. "Financing Modeling of Renewable Energy."
9. Saxena, R. C., et al. "Biomass-based energy fuel through biochemical routes: A review." Renewable and sustainable energy reviews 13.1 (2009): 167-178.
10. Bazmi, Aqeel Ahmed., et al. "Progress and challenges in utilization of palm oil biomass as fuel for decentralized electricity generation." Renewable and sustainable energy reviews 15.1 (2011): 574-583.
11. Sims, Ralph EH, et al. "An overview of second generation biofuel technologies." Bioresource technology 101.6 (2010): 1570-1580.
12. Haase, Martina, et al. "Prospective assessment of energy technologies: a comprehensive approach for sustainability assessment." Energy, Sustainability and Society 12.1 (2022): 1-41.
13. Robinson, Allison M., et al. "Bifunctional catalysts for upgrading of biomass-derived oxygenates: a review." ACS catalysis 6.8 (2016): 5026-5043.
14. Vamvuka, D. "Bio-oil, solid and gaseous biofuels from biomass pyrolysis processes—an overview." International journal of energy research 35.10 (2011): 835-862.
15. Oh, You-Kwan, et al. "Recent developments and key barriers to advanced biofuels: A short review." Bioresource Technology 257 (2018): 320-333.
16. Davaritouchaee, Maryam, et al. "Effect of reactive oxygen species on biomass structure in different oxidative processes." Industrial crops and products 137 (2019): 484-494.
17. Zhang, L., et al. "Overview of recent advances in thermo-chemical conversion of biomass." Energy conversion and management 51.5 (2010): 969-982.

18. Ma, Longlong, et al. "A review of thermal–chemical conversion of lignocellulosic biomass in China." Biotechnology Advances 30.4 (2012): 859-873.
19. Lewandowski, W. M., et al. "Thermal biomass conversion: A review." Processes 8.5 (2020): 516.
20. Akhade, Sneha A., et al. "Electrocatalytic hydrogenation of biomass-derived organics: a review." Chemical Reviews 120.20 (2020): 11370-11419.
21. Yang, Ming, et al. "Recent Progress on Electrocatalytic Valorization of Biomass-Derived Organics." Energy & Environmental Materials 5.4 (2022): 1117-1138.
22. Zhang, Lijuan, et al. "A review of thermal catalytic and electrochemical hydrogenation approaches for converting biomass-derived compounds to high-value chemicals and fuels." Fuel Processing Technology 226 (2022): 107097.
23. Bridgwater, Anthony V. "Renewable fuels and chemicals by thermal processing of biomass." Chemical Engineering Journal 91.2-3 (2003): 87-102.
24. Khodaei, Hassan, et al. "An overview of processes and considerations in the modelling of fixed-bed biomass combustion." Energy 88 (2015): 946-972.
25. Jenkins, Robert G. "Thermal gasification of biomass—a primer." Bioenergy. Academic Press, 2020.
26. Chhiti, Younes, and Mohammed Kemiha. "Thermal conversion of biomass, pyrolysis and gasification." International Journal of Engineering and Science (IJES) 2.3 (2013): 75-85.
27. Ling, Jester Lih Jie, et al. "A comparative review on advanced biomass oxygen fuel combustion technologies for carbon capture and storage." Energy (2023): 128566.
28. Demirbas, A. (2007). “Combustion of biomass. Energy sources, Part A: Recovery, utilization, and environmental effects.” 29(6), 549-561.
29. Gupta, A. K., and W. Cichonski. "Ultra-high temperature steam gasification of biomass and solid wastes." Environmental Engineering Science 24.8 (2007): 1179-1189.
30. Luo, Zhongyang, and Jinsong Zhou. "Thermal conversion of biomass." Handbook of Climate Change Mitigation and Adaptation. Cham: Springer International Publishing, 2022. 965-1021.
31. Zhao, Bin, et al. "Effect of pyrolysis temperature, heating rate, and residence time on rapeseed stem derived biochar." Journal of Cleaner Production 174 (2018): 977-987.

32. Liu, Tengyi, and Hiroshi Yabu. "Biomass-Derived Electrocatalysts: Low-Cost, Robust Materials for Sustainable Electrochemical Energy Conversion." Advanced Energy and Sustainability Research 5.1 (2024): 2300168.
33. Du, Lei, et al. "Electrocatalytic valorisation of biomass derived chemicals." Catalysis Science & Technology 8.13 (2018): 3216-3232.
34. Ochedi, Friday O., et al. "Photocatalytic, electrocatalytic and photoelectrocatalytic conversion of carbon dioxide: a review." Environmental Chemistry Letters 19 (2021): 941-967.
35. Wang, Hong, et al. "Phenolic wastewater treatment by an electrocatalytic membrane reactor." Catalysis Today 236 (2014): 121-126.
36. Neophytides, S. G., et al. "Electrochemical enhancement of a catalytic reaction in aqueous solution." Nature 370.6484 (1994): 45-47.
37. Poizot, Philippe, and Franck Dolhem. "Clean energy new deal for a sustainable world: from non-CO_2 generating energy sources to greener electrochemical storage devices." Energy & Environmental Science 4.6 (2011): 2003-2019.
38. Mehnert, Christian P., et al. "Supported ionic liquid catalysis investigated for hydrogenation reactions." Chemical Communications 24 (2002): 3010-3011.
39. Zhong, George., et al. "Hydrogenation of simple aromatic molecules: a computational study of the mechanism." Journal of the American Chemical Society 129.4 (2007): 924-933.
40. Kuß, David A., et al. "Combined Computational and Experimental Investigation on the Mechanism of CO_2 Hydrogenation to Methanol with Mn-PNP-Pincer Catalysts." ACS Catalysis 12.24 (2022): 15310-15322.
41. Liu, Cuibo, et al. "Designed Nanomaterials for Electrocatalytic Organic Hydrogenation Using Water as the Hydrogen Source." Accounts of Chemical Research (2023): 21170-21175.
42. Gianolio, Diego, et al. "Interfacial chemistry in the electrocatalytic hydrogenation of CO2 over C-Supported Cu-Based systems." ACS catalysis 13.9 (2023): 5876-5895.

43. Sanyal, Udishnu, et al. "Simultaneous electrocatalytic hydrogenation of aldehydes and phenol over carbon-supported metals." Journal of Applied Electrochemistry 51 (2021): 27-36.
44. Xue, Yinghao, et al. "Electrocatalytic hydrogenation boosts reduction of nitrate to ammonia over single-atom Cu with Cu (I)-N_3C_1 sites." Environmental Science & Technology 56.20 (2022): 14797-14807.
45. Han, Chenhui, et al. "Electrocatalytic hydrogenation of alkenes with Pd/carbon nanotubes at an oil–water interface." Nature Catalysis 5.12 (2022): 1110-1119.
46. Singh, Nirala, et al. "Electrocatalytic hydrogenation of phenol over platinum and rhodium: unexpected temperature effects resolved." Acs Catalysis 6.11 (2016): 7466-7470.
47. Zheng, Min, et al. "Recent Advances in Electrocatalytic Hydrogenation Reactions on Copper-Based Catalysts." Advanced Materials (2024): 2307913.
48. Santana, Diogo S., et al. "Electrocatalytic hydrogenation of organic compounds using a nickel sacrificial anode." Journal of Electroanalytical Chemistry 569.1 (2004): 71-78.
49. Anibal, Jacob, and Bingjun Xu. "Electroreductive C–C coupling of furfural and benzaldehyde on Cu and Pb surfaces." ACS Catalysis 10.19 (2020): 11643-11653.
50. Song, Xianmeng, et al. "Boosting CO_2 electrocatalytic reduction to ethylene via hydrogen-assisted C–C coupling on Cu_2O catalysts modified with Pd nanoparticles." Nano Energy 122 (2024): 109275.
51. Negishi, E-I. Huang Z. "Wang G. Mohan S. Wang C. Hattori H." Acc. Chem. Res 41 (2008): 1474-1485.
52. Suzuki, Akira. "The Suzuki reaction with arylboron compounds in arene chemistry." Modern Arene Chemistry (2002): 53-106.
53. Heck, Richard F. "Palladium reagents in organic syntheses." (No Title) (1985).
54. Yang, Fa, et al. "Bismuthene for highly efficient carbon dioxide electroreduction reaction." Nature communications 11.1 (2020): 1088.
55. Tan, Xinyi, et al. "Recent advances in innovative strategies for the CO_2 electroreduction reaction." Energy & Environmental Science 14.2 (2021): 765-780.
56. Lu, Qi, et al. "A selective and efficient electrocatalyst for carbon dioxide reduction." Nature communications 5.1 (2014): 3242.

57. Nguyen, Tu N., and Cao-Thang Dinh. "Gas diffusion electrode design for electrochemical carbon dioxide reduction." Chemical Society Reviews 49.21 (2020): 7488-7504.
58. Huang, Yun., et al. "Effects of electrolyte anions on the reduction of carbon dioxide to ethylene and ethanol on copper (100) and (111) surfaces." ChemSusChem 11.18 (2018): 3299-3306.
59. Wang, Yuhang., et al. "Designing copper-based catalysts for efficient carbon dioxide electroreduction." Advanced Materials 33.46 (2021): 2005798.
60. Zhu, Qinggong, et al. "Carbon dioxide electroreduction to C_2 products over copper-cuprous oxide derived from electrosynthesized copper complex." Nature communications 10.1 (2019): 3851.
61. Birhanu, Mulatu Kassie, et al. "Copper and copper-based bimetallic catalysts for carbon dioxide electroreduction." Advanced Materials Interfaces 5.24 (2018): 1800919.
62. Liu, Cong, et al. "Catalytic upgrading of biomass-derived compounds via C–C coupling reactions: Computational and experimental studies of acetaldehyde and furan reactions in HZSM-5." The Journal of Physical Chemistry C 119.42 (2015): 24025-24035.
63. Yu, Jia, et al. "Electroreductive coupling of benzaldehyde by balancing the formation and dimerization of the ketyl intermediate." Nature Communications 13.1 (2022): 7909.
64. Chadderdon, Xiaotong H., et al. "Mechanisms of furfural reduction on metal electrodes: Distinguishing pathways for selective hydrogenation of bioderived oxygenates." Journal of the American Chemical Society 139.40 (2017): 14120-14128.
65. Wang, Lu-Jun, et al. "Electroreductive cross-coupling between aldehydes and ketones or imines via cathodically generated dianions." Green Chemistry 24.21 (2022): 8386-8392.
66. Villalobos, Janette M., et al. "A new paradigm for carbon− carbon bond formation: aerobic, copper-templated cross-coupling." Journal of the American Chemical Society 129.51 (2007): 15734-15735.
67. Cuesta, Angel, et al. "Mechanism of the electrocatalytic oxidation of formic acid on metals." ACS Catalysis 2.5 (2012): 728-738.
68. Mostaghimi, Amir Hassan Bagherzadeh, et al. "A review on electrocatalytic oxidation of methane to oxygenates." Journal of Materials Chemistry A 8.31 (2020): 15575-15590.

69. Zhou, Hua, et al. "Electrocatalytic oxidative upgrading of biomass platform chemicals: from the aspect of reaction mechanism." Chemical Communications 58.7 (2022): 897-907.
70. Ding, Hui, et al. "Structural transformation of heterogeneous materials for electrocatalytic oxygen evolution reaction." Chemical Reviews 121.21 (2021): 13174-13212.
71. Zhuo, Qiongfang, et al. "Electrocatalytic Oxidation Processes for Treatment of Halogenated Organic Pollutants in Aqueous Solution: A Critical Review." ACS ES&T Engineering 2.10 (2022): 1756-1775.
72. Sirés, Ignasi, et al. "Electrochemical advanced oxidation processes: today and tomorrow. A review." Environmental Science and Pollution Research 21 (2014): 8336-8367.
73. Wu, Yi, et al. "High-efficiency electrochemical hydrogenation of biomass-derived benzaldehyde compounds via a durable and versatile dendritic-like Pd/Cu-CF electrocatalyst." Fuel Processing Technology 237 (2022): 107436.
74. Gong, Li, et al. "Semiconductor nanosheets for electrocatalytic self-coupling of benzaldehyde to hydrobenzoin." Chemical Engineering Journal 479 (2024): 147612.
75. Song, Yang, et al. "Hydrogenation of benzaldehyde via electrocatalysis and thermal catalysis on carbon-supported metals." Journal of Catalysis 359 (2018): 68-75.
76. Singh, Nirala, et al. "Aqueous phase catalytic and electrocatalytic hydrogenation of phenol and benzaldehyde over platinum group metals." Journal of Catalysis 382 (2020): 372-384.
77. Cheng, Guanhua, et al. "Critical role of solvent-modulated hydrogen-binding strength in the catalytic hydrogenation of benzaldehyde on palladium." Nature Catalysis 4.11 (2021): 976-985.
78. Saadi, A., Z. Rassoul, and M. M. Bettahar. "Gas phase hydrogenation of benzaldehyde over supported copper catalysts." Journal of Molecular Catalysis A: Chemical 164.1-2 (2000): 205-216.
79. Yuk, Simuck F., et al. "First-principle investigation on catalytic hydrogenation of benzaldehyde over Pt-group metals." Catalysis Today 388 (2022): 208-215.
80. Lopez-Ruiz, Juan A., et al. "Kinetic investigation of the sustainable electrocatalytic hydrogenation of benzaldehyde on Pd/C: effect of electrolyte composition and half-cell potentials." ACS Sustainable Chemistry & Engineering 6.12 (2018): 16073-16085.

81. Oh, Hyung-Suk, et al. "Electrochemical catalyst–support effects and their stabilizing role for IrO_x nanoparticle catalysts during the oxygen evolution reaction." Journal of the American Chemical Society 138.38 (2016): 12552-12563.
82. Rao, Radhika G., et al. "Interfacial charge distributions in carbon-supported palladium catalysts." Nature communications 8.1 (2017): 340.
83. Koh, Katherine, et al. "Electrochemically tunable proton-coupled electron transfer in Pd-catalyzed benzaldehyde hydrogenation." Angewandte Chemie 132.4 (2020): 1517-1521.
84. Gong, Li, et al. "Enhanced electrochemical hydrogenation of benzaldehyde to benzyl alcohol on Pd@ Ni-MOF by modifying the adsorption configuration." ACS Applied Materials & Interfaces (2024).
85. Anibal, Jacob, Arnav Malkani, and Bingjun Xu. "Stability of the ketyl radical as a descriptor in the electrochemical coupling of benzaldehyde." Catalysis Science & Technology 10.10 (2020): 3181-3194.
86. Murzin, Dmitry Yu. "Solvent effects in catalysis: implementation for modelling of kinetics." Catalysis Science & Technology 6.14 (2016): 5700-5713.
87. Li, Yan, et al. "Solvent effects on heterogeneous catalysis in the selective hydrogenation of cinnamaldehyde over a conventional Pd/C catalyst." Catalysis Science & Technology 8.14 (2018): 3580-3589.
88. Yoshida, Hiroshi, et al. "Solvent effects in heterogeneous selective hydrogenation of acetophenone: differences between Rh/C and Rh/Al_2O_3 catalysts and the superiority of water as a functional solvent." Green Chemistry 17.3 (2015): 1877-1883.
89. Klaewkla, Raweewan, Matthias Arend, and Wolfgang F. Hoelderich. A review of mass transfer controlling the reaction rate in heterogeneous catalytic systems. Vol. 5. Rijeka: INTECH Open Access Publisher, 2011.
90. Sun, Qi, et al. "Creating solvation environments in heterogeneous catalysts for efficient biomass conversion." Nature Communications 9.1 (2018): 3236.
91. Li, Hu, and Richard L. Smith Jr. "Solvents take control." Nature Catalysis 1.3 (2018): 176-177.
92. Singh, Nirala, et al. "Impact of pH on aqueous-phase phenol hydrogenation catalyzed by carbon-supported Pt and Rh." ACS Catalysis 9.2 (2018): 1120-1128.

93. Hu, Fei, et al. "Amorphous metallic NiFeP: a conductive bulk material achieving high activity for oxygen evolution reaction in both alkaline and acidic media." Advanced Materials 29.32 (2017): 1606570.
94. Zhao, Yige, et al. "Sulfur vacancy-promoted highly selective electrosynthesis of functionalized aminoarenes via transfer hydrogenation of nitroarenes with H2O over a Co3S4− x nanosheet cathode." CCS Chemistry 3.1 (2021): 507-515.
95. Xia, Rong, et al. "Electrochemical reduction of acetonitrile to ethylamine." Nature Communications 12.1 (2021): 1-8.
96. Chong, Xiaodan, et al. "Potential-tuned selective electrosynthesis of azoxy-, azo-and amino-aromatics over a CoP nanosheet cathode." National science review 7.2 (2020): 285-295.
97. Zhou, Ling, et al. "pH-Induced selective electrocatalytic hydrogenation of furfural on Cu electrodes." Chinese Journal of Catalysis 43.12 (2022): 3142-3153.

Chapter 2

Mechanism of electrocatalytic H_2 evolution, carbonyl hydrogenation and carbon – carbon coupling on Cu

Aqueous-phase electrocatalytic hydrogenation of benzaldehyde on Cu leads not only to benzyl alcohol (the carbonyl hydrogenation product), but Cu also catalyzes carbon-carbon coupling to hydrobenzoin. The catalyst surface is primarily covered with the organic substrate; H* coverage is low. Mechanistically, the first H addition to the carbonyl O of an adsorbed benzaldehyde molecule leads to a surface-bound hydroxy intermediate. The hydroxy intermediate then undergoes a second and rate-determining H addition to its α-C to form benzyl alcohol. The H additions occur predominantly via the proton-coupled electron transfer mechanism. In a parallel reaction, the radical α-C of the hydroxy intermediate attacks the electrophilic carbonyl C of a physisorbed benzaldehyde molecule to form the C-C bond, which is rate-determining. The C-C coupling is accompanied by the protonation of the formed alkoxy radical intermediate, coupled with electron transfer from the surface of Cu, to form hydrobenzoin.

This chapter is based on the article: Hongwen Chen et al. Mechanism of electrocatalytic H_2 evolution, carbonyl hydrogenation and carbon – carbon coupling on Cu (***Journal of the American Chemical Society***, 2024, 146, 20, 13949–13961). Hongwen Chen performed the experiments, did the data analysis and wrote the manuscript.

2.1 Introduction

Upgrading lignocellulosic biomass to value-added chemicals is an emergent technology that will contribute to replace crude-oil as a carbon source for energy carriers and fine chemicals.[1-4] Upgrading biomass typically involves reduction of biomass-derived oxygenated compounds[5,6] (to increase their stability) and C–C coupling[7,8] (to increase the molecular weight). Aqueous phase electrochemical reduction, i.e., hydrogenation (ECH) of biomass-derived oxygenates, such as alcohols, phenols, aldehydes, ketones, and carboxylic acids, is one of the promising strategies.[9-11] ECH has been shown to successfully reduce the aromatic rings in aromatics,[12,13] carbonyl groups in aldehydes and ketones,[14-16] as well as C=C double bonds in unsaturated carboxylic acids.[17,18] ECH, in addition to reduction, has also been shown to catalyze C–C bond formation in benzaldehyde and furfural derivates.[19,20]

The upgrading of biomass to liquid biofuels via thermo-catalytic hydrogenation (TCH) requires elevated H_2 pressure and high temperatures.[21,22] ECH, on the other hand, generates hydrogen in situ from an aqueous electrolyte under an external electric potential, which typically leads to high equilibrium pressures. Rather than forming H_2, the formed surface hydrogen atoms (H*) can also react with (the biomass-derived) organic substrates under mild reaction conditions. ECH, therefore, has several advantages including lower operating temperatures, no requirement of external H_2 supply, and easy integration with renewable power harvesting.[23,24]

The carbonyl functional groups that are abundantly present in bio-oils, predominantly as aromatic aldehydes and ketones, are prone to polymerization. The reduction of these carbonyl groups is therefore required to increase the stability of bio-oils. Benzaldehyde, the simplest aromatic aldehyde, is an ideal model compound to investigate low-temperature electroreduction of carbonyl groups present in the bio-oils. Furthermore, benzaldehyde and furfural derivatives, following electroreductive C–C coupling, have been suggested as potential source of high-quality fuels and value-added chemicals.[25-27]

Benzaldehyde hydrogenation, both thermochemical and electrochemical, has been investigated in detail on noble metals (e.g., Pt, Pd, Ru, and Rh) as well as base metals (e.g., Cu, Ni, and Pb).[19,28-32] **Scheme 2-1** shows the two possible products resulting from H addition and

C–C coupling, viz., benzyl alcohol and hydrobenzoin. Although several studies have investigated in detail benzyl alcohol formation, limited effort has been devoted to understand electrochemical C–C coupling to produce hydrobenzoin. A primary reason for this is that hydrobenzoin has been observed as a product only on a few catalysts.[20,33,34]

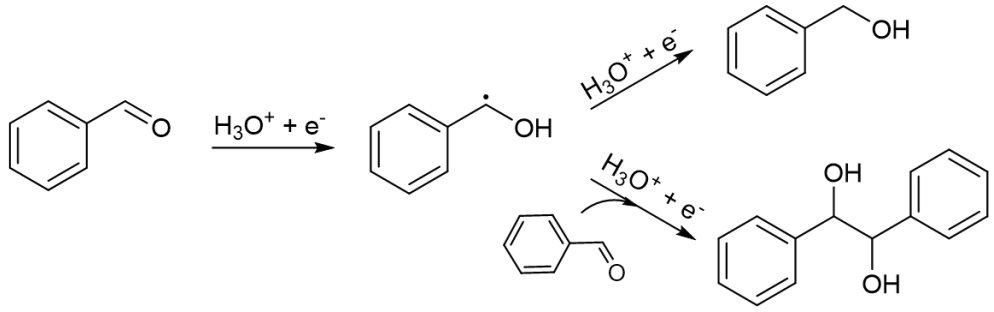

Scheme 2-1. Hydrogenation of benzaldehyde to benzyl alcohol and hydrobenzoin.

ECH of benzaldehyde to benzyl aclohol (and to hydrobenzoin when coupled with C–C bond formation) requires two successive H addition steps. The H addition has been proposed to proceed via two distinct mechanisms: (i) direct hydrogenation of adsorbed organic substrate by a surface hydride species (typically proceeding via Langmuir-Hinshelwood (LH) kinetics and often referred to as the LH mechanism),[30] or (ii) proton-coupled electron-transfer (PCET) mechanism.[28,35] Koh et al. proposed PCET mechanism for benzaldehyde hydrogenation on Pd.[35] Singh et al., on the other hand, investigated aqueous phase hydrogenation of benzaldehyde on Pt group metals and proposed a LH mechanism for H addition.[29]

The effects of solvents and co-reactants on benzaldehyde hydrogenation have also been investigated. For example, Sanyal et al. showed that the presence of polar co-adsorbates such as phenol enhance the rate of benzaldehyde ECH on carbon-supported metals via hydrogen bonding.[36] More recently, Cheng et al. investigated the role of solvents in catalytic hydrogenation of benzaldehyde and showed that solvents affect the binding strength of adsorbed H, resulting in different hydrogenation rates.[37] Overall, the kinetics and mechanism of benzaldehyde ECH to benzyl alcohol have been extensively investigated, both experimentally and computationally.[30,38-40]

In comparison, the reaction path for the reductive electrocatalytic conversion of benzaldehyde to hydrobenzoin were only speculatively addressed. It has been proposed that C–

C coupling occurs primarily via the LH mechanism involving the reaction of two surface ketyl radicals.[19,20] The ability of a catalyst to form and stabilize the ketyl intermediate has been proposed as a key descriptor of its ability to promote C–C coupling.[33] Interestingly. Evidence for ketyl radicals was observed on Cu, which promotes C–C coupling, but not on Pd or Pt.[33]

With the goal of understanding these mechanistic pathways, we report here a detailed kinetic and mechanistic study of ECH of benzaldehyde to both benzyl alcohol and hydrobenzoin on Cu/C. Using isotope labelling studies, we show that the rate-determining step for benzyl alcohol formation is the second H addition, while that for hydrobenzoin formation is the C–C coupling. Combining experimental evidence with theoretical simulations using periodic density functional theory (DFT), we postulate the possible reaction pathways for hydrobenzoin, benzyl alcohol, and H_2 formation during benzaldehyde ECH on Cu/C.

2.2 Materials and methods

2.2.1 Chemicals

Benzaldehyde (99.5%), benzyl alcohol (99.8%), hydrobenzoin (99.0%), copper (II) acetate (99.9%), palladium (II) acetate (99.9%), acetic acid (99.8%), sodium acetate (99.0%), 2-propanol (99.5%), acetone (99.9%), diphenyl ether (99.0%), ethyl acetate (99.5%), *t*-butanol (99.5%), 2-mercaptobenzothiazole (97%) and D_2O (99.9 atom% D) were purchased from Sigma-Aldrich and used without further purification. Deionized (DI) water (18.2 $M\Omega \cdot cm^{-1}$) was used to prepare all aqueous solutions.

2.2.2 Catalyst synthesis

Cu/C (~5 wt.-% metal loading) was prepared *via* incipient-wetness impregnation method. An aqueous solution of copper (II) acetate was added dropwise to a Vulcan® XC72R carbon black (QUINTECH) support, mixed thoroughly, and dried overnight at 333 K. The resulting dried material was first treated in 100 $mL \cdot min^{-1}$ N_2 at 673 K (temperature ramp: 10 $K \cdot min^{-1}$) for 4 h, followed by reduction in 100 $mL \cdot min^{-1}$ H_2 at 623 K (temperature ramp: 10 $K \cdot min^{-1}$) for 4 h. These reduced catalysts are referred to as Cu/C. For the preparation of ozone-treated Cu/C catalyst, the carbon black support was first treated in O_3 at room temperature for 2 – 4 h, followed by deposition of Cu *via* the incipient-wetness impregnation method described above.

These O_3-treated catalysts are referred to as Cu/C/O_3-2h and Cu/C/O_3-4h, respectively.

The Pd/C (~5 wt.-% metal loading) catalyst was also prepared *via* incipient-wetness impregnation method described above using palladium (II) acetate as the metal precursor. The prepared Pd/C catalyst was first treated in 100 mL·min^{-1} N_2 at 453 K (temperature ramp: 5 K·min^{-1}) for 2 h, followed by reduction in 100 mL·min^{-1} H_2 at 523 K (temperature ramp: 5 K·min^{-1}) for 2 h.

2.2.3 Carbon felt pretreatment

Carbon felt (Sigma-Aldrich, 3.0 cm × 1.5 cm) was immersed sequentially in acetone, DI water, and acetone again for at least 30 min each under ultrasonication treatment at ambient temperature. Finally, the treated carbon felt was dried in an oven at 333 K for 12 h.

2.2.4 Electrode preparation

The synthesized Cu/C (~10 mg) was dispersed in a 1:1 solution of 1 mL 2-propanol and 1 mL DI water for 30 min under ultrasonication treatment at room temperature. The catalyst ink was then deposited on both sides of the pretreated carbon felt. The carbon felt electrode (containing Cu/C catalyst) was finally dried overnight in an oven at 333 K.

2.2.5 Nafion membrane pretreatment

The Nafion-117 proton exchange membrane (Ion Power) was first immersed in a 3% H_2O_2 solution for 1 h at 353 K. The Nafion membrane was then immersed in DI water at 353 K for 2 h. Subsequently, the membrane was immersed in 1 mol·L^{-1} H_2SO_4 at 353 K for 1 h. Finally, the Nafion membrane was washed several times with DI water and stored in DI water under ambient conditions.

2.2.6 Electrochemical measurements

All electrochemical experiments were performed using a BioLogic VSP-300 workstation using a two-compartment batch electrolysis cell (Supplementary **Figure S2-1**). Cu/C deposited on a carbon felt was used as the working electrode. A double-junction Ag/AgCl (eDAQ) and a Pt wire (Sigma-Aldrich) were used as the reference electrode and counter electrode, respectively. The anode and cathode compartments were separated by the pretreated Nafion

membrane. The reference Ag/AgCl electrode was calibrated against a reversible hydrogen electrode (RHE), and all the potentials herein are reported relative to the RHE, per the following equation.

$$E_{RHE} = E_{Ag/AgCl} + 0.197 + 0.0591 \cdot pH \quad (2\text{-}1)$$

where E_{RHE} and $E_{Ag/AgCl}$ are electrode potentials relative to RHE and Ag/AgCl electrode potentials, respectively.

All electrochemical experiments were performed under ambient conditions. N_2 gas (~25 $mL \cdot min^{-1}$) was continuously bubbled through the electrolyte solution throughout the reaction to remove any dissolved gases. A stirring rate of 500 rpm allowed complete dissolution of organic in the electrolyte solution and overcame the mass transfer limitations (**Figure S2-2**). The solution resistance between working and reference electrodes was measured by potentiostatic electrochemical impedance spectroscopy (PEIS) and compensated (~85%) by the electrochemical workstation. Prior to the reaction, the catalyst was polarized at –40 mA for ~20 min to ensure complete reduction of the metal.

The potentiodynamic linear sweep voltammetry (LSV) measurements were performed in either pure electrolyte solution or 20 mM benzaldehyde solution at a scan rate of 1 $mV \cdot s^{-1}$.

2.2.7 Product analysis

The course of the ECH experiments was followed by periodically withdrawing aliquots of ~1 mL from the cathode compartment. The products in the aqueous electrolyte solution were extracted with ~0.5 ml ethyl acetate. The extract was then analyzed by an offline gas chromatograph coupled with a mass spectrometer (Agilent 7890B GC/5977A MSD). The carbon balance between the reactants converted and formed products was >95% in all cases.

The initial rate towards a product i (in terms of H consumed per gram metal) was calculated from the product i formed vs. reaction time plots using the following equation.

$$r_i = \frac{m_i \times \epsilon_i}{w_{cat} \times x_{metal}} \quad (2\text{-}2)$$

where m_i is the initial slope, w_{cat} is the amount of catalyst, x_{metal} is the metal loading on the catalyst (as weight fraction), and ϵ_i is the number of H atoms required to form the product i. The initial slope corresponds to the linear region of product i formed vs. reaction time plot

(typically 0 – 20 min).

The electron consumption towards H_2 formation was indirectly estimated from the difference in the total electron consumption and the H (and the corresponding electron) consumption towards the formation of other products. The amount of H_2 formed (n_{H_2}) in mol was then calculated using the following equation.

$$n_{H_2} = \frac{q_{H_2}}{2 \cdot F} \tag{2-3}$$

where q_{H_2} is the electron consumption towards H_2 formation, and F is the Faraday's constant. An exemplary plot is shown in Supplementary **Figure S2-3**. Additional calculation details are described in Supplementary Information **Section S2-3**.

2.2.8 Computational methods

All quantum chemical calculations were performed on a periodic electrode-electrolyte interface model using the Vienna ab initio simulation package (VASP) with a plane wave basis set.[41-44] The simulation were performed on a 4 × 4 × 4 supercell of Cu(111) surface, cleaved from bulk Cu with lattice constant of 3.59 Å, and a vacuum of at least 10 Å above the water layer. Implicit solvation model with additional explicit water molecules was used in all simulations. Detailed computational details are provided in the Supplementary Information **Section S2-4**.

2.3 Results and discussion

Cu/C catalyst (~5 wt.-% metal loading) was synthesized via incipient-wetness impregnation method using copper (II) acetate as the Cu source and Vulcan carbon black as the support. The specific surface area of the catalyst was estimated to be ~223 $m^2 \cdot g_{cat}^{-1}$ from N_2 adsorption-desorption measurements (Supplementary **Figure S2-4**). The formation of metallic Cu nanoparticles in the Cu0 oxidation state was confirmed by X-ray absorption near edge structure (XANES) measurements (Supplementary **Figure S2-5a**). Furthermore, the extended X-ray absorption fine structure (EXAFS) analysis indicated a Cu–Cu coordination number of ~10 (Supplementary **Figure S2-5b** and **Table S2-1**), suggesting the formation of large Cu nanoparticles. The formation of large nanoparticles was also confirmed by transmission electron microscopy (TEM) images of the synthesized catalyst (Supplementary **Figure S2-6**). Lastly, X-

ray diffraction (XRD) measurements of Cu/C indicated Cu (111) to be the most abundant facet in the formed Cu nanoparticles (Supplementary **Figure S2-7**).

2.3.1 H_2 evolution reaction (HER) on Cu in the absence of benzaldehyde

We first investigated the H_2 evolution reaction (HER) on Cu/C in the absence of an organic substrate. **Figure 2-1** shows the H_2 yield (in mol H consumed per gram metal) as a function of reaction time at an applied external potential (η) of –0.5 V vs. RHE on Cu/C. The H_2 yield during HER on Pd/C at η = –0.2 V vs. RHE is also shown for comparison. The HER rate on Cu/C was estimated to be ~3.7 $mmol_H \cdot g_{Cu}^{-1} \cdot s^{-1}$, while the HER rate on Pd/C was ~1.9 $mmol_H \cdot g_{Pd}^{-1} \cdot s^{-1}$. Significantly higher overpotential required to achieve similar HER rates on Cu/C suggests a weaker hydrogenation ability of Cu, compared to Pd.

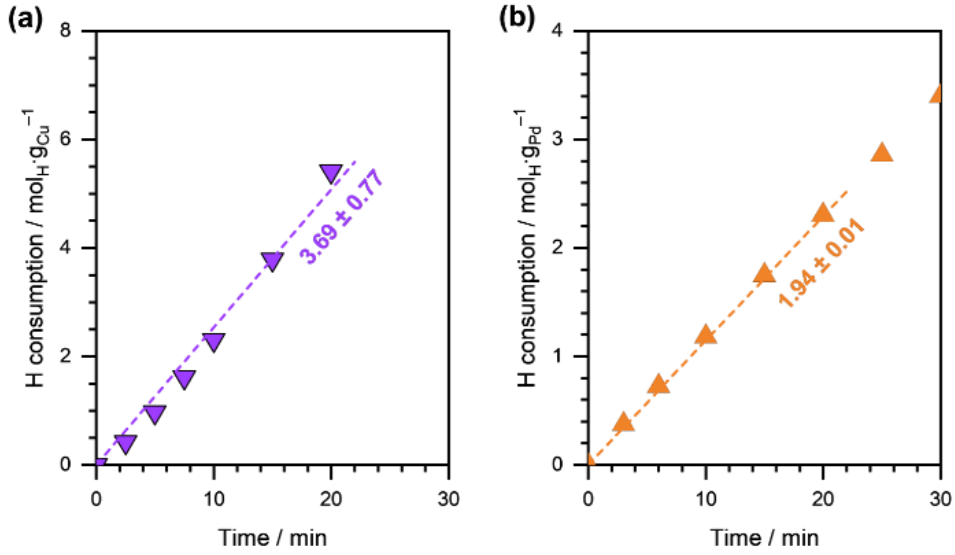

Figure 2-1. H_2 evolution as a function of reaction time during HER on (a) Cu/C, and (b) Pd/C. Reaction conditions: η = –0.5 V vs. RHE on Cu/C and η = –0.2 V vs. RHE on Pd/C, 1.5 M acetate buffer solution (pH ~4.6), room temperature, ambient pressure. The dashed lines are linear fits, and the reported numbers are initial HER rates in $mmol_H \cdot g_{metal}^{-1} \cdot s^{-1}$.

2.3.2 Mechanism of H_2 evolution on Cu in the absence of benzaldehyde

The H_2 evolution on metal electrodes has been described in terms of the Volmer-Heyrovsky-Tafel mechanism (illustrated in **Scheme 2-2**).[45] The Volmer step is a PCET step that involves the adsorption of a solvated proton (H_3O^+) on the surface of the electrode, coupled with simultaneous electron transfer from the surface, to form H*. The Heyrovsky step is an Eley-Rideal (ER)-type PCET step wherein the surface H* reacts with a solvated proton and an

electron to form H_2. The Tafel step, on the other hand, is an LH-type surface recombination of two H* to form H_2.

$$H_3O^+ + e^- + * \rightleftharpoons H^* + H_2O \quad \text{(Volmer)}$$

$$H_3O^+ + e^- + H^* \rightleftharpoons H_2 + H_2O + * \quad \text{(Heyrovsky)}$$

$$H^* + H^* \rightleftharpoons H_2 + 2^* \quad \text{(Tafel)}$$

Scheme 2-2. Volmer, Heyrovsky, and Tafel steps for HER on metal electrodes.

Both Volmer and Heyrovsky steps follow the PCET mechanism; therefore, their rates can be expressed as

$$r_{Volmer} = k_{Volmer} \cdot e^{-\alpha f \eta} \cdot \theta_* \cdot a_{H_3O^+} \tag{2-4}$$

$$r_{Heyrovsky} = k_{Heyrovsky} \cdot e^{-\alpha f \eta} \cdot \theta_H \cdot a_{H_3O^+} \tag{2-5}$$

where k_{Volmer} and $k_{Heyrovsky}$ are the respective kinetic rate constants, α is the electron transfer coefficient, f denotes F/RT (where F, R, and T denote the Faraday constant, the universal gas constant, and the temperature, respectively), θ_* and θ_H are the surface coverage of empty sites ($*$) and H*, respectively, and $a_{H_3O^+}$ is the concentration of hydronium ions (equal to their concentration under these conditions). In contrast, the rate of the LH-type Tafel step is expressed as

$$r_{Tafel} = k_{Tafel} \cdot \theta_H^2 \tag{2-6}$$

where k_{Tafel} is the kinetic rate constant of the Tafel step and θ_H is the surface coverage of H*.

To determine the kinetically rate-determining step (rds) for H_2 evolution on Cu, we estimated the Tafel slope of HER on Cu/C in the pure electrolyte solution. Theoretically (at T = 298 K and α = 0.5), the Tafel slope is equal to ~120 mV·dec^{-1} if the Volmer step is the rate-determining step.[45] On the other hand, if the rate-determining step is the Heyrovsky step or the Tafel step, the Tafel slope is equal to ~40 mV·dec^{-1} or ~30 mV dec^{-1}, respectively.[45,46] Furthermore, at high H* coverages (*i.e.*, $\theta_H \approx 1$), theoretically, the Tafel slope becomes equal to ~120 mV·dec^{-1} in the case of Heyrovsky step being rate-determining or equal to ∞ if the Tafel step is rate-determining.[45,46]

Figure 2-2a shows the linear sweep voltammetry (LSV) curve of HER on Cu/C. The corresponding Tafel curve is presented in **Figure 2-2b**. Based on the LSV curve, we estimated the onset potential of HER on Cu/C to be approximately equal to –0.41 V vs. RHE. Additionally, we note that at low overpotentials (*i.e.*, η > –0.4 V vs. RHE), the Tafel slope was equal to ~30 mV dec^{-1}, clearly suggesting that the Tafel step is the rate-determining step for H_2 evolution. In other words, the HER on Cu/C (in the absence of organic substrate) proceeds *via* the Volmer-Tafel(rds) pathways under the applied reaction conditions. We also note that the value of Tafel slope increased with increasing overpotential, reaching ~395 mV·dec^{-1} at η = –0.6 V vs. RHE. The value of Tafel slope was equal to ~250 mV·dec^{-1} at η = –0.5 V vs. RHE. These higher values of the Tafel slope indicate high surface coverage of H* at higher overpotentials.[45,46]

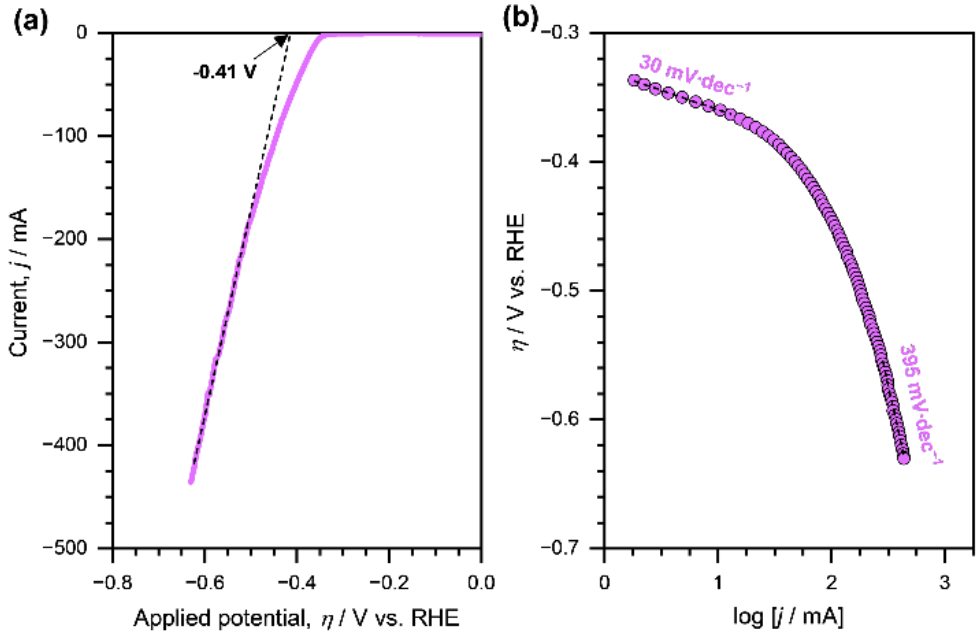

Figure 2-2. (a) Linear sweep voltammetry curve (scan rate = 1 mV·s^{-1}) of HER in pure electrolyte on Cu/C (b) Tafel curve of HER in pure electrolyte on Cu/C. The dashed lines are linear fits, and the reported numbers are Tafel slopes. Reaction conditions: η = –0.5 V vs. RHE, 1.5 M acetate buffer solution (pH ~4.6), room temperature, ambient pressure.

We also investigated the effect of hydronium ion concentration ($a_{H_3O^+}$) on HER by varying the pH of the electrolyte solution (shown in **Figure 2-3a**). We can clearly see that the HER rate showed almost no dependence on $a_{H_3O^+}$; *i.e.*, the reaction-order was approximately zero. Furthermore, we also performed HER on Cu/C catalysts with acid-functionalized support. Acid-functionalization of the support *via* O_3 treatment has been shown to increase $a_{H_3O^+}$ near the

surface of the electrode, thus enhancing the rates of elementary steps involving PCET.[35] **Figure 2-3b** shows the effect of O_3 treatment of the carbon support on the HER rates. Again, we can clearly see that the HER rates remained unchanged after O_3 treatment.

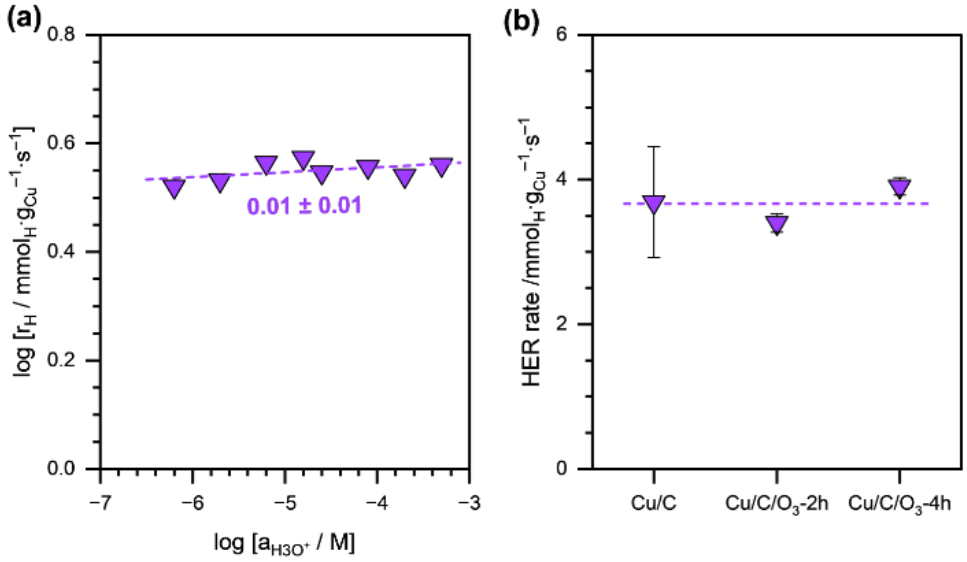

Figure 2-3. (a) HER rates as a function of $a_{H_3O^+}$ (pH 3.2 – 6.3) on Cu/C. The dashed line is a linear fit and the reported number is the calculated reaction order. (b) HER rates in pure electrolyte solution on Cu/C, Cu/C/O_3-2h, and Cu/C/O_3-4h catalysts at pH ~4.6. The dashed line is a guide to the eye. Reaction conditions: η = –0.5 V vs. RHE, 1.5 M acetate buffer solution (pH ~4.6), room temperature, ambient pressure.

From **Eq. 2-4** and **Eq. 2-5**, it can be deduced that r_{Volmer} and $r_{Heyrovsky}$ are dependent on η and $a_{H_3O^+}$. On the other hand, r_{Tafel} is independent of η or $a_{H_3O^+}$ (**Eq. 2-6**) at high H* coverages (*i.e.*, $\theta_H \approx 1$). It must however be noted that at low coverages of H* (*i.e.*, when $\theta_H \ll 1$), θ_H itself varies with η and $a_{H_3O^+}$ (due to its dependence on the reversible rate of the Volmer step). Therefore, r_{Tafel} indirectly depends on η and $a_{H_3O^+}$ when $\theta_H \ll 1$. The zero-order dependence of HER on $a_{H_3O^+}$ (**Figure 2-3a**), therefore, suggests high H* on the surface of Cu (*i.e.*, $\theta_H \approx 1$). The Volmer step, therefore, can be assumed to be equilibrated under these reaction conditions. Furthermore, the invariance of HER rates with $a_{H_3O^+}$ clearly suggests that the kinetically relevant step for H_2 evolution on Cu/C is not a PCET step. As both Volmer and Heyrovsky steps follow the PCET mechanism, we conclude that the rate-determining step for H_2 evolution on Cu/C, in the absence of an organic substrate, is the Tafel step and HER on Cu follows the Volmer-Tafel(rds) pathway. **Scheme 2-3** illustrates the

postulated mechanism for H_2 evolution on Cu/C in the absence of an organic substrate.

We must note here that, based on the obtained Tafel slopes, the rate-determining step for HER on Cu-based electrocatalysts has also been proposed to be the Volmer step or the Heyrovsky step under different reaction conditions. For example, Sharifi-Asl *et al.* suggested Volmer step to be the rate-determining step (Tafel slope = 87 – 120 mV·dec^{-1}) for HER on pure Cu electrodes.[47] The higher Tafel slope in their case is likely due to low $a_{H_3O^+}$ (pH = 5.7 – 9.2) employed in their studies. Xue *et al.*, on the other hand, concluded that the HER on Cu@graphdiyne core-shell electrocatalysts proceeds *via* the Volmer-Heyrovsky(rds) mechanism (Tafel slope ~69 mV·dec^{-1}).[48] We speculate that the higher Tafel slope in this case could be due to the higher scan rate (5 mV·s^{-1}) employed during the LSV measurements. The scan rate has been shown to affect the Tafel slopes in the potentiodynamic LSV measurements.[49] Interestingly, it has been proposed that the HER proceeds *via* the Volmer-Tafel(rds) mechanism on Cu-based metal organic frameworks.[50,51] Based on the kinetic investigations and LSV measurements, we conclude that the Tafel step is the rate-determining step for HER on Cu/C and that the HER proceeds *via* the Volmer-Tafel(rds) pathway on Cu/C.

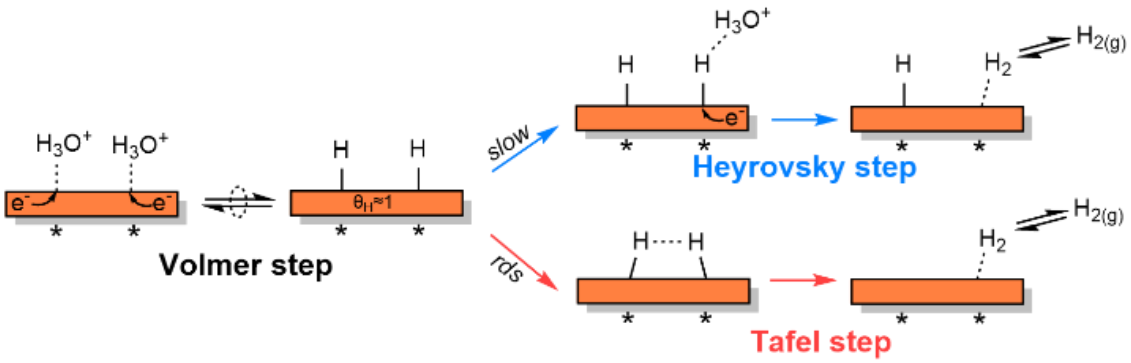

Scheme 2-3. Reaction mechanism for H_2 evolution on Cu/C in the absence of benzaldehyde.

2.3.3 ECH of benzaldehyde on Cu

Let us now look at the aqueous-phase ECH of benzaldehyde on Cu/C. The LSV curve of benzaldehyde ECH on Cu/C is presented in the Supplementary **Figure S2-8**. The onset potential of benzaldehyde ECH on Cu/C was estimated to be –0.4 V vs. RHE. **Figure 2-4** shows the concentration profiles of reactants and products during benzaldehyde ECH on Cu/C at η = –0.5 V vs. RHE. The concentration profiles during benzaldehyde ECH on Pd/C (at η = –0.2 V vs. RHE) are also shown. First of all, it is noteworthy that Cu, unlike Pd, in addition to C=O

hydrogenation to benzyl alcohol, catalyzed C-C coupling to hydrobenzoin. No other by-products were observed. Based on the yield vs. conversion plots (Supplementary **Figure S2-9**), it can be established that both benzyl alcohol and hydrobenzoin are kinetically primary products. We must also mention here that the carbon support showed negligible activity towards benzaldehyde ECH under the same reaction conditions (Supplementary **Figure S2-10**).

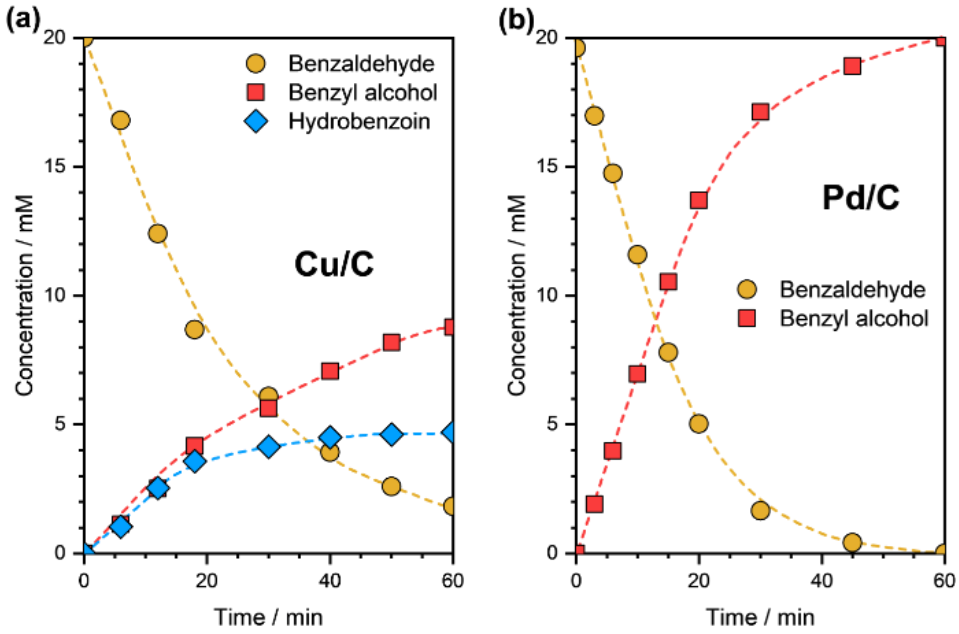

Figure 2-4. Concentration profiles of reactants and products during benzaldehyde ECH on (a) Cu/C, and (b) Pd/C. Reaction conditions: 20 mM benzaldehyde, η = –0.5 V vs. RHE on Cu/C and η = –0.2 V vs. RHE on Pd/C, 1.5 M acetate buffer solution (pH ~4.6), room temperature, ambient pressure. The dashed lines are guides to the eye.

Figure 2-5 shows the H consumption towards different products as a function of reaction time during benzaldehyde ECH on Cu/C and Pd/C. The total H consumption rate on Pd/C was estimated to be ~2.3 $mmol_H \cdot g_{Pd}^{-1} \cdot s^{-1}$, and the overall Faradaic efficiency towards benzaldehyde conversion was almost 100%. Interestingly, the total H consumption rate was similar on Cu/C (~2.4 $mmol_H \cdot g_{Cu}^{-1} \cdot s^{-1}$) albeit at a much higher overpotential, again indicating the weaker hydrogenation ability of Cu compared to Pd. However, similar rates of benzyl alcohol and hydrobenzoin formation on Cu (~1.2 and ~1.1 $mmol_H \cdot g_{Cu}^{-1} \cdot s^{-1}$, respectively) highlight its remarkable ability to catalyze both C=O hydrogenation and C-C coupling reactions. The overall Faradaic efficiency of Cu/C towards benzaldehyde conversion was also high (almost 92%), while the overall Faradaic selectivities towards benzyl alcohol and hydrobenzoin formation were ~48% and ~44%, respectively. Lastly, it must be noted that the H_2 formation rate on Cu/C

in the presence of benzaldehyde (~0.2 $mmol_H \cdot g_{Cu}^{-1} \cdot s^{-1}$; **Figure 2-5a**) was significantly lower than that in its absence (~3.7 $mmol_H \cdot g_{Cu}^{-1} \cdot s^{-1}$; **Figure 2-1a**) suggesting low H* coverage in the presence of benzaldehyde.

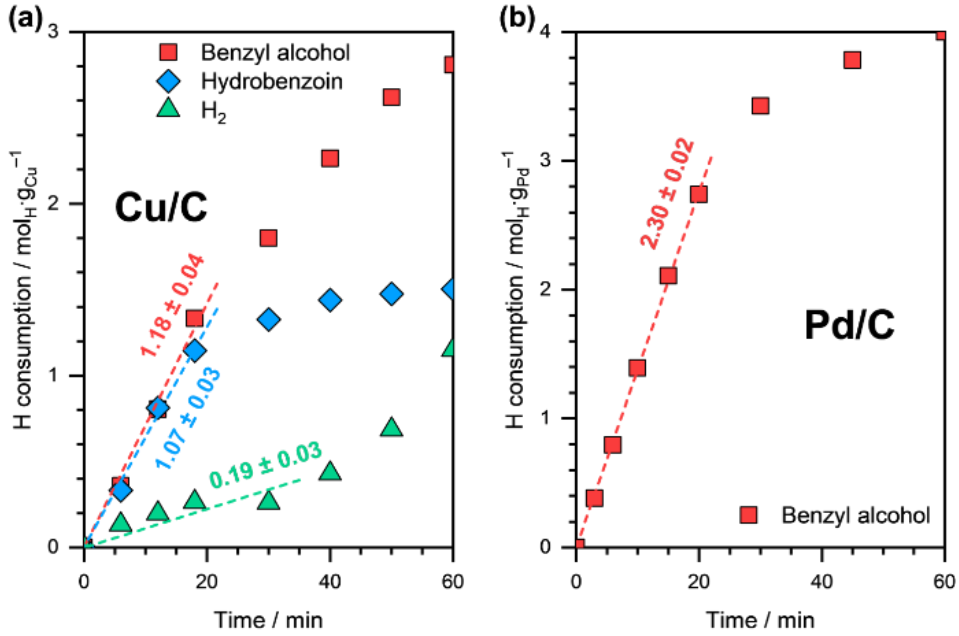

Figure 2-5. H consumption towards benzyl alcohol, hydrobenzoin, and H_2 formation as a function of reaction time during benzaldehyde ECH on (a) Cu/C, and (b) Pd/C. Reaction conditions: 20 mM benzaldehyde, η = –0.5 V vs. RHE on Cu/C and η = –0.2 V vs. RHE on Pd/C, 1.5 M acetate buffer solution (pH ~4.6), room temperature, ambient pressure. The dashed lines are linear fits and the reported numbers are the initial rates in $mmol_H \cdot g_{metal}^{-1} \cdot s^{-1}$.

Figure 2-6 shows the effects of initial benzaldehyde concentration (a_{BZ}), $a_{H_3O^+}$, and η on benzaldehyde ECH on Cu/C. The reaction orders in benzaldehyde for benzyl alcohol and hydrobenzoin formation were estimated to be ~0.05 (approximately zero-order) and ~0.99 (approximately first-order), respectively. HER, in the presence of benzaldehyde, also showed almost zero-order dependence on a_{BZ}. We further note that the product formation rates increased modestly with $a_{H_3O^+}$ and the reaction orders in H_3O^+ for benzyl alcohol, hydrobenzoin, and H_2 formation were estimated to be ~0.27, ~0.20, and ~0.18, respectively. Finally, it can be clearly seen that both benzyl alcohol and hydrobenzoin formation rates showed a similar dependence on η and increased with increasing overpotential.

We note here that a_{BZ}, $a_{H_3O^+}$ and η, all had an impact on the products selectivity during benzaldehyde ECH on Cu/C (Supplementary **Figure S2-11**). The hydrobenzoin selectivity

gradually increased while benzyl alcohol selectivity gradually decreased with increasing a_{BZ} (Supplementary **Figure S2-11a**). Similarly, hydrobenzoin selectivity initially increased with η (from –0.4 to –0.5 V vs. RHE) but then remained invariant with a further increase in η (Supplementary **Figure S2-11b**). Lastly, electrolyte pH (or $a_{H_3O^+}$) had no effect on benzyl alcohol and hydrobenzoin selectivity (Supplementary **Figure S2-11c**) and the two remained almost constant in the investigated pH range (3.2 – 6.3). Interestingly, the H_2 Faradaic selectivity remained low (<0.1) under the investigated reaction conditions indicating high Faradic efficiency towards benzaldehyde conversion.

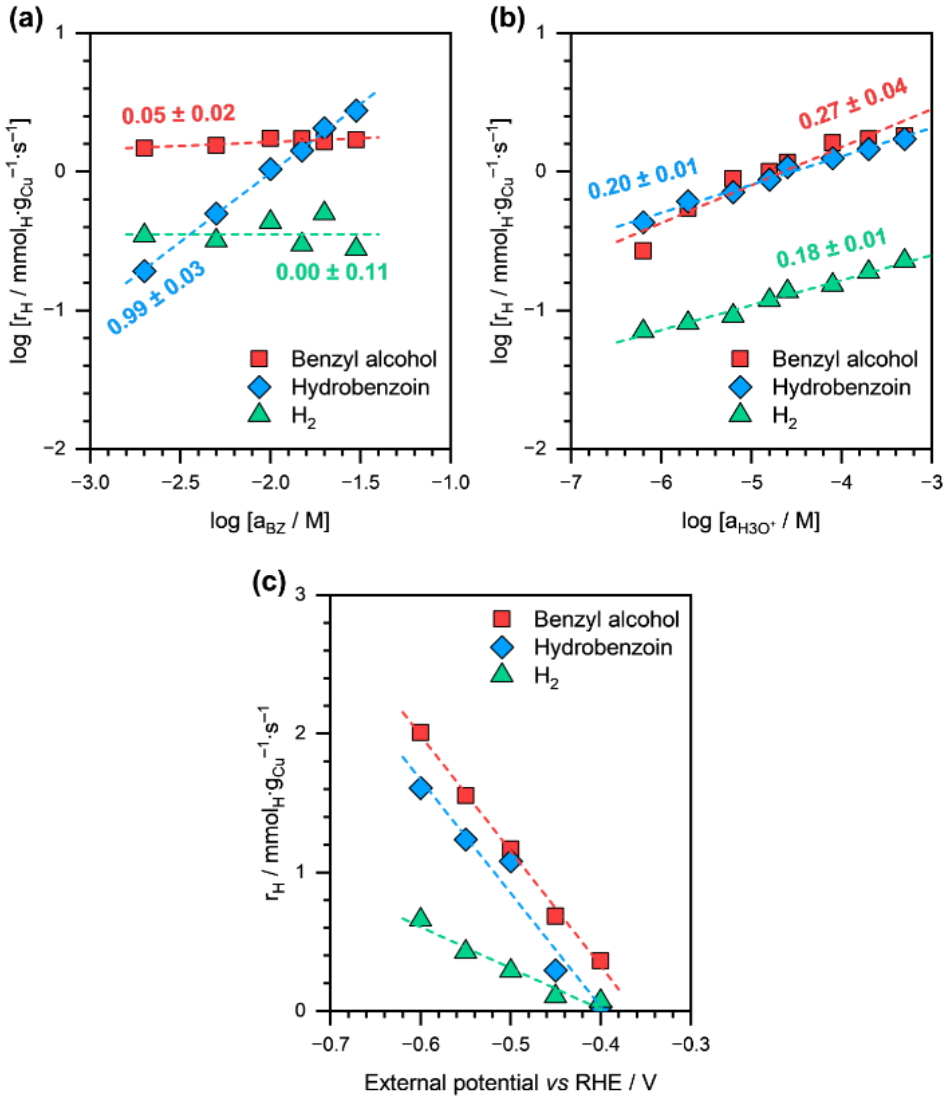

Figure 2-6. Benzyl alcohol, hydrobenzoin, and H_2 formation rates, during benzaldehyde ECH on Cu/C, as a function (a) initial benzaldehyde concentration (a_{BZ}), (b) H_3O^+ activity ($a_{H_3O^+}$), and (c) η. Reaction conditions: 2 – 30 mM benzaldehyde, η = –0.4 to –0.6 V vs. RHE, 1.5 M acetate buffer solution (pH 3.2 – 6.3), room temperature, ambient pressure. The dashed lines are linear fits, and the reported numbers are estimated reaction orders.

Figure 2-7a shows the Arrhenius-type plots for benzyl alcohol, hydrobenzoin, and H_2 formation during benzaldehyde ECH on Cu/C. The apparent activation energy (E_a) for benzyl alcohol and hydrobenzoin formation was estimated to be ~28 kJ·mol^{-1} and ~2 kJ·mol^{-1}, respectively. The corresponding apparent pre-exponential factors were 7 ×10^4 and 2 × 10^1, respectively. The E_a for benzyl alcohol formation on Cu/C was similar to that reported on Pt/C and Rh/C (~25 kJ·mol^{-1} and ~21 kJ·mol^{-1} at η = –0.7 V vs. Ag/AgCl, respectively).[28] The E_a for H_2 formation was estimated to be ~34 kJ·mol^{-1} (**Figure 2-7a**) while the corresponding apparent pre-exponential factor was 1 × 10^5. Interestingly, Sharifi-Asl *et al.* also estimated similar activation energy for HER on Cu electrode (E_a ~32 kJ·mol^{-1}).[47]

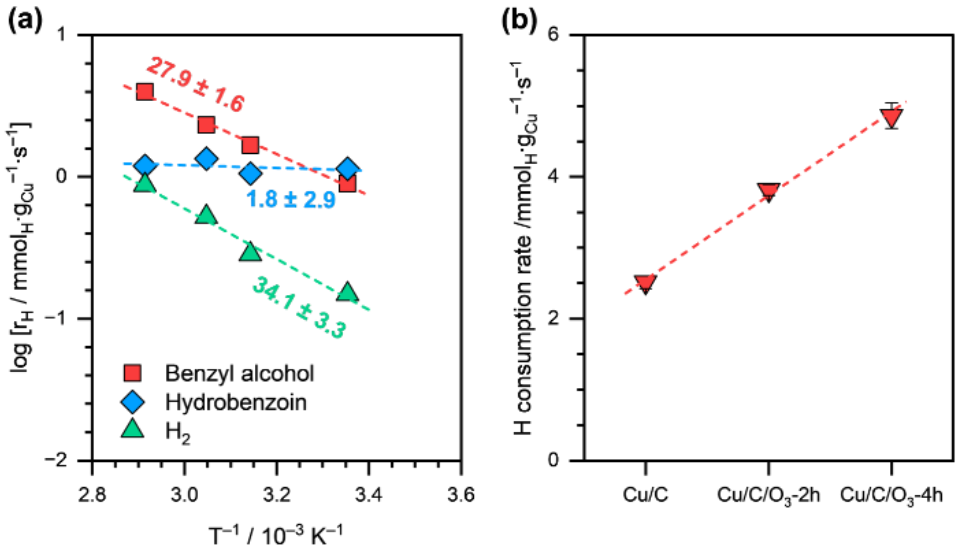

Figure 2-7. (a) Arrhenius-type plots for benzyl alcohol, hydrobenzoin, and H_2 formation during benzaldehyde ECH on Cu/C. The dashed lines are linear fits and the reported number are E_a in kJ·mol^{-1}. (b) Total H consumption rates during benzaldehyde ECH on Cu/C, Cu/C/O_3-2h, and Cu/C/O_3-4h. Dashed line is a guide to the eye. Reaction conditions: 20 mM benzaldehyde, η = –0.5 V vs. RHE, 1.5 M acetate buffer solution (pH ~4.6), 298 – 353 K reaction temperature, ambient pressure.

Figure 2-7b shows the effect of acid functionalization of the carbon support on the total H consumption rates on Cu/C during benzaldehyde ECH. The individual rates and Faradaic selectivities of benzyl alcohol, hydrobenzoin, and H_2 formation on the O_3-treated catalysts are compiled in Supplementary **Table S2-2**. It must be noted that all catalysts showed at least 90% Faradaic efficiency towards benzaldehyde conversion. Interestingly, both O_3-treated catalysts, *i.e.*, Cu/C/O_3-2h and Cu/C/O_3-4h, showed increasingly higher H consumption rates for benzaldehyde ECH. In fact, the ECH rate almost doubled from ~2.4 $mmol_H \cdot g_{Cu}^{-1} \cdot s^{-1}$ on Cu/C

to ~4.9 $mmol_H \cdot g_{Cu}^{-1} \cdot s^{-1}$ on Cu/C/O_3-4h. Furthermore, benzyl alcohol and hydrobenzoin formation rates also increased individually upon O_3 treatment (Supplementary **Table S2-2**). Lastly, we note that the HER rates (in the presence of benzaldehyde) also increased substantially from ~0.24 $mmol_H \cdot g_{Cu}^{-1} \cdot s^{-1}$ on Cu/C to ~0.51 $mmol_H \cdot g_{Cu}^{-1} \cdot s^{-1}$ on Cu/C/O_3-4h.

2.3.4 H_2 evolution during benzaldehyde ECH on Cu

Let us first discuss H_2 formation on Cu/C in the presence of benzaldehyde. First, we note that the HER rate in the presence of benzaldehyde (~0.2 $mmol_H \cdot g_{Cu}^{-1} \cdot s^{-1}$; **Figure 2-5a**) was much lower than the HER rate in its absence (~3.7 $mmol_H \cdot g_{Cu}^{-1} \cdot s^{-1}$; **Figure 2-1a**). We concluded above that the kinetically rate-determining step for HER on Cu/C is the Tafel step and that the HER on Cu/C follows the Volmer-Tafel(rds) mechanism. As r_{Tafel} is second order in θ_H (**Eq. 2-6**), the substantially lower HER rate in the presence of benzaldehyde suggests that $\theta_H \ll 1$ under benzaldehyde ECH reaction conditions. Additionally, the almost zero-order dependence of benzyl alcohol formation on a_{BZ} (**Figure 2-6a**) indicates high surface coverage of the organic substrate. Assuming competitive adsorption between BZ* and H* for the same sites on the Cu surface, we postulate that H* coverage must be low in the presence of benzaldehyde. The low H* coverage is also evidenced by the high FE towards benzaldehyde conversion on Cu/C (>90%) under benzaldehyde ECH reaction conditions.

Remarkably, the HER rates, in the presence of benzaldehyde, increased with increasing $a_{H_3O^+}$ (**Figure 2-6b**) and η (**Figure 2-6c**). This trend contrasts with that observed in the absence of benzaldehyde, where HER rates showed an almost no dependence on $a_{H_3O^+}$ (**Figure 2-3a**). Furthermore, in the presence of benzaldehyde, O_3 treatment of the carbon support almost doubled the HER rate from ~0.24 $mmol_H \cdot g_{Cu}^{-1} \cdot s^{-1}$ on Cu/C to ~0.51 $mmol_H \cdot g_{Cu}^{-1} \cdot s^{-1}$ on Cu/C/O_3-4h (Supplementary **Table S2-2**). This result is again in contrast to the results obtained in the absence of benzaldehyde, where the HER rates remained almost invariant after the O_3 treatment of the carbon support (**Figure 2-3b**). We recall here that at low H* coverages (*i.e.*, $\theta_H \ll 1$), θ_H is dependent on the reversible rate of Volmer step, which in turn is dependent on both $a_{H_3O^+}$ and η (**Eq. 2-4**). The clear dependence of HER rates on $a_{H_3O^+}$ and η, therefore, suggests that $\theta_H \ll 1$ under benzaldehyde ECH reaction conditions.

We further note here that r_{Tafel} and $r_{Heyrovsky}$ are both dependent on θ_H (**Eq. 2-6** and **Eq. 2-5**, respectively); however, the kinetic dependence of r_{Tafel} on θ_H is second-order, while that of $r_{Heyrovsky}$ is first-order. Therefore, under benzaldehyde ECH reaction conditions, it is also possible that $r_{Tafel} < r_{Heyrovsky}$ at low H* coverages. In other words, when $\theta_H \ll 1$, the H_2 formation could occur *via* the Heyrovsky step. As Heyrovsky step follows the PCET mechanism, the change in the mechanism of H_2 evolution from Volmer-Tafel to Volmer-Heyrovsky could also explain the dependence of HER rates on $a_{H_3O^+}$ and η. Although it is not possible to confirm this shift in the mechanism from our kinetic investigations, we can unequivocally conclude that the surface coverage of H* is low (*i.e.*, $\theta_H \ll 1$) on Cu/C under benzaldehyde ECH reaction conditions.

2.3.5 Mechanism for benzyl alcohol formation during benzaldehyde ECH on Cu

Benzyl alcohol formation from benzaldehyde requires two successive H additions to the benzaldehyde molecule. These H additions have been postulated to proceed *via* two distinct pathways: the hydroxy pathway and the alkoxy pathway (illustrated in **Scheme 2-4**). In the hydroxy pathway, the carbonyl O of the adsorbed benzaldehyde (ArCHO*) is hydrogenated first to form a surface hydroxy intermediate (ArCHOH*), followed by a second H addition to its α-C to form benzyl alcohol. In the alkoxy pathway, on the other hand, the carbonyl C atom is first hydrogenated to form an alkoxy intermediate ($ArCH_2O$*), followed by hydrogenation of the O to form benzyl alcohol.

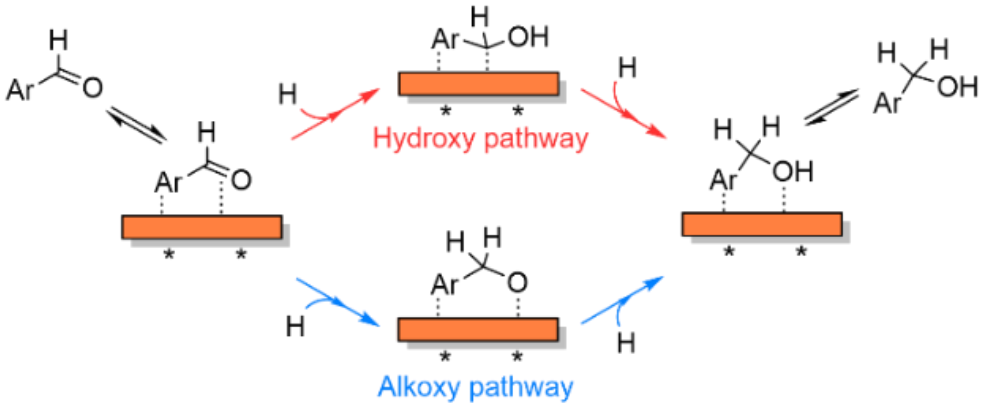

Scheme 2-4. Mechanism for benzyl alcohol formation during benzaldehyde ECH *via* the alkoxy and hydroxy pathways.

We performed isotope labelling studies to distinguish between the alkoxy and the hydroxy

pathways for benzyl alcohol formation. Cheng *et al.* have previously shown that during benzaldehyde hydrogenation (on Pd/C), the addition of D to the carbonyl C *via* the alkoxy pathway forms ArCHDO* and would inevitably result in the formation of some deuterated benzaldehyde (ArCDO*) due to the reversibility of this step.[37] On the other hand, addition of D to the carbonyl O *via* the hydroxy pathway forms ArCHOD*. The reverse reaction, in this case, would only form non-deuterated benzaldehyde (ArCHO*). Therefore, the presence of deuterated benzaldehyde in the electrolyte can be used to distinguish between the two pathways. In the case of benzaldehyde ECH, the solvent (*i.e.*, H_2O) is the source of H. Therefore, we performed benzaldehyde ECH on Cu/C using D_2O as a solvent instead of H_2O. However, we did not detect any deuterated benzaldehyde (*i.e.*, ArCDO) in the electrolyte solution even after 90 min of reaction. These results, therefore, suggest that the hydroxy pathway must be the preferred pathway for H addition during benzaldehyde ECH on Cu.

We also note that hydrobenzoin formation during benzaldehyde ECH involves C-C coupling between two partially hydrogenated benzaldehyde. Hydrobenzoin formation, therefore, necessitates H addition to the carbonyl O atom of each benzaldehyde and C-C bond formation between the corresponding α-C atoms. A preferential H addition to the carbonyl C *via* the alkoxy pathway would saturate the C atom and, therefore, inhibit C-C coupling. As hydrobenzoin was observed in significant quantities during benzaldehyde ECH (**Figure 2-4a**), we conclude that the hydroxy pathway is the preferred pathway for H addition on Cu/C under the investigated benzaldehyde ECH reaction conditions.

Let us now discuss the H addition mechanism during benzaldehyde ECH to benzyl alcohol. These H additions could occur either *via* the PCET mechanism or *via* the LH-type surface mechanism. The LH pathway involves the reaction of an adsorbed benzaldehyde with surface H* species. The PCET mechanism, on the other hand, involves an ER-type reaction of an adsorbed benzaldehyde with a solvated H_3O^+, coupled with a concerted electron transfer from the catalyst's surface. The rate of H addition *via* the PCET mechanism ($r_{H,PCET}$) can be expressed as

$$r_{H,PCET} = k_{H,PCET} \cdot e^{-\alpha f \eta} \cdot \theta_{BZ} \cdot a_{H_3O^+} \tag{2-7}$$

where $k_{H,PCET}$ is the kinetic rate constant and θ_{BZ} is the surface coverage of adsorbed benzaldehyde. The rate of H addition *via* the LH mechanism ($r_{H,LH}$), on the other hand, takes

the following form

$$r_{H,LH} = k_{H,LH} \cdot \theta_{BZ} \cdot \theta_H \quad (2\text{-}8)$$

Where $k_{H,LH}$ is the kinetic rate constant and θ_H is the surface coverage of H*. Based on these rate equations, we can clearly see that the $r_{H,PCET}$ depends on $a_{H_3O^+}$ and η, while $r_{H,LH}$ depends on θ_H.

We recall that the benzyl alcohol formation rates showed a positive dependence on both $a_{H_3O^+}$ (**Figure 2-6b**), η (**Figure 2-6c**), and on O_3 treatment of the carbon support (Supplementary **Table S2-2**), thus suggesting that the kinetically relevant step for benzyl alcohol formation (either the first or the second H addition) involves PCET. However, we must note here that these results do not exclude the H addition *via* the LH step. We have concluded above that $\theta_H \ll 1$ in the presence of benzaldehyde and that H* coverage increases with $a_{H_3O^+}$ and η. The increase in θ_H would consequentially also increase $r_{H,LH}$ thus explaining the above trends.

To conclusively distinguish between PCET and LH pathways for H addition, we performed benzaldehyde ECH on Cu/C in the presence of *t*-butanol (*t*-BuOH), a specific quenching agent towards surface H*. The obtained results are presented in the Supplementary **Figure S2-12**.[52-54] **Figure 2-8** shows the initial benzaldehyde conversion rates (r_{BZ}) on Cu/C (at varying a_{BZ}) in the presence or absence of t-BuOH. First of all, it can be clearly seen that r_{BZ} decreased in the presence of t-BuOH in all cases. This decrease clearly suggests that the LH pathway contributes, at least to some extent, towards H addition. Using r_{BZ} as a quantitative indicator, we estimated that the contribution of LH pathway towards H addition is ~20% irrespective of initial benzaldehyde concentration. Based on these results, we conclude that PCET is the dominating pathway for H addition on Cu/C, contributing ~80% towards H addition under the investigated reaction conditions.

We also performed HER on Cu/C (in the pure electrolyte solution) in the presence of *t*-BuOH (Supplementary **Figure S2-13**), and the corresponding H_2 formation rates are also shown in **Figure 2-8**. It can be seen that the HER rates, in pure electrolyte solution, decreased substantially from ~2.1 $mmol_{H2} \cdot g_{Cu}^{-1} \cdot s^{-1}$ without t-BuOH to ~0.6 $mmol_{H2} \cdot g_{Cu}^{-1} \cdot s^{-1}$ in the presence of ~200 mM t-BuOH, i.e., a decrease of more than 70%. As we have noted above, the

HER on Cu/C occurs via the Tafel step, which is an LH-type surface recombination of two H* species. A more significant decrease in the HER rates in the presence of t-BuOH, in this case, is therefore expected.

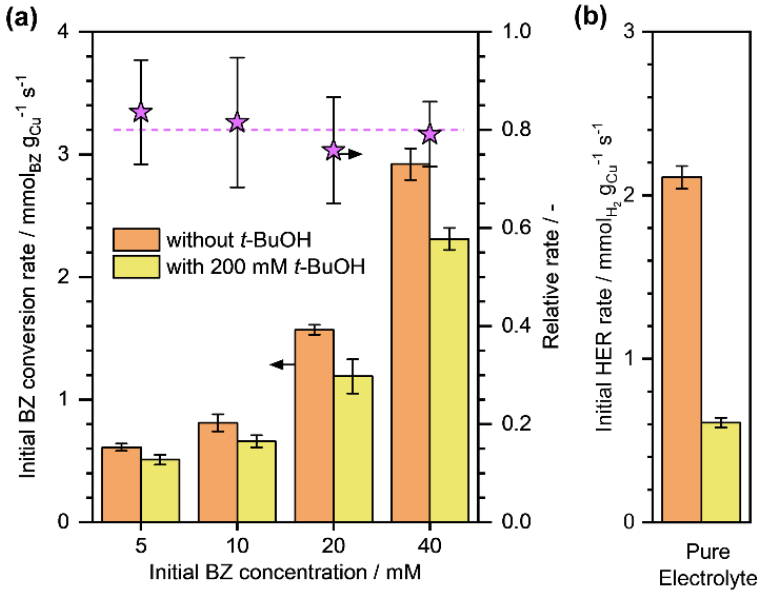

Figure 2-8. (a) Initial benzaldehyde conversion rates during benzaldehyde ECH, and initial HER rates in pure electrolyte solution, on Cu/C with and without 200 mM t-BuOH. The relative rates in the presence of t-BuOH are also reported. Reaction conditions: 0 – 40 mM benzaldehyde, η = –0.5 V vs. RHE, 1.5 M acetate buffer solution (pH ~4.6), room temperature, ambient pressure.

The protonation and electron transfer processes during H addition have also been described as either inner-sphere or outer-sphere processes.[8] The inner-sphere reactions occur on the electrode surface while outer-sphere reactions occur in the solvent layer and do not require a strong interaction between the reactants or intermediates and the electrode surface. Self-assembled monolayers of organothiols have been shown to inhibit the inner-sphere reactions but not the outer-sphere reactions.[8] Therefore, we performed benzaldehyde ECH in the presence of 10 mM 2-mercaptobenzothiazole (MBT) to distinguish between the inner-sphere and outer-sphere reactions and the results are reported in Supplementary **Figure S2-14**. It can be seen that both hydrobenzoin and benzyl alcohol formation decreased significantly in the presence of MBT, thus clearly indicating that the reactions involved in the formation of benzyl alcohol and hydrobenzoin during benzaldehyde ECH are inner-sphere processes and occur on the surface of Cu.

Next, to elucidate the kinetically relevant steps for benzyl alcohol and hydrobenzoin

formation during benzaldehyde ECH, we performed isotope labelling experiments. **Figure 2-9** shows the initial benzyl alcohol and hydrobenzoin formation rates during benzaldehyde ECH on Cu/C in H_2O or D_2O as solvent. We can see that the benzyl alcohol formation rate decreased from ~1.2 $mmol_H \cdot g_{Cu}^{-1} \cdot s^{-1}$ in H_2O to ~0.5 $mmol_H \cdot g_{Cu}^{-1} \cdot s^{-1}$ in D_2O. This corresponds to a strong primary kinetic isotope effect (KIE) of r_H/r_D = 2.4/1. The strong primary KIE suggests that H addition (either the first or the second) is the rate-determining step for benzyl alcohol formation. In contrast, the hydrobenzoin formation rate increased only slightly when the solvent was changed to D_2O, corresponding to an inverse secondary KIE of r_H/r_D = 1/1.08. The weak (secondary) KIE suggests that H is not directly involved in the kinetically relevant step for hydrobenzoin formation. Therefore, we conclude that the rate-determining step for hydrobenzoin formation is the C-C bond formation. The different rate-determining steps for benzyl alcohol and hydrobenzoin formation is also supported by the different E_a (~28 $kJ \cdot mol^{-1}$ and ~2 $kJ \cdot mol^{-1}$, respectively; **Figure 2-7a**).

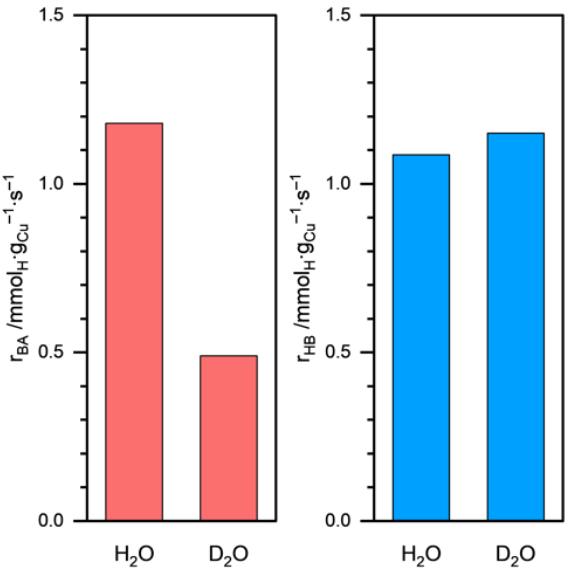

Figure 2-9. Benzyl alcohol and hydrobenzoin formation rates during benzaldehyde ECH on Cu/C in H_2O or D_2O solvent. Reaction conditions: 20 mM benzaldehyde, η = –0.5 V vs. RHE, 1.5 M acetate buffer solution (pH ~4.6), room temperature, ambient pressure.

2.3.6 Mechanism for hydrobenzoin formation during benzaldehyde ECH on Cu

Let us now focus on C-C coupling during benzaldehyde ECH on Cu/C. The C-C coupling during hydrobenzoin formation could occur either *via* an LH-type mechanism or *via* an ER-type mechanism (as illustrated in **Scheme 2-5**). The LH pathway involves a reaction between

two surface intermediates, while the ER-type mechanism involves the reaction of an adsorbed intermediate with a physisorbed benzaldehyde molecule. The rates of C-C coupling *via* the LH-type ($r_{C-C,LH}$) or the ER-type ($r_{C-C,ER}$) mechanisms can be expressed as

$$r_{C-C,LH} = r_{C-C,LH} \cdot (\theta_{BZ'})^2 \quad (2\text{-}9)$$

$$r_{C-C,ER} = r_{C-C,ER} \cdot \theta_{BZ'} \cdot a_{BZ} \quad (2\text{-}10)$$

where $k_{C-C,LH}$ and $k_{C-C,ER}$ are the respective kinetic rate constants, $\theta_{BZ'}$ is the surface coverage of adsorbed intermediate, and a_{BZ} is the concentration of benzaldehyde.

We have shown above that, under the applied reaction conditions, the surface of Cu is saturated with the organic substrate, *i.e.*, $\theta_{BZ'} \approx 1$. Therefore, under these conditions, the reaction orders in benzaldehyde for the LH-type and ER-type C-C coupling pathways are expected to be zero and one, respectively. We recall that the hydrobenzoin formation showed a reaction order of approximately one in a_{BZ} (**Figure 2-6a**). Therefore, we conclude here that hydrobenzoin formation on Cu/C proceeds *via* the ER-type mechanism wherein an adsorbed surface intermediate reacts with a physisorbed benzaldehyde.

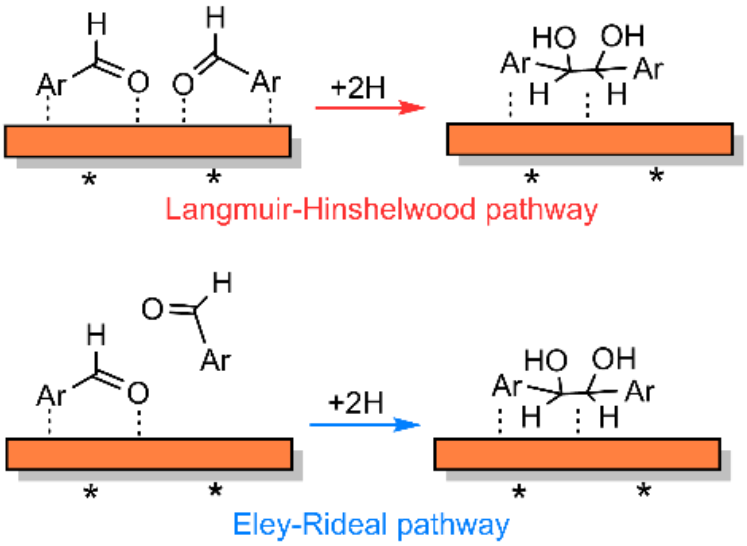

Scheme 2-5. LH- and ER-type pathways for C-C coupling.

Hydrobenzoin formation, in addition to the C-C coupling step, requires H addition to the carbonyl O atoms of the involved benzaldehyde molecules. The proposed ER-type C-C coupling could, therefore, occur before or after the hydrogenation of the adsorbed intermediate. In other words, the physisorbed benzaldehyde molecule could react with either (i) an adsorbed BZ* (ArCHO*), *i.e.*, prior to the first H addition or (ii) a surface hydroxy intermediate

(ArCHOH*) formed after the first H addition. It must be noted that the C-C coupling between a physisorbed benzaldehyde and adsorbed BZ* (ArCHO*) would form benzoin (following an intramolecular H transfer). However, we did not observe benzoin as a by-product during benzaldehyde ECH on Cu/C. The possibility that any benzoin formed is rapidly hydrogenated to hydrobenzoin (under the applied reaction conditions) was investigated by performing ECH of benzoin on Cu/C under the same reaction conditions. The ECH of ~20 mM aqueous solution of benzoin on Cu/C at η = –0.5 V vs. RHE in 1.5 M acetate buffer solution (pH ~4.6) showed negligible conversion to hydrobenzoin. These results, therefore, clearly suggest that the occurrence of C-C coupling before the first H addition step is unlikely. Therefore, we conclude that C-C coupling occurs after the first H addition and involves a partially hydrogenated surface hydroxy intermediate (ArCHOH*). The formation and stabilization of partially hydrogenated benzaldehyde (as ketyl radical species) on the surface of Cu has been observed experimentally.[19,20,33]

Finally, it is worth mentioning here that a fast second H addition to the surface hydroxy intermediate would result in the formation of primarily benzyl alcohol and, therefore, inhibit hydrobenzoin formation *via* C-C coupling. As hydrobenzoin was observed in significant quantities on Cu/C, we conclude that the second H addition has a lower rate constant than the first H addition and is, therefore, the rate-determining step for benzyl alcohol formation. The first H addition that forms the hydroxy intermediate can be assumed to be fast and equilibrated under the applied reaction conditions.

2.3.7 Molecular simulations

To further validate the postulated reaction pathways for benzyl alcohol and hydrobenzoin formation during benzaldehyde ECH on Cu, we simulated H addition and C-C coupling pathways using periodic DFT calculations on the Cu(111) surface (the most abundant facet evident from XRD). The simulations were performed on a system comprising a benzaldehyde molecule adsorbed flat (at ~2.45 Å) on the Cu(111) surface. Charges were calculated using the Bader charge analysis. An implicit solvation model with additional explicit water molecules was employed in all simulations (refer to the Experimental Methods section for more details on the computational methodology). **Table 2-1** shows the calculated energy barriers (ΔE_{TS}) for the

first H addition, the second H addition, and the C-C coupling steps at the specified surface potentials relative to the RHE ($U_{i,RHE}$). The $U_{i,RHE}$ of the Cu(111) surface was estimated from its work function (φ).

Table 2-1. Energy barriers (ΔE_{TS}) of different reaction steps for benzyl alcohol and hydrobenzoin formation on Cu(111) surface at the specified surface potential ($U_{i,RHE}$).

Reaction step	ΔE_{TS} / kJ·mol^{-1}	$U_{i,RHE}$[a] / V vs. RHE
First H addition	~26[b], ~46[c]	–0.42
Second H addition	~81[b]	–0.54
C-C coupling	~36	–0.42

[a] Estimated at pH = 4.6 and T = 300 K
[b] PCET mechanism
[c] LH-type surface mechanism

Let us first look at the formation of surface hydroxy intermediate, *i.e.*, first H addition, *via* the PCET mechanism. The first PCET step was simulated by adding a proton to the water layer above the adsorbed benzaldehyde molecule (and a corresponding electron to the Cu surface). The initial (IS), transition (TS‡), and final states (FS) for the first PCET step are shown in **Figure 2-10a**. During the simulations, we observed that the carbonyl O of benzaldehyde (O_b) was H-bonded to the nearby H_2O_w (or $H_3O_w^+$) molecules. In the PCET step, the proton was transferred from a H-bonded $H_3O_w^+$ to O_b, and the electron was simultaneously transferred from the Cu surface. An increase in the total Bader charge on the Cu surface (from +0.67 to +0.91) indicated that the electron was transferred from the surface of the catalyst to the adsorbed intermediate. The energy barrier for the first PCET step was estimated to be ~26 kJ·mol^{-1} (**Table 2-1**). First of all, the low energy barrier suggests that the first H addition, in agreement with the experimental findings, is fast and can be assumed to be equilibrated under the applied reaction conditions. Additionally, we also noted that the total Bader charge on the Cu surface and the O_b–H interatomic distance in the TS‡ were closer to that in the FS compared to that in the IS, indicating a late transition state for the first H addition.

We also simulated the first H addition *via* the LH-type surface reaction between an adsorbed H* and an adsorbed benzaldehyde (illustrated in Supplementary **Figure S2-15**). The energy barrier for this step was estimated to be ~46 kJ·mol^{-1} (**Table 2-1**). The relatively higher barrier for the surface H addition corroborates our experimental findings that H addition on Cu/C

occurs primarily *via* the PCET mechanism.

Next, we simulated the second H addition to the α-C of the surface hydroxy intermediate *via* PCET to form BA*. For this, we added another proton to the water layer above the adsorbed hydroxy intermediate (ArCHOH*) and a corresponding electron to the Cu surface. We again observed that the hydroxy O (O_b) was H-bonded to the nearby H_2O_w (or $H_3O_w^+$) molecules. In the second PCET step, the H^+ was transferred from a nearby $H_3O_w^+$ to the α-C (C_b) of the hydroxy intermediate, as illustrated in **Figure 2-10b**. The proton transfer was coupled with electron transfer from the surface of Cu. Similar to the first PCET step, the increase in the Bader charge on the Cu surface (from +0.71 to +0.86) indicated that the electron was transferred from the surface to the adsorbed intermediate. The energy barrier for the second PCET was estimated to be ~81 kJ·mol^{-1} (**Table 2-1**). We note that this barrier is significantly higher than that calculated for the first H addition (ΔE_{TS} ~26 kJ·mol^{-1}). In agreement with the experimental evidence, the higher energy barrier for the second H addition clearly suggests that it must be the rate-determining step for benzyl alcohol formation. The higher barrier for H addition to the α-C (*i.e.*, second H addition) compared to carbonyl O (*i.e.*, first H addition) is likely due to the hydrophilic nature of the O atom. Lastly, the similar total Bader charge on the Cu surface in the TS‡ and the IS, as well as a relatively large C_b–H interatomic distance in the TS‡, indicates an early transition state for the second H addition.

Finally, let us discuss the formation of hydrobenzoin *via* the C-C coupling reaction between a surface hydroxy intermediate and a (physisorbed) benzaldehyde (illustrated in **Figure 2-10c**). For this, we placed a benzaldehyde molecule next to the adsorbed hydroxy intermediate (as well as a proton to the water layer above and an electron to the Cu surface). The C-C bond formation involved an attack on the electrophilic carbonyl C (C_b) of the physisorbed benzaldehyde molecule by the radical α-C (C_h) of the hydroxy intermediate. Interestingly, during the simulations, the C-C bond formation was immediately followed by a fast barrier-less protonation of the radical O (O_b) of the formed alkoxy radical and a concerted electron transfer from the surface of Cu to form HB*. In other words, the C-C coupling was immediately followed by a fast barrier-less PCET to directly form HB*. The increase in the Bader charge on the Cu surface from the IS (+0.67) to the FS (+1.32) indicates electron transfer from the surface of Cu to the adsorbed intermediate. We also note that the total Bader charge on the Cu surface

in the TS‡ was similar to that in the IS, thus indicating that electron transfer had not occurred up to the transition state. The energy barrier for the C-C bond formation was estimated to be ~36 kJ·mol^{-1} (**Table 2-1**).

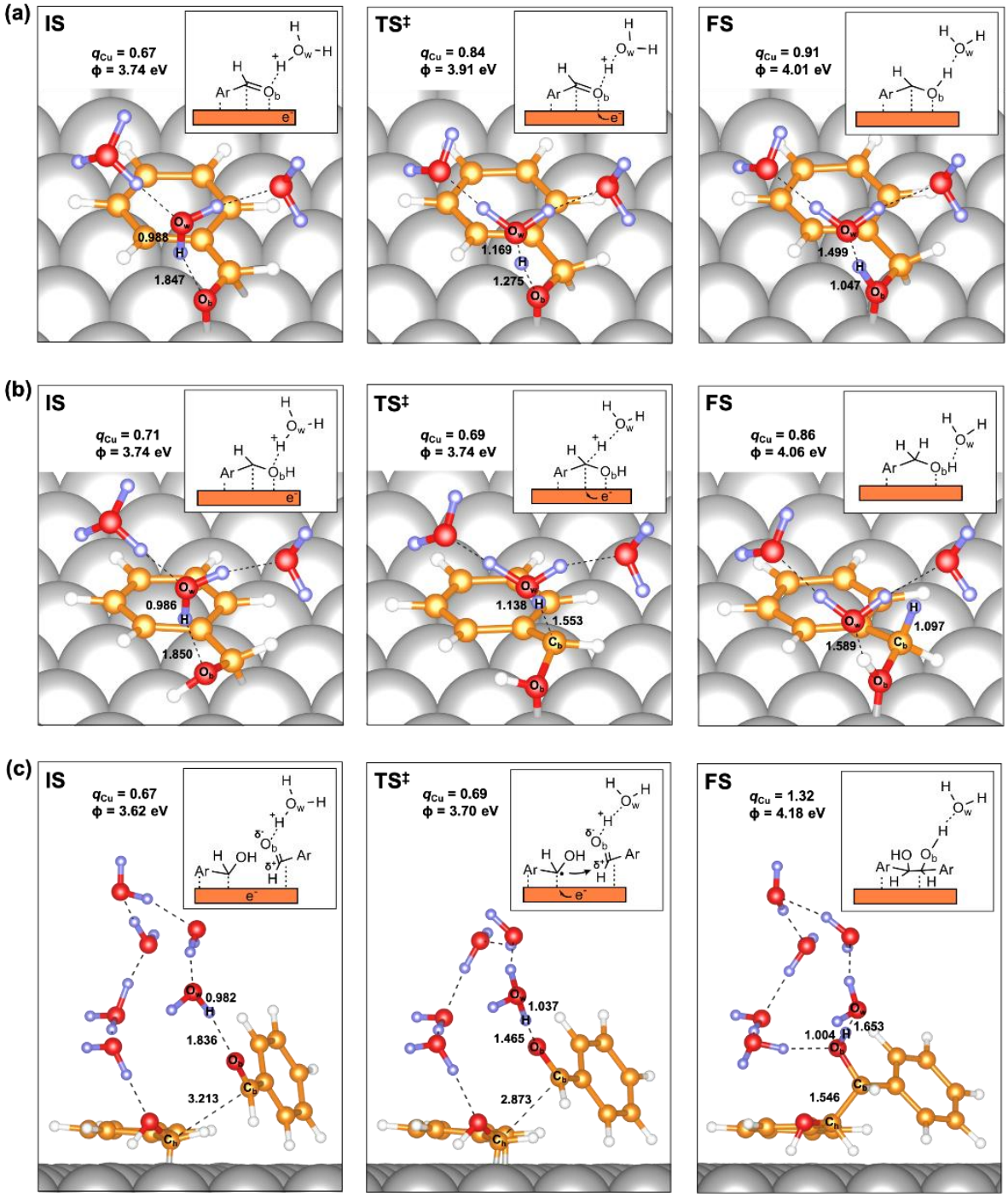

Figure 2-10. Initial (IS), transition (TS‡), and final states (FS) of (a) the first H addition *via* PCET, and (b) the second H addition *via* PCET, for BA* formation, and (c) C-C coupling followed by fast PCET, for HB* formation on the Cu(111) surface. The estimated Bader charges on the Cu surface (q_{Cu}) and the corresponding work-functions (φ) are also shown. The reported number are interatomic distances in Å. Cu: grey, C: orange, O: red, H: while/purple.

Based on these first-principle molecular simulations, the energy barriers for benzyl alcohol A and hydrobenzoin formation have been estimated to be ~81 kJ·mol^{-1} and ~36 kJ·mol^{-1}, respectively. The molecular simulations, therefore, predict that the true activation energy of benzyl alcohol formation must be higher than that for hydrobenzoin formation. This difference in the energy barriers agrees qualitatively with the experimentally observed E_a for benzyl alcohol and hydrobenzoin formation (~28 kJ·mol^{-1} and ~2 kJ·mol^{-1}, respectively; **Figure 2-7a**). Finally, we note here that the mechanism of C-C coupling on Cu has been previously described in terms of the surface combination of two radical intermediates.[19,20] The formation of these radical intermediates has been observed experimentally on Cu using infrared spectroscopy. Furthermore, the ability of Cu to stabilize these radical species has been proposed as a key descriptor of its ability to promote C-C coupling.[33] However, based on the kinetic measurements (*e.g.*, first-order reaction kinetics in a_{BZ} for hydrobenzoin formation), assisted by first-principle periodic DFT calculations, we propose here that the C-C coupling on Cu/C, at least under the investigated reaction conditions, follows an ER-type mechanism involving the reaction of a partially hydrogenated hydroxy (radical) intermediate with a physisorbed benzaldehyde molecule. The C-C bond formation is followed by a fast barrier-less PCET to form hydrobenzoin.

2.3.8 Overall mechanism for benzaldehyde ECH on Cu

Combining the experimental and computational evidence, we now postulate the overall mechanism of benzaldehyde ECH to benzyl alcohol and hydrobenzoin on Cu/C (illustrated in **Scheme 2-6**). First, benzaldehyde (ArCHO) adsorbs reversibly on a vacant site ($*$) on the surface of Cu. The surface is predominantly covered with the organic substrate and H* coverage is low under the applied reaction conditions. The adsorbed benzaldehyde (ArCHO*) undergoes a fast (and equilibrated) first PCET to the carbonyl O to form a surface hydroxy intermediate (ArCHOH*). The formed hydroxy intermediate follows two parallel reaction pathways. In the first pathway, ArCHOH* undergoes a second PCET on its α-C to form adsorbed benzyl alcohol *, which finally desorbs form the surface to form benzyl alcohol. This second H addition is the rate-determining step for benzyl alcohol formation. In a parallel reaction, the electrophilic carbonyl C of a nearby physisorbed benzaldehyde molecule (Ar$C^{\delta+}HO^{\delta-}$) is attacked by the

radical α-C of the hydroxy intermediate (ArC˙HOH*) to form the C-C bond. The C-C coupling is followed by a fast barrier-less PCET to the radical O of the formed alkoxy radical intermediate to form HB*, which finally desorbs from the surface of Cu to form hydrobenzoin. The C-C bond formation is the rate-determining step for benzaldehyde ECH to hydrobenzoin.

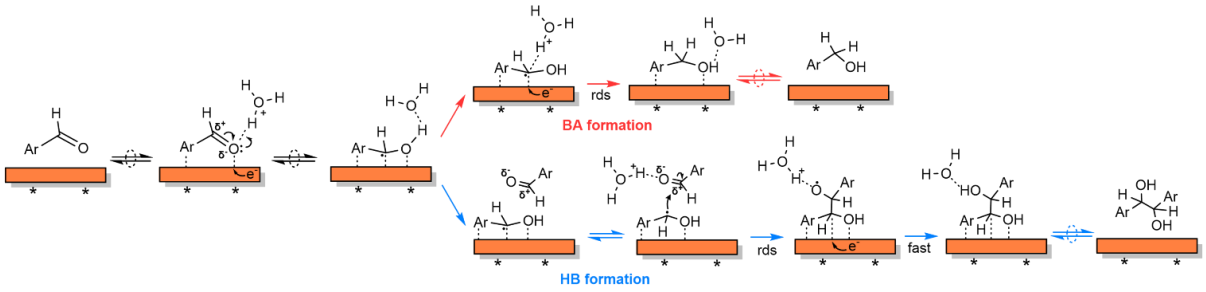

Scheme 2-6. Proposed mechanism for hydrobenzoin and benzyl alcohol formation during benzaldehyde ECH on Cu/C.

2.4 Conclusion

Benzaldehyde ECH on Cu/C forms two primary products, *viz.*, benzyl alcohol (the C=O hydrogenation product) and hydrobenzoin (the C-C coupling product), with an overall Faradaic efficiency of >90% at η = –0.5 V vs. RHE. The Faradaic selectivities towards benzyl alcohol and hydrobenzoin formation were ~48% and ~44%, respectively. In the absence of organic substrate, the H_2 evolution on Cu/C follows the Volmer-Tafel(rds) mechanism. Under benzaldehyde ECH reaction conditions, on the other hand, the surface of Cu is predominantly covered with the organic substrate and the coverage of H* is low. The adsorbed benzaldehyde undergoes a fast (equilibrated) first PCET on the carbonyl O to form a hydroxy intermediate. The hydroxy intermediate then undergoes a second (rate-determining) PCET on its α-C to form benzyl alcohol. In a parallel reaction, the electrophilic carbonyl C of a physisorbed benzaldehyde molecule is attacked by the radical α-C of the hydroxy intermediate to form the C-C bond. The C-C coupling is followed by a fast barrier-less second PCET to form hydrobenzoin. The C-C coupling is the rate-determining step for hydrobenzoin formation.

2.5 Supporting information

2.5.1. Additional experimental methods

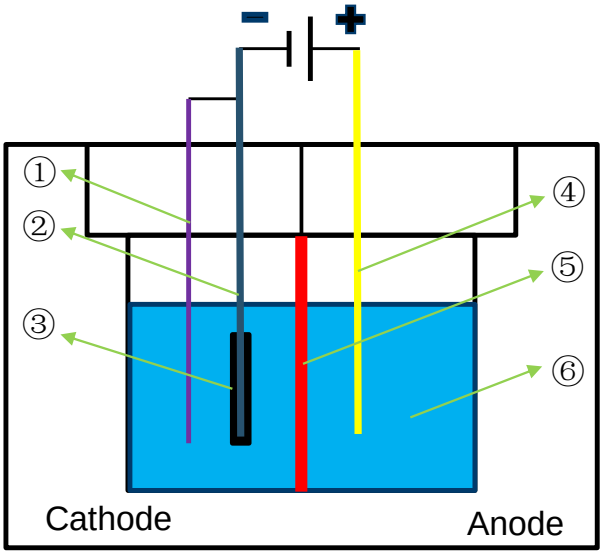

Figure S2-1. Schematic of the two-compartment cell used for all electrochemical experiments. (1) Ag/AgCl reference electrode; (2) Titanium rod; (3) Catalyst on a carbon felt (working electrode); (4) Counter electrode (Pt wire); (5) Nafion membrane; (6) Electrolyte solution.

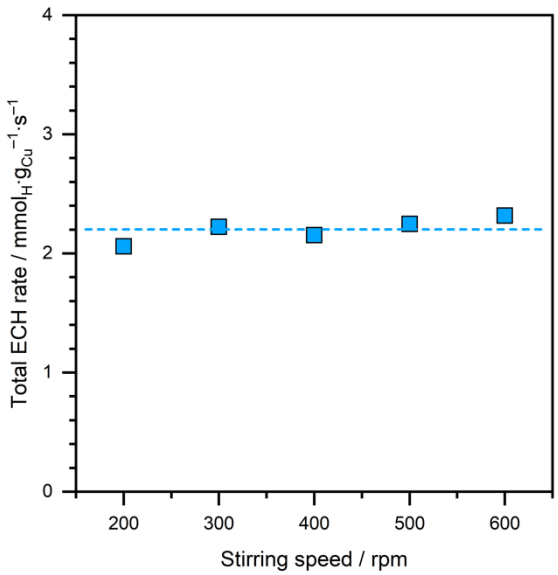

Figure S2-2. Total benzaldehyde ECH rate as a function of stirring speed of the rotor. Reaction conditions: 20 mM benzaldehyde, applied potential –0.5 V *vs* RHE, 1.5 M acetate buffer solution (pH ~4.6), room temperature, ambient pressure. The dashed line is a guide to the eye.

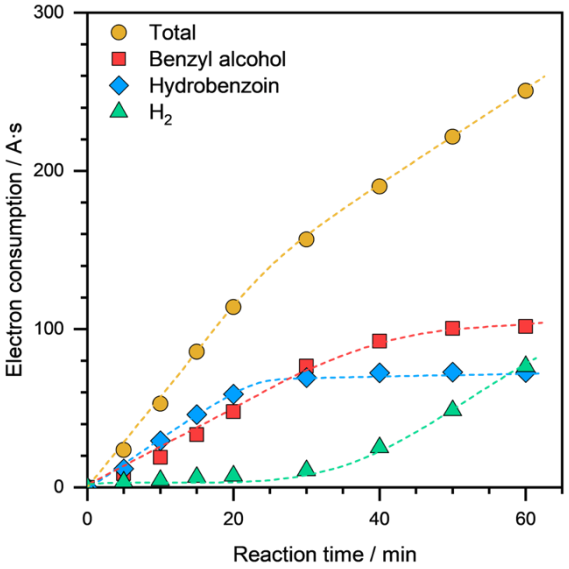

Figure S2-3. Electron consumption (in A·s) during benzaldehyde ECH on Cu/C. Reaction conditions: 20 mM benzaldehyde, applied potential –0.5 V vs RHE on Cu/C, 1.5 M acetate buffer solution (pH ~4.6), room temperature, ambient pressure. The dashed lines are guides to the eye.

The electron consumption (and simultaneously H^+ consumption) towards H_2 evolution (q_{H_2}) was calculated using the following relation

$$q_{H_2} = q_{total} - q_{BA} - q_{HB} \tag{2-11}$$

where q_{total}, q_{BA}, and q_{HB} are the total electron consumption, and electron consumption towards benzyl alcohol and hydrobenzoin formation, respectively.

2.5.2. Additional Catalyst Characterization

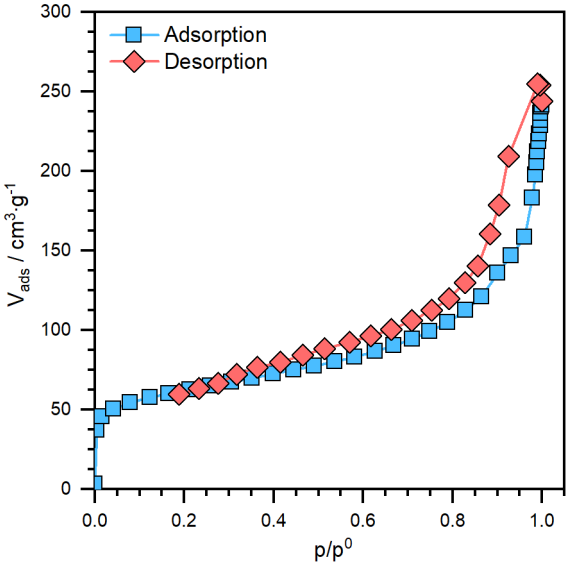

Figure S2-4. N_2 physisorption isotherm on Cu/C. The N_2 adsorption-desorption isotherms were determined at 77 K on a PMI automated BET sorptometer. Prior to measurements, the sample was outgassed at 523 K for 2 h. The surface area of the catalysts was estimated to be ~223 $m^2 \cdot g_{cat}^{-1}$ by the Brunauer-Emmett-Teller (BET) method.

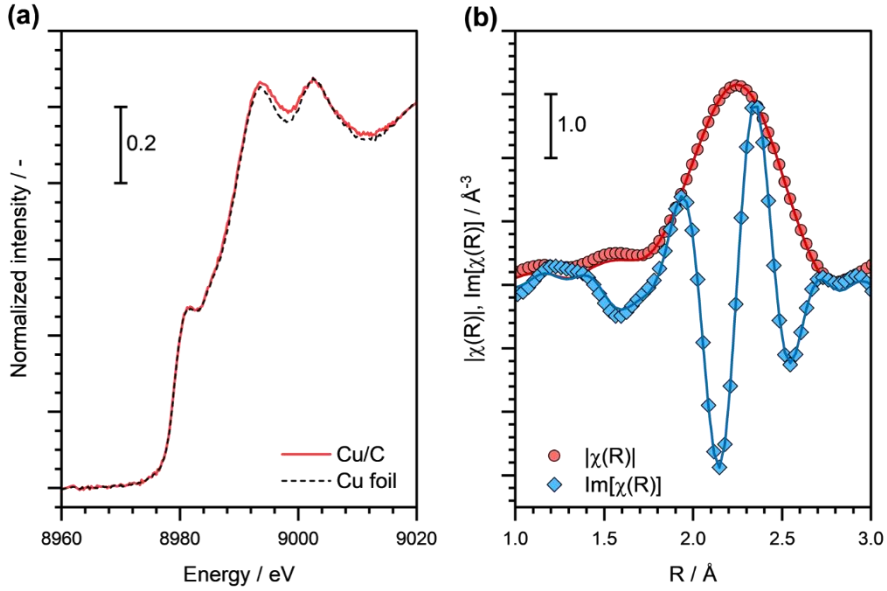

Figure S2-5. (a) X-ray absorption near edge structure (XANES) of Cu/C. The XANES of Cu reference foil is also shown for comparison. (b) Fourier-transformed extended x-ray absorption fine structure (FT-EXAFS) of Cu/C. Experimental data are shown as closed symbols and the corresponding fits are shown as solid lines.

Table S2-1. Fitting results: coordination numbers (CN), interatomic distances (*d*), and Debye-Waller factors (σ^2), for EXAFS of Cu/C and Cu reference foil. Fitting parameters: $S_0^2 = 0.93$, $\Delta E_0 = 4.5$ Å. The fitting was performed simultaneously on k^1-, k^2-, and k^3- weighted data in *q*-space (k-range: 2.4 – 11.5 $Å^{-1}$ and R-range: 1 – 3 Å).

	$CN_{Cu–Cu}$	$d_{Cu–Cu}$ /Å	$\sigma^2 \times 10^3$ /$Å^2$
Cu/C	10.1 ± 0.6	2.545 ± 0.002	8.6 ± 0.5
Cu foil	12[a]	2.544 ± 0.002	9.0 ± 0.4

[a]This parameter was fixed during the fit.

The Cu K-edge X-ray absorption spectroscopy (XAS) measurements were performed using an easyXAFS300+ spectrometer system equipped with a ProtoXRD XRT60 x-ray tube and AXAS-M silicon drift detector (SDD) from KETEK GmbH. Monochromatic x-rays were obtained using a Si553 spherically bent crystal analyzers.

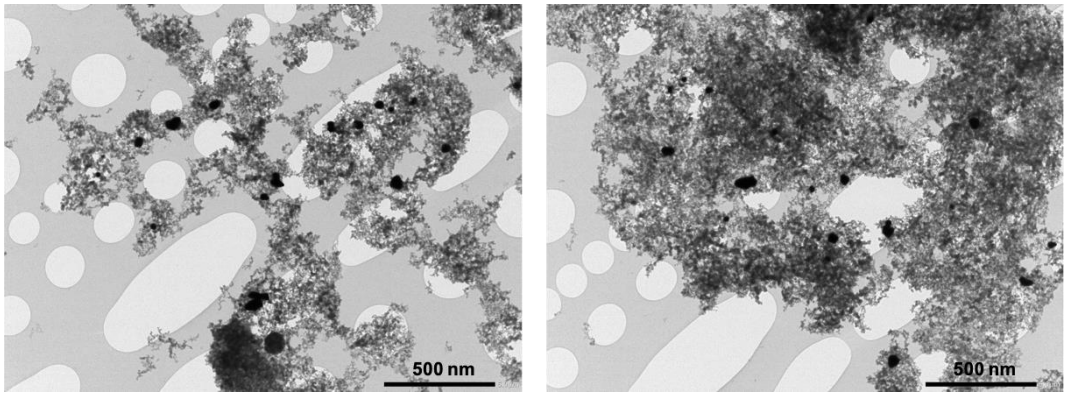

Figure S2-6. Transmission electron microscopy (TEM) images of Cu/C. The TEM micrographs were recorded on a JEOL JEM-2011 scanning TEM with an accelerating voltage of 120 keV.

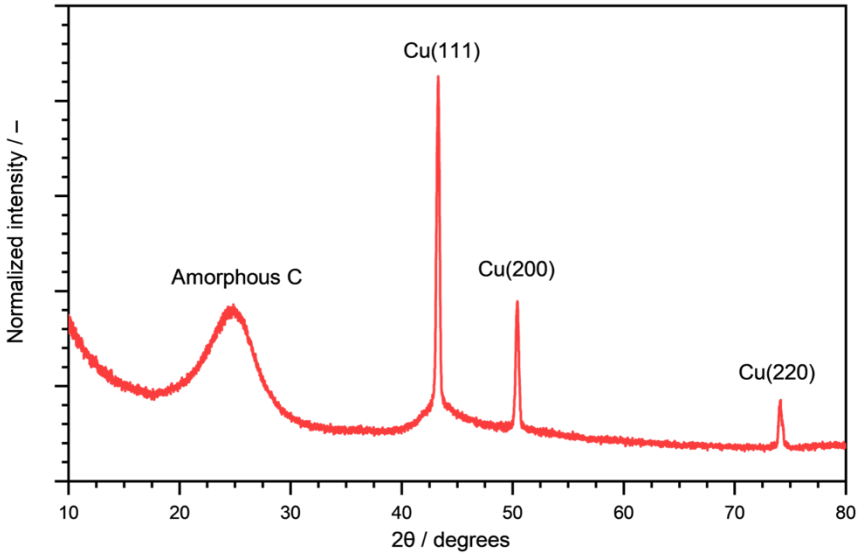

Figure S2-7. Powder X-ray diffractogram of Cu/C. The X-ray diffraction pattern was collected using a Philips X'Pert Pro System, with Cu-Kα radiation source operating at 45 kV and 40 mA. The sample was measured with a scanning rate of 0.02 degree·s^{-1} in 2θ range between 10° and 80°.

2.5.3. Supplementary Figures and Tables

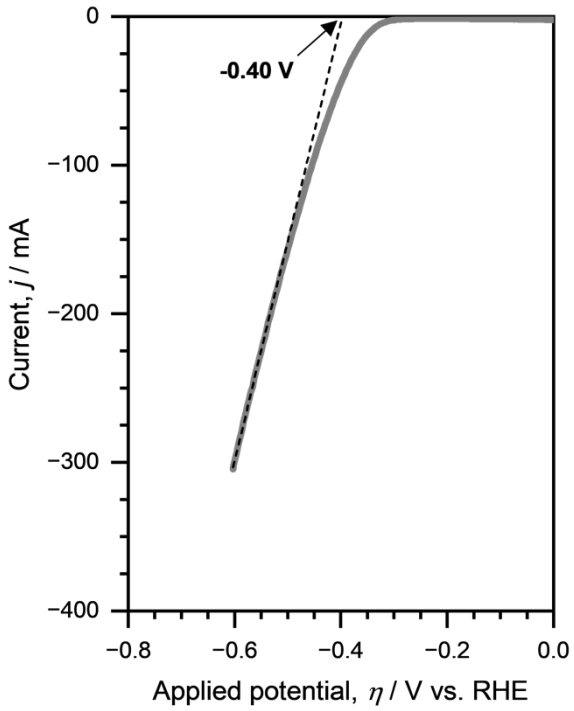

Figure S2-8. (a) Linear sweep voltammetry (LSV) curves (scan rate = 1 $mV \cdot s^{-1}$) on Cu/C with 20 mM benzaldehyde. Reaction conditions: 20 mM benzaldehyde, 1.5 M acetate buffer solution (pH ~4.6), room temperature, ambient pressure.

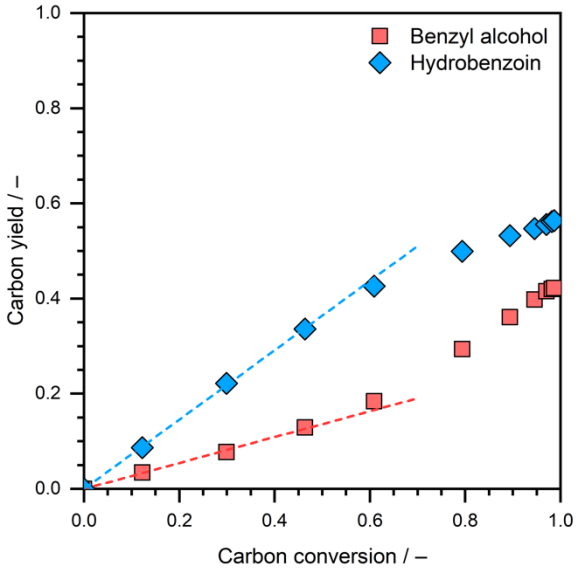

Figure S2-9. Yield *versus* conversion (on a carbon basis) plots during benzaldehyde ECH on Cu/C. Reaction conditions: 20 mM benzaldehyde, applied potential –0.5 V *vs* RHE, 1.5 M acetate buffer solution (pH ~4.6), room temperature, ambient pressure. The dashed lines are linear fits.

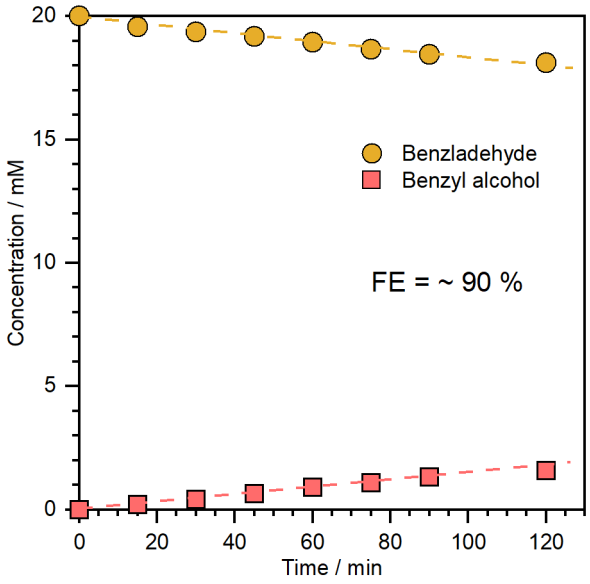

Figure S2-10. Concentration profiles of reactants and products during benzaldehyde ECH on carbon black. Reaction conditions: 20 mM benzaldehyde, η = –0.5 V vs. RHE, 1.5 M acetate buffer solution (pH ~4.6), room temperature, ambient pressure. The dashed lines are guides to the eye.

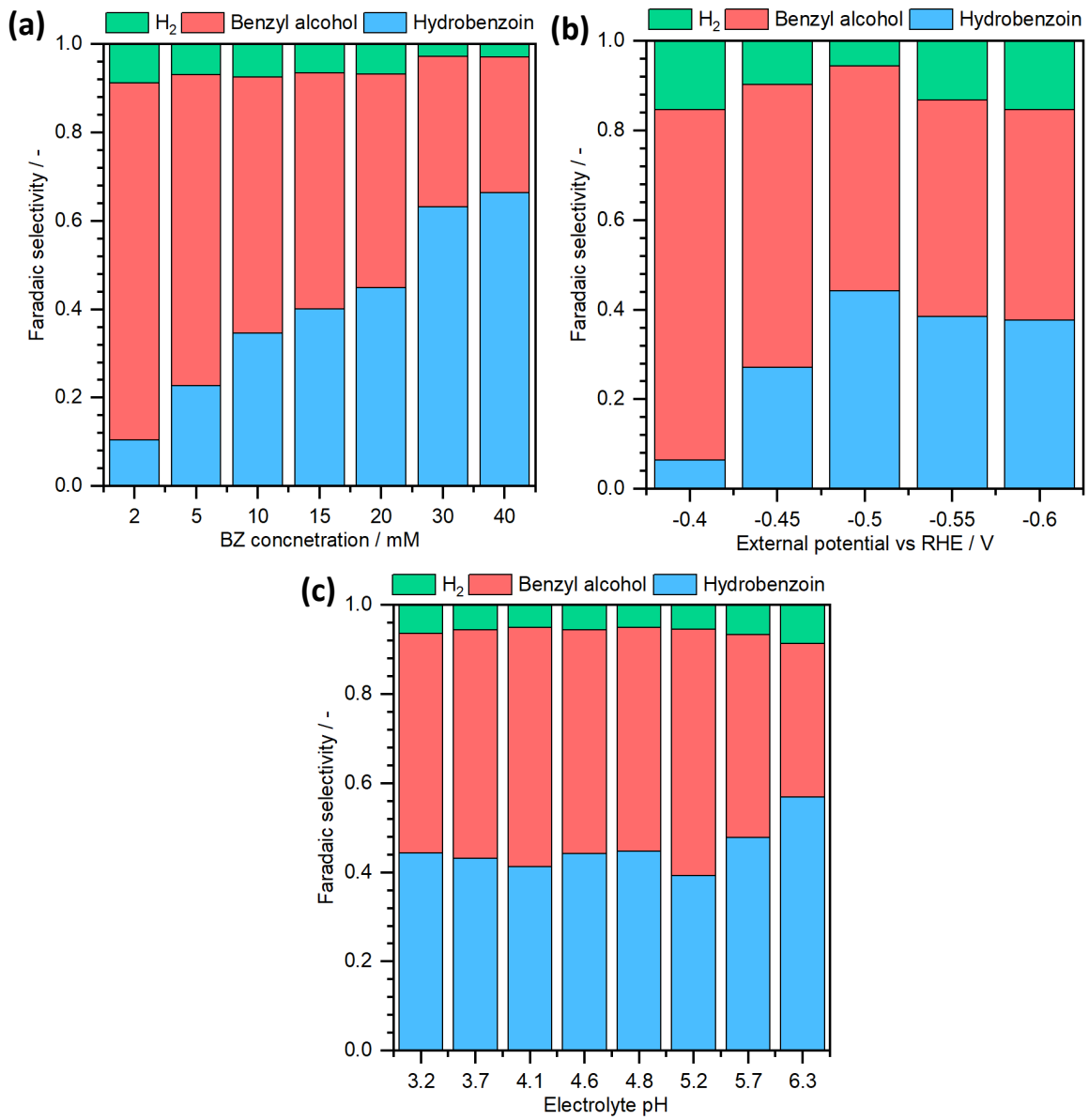

Figure S2-11. Benzyl alcohol, hydrobenzoin, and H_2 Faradic efficiency, during benzaldehyde ECH on Cu/C, as a function (a) initial benzaldehyde concentration (a_{BZ}), (b) η, and (c) H_3O^+ activity ($a_{H_3O^+}$). Reaction conditions: 2 – 40 mM benzaldehyde, η = –0.4 to –0.6 V vs. RHE, 1.5 M acetate buffer solution (pH 3.2 – 6.3), room temperature, ambient pressure.

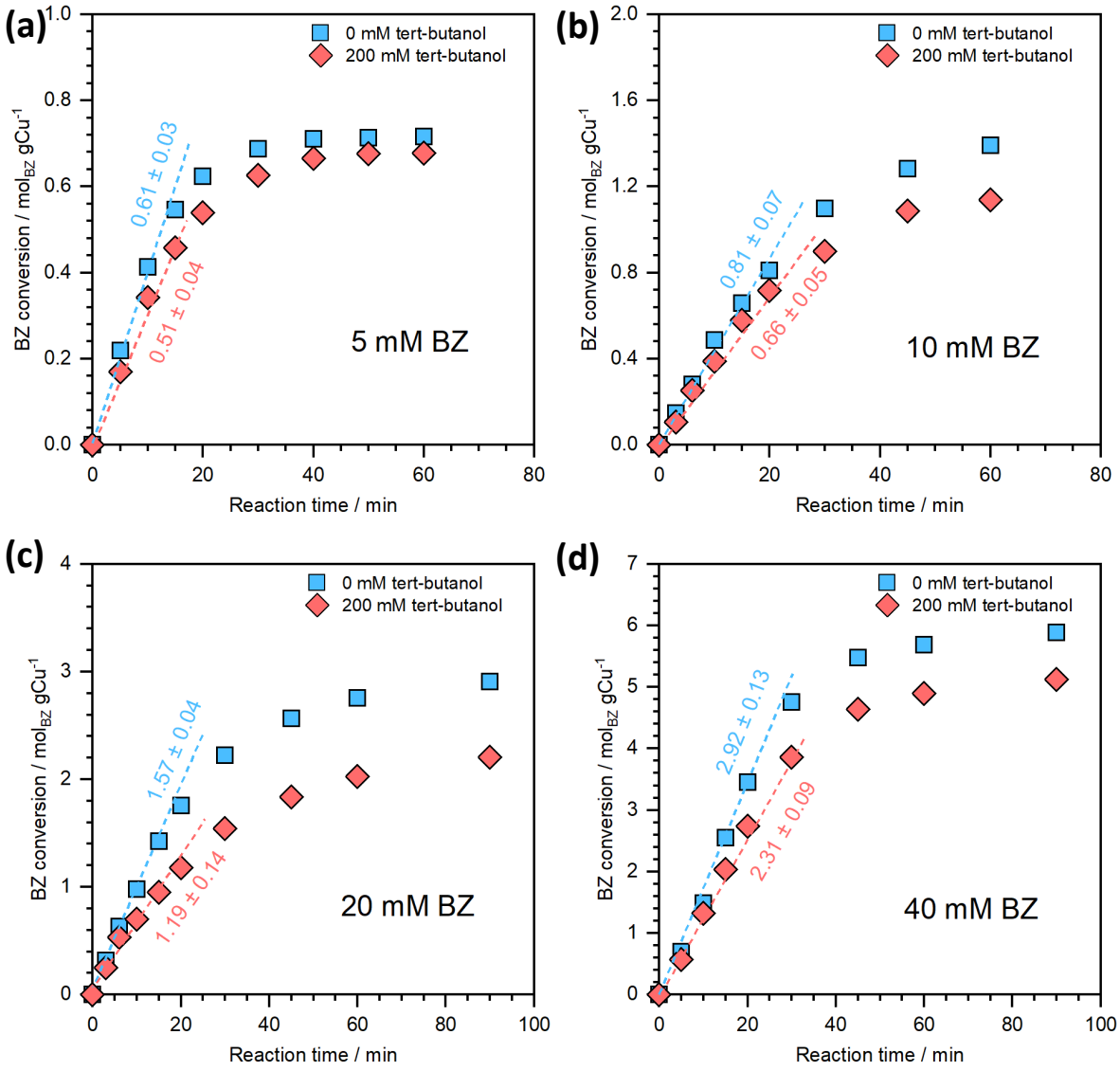

Figure S2-12. Benzaldehyde conversion as a function of reaction time during benzaldehyde ECH with or without *t*-butanol (*t*-BuOH) on Cu/C with initial benzaldehyde concentration of 5 mM (a), 10 mM (b), 20 mM (c) and 40 mM (d). Reaction conditions: 5 - 40 mM benzaldehyde, 0 mM or 200 mM *t*- BuOH, η = –0.5 V vs. RHE, 1.5 M acetate buffer solution (pH ~4.6), room temperature, ambient pressure. The dashed lines are linear fits, and the reported numbers are the initial benzaldehyde conversion rates in $mmol_{BZ} \cdot g_{Cu}^{-1} \cdot s^{-1}$.

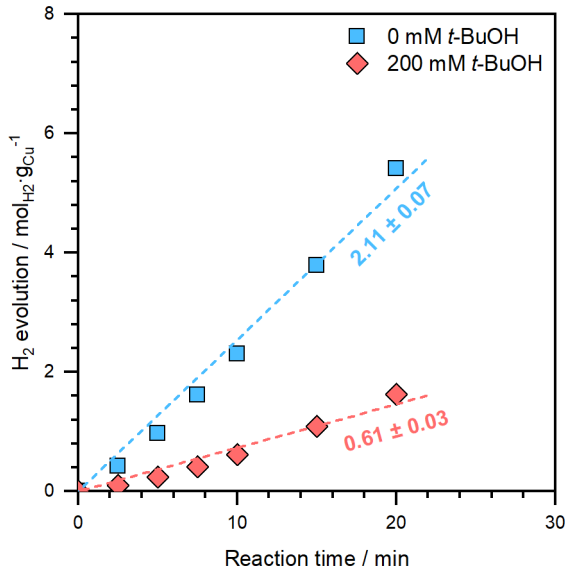

Figure S2-13. H_2 evolution as a function of reaction time during HER with or without *t*- BuOH on Cu/C. Reaction conditions: 0 mM or 200 mM *t*- BuOH, η = –0.5 V *vs* RHE, 1.5 M acetate buffer solution (pH ~4.6), room temperature, ambient pressure. The dashed lines are linear fits, and the reported numbers are the initial HER rates in $mmol_{H2}·g_{Cu}^{-1}·s^{-1}$.

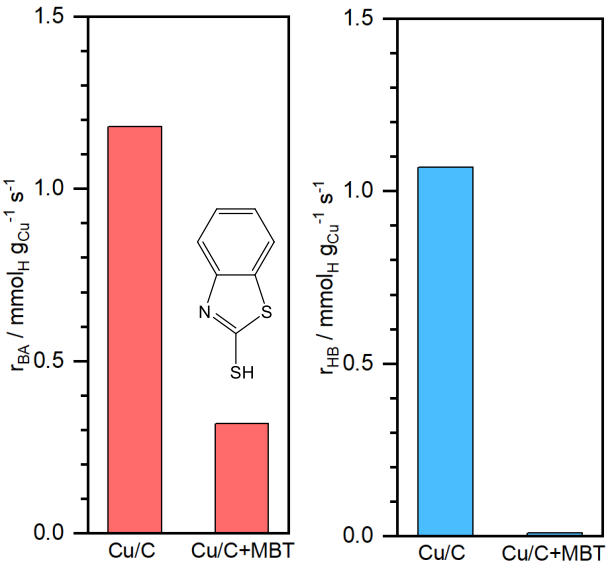

Figure S2-14. Benzyl alcohol and hydrobenzoin formation rates during benzaldehyde ECH on Cu/C and Cu/C-MBT electrodes. Reaction conditions: 20 mM benzaldehyde, η = –0.5 V vs. RHE, 1.5 M acetate buffer solution (pH ~4.6), room temperature, ambient pressure.

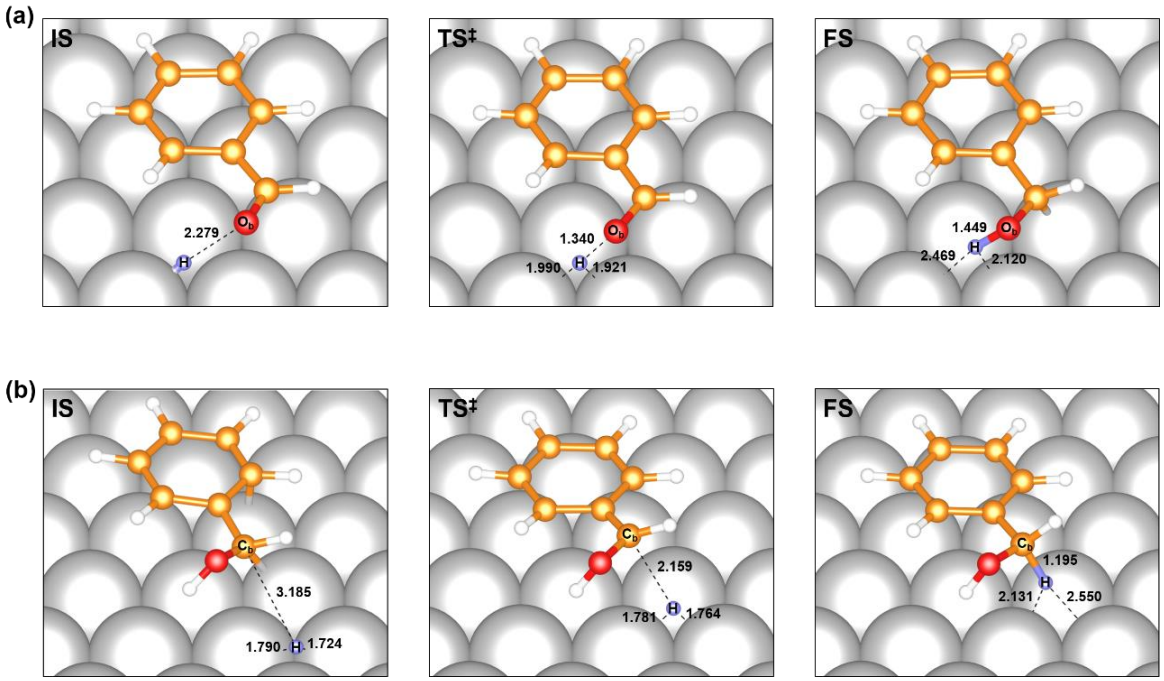

Figure S2-15. Initial (IS), transition (TS‡), and final (FS) states for H addition to adsorbed benzaldehyde molecule *via* the Langmuir-Hinshelwood type surface reaction between BZ* and H* on Cu(111) surface.

Table S2-2. Initial rates (in $mmol_{H}{\cdot}g_{Cu}^{-1}{\cdot}s^{-1}$) of benzyl alcohol, hydrobenzoin, and H_2 formation during benzaldehyde ECH on Cu/C, Cu/C/O_3-2h, and Cu/C/O_3-4h. The corresponding Faradaic selectivities are shown in parentheses. Reaction conditions: 20 mM benzaldehyde, applied potential –0.5 V *vs* RHE, 1.5 M acetate buffer solution (pH ~4.6), room temperature ambient pressure.

	Cu/C	Cu/C/O_3-2h	Cu/C/O_3-4h
Benzyl alcohol	1.23 (0.48)	2.27 (0.57)	2.28 (0.44)
Hydrobenzoin	1.09 (0.43)	1.41 (0.36)	2.40 (0.46)
H_2	0.24 (0.09)	0.29 (0.07)	0.51 (0.10)

2.5.4. Additional Calculation Details

The conversion of a reactant i at a given time t was estimated by

$$\chi_i(t) = \frac{n_i(t)}{n_i^0} \qquad (2\text{-}12)$$

where $n_i(t)$ is the amount of reactant detected at time t and n_i^0 is the initial amount of reactant in the electrolyte.

Similarly, the yield of a product j with respect to a reactant i at any given time t was estimated by

$$Y_j(t) = \frac{n_j(t)}{n_i^0} \quad (2\text{-}13)$$

where $n_j(t)$ is the amount of reactant j detected at time t and n_i^0 is the initial amount of reactant i in the electrolyte solution.

The initial ECH rate of a product i (in terms of H consumed per gram metal) was calculated from the initial slope (m_i) of the product i formed *vs* time plot using the following equation

$$r_i = \frac{m_i \times \epsilon_i}{w_{cat} \times x_{metal}} \quad (2\text{-}14)$$

where w_{cat} is the amount of catalyst, x_{metal} is the metal loading on the catalyst (as weight fraction), and ϵ_i is the number of H atoms required to form the product i.

The Faradaic efficiency towards the formation of a product i was estimated by

$$FE_i = \frac{q_i}{q_{total}} \quad (2\text{-}15)$$

where q_i is the electrons consumed towards formation of product i, and q_{total} is the total electrons consumed.

2.5.5. Additional Computational Details

All quantum chemical calculations were performed on a periodic electrode-electrolyte interface model using the Vienna *ab initio* simulation package (VASP) with a plane wave basis set.[41-44] The single-electron wavefunctions were estimated using the employed basis set truncated at an energy cut-off of 400 eV. The k-points for these wavefunction calculations were sampled from a grid size 2 × 2 × 1 in the Brillouin zone. The partial occupancies were set for each orbital using the Methfessel-Paxton scheme to smoothen the wavefunctions.[55] Using projector augmented-wave (PAW) method, the core electrons were treated with the frozen-core approximations, while the valence electron wavefunctions were calculated using the plane wave basis set.[56] Further, to determine electron density from these wavefunctions, the electron self-interaction contribution in the Hartree potential was corrected using generalized gradient approximation (GGA) Perdew-Burke-Ernzerhof (PBE) exchange correlation functional with additional dispersion corrections using the Becke-Johnson (BJ) damping scheme.[57,58] The open-

source VASPsol package was used to implement implicit solvent in all *ab initio* simulations.[59] The Bader charge analysis was performed using the code available from Henkelman and co-workers.[60]

All simulations were performed on a 4 × 4 × 4 supercell of Cu(111) surface, cleaved from bulk Cu with lattice constant of 3.59 Å, and a vacuum of at least 10 Å above the water layer. The top two layers of the Cu(111) slab, representing the surface atoms were not constrained during simulations, while the bottom two layers were fixed representing bulk Cu. The electrode-electrolyte interface was modelled using 15 explicit H_2O molecules in addition to one proton and reaction intermediates above the Cu(111) surface. The system was first relaxed using *ab initio* molecular dynamics (AIMD) simulations. The AIMD simulations were performed using a canonical ensemble at constant temperature (300 K) and volume (NVT). To maintain constant temperature, Nosé-Hoover thermostat was employed with a time constant of 0.01 ps. AIMD simulation were carried out for at least 5 ps with a time step of 0.5 fs while maintaining the energy and force convergence at 1×10^{-5} eV and 5×10^{-2} eV·Å^{-1}, respectively. The selected configurations from AIMD simulations were further optimized using density functional theory (DFT). Three different reaction pathways were investigated: first H addition, second H addition, and C–C coupling. The H addition *via* PCET mechanism was modelled by adding a H^+ to the water layer near the interface and an e^- to the metal surface, while the Langmuir-Hinshelwood type surface hydrogenation was modeled using H atoms (H*) adsorbed on Cu. The transition states (TS) for each step were identified using the climbing image-nudged elastic band technique (cl-NEB).[61] For this, eight frames were developed between the initial state (IS) and the final state (FS) to observe a minimum energy path along the reaction coordinate.

We note that the workfunction (ϕ), or the surface potential (U), of the metal surface varies between the IS, TS, and FS, especially in the PCET steps. The obtained potential energies were therefore corrected using the method developed by Chan and Norskov.[62] Based on this method, the difference in the energy between state 1 and state 2 at a given potential is given by

$$E_2(\phi_1) - E_1(\phi_1) = E_2(\phi_2) - E_1(\phi_1) + \frac{(q_2 - q_1)(\phi_2 - \phi_1)}{2} \qquad (2\text{-}16)$$

where ϕ_i is the work function at state i and q_i is the charge on the surface (with adsorbates) at state i. For all states, the charge was estimated using Bader charge analysis. Furthermore,

the work function (ϕ_i) at state i was related to the surface potential of Cu(III) surface using the following relation

$$U_{i,SHE} = \frac{\phi_i - \phi_{SHE}}{e} \qquad (2\text{-}17)$$

where $U_{i,SHE}$ is the surface potential of Cu(111) relative to SHE at state i, and ϕ_i and ϕ_{SHE} are the work functions of Cu(111) at state i and that of SHE (equal to 4.44 eV), respectively.

2.6 References

1. Iris, K. M. "Mechanistic understanding of the catalytic hydrogenation of bio-derived aromatics." Green Chemistry 23.23 (2021): 9239-9253.
2. Chheda, Juben N., and James A. Dumesic. "An overview of dehydration, aldol-condensation and hydrogenation processes for production of liquid alkanes from biomass-derived carbohydrates." Catalysis Today 123.1-4 (2007): 59-70.
3. Serrano-Ruiz, Juan Carlos, Rafael Luque, and Antonio Sepúlveda-Escribano. "Transformations of biomass-derived platform molecules: from high added-value chemicals to fuels via aqueous-phase processing." Chemical Society Reviews 40.11 (2011): 5266-5281.
4. Jahirul, Mohammad I., et al. "Biofuels production through biomass pyrolysis—a technological review." Energies 5.12 (2012): 4952-5001.
5. Chheda, Juben N., George W. Huber, and James A. Dumesic. "Liquid-phase catalytic processing of biomass-derived oxygenated hydrocarbons to fuels and chemicals." Angewandte Chemie International Edition 46.38 (2007): 7164-7183.
6. Robinson, Allison M., Jesse E. Hensley, and J. Will Medlin. "Bifunctional catalysts for upgrading of biomass-derived oxygenates: a review." ACS catalysis 6.8 (2016): 5026-5043.
7. Gürbüz, Elif I., Edward L. Kunkes, and James A. Dumesic. "Integration of C–C coupling reactions of biomass-derived oxygenates to fuel-grade compounds." Applied Catalysis B: Environmental 94.1-2 (2010): 134-141.
8. Chadderdon, Xiaotong H., et al. "Mechanisms of furfural reduction on metal electrodes: Distinguishing pathways for selective hydrogenation of bioderived oxygenates." Journal of the American Chemical Society 139.40 (2017): 14120-14128.

9. Akhade, Sneha A., et al. "Electrocatalytic hydrogenation of biomass-derived organics: a review." Chemical reviews 120.20 (2020): 11370-11419.
10. Yang, Ming, et al. "Recent progress on electrocatalytic valorization of biomass-derived organics." Energy & Environmental Materials 5.4 (2022): 1117-1138.
11. Li, Kui, and Yujie Sun. "Electrocatalytic upgrading of biomass-derived intermediate compounds to value-added products." Chemistry–A European Journal 24.69 (2018): 18258-18270.
12. Song, Yang, et al. "Integrated catalytic and electrocatalytic conversion of substituted phenols and diaryl ethers." Journal of catalysis 344 (2016): 263-272.
13. Song, Yang, et al. "Aqueous phase electrocatalysis and thermal catalysis for the hydrogenation of phenol at mild conditions." Applied Catalysis B: Environmental 182 (2016): 236-246.
14. Bondue, C. J., and M. T. M. Koper. "A mechanistic investigation on the electrocatalytic reduction of aliphatic ketones at platinum." Journal of catalysis 369 (2019): 302-311.
15. Kwon, Youngkook, et al. "Electrocatalytic conversion of furanic compounds." ACS Catalysis 6.10 (2016): 6704-6717.
16. Sanyal, Udishnu, et al. "Electrocatalytic hydrogenation of oxygenated compounds in aqueous phase." Organic Process Research & Development 22.12 (2018): 1590-1598.
17. Matthiesen, John E., et al. "Electrochemical conversion of muconic acid to biobased diacid monomers." ACS Sustainable Chemistry & Engineering 4.6 (2016): 3575-3585.
18. Matthiesen, John E., et al. "Electrochemical conversion of biologically produced muconic acid: key considerations for scale-up and corresponding technoeconomic analysis." ACS Sustainable Chemistry & Engineering 4.12 (2016): 7098-7109.
19. Anibal, Jacob, and Bingjun Xu. "Electroreductive C–C coupling of furfural and benzaldehyde on Cu and Pb surfaces." ACS Catalysis 10.19 (2020): 11643-11653.
20. Yu, Jia, et al. "Electroreductive coupling of benzaldehyde by balancing the formation and dimerization of the ketyl intermediate." Nature Communications 13.1 (2022): 7909.
21. Zhang, Xingguang, Karen Wilson, and Adam F. Lee. "Heterogeneously catalyzed hydrothermal processing of C_5–C_6 sugars." Chemical reviews 116.19 (2016): 12328-12368.
22. Wan, Yan, and Jong-Min Lee. "Toward value-added dicarboxylic acids from biomass

derivatives via thermocatalytic conversion." ACS Catalysis 11.5 (2021): 2524-2560.

23. Wang, Suheng, et al. "Highly efficient ethylene production via electrocatalytic hydrogenation of acetylene under mild conditions." Nature Communications 12.1 (2021): 7072.
24. Zhang, Lijuan, et al. "A review of thermal catalytic and electrochemical hydrogenation approaches for converting biomass-derived compounds to high-value chemicals and fuels." Fuel Processing Technology 226 (2022): 107097.
25. Huang, Yao-Bing, et al. "Production of high quality fuels from lignocellulose-derived chemicals: a convenient C–C bond formation of furfural, 5-methylfurfural and aromatic aldehyde." Rsc Advances 2.30 (2012): 11211-11214.
26. Mou, Zehuai, Shuo Kelvin Feng, and Eugene YX Chen. "Bio-based difuranic polyol monomers and their derived linear and cross-linked polyurethanes." Polymer Chemistry 7.8 (2016): 1593-1602.
27. Liu, Dajiang, and Eugene Y-X. Chen. "Diesel and alkane fuels from biomass by organocatalysis and metal–acid tandem catalysis." ChemSusChem 6.12 (2013): 2236-2239.
28. Song, Yang, et al. "Hydrogenation of benzaldehyde via electrocatalysis and thermal catalysis on carbon-supported metals." Journal of Catalysis 359 (2018): 68-75.
29. Singh, Nirala, et al. "Aqueous phase catalytic and electrocatalytic hydrogenation of phenol and benzaldehyde over platinum group metals." Journal of catalysis 382 (2020): 372-384.
30. Yuk, Simuck F., et al. "First-principle investigation on catalytic hydrogenation of benzaldehyde over Pt-group metals." Catalysis Today 388 (2022): 208-215.
31. Lopez-Ruiz, Juan A., et al. "Understanding the role of metal and molecular structure on the electrocatalytic hydrogenation of oxygenated organic compounds." ACS Catalysis 9.11 (2019): 9964-9972.
32. Andrews, Evan, et al. "Performance of base and noble metals for electrocatalytic hydrogenation of bio-oil-derived oxygenated compounds." ACS sustainable chemistry & engineering 8.11 (2020): 4407-4418.
33. Anibal, Jacob, Arnav Malkani, and Bingjun Xu. "Stability of the ketyl radical as a descriptor in the electrochemical coupling of benzaldehyde." Catalysis Science & Technology 10.10 (2020): 3181-3194.

34. Guena, Thierry, and Derek Pletcher. "Electrosyntheses from aromatic aldehydes in a flow cell. Part I. The reduction of benzaldehyde." Acta Chemica Scandinavica 52 (1998): 23-31.
35. Koh, Katherine, et al. "Electrochemically tunable proton-coupled electron transfer in Pd-catalyzed benzaldehyde hydrogenation." Angewandte Chemie 132.4 (2020): 1517-1521.
36. Sanyal, Udishnu, et al. "Hydrogen bonding enhances the electrochemical hydrogenation of benzaldehyde in the aqueous phase." Angewandte Chemie 133.1 (2021): 294-300.
37. Cheng, Guanhua, et al. "Critical role of solvent-modulated hydrogen-binding strength in the catalytic hydrogenation of benzaldehyde on palladium." Nature Catalysis 4.11 (2021): 976-985.
38. Lopez-Ruiz, Juan A., et al. "Kinetic investigation of the sustainable electrocatalytic hydrogenation of benzaldehyde on Pd/C: effect of electrolyte composition and half-cell potentials." ACS sustainable chemistry & engineering 6.12 (2018): 16073-16085.
39. Nguyen, Manh-Thuong, et al. "Electro-reduction of organics on metal cathodes: A multiscale-modeling study of benzaldehyde on Au (111)." Catalysis Today 350 (2020): 39-46.
40. Cantu, David C., et al. "A combined experimental and theoretical study on the activity and selectivity of the electrocatalytic hydrogenation of aldehydes." ACS Catalysis 8.8 (2018): 7645-7658.
41. Kresse, Georg, and Jürgen Furthmüller. "Efficiency of ab-initio total energy calculations for metals and semiconductors using a plane-wave basis set." Computational materials science 6.1 (1996): 15-50.
42. Kresse, Georg, and Jürgen Furthmüller. "Efficient iterative schemes for ab initio total-energy calculations using a plane-wave basis set." Physical review B 54.16 (1996): 11169.
43. Kresse, Georg, and Jürgen Hafner. "Ab initio molecular-dynamics simulation of the liquid-metal–amorphous-semiconductor transition in germanium." Physical Review B 49.20 (1994): 14251.
44. Kresse, Georg, and Jürgen Hafner. "Ab initio molecular dynamics for liquid metals." Physical review B 47.1 (1993): 558.
45. Shinagawa, Tatsuya, Angel T. Garcia-Esparza, and Kazuhiro Takanabe. "Insight on Tafel slopes from a microkinetic analysis of aqueous electrocatalysis for energy conversion."

Scientific reports 5.1 (2015): 13801.

46. Lasia, Andrzej. "Mechanism and kinetics of the hydrogen evolution reaction." international journal of hydrogen energy 44.36 (2019): 19484-19518.
47. Sharifi-Asl, Samin, and Digby D. Macdonald. "Investigation of the kinetics and mechanism of the hydrogen evolution reaction on copper." Journal of The Electrochemical Society 160.6 (2013): H382.
48. Xue, Yurui, et al. "Self-catalyzed growth of Cu@ graphdiyne core–shell nanowires array for high efficient hydrogen evolution cathode." Nano Energy 30 (2016): 858-866.
49. Anantharaj, Sengeni, et al. "The pitfalls of using potentiodynamic polarization curves for Tafel analysis in electrocatalytic water splitting." ACS Energy Letters 6.4 (2021): 1607-1611.
50. Raoof, Jahan-Bakhsh, et al. "MOF-derived Cu/nanoporous carbon composite and its application for electro-catalysis of hydrogen evolution reaction." Energy 90 (2015): 1075-1081.
51. Nivetha, Ravi, et al. "Cu based Metal Organic Framework (Cu-MOF) for electrocatalytic hydrogen evolution reaction." Materials Research Express 7.11 (2020): 114001.
52. Gu, Zhenao, et al. "Simultaneous phenol removal and resource recovery from phenolic wastewater by electrocatalytic hydrogenation." Environmental Science & Technology 56.7 (2022): 4356-4366.
53. Mao, Ran, et al. "Enhanced indirect atomic H* reduction at a hybrid Pd/graphene cathode for electrochemical dechlorination under low negative potentials." Environmental Science: Nano 5.10 (2018): 2282-2292.
54. Buxton, George V., et al. "Critical Review of rate constants for reactions of hydrated electrons, hydrogen atoms and hydroxyl radicals (· OH/· O^- in Aqueous Solution." Journal of physical and chemical reference data 17.2 (1988): 513-886.
55. Methfessel, M. P. A. T., and A. T. Paxton. "High-precision sampling for Brillouin-zone integration in metals." physical review B 40.6 (1989): 3616.
56. Blöchl, Peter E. "Projector augmented-wave method." Physical review B 50.24 (1994): 17953.
57. Grimme, Stefan, Stephan Ehrlich, and Lars Goerigk. "Effect of the damping function in

dispersion corrected density functional theory." Journal of computational chemistry 32.7 (2011): 1456-1465.

58. Hammer, B. H. L. B., Lars Bruno Hansen, and Jens Kehlet Nørskov. "Improved adsorption energetics within density-functional theory using revised Perdew-Burke-Ernzerhof functionals." Physical review B 59.11 (1999): 7413.
59. Mathew, Kiran, et al. "Implicit solvation model for density-functional study of nanocrystal surfaces and reaction pathways." The Journal of chemical physics 140.8 (2014).
60. Tang, W., E. Sanville, and G. Henkelman. "A grid-based Bader analysis algorithm without lattice bias." Journal of Physics: Condensed Matter 21.8 (2009): 084204.
61. Henkelman, Graeme, Blas P. Uberuaga, and Hannes Jónsson. "A climbing image nudged elastic band method for finding saddle points and minimum energy paths." The Journal of chemical physics 113.22 (2000): 9901-9904.
62. Chan, Karen, and Jens K. Nørskov. "Electrochemical barriers made simple." The journal of physical chemistry letters 6.14 (2015): 2663-2668.

Chapter 3

Electrocatalytic conversion of benzaldehyde on Cu in alkaline media

Aqueous phase electrochemical hydrogenation (ECH) of benzaldehyde on Cu/C under alkaline conditions ($pH = 9.1 – 12.3$) forms benzyl alcohol and hydrobenzoin with high selectivity towards the C–C coupling product (Faradaic selectivity towards hydrobenzoin ≥ 0.84). The rate-determining step (RDS) for benzyl alcohol formation is the H addition to the radical α-C of the surface hydroxy intermediate, while that for hydrobenzoin formation is the H addition to the carbonyl O of the adsorbed benzaldehyde molecule. The subsequent C–C bond formation and H addition steps are fast. In the absence of benzaldehyde (i.e., in a pure electrolyte solution), the RDS for H_2 evolution reaction (HER) on Cu/C in alkaline media is the dissociation of H_2O on the surface to form H* (i.e., the Volmer step). The H addition in alkaline media occurs primarily via a proton-coupled electron-transfer (PCET) type mechanism wherein H_2O molecules act as the proton source (forming OH^- in the process). The high selectivity towards C–C coupling in alkaline media is due to slow H addition kinetics, which can be attributed to a shift in the H source – from solvated hydronium ions in acidic media to water molecules in alkaline media. The electrolyte pH and the concentration of Na^+ cations influence the kinetics of HER and benzaldehyde ECH. Increasing the electrolyte pH enhances the activity by indirectly increasing the near-surface Na^+ concentration, which in turn influences the kinetics of H addition steps by favoring the dissociation of H_2O.

This chapter is based on the article: Hongwen Chen et al. Electrocatalytic conversion of benzaldehyde on Cu in alkaline media (submitted to ***Journal of the American Chemical Society***). Hongwen Chen performed the experiments, did the data analysis and wrote the manuscript.

3.1 Introduction

The demand for energy carriers coupled with critical climate change concerns resulting from fossil fuel usage has driven considerable efforts in developing sustainable and eco-friendly energy storage and transformative technologies.[1-3] Biomass is a renewable carbon resource; its employment does not disrupt the carbon equilibrium of our existing ecosystem, as it sequesters carbon that is currently in the atmosphere.[4, 5] However, adding biomass to the present carbon-based economy requires its upgrading to fuel-range hydrocarbons and value-added chemicals.

Thermochemical upgrading of biomass typically involves the reduction (or hydrogenation) and eventually elimination of oxygenated functional groups or C–C coupling to increase the molecular weight at elevated temperatures and pressures.[6, 7] Electrochemical hydrogenation (ECH) is a viable alternative wherein hydrogen is generated in situ from an aqueous electrolyte solution when an external electric field is applied. The formed hydride species (H*) can subsequently react with the biomass-derived organic substrates under milder reaction conditions.[8-11]

Benzaldehyde, the simplest aldehyde molecule, is an ideal model compound to investigate the electrochemical reduction of carbonyl groups and C–C coupling. During benzaldehyde ECH on metal electrodes, two primary products have been reported: (i) benzyl alcohol as the carbonyl hydrogenation product and (ii) hydrobenzoin as the C–C coupling product. Although benzaldehyde hydrogenation to benzyl alcohol has been observed on several metal-based electrocatalysts (*e.g.*, Pd, Pt, Rh, and Cu),[12-15] its electroreduction to hydrobenzoin has been observed only on Cu- and Pb-based electrocatalysts.

We have recently reported on the ability of Cu to catalyze both C=O hydrogenation and C–C coupling ECH reaction.[16] Both benzyl alcohol and hydrobenzoin were reported as the primary products with similar Faradaic selectivities (~45%).[16] In the proposed mechanism, an adsorbed benzaldehyde molecule undergoes the first H addition on its carbonyl O to form a surface hydroxy intermediate, which subsequently undergoes a second H addition on its α-C to form benzyl alcohol. In a parallel reaction, the radical α-C of the hydroxy intermediate is attacked by the electrophilic carbonyl C of a physisorbed benzaldehyde molecule in an Eley-Rideal (ER)-type reaction to form the C–C bond. The C–C bond formation was accompanied by a fast H

addition to the radical O of the alkoxy intermediate to form hydrobenzoin. Combining kinetic and isotopic studies with first-principle molecular simulations, we showed that second H addition is the RDS for benzyl alcohol formation, while C–C bond formation is the RDS for hydrobenzoin formation.[16]

The composition of the electrolyte plays a vital role in determining the kinetics and mechanism of hydrogenation reactions. For example, Zhang et al. reported that the presence of alcohol in water-based electrolytes has a negative impact on benzaldehyde hydrogenation rate and Faradic efficiency towards benzaldehyde conversion due to decreased activity of the hydronium ions.[19] Electrolyte pH also plays an important role in the H_2 evolution and biomass hydrogenation reactions. In acidic electrolytes, for example, the hydronium ion activity, or in other words the electrolyte pH, has been shown to kinetically affect the hydrogenation rates.[17-21] Goyal et al. have shown that the activity of cations in the electrolyte also plays a central role in stabilizing the transition state of the rate determining Volmer step by favorably interacting with the dissociating H_2O molecule.[22, 23]

The HER kinetics in alkaline media are typically slow compared to those in acidic media. For example, the HER rate on Pt electrodes is generally ~2 to 3 orders of magnitude lower in alkaline solutions than in acidic solutions.[24] The slow HER kinetics in alkaline media is conventionally attributed to stronger binding of H to the metal surface, electrode-electrolyte interactions, as well as structural organization of the solvent molecules near the metal surface.[25-28] Notably, although solvated H_3O^+ ions have been proposed as the H source for both ECH and HER reactions in acidic media, Zhao et al., based on D_2O-labeling experiments, showed that molecular H_2O is the H source during the ECH of nitroarenes in alkaline media.[29] Water adsorbed on the surface of electrodes has also been identified as the proton source for electrochemical reduction reactions.[30] Finally, it has been suggested that the required dissociation of H_2O at the metal interface introduces an additional energy barrier, thus, decreasing the HER activity.[31]

Due to the slow HER kinetics, the electroreduction of organic substrates in alkaline media has been of interest owing to high Faradic efficiency towards organic conversion that has been observed in some cases.[32, 33] For example, Xia et al. reported that Cu nanoparticles exhibit high Faradaic efficiency (~96%) towards ethylamine conversion in alkaline solutions (at $\eta = -0.29$

V vs RHE) due to the suppressed competing HER on the cathode.[33] Chong et al. also reported very high Faradic efficiency (~95%) in alkaline media for the electroreduction of nitroarenes on CoP nanosheet cathodes.[32]

Alkaline electrolytes have also been suggested to provide a good platform for C–C coupling reactions.[34, 35] For example, Xiao et al. reported electro-hydrodimerization of furfural to hydrofuroin on a carbon electrode with a yield towards hydrofuroin of ~94% and a Faradaic efficiency of ~93% in a batch electrolyzer.[35] Dixit et al. have suggested that the presence of H* on the catalyst's surface significantly affects the product selectivity during furfural ECH in alkaline media.[34]

Thus, performing ECH in alkaline media has several advantages including suppressed HER and better selectivity towards C–C coupling products. Although several studies have investigated HER and electrochemical reduction of C_1 molecules (like CO and CO_2) in alkaline conditions, a detailed kinetic and mechanistic understanding of electroreduction of biomass-derived platform chemicals in alkaline media does not exist to our knowledge. In this work, we present a detailed kinetic and mechanistic investigation of HER and benzaldehyde ECH (to benzyl alcohol and hydrobenzoin) on Cu/C in alkaline electrolyte solutions ($pH = 9.1 – 12.3$).

3.2 Materials and methods

3.2.1 Chemicals

Benzaldehyde (99.5%), benzyl alcohol (99.8%), hydrobenzoin (99.0%), copper (II) acetate (99.9%), acetic acid (99.8%), sodium acetate (99.0%), sodium hydroxide (99.0%), sodium chloride (99.0%), 2-propanol (99.5%), diphenyl ether (99.0%), ethyl acetate (99.5%), *tert*-butanol (99.5%), 2-mercaptobenzothiazole (97%) and D_2O (99.9 atom% D) were purchased from Sigma-Aldrich and were used without further purification. Deionized (DI) water (18.2 $M\Omega \cdot cm^{-1}$) was used to prepare all aqueous solutions.

3.2.2 Catalyst synthesis

Cu/C (~5 wt.-% metal loading) was prepared *via* a previously described incipient-wetness impregnation method.[16] An aqueous solution of copper (II) acetate was added dropwise to a Vulcan XC72R carbon black (QUINTECH) support, mixed thoroughly, and dried overnight at

333 K. The resulting dried material was first treated in 100 mL·min^{-1} N_2 at 673 K (temperature ramp: 10 K·min^{-1}) for 4 h, followed by reduction in 100 mL·min^{-1} H_2 at 623 K (temperature ramp: 10 K·min^{-1}) for 4 h. These reduced catalysts are referred to as Cu/C. For the preparation of O_3-treated Cu/C catalyst, the carbon black support was first treated in O_3 at room temperature for 2 h or 4 h, followed by deposition of Cu *via* the incipient-wetness impregnation method described above. These O_3-treated catalysts are referred to as Cu/C/O_3-2h and Cu/C/O_3-4h, respectively.

3.2.3 Carbon felt pre-treatment.

Carbon felt (Sigma-Aldrich, 3.0 cm × 1.5 cm) was immersed sequentially in acetone, DI water, and acetone again for at least 30 min each under ultrasonication treatment at room temperature. Finally, the carbon felt was dried in an oven at 333 K for 12 h and stored for further use.

3.2.4 Electrode preparation.

The synthesized Cu/C catalyst (~10 mg) was dispersed in a solution of 1 mL 2-propanol and 1 mL DI water for 30 min under ultrasonication treatment at room temperature. The ink containing catalyst was then deposited on both sides of the pre-treated carbon felt. The carbon felt electrode (containing Cu/C) was then dried overnight in an oven at 333 K.

3.2.5 Nafion membrane pre-treatment.

A Nafion-117 proton exchange membrane (Ion Power) was first immersed in a 3 vol.-% H_2O_2 solution for ~1 h at 353 K. The membrane was then immersed in DI water at 353 K for 2 h. Subsequently, the membrane was immersed in 1 M H_2SO_4 at 353 K for ~1 h. Finally, the membrane was washed several times with DI water and stored in DI water under ambient conditions for further use.

3.2.6 Electrochemical measurements

All electrochemical experiments were performed using a BioLogic VSP-300 workstation using a two-compartment batch electrolysis cell. Cu/C deposited on a carbon felt was used as the working electrode. A double-junction Ag/AgCl (eDAQ) and a Pt wire (Sigma-Aldrich) were used as the reference electrode and counter electrode, respectively. The anode and cathode compartments were separated by the pretreated Nafion membrane. The reference Ag/AgCl

electrode was calibrated against a reversible hydrogen electrode (RHE), and all the potentials herein are reported relative to the RHE, per the following equation:

$$E_{RHE} = E_{\frac{Ag}{AgCl}} + 0.197 + 0.0591 \cdot pH \quad (1)$$

where E_{RHE} and $E_{\frac{Ag}{AgCl}}$ are electrode potentials relative to RHE and Ag/AgCl electrode potentials, respectively.

All electrochemical experiments were performed under ambient conditions. N_2 gas (~ 25 $mL \cdot min^{-1}$) was continuously bubbled through the electrolyte solution throughout the reaction to remove any dissolved gases. A stirring rate of 500 rpm allowed complete dissolution of organic in the electrolyte solution and overcame the mass transfer limitations. The solution resistance between working and reference electrodes was measured by potentiostatic electrochemical impedance spectroscopy (PEIS) and compensated (~85%) by the electrochemical workstation. Prior to the reaction, the catalysts were polarized at -40 mA for at least 20 min to ensure the complete reduction of the metal.

The LSV measurements were performed in either pure electrolyte or 20 mM benzaldehyde solution at a scan rate of 1 $mV \cdot s^{-1}$.

3.2.7 Product analysis

The course of benzaldehyde ECH experiments was followed by periodically withdrawing aliquots of ~1 mL from the cathode compartment. The products in the aqueous electrolyte were extracted with 0.5 ml ethyl acetate. The extract was then analyzed using an offline gas chromatograph coupled with a mass spectrometer (Agilent 7890B GC/5977A MSD).

The electron consumption towards H_2 formation was indirectly estimated from the difference in total electron consumption and electron consumption towards the formation of benzyl alcohol and hydrobenzoin. The amount of H_2 formed was calculated using the following equation:

$$n_{H_2} = \frac{q_{H_2}}{2 \cdot F} \quad (2)$$

where n_{H_2} is the amount of H_2 formed, q_{H_2} is the electron consumption towards H_2 formation, and F is the Faraday's constant.

3.2.8 Computational methods.

All quantum chemical calculations were performed on a periodic electrode-electrolyte

interface model using the Vienna ab initio simulation package (VASP) with a plane wave basis set.[41-44] The simulation were performed on a 4 × 4 × 4 supercell of Cu(111) surface, cleaved from bulk Cu with lattice constant of 3.59 Å, and a vacuum of at least 10 Å above the water layer. Implicit solvation model with additional explicit water molecules was used in all simulations. Detailed computational details are provided in the Supplementary Information **Section S3-3**.

3.3 Results and discussion

A Cu/C catalyst (with ~5 wt.-% Cu loading) was synthesized via a previously described incipient-wetness impregnation method using Vulcan carbon black as the support.[16] Detailed characterization of the synthesized Cu/C catalyst, including N_2 physisorption, X-ray absorption spectroscopy, X-ray diffraction and transmission electron microscopy have been reported previously.[16]

3.3.1 Mechanism of H_2 Evolution Reaction on Cu/C.

Let us first look at the H_2 formation on Cu/C in the absence of any organic substrate (i.e., in pure electrolyte solution). The mechanism of HER on metallic surfaces is typically described in terms of Volmer, Heyrovsky and Tafel steps.[22, 31] The Volmer step is a PCET process that forms surface hydrides (H*). It is followed by Heyrovsky and Tafel steps. The Heyrovsky step is an ER-type step wherein H* reacts with a proton (coupled with an electron transfer from the electrode's surface) to form H_2, whereas the Tafel step is a Langmuir-Hinshelwood (LH)-type surface recombination of two H* species to form H_2. In acidic solutions, solvated H_3O^+ ions act as proton donors in the Volmer and Heyrovsky steps. In alkaline media, on the other hand, the source of protons are the H_2O molecules.[22, 23] **Scheme 3-1** illustrates the HER steps in acidic and alkaline media in terms of the Volmer, Heyrovsky and Tafel steps.

The rates of Volmer, Heyrovsky and Tafel steps in alkaline media can be expressed as:

$$r_{Volmer} = k_{Volmer} \cdot e^{-\alpha f \eta} \cdot \theta_* \cdot a_{H_2O} \quad (3\text{-}1)$$

$$r_{Heyrovsky} = k_{Heyrovsky} \cdot e^{-\alpha f \eta} \cdot \theta_H \cdot a_{H_2O} \quad (3\text{-}2)$$

$$r_{Tafel} = k_{Tafel} \cdot \theta_H^2 \quad (3\text{-}3)$$

where k_{Volmer}, $k_{Heyrovsky}$ and k_{Tafel} are the respective kinetic rate constants, α is the electron transfer coefficient, f denotes F/RT (where F, R, and T denote the Faraday constant, the universal gas constant, and the temperature, respectively), θ_* and θ_H are the surface coverage of empty sites ($*$) and H*, respectively, and a_{H_2O} is the activity of water near the electrode's surface (*i.e.*, in the Helmholtz layer).

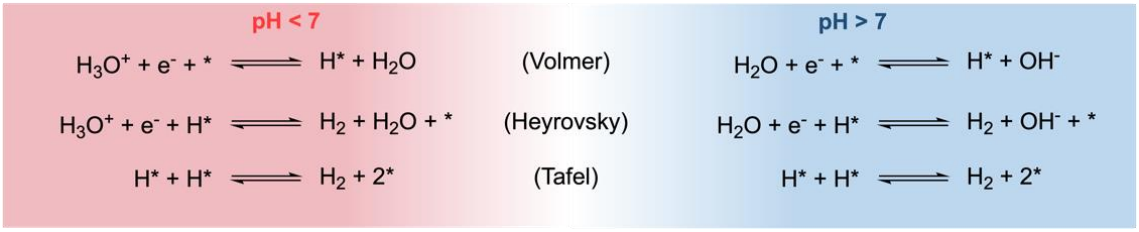

Scheme 3-1. Volmer, Heyrovsky, and Tafel steps for HER in acidic and alkaline media.

Figure 3-1a shows the linear sweep voltammetry (LSV) curve under HER conditions (i.e., in pure electrolyte solution) on Cu/C in alkaline electrolyte ($pH = 11.3$). Extrapolating the linear region of LSV curve, the onset potential of HER on Cu/C in alkaline media was estimated to be approximately –0.66 V vs RHE, which is significantly lower than the previously-reported value of –0.41 V vs RHE in acidic media (at $pH = 4.6$).[16] The more negative onset potential in alkaline conditions indicates relatively slower HER kinetics in alkaline media compared to acidic media.

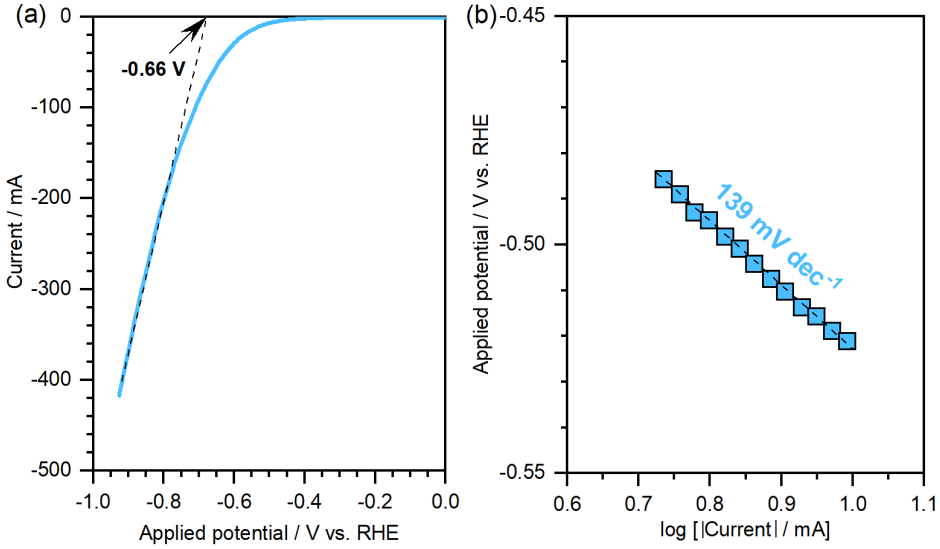

Figure 3-1. (a) LSV curve (scan rate = 1 mV·s^{-1}) and (b) Tafel curve under HER conditions on Cu/C in alkaline media ($pH \approx 11.3$). The dashed lines are fits to the linear region, and the reported numbers are the onset potential in (a) and the Tafel slope in (b). Reaction conditions: 0.01 M NaOH/ 0.99 M NaCl (pH ~11.3), room temperature, ambient pressure.

Next, we elucidated the RDS for HER on Cu/C from the cathodic Tafel slopes (β_c) obtained

from the LSV measurements. Theoretically, at $T = 298$ K and $\alpha = 0.5$, $\beta_c \cong 120$ mV·dec^{-1} if the Volmer step is the RDS.[36, 37] On the other hand, if the Heyrovsky or Tafel steps are the RDS, then $\beta_c \cong 40$ mV·dec^{-1} or $\beta_c \cong 30$ mV·dec^{-1}, respectively.[36, 37] The obtained Tafel slope under HER conditions on Cu/C in alkaline media is also reported in **Figure 3-1b**. Under alkaline conditions, the Tafel slope was estimated to be approximately 139 mV·dec^{-1}, suggesting that the Volmer step is the RDS for HER. In other words, H_2O dissociation on the surface of Cu determines the rate of H_2 formation.

Figure 3-2 shows the H_2 yield as a function of reaction time on Cu/C in alkaline media at $\eta = -0.5$ vs RHE. The estimated initial HER rates are also reported. As expected, the HER rate was very low ($r_H \leq 0.01$ mmol·g$_{Cu}^{-1}$·s^{-1}) under these reaction conditions. In comparison, the HER rate in acidic electrolyte ($pH = 4.6$) at $\eta = -0.5$ V vs RHE was significantly higher ($r_H \cong 3.69$ mmol·g$_{Cu}^{-1}$·s^{-1}).[16] The negligible HER rate indicates slower H addition kinetics in alkaline media compared to acidic media. We also note here that, expectedly, the HER rate increased substantially (to $r_H \cong 2.20$ mmol·g$_{Cu}^{-1}$·s^{-1}) at a higher applied overpotential ($\eta = -0.7$ vs RHE).

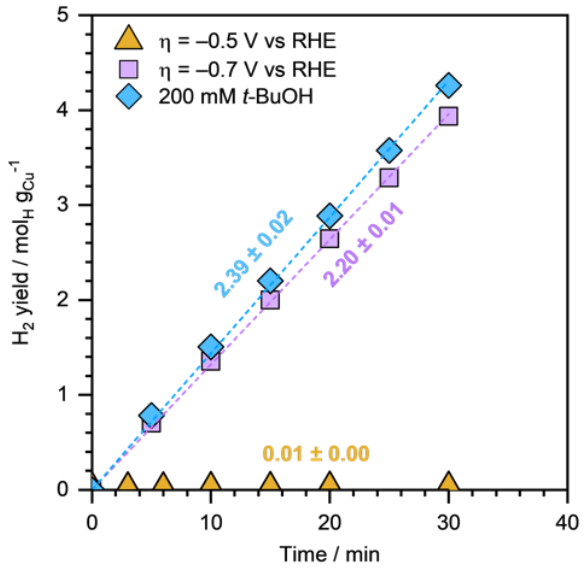

Figure 3-2. H_2 yield as a function of reaction time during HER on Cu/C at (i) $\eta = -0.5$ V vs RHE (triangles), (ii) $\eta = -0.7$ V vs RHE (squares), and (iii) $\eta = -0.7$ V vs RHE in the presence of ~200 mM *t*-BuOH (diamonds). The dashed lines are linear fits, and the reported numbers are initial HER rates in mmol$_H$·g$_{Cu}^{-1}$·s^{-1}. Reaction conditions: 0.01 M NaOH/0.99 M NaCl ($pH = 11.3$), room temperature, ambient pressure.

To further confirm the RDS for HER in alkaline media, we performed HER on Cu/C (at $\eta =$

–0.7 V vs RHE) in the presence of *t*-butanol (*t*-BuOH), which is known to reduce the amount of surface H*.[38-40] The H_2 yield and the initial HER rates in the presence of ~200 mM *t*-BuOH are presented in **Figure 3-2**. We note that in alkaline conditions (at $pH = 11.3$), the HER rate was not impacted by the presence of *t*-BuOH. In contrast, we have previously shown that in slightly acidic conditions (at $pH = 4.6$), the HER rate decreased significantly (up to ~75%) in the presence of *t*-BuOH suggesting that H* species were involved in the rate-determining Tafel step.[16] Therefore, the invariance of HER rates to the presence of *t*-BuOH suggests that the surface H* species are not a reactant in the RDS in alkaline media. As both Heyrovsky and Tafel steps involve the surface H* species (**Scheme 3-1**), we conclude that the Volmer step is the RDS for HER on Cu/C in alkaline conditions.

We recall that, based on similar Tafel analysis and *t*-BuOH co-reactant experiments, we have previously concluded that, in acidic solutions (i.e., $pH = 4.6$), the RDS for HER is the Tafel step and that HER on Cu/C follows the Volmer-Tafel mechanism. In other words, $r_{Tafel} < r_{Volmer}$ in acidic conditions. This difference suggests that H_3O^+ dissociation (in acidic solutions) must be relatively fast in comparison to H_2O dissociation (in alkaline solutions). It must also be noted that the acid dissociation constant (pK_a) of H_3O^+ ($pK_a = -1.7$).is significantly lower than that of H_2O ($pK_a = 14$). Therefore, we attribute the slower HER kinetics in alkaline media to the weaker dissociation and protonation ability of H_2O compared to that of H_3O^+.

3.3.2 Effect of Electrolyte pH and Na^+ Concentration on HER

Figure 3-3a shows the LSV curves under HER conditions on Cu/C at different electrolyte pH values ($pH = 9.1 – 12.3$) but at a constant Na^+ activity ($a_{Na^+} = 1$ M) via addition of NaOH and NaCl to the solution. The corresponding Tafel slopes are presented in **Figure 3-3b**. We can see that HER activity (represented by the magnitude of the measured electron current in **Figure 3-3a**) increased significantly and monotonically with the electrolyte pH. Interestingly, the measured Tafel slopes decreased systematically with increasing pH (from $\beta_c \cong 212$ mV·dec^{-1} at $pH = 9.1$ to $\beta_c \cong 129$ mV·dec^{-1} at $pH = 12.3$). Tafel slope values greater than 120 mV·dec^{-1} typically indicate that the reaction is controlled by H_2O dissociation and that the RDS is the first electron transfer.[41] Overall, these results suggest that electrolyte

pH, or the concentration of OH^- ions (a_{OH^-}), positively impacts the HER activity on Cu/C in alkaline conditions.

As discussed earlier, the RDS for HER on Cu/C in alkaline conditions is the Volmer step. As neither H^+ nor OH^- ions are the reactants in the RDS of HER (**Scheme 3-1**), we expect that the HER kinetics must be independent of pH. Notably, Goyal et al. also reported similar pH dependence for HER on Au-based catalysts even though Volmer step was elucidated to be rate determining.[22] They suggested that increasing electrolyte pH tunes the near-surface concentration of cations (in the Helmholtz layer).[22, 23] They further suggested that the cations near the electrode surface enhance the HER activity by favorably interacting with the dissociating H_2O molecules.[22, 23]

We also investigated the effect of Na^+ concentration (a_{Na^+}) on HER activity. **Figure 3-3c** shows the LSV curves under HER conditions on Cu/C at different Na^+ concentrations (a_{Na^+} = 250 – 1500 mM), however, at a constant electrolyte pH = 9.1. **Figure 3-3d** shows the corresponding reaction order plots ($\log|j|$ versus $\log a_{Na^+}$) at different values of applied external potential (η). We can see that the HER rates, again measured as the current density, increased monotonically with increasing a_{Na^+}. Furthermore, the reaction orders estimated at different η values were also positive (ranging between ~0.31 at η = –0.80 V vs RHE and ~0.62 at η = –0.65 V vs RHE). The overall positive dependence of HER rates on a_{Na^+} confirms that increasing the (near-surface) Na^+ concentration (in the Helmholtz layer) positively affects the kinetics of HER on Cu/C in alkaline electrolytes.

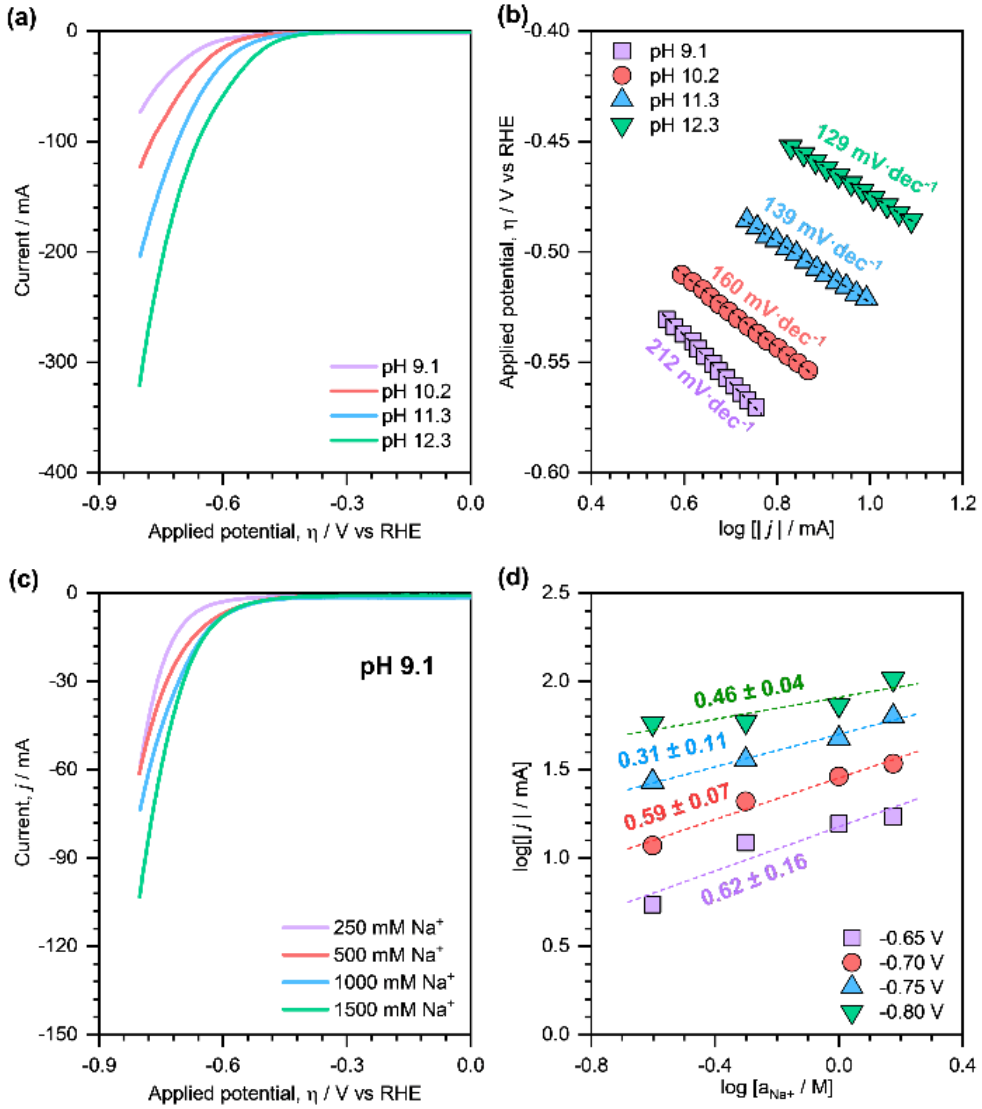

Figure 3-3. (a) LSV curves and (b) Tafel curves under HER conditions on Cu/C at different pH. (c) LSV curves under HER conditions on Cu/C in 0.0001 M NaOH and different concentration of Na^+. (d) Reaction order plots at $pH = 9.1$ on Cu/C. The dashed lines are linear fits, and the reported numbers are Tafel slopes in (b) and reaction orders in (d). Reaction conditions: NaOH/NaCl electrolyte ($pH = 9.1 – 12.3$), room temperature, ambient pressure.

3.3.3 ECH and C–C Coupling of benzaldehyde on Cu/C

Now, let us focus on the ECH of benzaldehyde on Cu/C in alkaline media ($pH = 9.1 – 12.3$). **Figure 3-4** shows a comparison between LSV curves obtained under benzaldehyde ECH and HER reaction conditions in alkaline media ($pH = 11.3$). We can clearly see that the magnitude of the current density on Cu/C in the presence of ~20 mM benzaldehyde was significantly higher than that in its absence. Additionally, in the presence of benzaldehyde, the onset potential was estimated to be –0.51 V vs RHE (compared to –0.66 V vs RHE in its absence). Therefore, based on the higher current density and positively shifted onset potential, we conclude that the

overall ECH activity on Cu/C is superior in the presence of benzaldehyde than in its absence. It must be mentioned here that the ECH rates of organic substrates are typically lower than the HER rates under the same reaction conditions.[42, 43] However, our results clearly indicate that in alkaline conditions on Cu/C, the rate of H addition to benzaldehyde-derived organic substrate (to form benzyl alcohol or hydrobenzoin) is higher than the corresponding rate of H addition to an adsorbed H* (to form H_2).

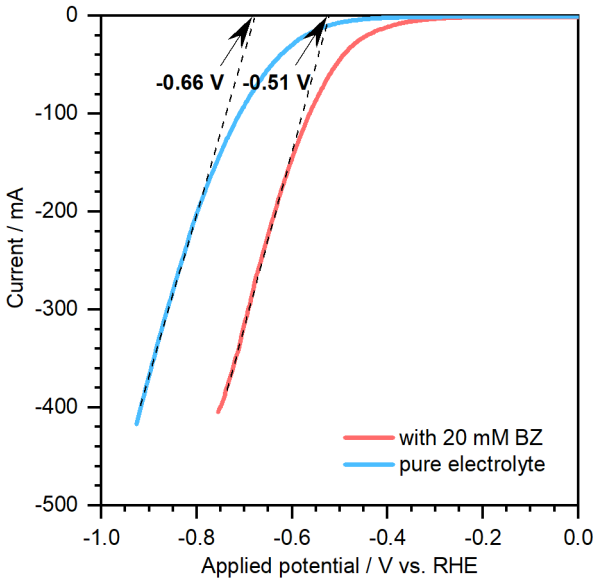

Figure 3-4. LSV curve (scan rate = 1 $mV \cdot s^{-1}$) on Cu/C in the presence of 20 mM benzaldehyde. The LSV curve under HER conditions is also shown for comparison. Reaction conditions: 20 mM benzaldehyde, 0.01 M NaOH/0.99 M NaCl (pH ~11.3), room temperature, ambient pressure.

Figure 3-5a shows the concentration profiles of benzaldehyde, benzyl alcohol, and hydrobenzoin during the ECH of ~20 mM benzaldehyde aqueous solution on Cu/C in alkaline media ($pH = 11.3$). Except benzyl alcohol and hydrobenzoin, no other major byproducts were observed during the reaction. Also, based on the yield versus conversion plots (Supplementary **Figure S3-1**), we conclude that both benzyl alcohol and hydrobenzoin are the kinetically primary products during benzaldehyde ECH under the applied reaction conditions. **Figure 3-5b** shows benzyl alcohol and hydrobenzoin yields as a function of reaction time during benzaldehyde ECH. From these plots, the initial benzyl alcohol and hydrobenzoin formation rates (in terms of mol H consumed) were estimated to be ~0.19 $mmol_H \cdot g_{Cu}^{-1} \cdot s^{-1}$ and ~1.08 $mmol_H \cdot g_{Cu}^{-1} \cdot s^{-1}$, respectively. Interestingly, H_2 formation was negligible (≤0.01 $mmol_H \cdot g_{Cu}^{-1} \cdot s^{-}$

[1]) under these reaction conditions, which resulted in almost 100% Faradaic efficiency towards organic conversion. The low H_2 formation during benzaldehyde ECH is consistent with the low HER rate (≤0.01 $mmol_H \cdot g_{Cu}^{-1} \cdot s^{-1}$; **Figure 3-2**) observed in the absence of benzaldehyde under similar reaction conditions (η = –0.5 V vs RHE and pH = 11.3). Lastly, we note that the total H consumption rate in the presence of benzaldehyde (~1.28 $mmol_H \cdot g_{Cu}^{-1} \cdot s^{-1}$) was significantly higher than the total H consumption rate in its absence (≤0.01 $mmol_H \cdot g_{Cu}^{-1} \cdot s^{-1}$) further suggesting that, in alkaline conditions, the rate of H addition to benzaldehyde (to form benzyl alcohol or hydrobenzoin) is higher than the rate of H addition to an adsorbed H* (to form H_2).

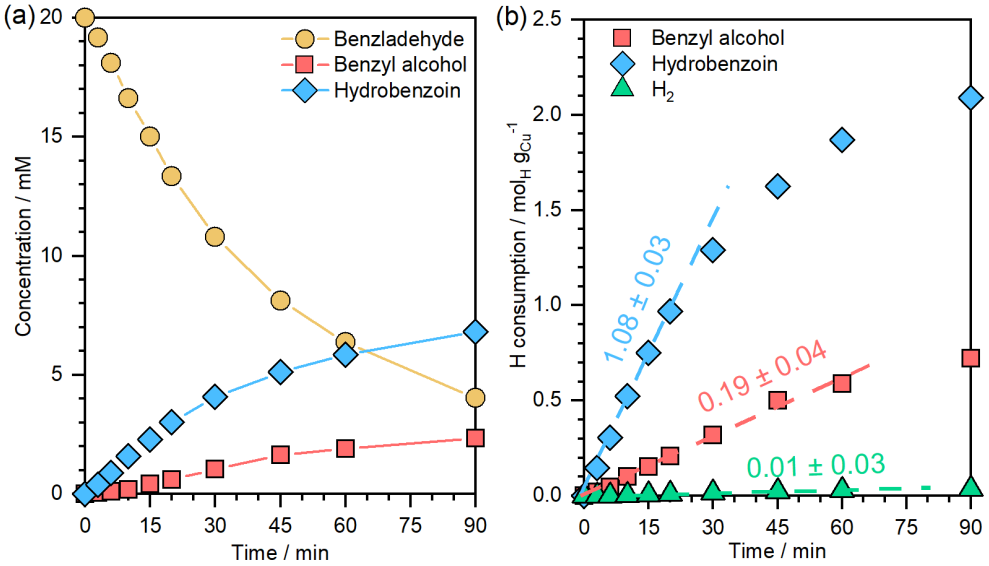

Figure 3-5. (a) Concentration profiles of reactants and products during benzaldehyde ECH on Cu/C, (b) H consumption yield towards benzyl alcohol, hydrobenzoin, and H_2 formation as a function of reaction time during benzaldehyde ECH on Cu/C. Reaction conditions: 20 mM benzaldehyde, η = –0.5 V vs RHE, 0.01 M NaOH/0.99 M NaCl (pH ~11.3), room temperature, ambient pressure. The dashed lines are linear fits, and the reported numbers are the initial rates in $mmol_H \cdot g_{Cu}^{-1} \cdot s^{-1}$.

The Faradaic selectivities towards benzyl alcohol and hydrobenzoin formation in alkaline conditions (at pH = 11.3 and η = –0.5 V vs RHE) were estimated to be ~0.16 and ~0.84, respectively. In comparison, we recall that the Faradaic selectivities towards benzyl alcohol and hydrobenzoin in acidic conditions (at pH = 4.6 and η = –0.5 V vs RHE) were reported to be ~0.48 and ~0.44, respectively.[16] These results clearly show that, in alkaline conditions, the Faradaic selectivity of benzaldehyde ECH towards hydrobenzoin formation is significantly higher than that towards benzyl alcohol formation, suggesting that alkaline conditions promote

C–C coupling.

3.3.4 H Addition Mechanism during benzaldehyde ECH on Cu

The H addition during ECH reactions can be either an inner-sphere process (occurring on the electrode surface) or an outer-sphere process (occurring in the solvent layer).[16, 44, 45] Organothiols, like 2-mercaptobenzothiazole (MBT), have been shown to specifically inhibit the inner-sphere reactions by forming a self-assembled monolayer. These self-assembled monolayers do not affect the outer-sphere reactions.[16, 44, 45] Therefore, we performed benzaldehyde ECH on Cu/C in the presence of ~10 mM MBT to distinguish between the inner-sphere and outer-sphere reactions, and the corresponding benzaldehyde conversion rates are presented in **Figure 3-6a** and **Figure 3-6b**. We can see that both benzyl alcohol and hydrobenzoin formation rates decreased significantly in the presence of MBT suggesting that the H addition during benzaldehyde ECH on Cu/C is primarily an inner-sphere process.

Next, to elucidate the role of surface H* in the H addition mechanism, we compare the H consumption rates for the HER and the benzaldehyde ECH reactions. The total H consumption rate during HER ($\leq$0.01 $mmol_H \cdot g_{Cu}^{-1} \cdot s^{-1}$) is significantly lower than the total H consumption rate during benzaldehyde ECH (~1.28 $mmol_H \cdot g_{Cu}^{-1} \cdot s^{-1}$) in alkaline media. We have concluded above that the Volmer step (i.e., formation of surface H*) is the RDS for HER on Cu/C. Thus, if surface H* is a reactant in the RDS for benzaldehyde ECH, the overall benzaldehyde conversion rate would need to be lower than 0.01 $mmol_H \cdot g_{Cu}^{-1} \cdot s^{-1}$. This is not the case, which suggests that the surface H* species are not involved in the H addition mechanism during benzaldehyde ECH on Cu/C in alkaline conditions. We also performed benzaldehyde ECH on Cu/C in the presence of ~200 mM *t*-BuOH, which reduced the amount of surface H* and the results are presented in Supplementary **Figure S3-2**.[38-40] The initial benzaldehyde conversion rates with and without *t*-BuOH are presented in **Figure 3-6c**. Evidently, the benzaldehyde conversion rate was unaffected by the presence of *t*-BuOH, clearly indicating that surface H* species do not participate in benzaldehyde ECH to benzyl alcohol or hydrobenzoin. Therefore, we conclude that in alkaline conditions, the H addition during benzaldehyde ECH on Cu/C does not involve surface H*.

We propose that H addition during benzaldehyde ECH proceeds via a PCET-type mechanism

wherein a proton is transferred to the adsorbed substrate coupled with an electron transfer from the surface of the electrode. The protons in this PCET-type mechanism could originate from either solvated H_3O^+ ions or H_2O molecules that are on/near the electrode surface as illustrated in **Scheme 3-2**. We note that although solvated H_3O^+ ions have been previously described as the protonating agents in acidic solution, they are unlikely to play a role for H addition in alkaline media due to their extremely low concentration.[34, 46]

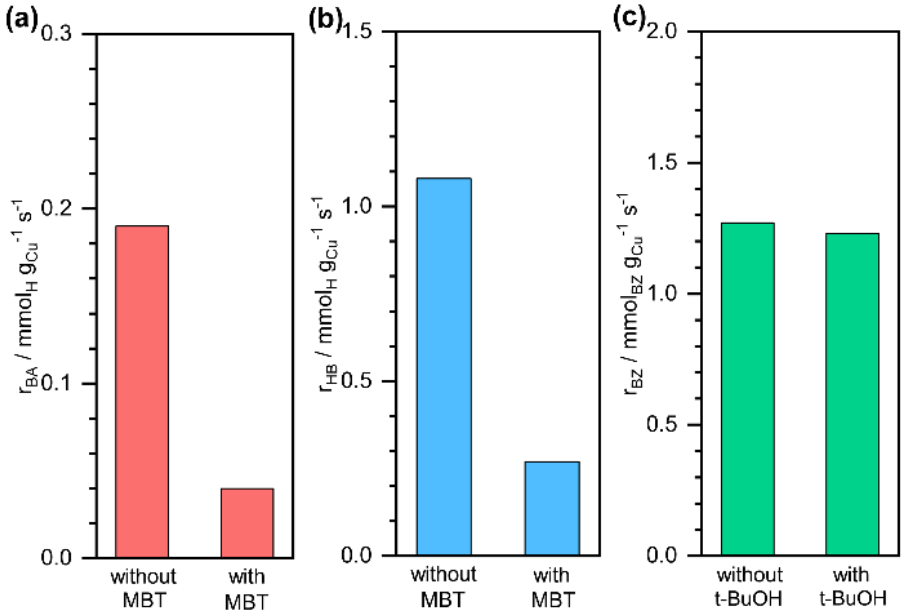

Figure 3-6. (a) Initial benzyl alcohol and (b) initial hydrobenzoin formation rates during benzaldehyde ECH on Cu/C without or with 10 mM MBT. (c) Initial benzaldehyde conversion rate during benzaldehyde ECH on Cu/C without or with 200 mM *t*-BuOH. Reaction conditions: 20 mM benzaldehyde, $\eta = -0.5$ V vs RHE, 0.01 M NaOH/ 0.99 M NaCl (pH ~11.3), room temperature, ambient pressure.

To elucidate the source of protons during H addition in alkaline conditions, we performed benzaldehyde ECH on acid-functionalized Cu/C catalysts. Acid-functionalization of the carbon support (via O_3 treatment) has been shown to increases H_3O^+ concentration near the surface of the electrode.[47] Therefore, we performed benzaldehyde ECH on O_3-treated Cu/C catalysts and the corresponding ECH rates are reported in Supplementary **Figure S3-3**. It can be seen that the total ECH activity was not affected by the acid-functionalization of the support, thus, confirming that, in alkaline electrolytes, H_3O^+ ions do participate in the H addition step. We have also excluded the role of surface H* in H addition by comparing the rate of H consumption in the electrolyte solutions with and without benzaldehyde (**Figure 3-2** and **Figure 3-5b**) as

well as the *t*-BuOH co-reaction experiments (**Figure 3-6c**). Furthermore, we note that hydroxide ions are also unlikely to be the source of protons due to the much higher energy required to deprotonate OH^- than H_2O. It is, therefore, likely that H_2O molecules act as the proton source during ECH reactions in alkaline media, forming OH^- in the process. Therefore, based on these experimental observations, we conclude that H addition in alkaline media proceed via a PCET-type mechanism wherein H_2O molecules act as proton source by dissociating near the organic substrate (as illustrated in **Scheme 3-2**). The dissociation is accompanied by a concerted electron transfer from the surface of the electrode to the organic substrate.

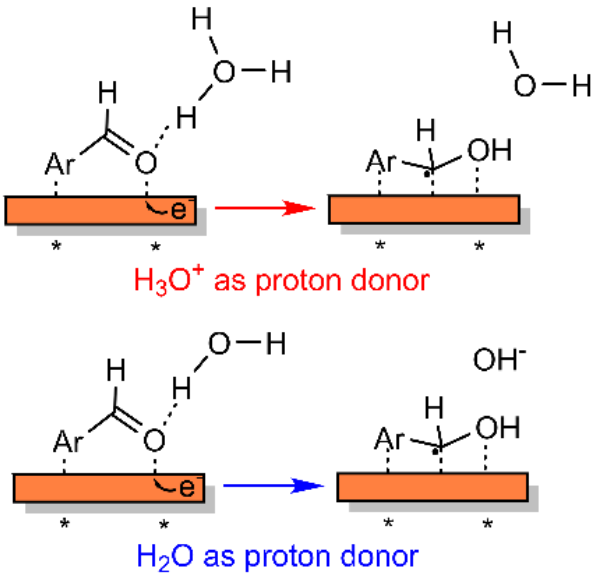

Scheme 3-2. Mechanism of PCET-type H addition during benzaldehyde ECH.

3.3.5 Reaction Mechanism of benzaldehyde ECH on Cu/C

Now let us discuss the mechanistic pathways for benzyl alcohol and hydrobenzoin formation from benzaldehyde during its ECH on Cu/C in alkaline media. First, we must note that benzyl alcohol formation from benzaldehyde requires two successive H addition steps to the adsorbed benzaldehyde molecule, one each to the carbonyl C and the carbonyl O atoms. Hydrobenzoin formation, on the other hand, in addition to the H addition to the carbonyl O atoms of two benzaldehyde molecules, requires C–C coupling between the carbonyl C atoms of the two benzaldehyde molecules. Formation of hydrobenzoin from benzaldehyde necessitates that the first H addition must occur on the carbonyl O atom to form the surface hydroxy intermediate

(*i.e.*, the hydroxy pathway); preferential first H addition to the carbonyl C atom (*i.e.*, the alkoxy pathway) will inhibit hydrobenzoin formation.[16]

To elucidate the kinetically relevant steps for benzyl alcohol and hydrobenzoin formation, we performed isotope labelling experiments. **Figure 3-7** shows the initial benzyl alcohol and hydrobenzoin formation rates during benzaldehyde ECH on Cu/C with H_2O or D_2O as solvents. Interestingly, both benzyl alcohol and hydrobenzoin formation rates decreased significantly when we changed the solvent from H_2O to D_2O. The benzyl alcohol formation rate decreased from ~0.19 $mmol_H \cdot g_{Cu}^{-1} \cdot s^{-1}$ in H_2O to ~0.01 $mmol_H \cdot g_{Cu}^{-1} \cdot s^{-1}$ in D_2O, corresponding to a strong primary kinetic isotope effect (KIE). Similarly, the hydrobenzoin formation rate decreased from ~1.1 $mmol_H \cdot g_{Cu}^{-1} \cdot s^{-1}$ in H_2O to ~0.2 $mmol_H \cdot g_{Cu}^{-1} \cdot s^{-1}$ in D_2O, also corresponding to a strong primary KIE.

The strong primary KIE in both cases suggests that, in alkaline conditions ($pH = 11.3$), H addition is involved in the RDS, and that one of the two H addition steps must be the RDS for both benzyl alcohol and hydrobenzoin formation. It is worth mentioning here that in acidic media (*i.e.*, $pH = 4.6$), using similar isotope labelling experiments, C–C coupling was shown to be the RDS for hydrobenzoin formation during benzaldehyde ECH on Cu/C.[16]

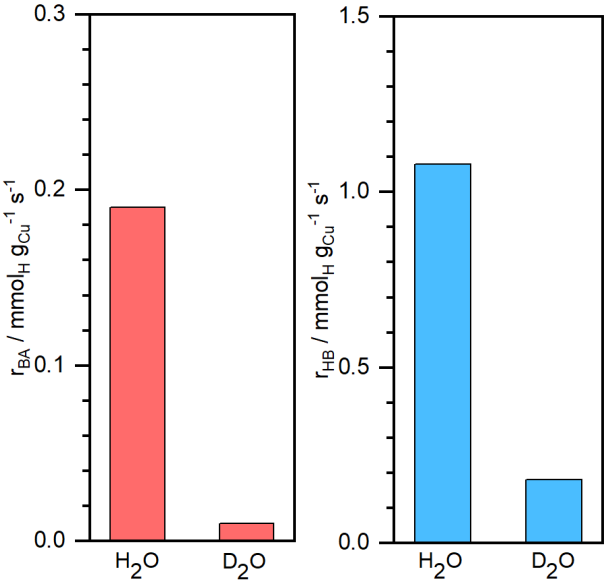

Figure 3-7. Benzyl alcohol (left panel) and hydrobenzoin (right panel) formation rates during benzaldehyde ECH on Cu/C in H_2O or D_2O solvents. Reaction conditions: 20 mM benzaldehyde, $\eta = -0.5$ V vs RHE, 0.01 M NaOH/ 0.99 M NaCl (pH ~11.3), room temperature, ambient pressure.

As we have noted earlier, both benzyl alcohol and hydrobenzoin formation pathways (from benzaldehyde) involve two separate H addition steps. The first H addition step is common for both pathways and involves H addition to the carbonyl O of an adsorbed BZ* to form a surface hydroxy intermediate. **Figure 3-8** shows the Arrhenius-type plots for benzyl alcohol and hydrobenzoin formation during benzaldehyde ECH on Cu/C under alkaline conditions. From these Arrhenius plots, the apparent activation energy barriers ($E_{a,app}$) for benzyl alcohol and hydrobenzoin formation were estimated to be ~51 kJ·mol^{-1} and ~11 kJ·mol^{-1}, respectively. The corresponding apparent pre-exponential factors (A_{app}) were estimated to be $\log A_{app} = 8.1 \pm 0.9$ and $\log A_{app} = 2.0 \pm 0.3$, respectively. The significantly different values of $E_{a,app}$ suggests that the RDS for benzyl alcohol and hydrobenzoin formation are different. Therefore, based on these different $E_{a,app}$ values, we conclude that, at least, the first H addition cannot be the RDS for both benzyl alcohol and hydrobenzoin formation.

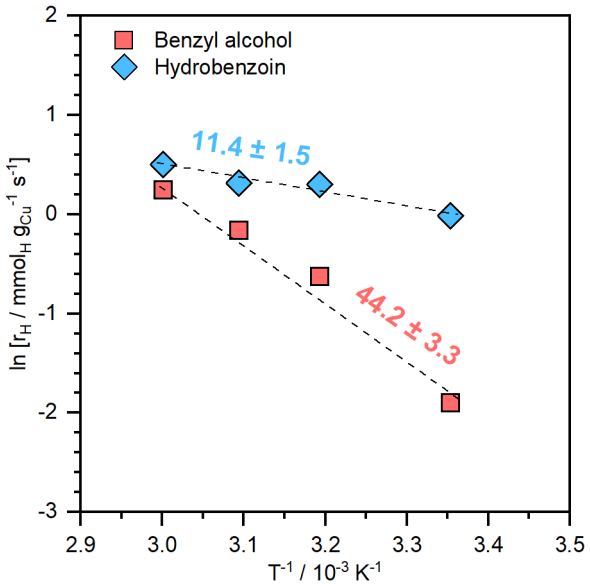

Figure 3-8. Benzyl alcohol and hydrobenzoin formation rates, during benzaldehyde ECH on Cu/C, as a function of temperature. Reaction conditions: 20 mM benzaldehyde, $\eta = -0.5$ V vs RHE, 0.01 M NaOH/ 0.99 M NaCl ($pH =$ ~11.3), $T =$ 298 – 333 K, ambient pressure. The dashed lines are linear fits, and the reported numbers are the apparent activation energies in kJ·mol^{-1}.

3.3.6 First-principle molecular simulations

We performed first-principle periodic DFT calculations on a Cu(111) surface to further elucidate the H addition and C–C coupling pathways during benzaldehyde ECH in alkaline media. The simulations were performed on a system comprising a benzaldehyde molecule

adsorbed flat on the surface. An implicit solvation model with (additional) 20 explicit H_2O molecules was employed in all simulations. Atomic charges were estimated using the Bader charge analysis. Initial configurations were sampled from ab initio molecular dynamics simulations, and then nudged elastic band calculations were carried out to determine the energy barriers. Refer to the Experimental Methods section for more details. Table 1 shows the calculated electronic energy barriers ($\Delta E_{TS}^{\ddagger}$) at 0 K for different reaction steps at $U_{i,RHE}$ = –0.5 V. The $U_{i,RHE}$ of the surface was estimated from its work function (ϕ).

First let us discuss the formation of BA* from BZ*. The initial (IS), transition (TS‡), and final states (FS) for the first H addition considered are illustrated in **Figure 3-9a**. In acidic media, a proton transfer was from a H_3O^+ ion near the carbonyl O atom of the benzaldehyde (O_b) and here we consider a water molecule in a similar configuration. We noted that during the molecular simulations, O_b was fluxionally H-bonded to the O atom (O_w) of a nearby water molecule. In the H addition step, H_w (in the form of a proton) was transferred from a nearby H-bonded water molecule to O_b and an electron was simultaneously transferred from the surface resulting in the formation of a surface-bound hydroxy intermediate and a corresponding OH^- ion in the water layer. The transfer of electron from the surface was evident as the total charge on the surface was higher in the FS as compared to the IS (**Figure 3-9a**).

The $\Delta E_{TS}^{\ddagger}$ for this first H addition step was estimated to be ~59 kJ·mol^{-1} at $U_{i,RHE}$ = –0.5 V (**Table 3-1**). We recall that, based on similar first-principle DFT calculations, the $\Delta E_{TS}^{\ddagger}$ for the first H addition step in acidic conditions (i.e., in the presence of a solvated H_3O^+ ion) was estimated to be ~26 kJ·mol^{-1}.[16] The fact that $\Delta E_{TS}^{\ddagger}$ is higher in alkaline conditions is consistent with stronger bonding of a proton in H_2O than in H_3O^+.

Next, we simulated the second H addition to the α-C of the surface hydroxy intermediate to form BA*. Following the mechanism in acidic solution but again with a H_2O molecule rather than H_3O^+, second H addition step involved H^+ transfer from a nearby water molecule to the α-C (C_b) of the hydroxy intermediate, as illustrated in **Figure 3-9b**. We observed that in the second H addition step, H^+ was transferred from a nearby H_2O_w molecule to C_b. The H^+ transfer was coupled with electron transfer from the surface resulting in the formation of BA* and a

corresponding OH^- ion in the water layer. The electron transfer from the surface to the intermediate is evident as the net charge on the surface was higher in the FS compared to the IS.

Table 3-1. Transition state (ΔE_{TS}) and final state (ΔE_{FS}) energies, relative to initial state, at 0 K for different reaction steps of benzyl alcohol and hydrobenzoin formation on Cu(111) surface at the specified surface potential ($U_{i,RHE}$).

Reaction step	$\Delta E_{TS}^{\ddagger}$ / kJ·mol^{-1}
First H addition	~59
BA* formation	~99
HB* formation	~38

[a] estimated at pH = 11.3 and T = 300 K.

The $\Delta E_{TS}^{\ddagger}$ for the second H addition step was estimated to be ~99 kJ·mol^{-1} (**Table 3-1**), which is significantly higher than the energy barrier for the first H addition ($\Delta E_{TS}^{\ddagger}$ ~59 kJ·mol^{-1}) and also higher than this step in acid media ($\Delta E_{TS}^{\ddagger}$ ~81 kJ·mol^{-1}). During molecular simulations, we observed that the nearby water molecules were primarily H-bonded to the O atom of the hydroxy intermediate (O_b), rather than the α-C. The H-bonded water molecule, that was considered to undergo reaction, therefore, had to move from O_b to the α-C for the H addition to occur. The higher barrier for H addition to the α-C is, therefore, likely due to stronger interaction of O atom with the water molecules. Lastly, based on the estimated electronic energy barriers, we conclude that the second H addition must be the rate-determining step for benzyl alcohol formation.

Next, let us discuss the formation of HB* via the C–C coupling reaction between a surface hydroxy intermediate and a nearby physisorbed benzaldehyde molecule. The obtained IS, TS‡, and FS are illustrated in **Figure 3-9c**. For these simulations, we placed a benzaldehyde molecule next to the adsorbed hydroxy intermediate in the Helmholtz layer and added an electron (net charge = –1) to the system. The C–C bond formation involved an attack on the electrophilic carbonyl C (C_b) of the physisorbed benzaldehyde molecule by the radical α-C (C_h) of the hydroxy intermediate.

Interestingly, the C–C bond formation was accompanied by a simultaneous transfer of a H^+ from a nearby water molecule to the O atom of the formed alkoxy intermediate (accompanied by electron transfer from the surface) to directly form HB*. The total charge on the surface increased in the FS compared to the IS indicating that the electron was transferred to the intermediate (**Figure 3-9c**). This observation is similar to that made during the simulations performed in acidic conditions (i.e., in the presence of a H_3O^+ ion) where we also observed that the C–C bond formation was accompanied by the simultaneous H addition to directly form HB*.[16] The $\Delta E_{TS}^{\ddagger}$ for HB* formation was estimated to be ~38 kJ·mol^{-1} from these molecular simulations (**Table 3-1**). This barrier was similar to that obtained from simulations in acidic conditions ($\Delta E_{TS}^{\ddagger}$ ~36 kJ·mol^{-1}). The smaller barrier for C–C bond formation compared to that of the first H addition ($\Delta E_{TS}^{\ddagger}$ ~59 kJ·mol^{-1}) suggests that C–C coupling is not the RDS for hydrobenzoin formation. This result is in line with the isotope labelling experiments (**Figure 3-7**) which also suggested that C–C coupling is not the RDS for hydrobenzoin formation in alkaline conditions.

Interestingly, during C–C coupling simulations, we noticed that the H^+ (which was added to the O atom of the alkoxide intermediate) was fluxional between the adsorbate and the solvated hydroxide ion (OH^-). Such fluxionality was not evident in the simulation performed under acidic conditions. Therefore, we also simulated the protonation of the alkoxide intermediate (formed after C–C coupling) to form HB* and the obtained IS, TS‡, and FS are illustrated in Supplementary **Figure S3-4**. During this step, the H^+ was transferred from a nearby water molecule (H_2O_w) to the negatively-charged alkoxide intermediate (formed after C–C coupling and electron transfer) resulting in the formation of HB* and a corresponding OH^- in the water layer. The $\Delta E_{TS}^{\ddagger}$ and ΔE_{FS} for this protonation step were negligible thus suggesting that this step is likely to be fast and equilibrated under the investigated reaction conditions.

Overall, these molecular simulations suggest that, in alkaline conditions, the rate of hydrobenzoin formation must be determined by the first H addition as the subsequent C–C coupling and H addition steps are fast. The overall electronic energy barrier for benzyl alcohol formation ($\Delta E_{TS}^{\ddagger}$ ~99 kJ·mol^{-1}) was higher than that for hydrobenzoin formation ($\Delta E_{TS}^{\ddagger}$ ~59

kJ·mol^{-1}), suggesting that the true activation energy of benzyl alcohol formation must be higher than that for hydrobenzoin formation. This is in qualitative agreement with the experimentally observed apparent activation energies for benzyl alcohol and hydrobenzoin formation (~51 kJ·mol^{-1} and ~11 kJ·mol^{-1}, respectively; **Figure 3-8**). Notably, the theoretical energy barriers for benzyl alcohol and hydrobenzoin formation were found to be higher in alkaline conditions (~99 kJ·mol^{-1} for benzyl alcohol formation and ~59 kJ·mol^{-1} for hydrobenzoin formation) than in acidic conditions (~81 kJ·mol^{-1} for benzyl alcohol formation and ~36 kJ·mol^{-1} for hydrobenzoin formation). This trend is also in qualitative agreement with the experimental results, where we estimated that the apparent activation energies for benzyl alcohol and hydrobenzoin formation were slightly higher in alkaline conditions (~51 kJ·mol^{-1} for benzyl alcohol formation and ~11 kJ·mol^{-1} for hydrobenzoin formation) than in acidic conditions (~28 kJ·mol^{-1} for benzyl alcohol formation and ~1.8 kJ·mol^{-1} for hydrobenzoin formation).

Lastly, we must mention here that it is not plausible to investigate many possible low energy configurations of the system due to computational expenses so there could be configurations that result in lower values of $\Delta E_{TS}^{\ddagger}$. This is especially true for the H additions steps which are sensitive to, for example, the structural configuration of water molecular near the electrode's surface or the O–H bond strength which could be affected by strong interaction of the H_2O molecule with the surface. However, we expect that the obtained energy barriers will remain higher than those in the case of H_3O^+ dissociation, so the conclusions comparing the acid and alkaline media and corresponding rate-determining steps would remain.

Finally, based on kinetic investigation and first-principle molecular simulations, the proposed mechanism for benzaldehyde ECH to benzyl alcohol and hydrobenzoin on Cu/C in alkaline media is illustrated in **Scheme 3-3**. In the proposed mechanism, first, a benzaldehyde molecule adsorbs (reversibly) on a vacant site ($*$) on the surface of Cu. Next, the adsorbed BZ* undergoes a first H addition to the carbonyl O atom to form a surface hydroxy intermediate. The surface hydroxy intermediate undergoes two parallel reactions. In the first case, the α-C of the hydroxy intermediate is hydrogenated to form BA*, which finally desorbs to form benzyl alcohol. The second H addition is the RDS for benzyl alcohol formation. In a parallel reaction, the radical α-C of the hydroxy intermediate is attacked by the electrophilic carbonyl C of a nearby

physisorbed benzaldehyde molecule (in the Helmholtz layer) to form an alkoxy intermediate. The C–C bond formation step is fast under these reaction conditions. The formed alkoxide species undergoes protonation to form HB*, which finally desorbs to form hydrobenzoin. The protonation is also fast and equilibrated under these reaction conditions. The first H addition is the RDS for hydrobenzoin formation.

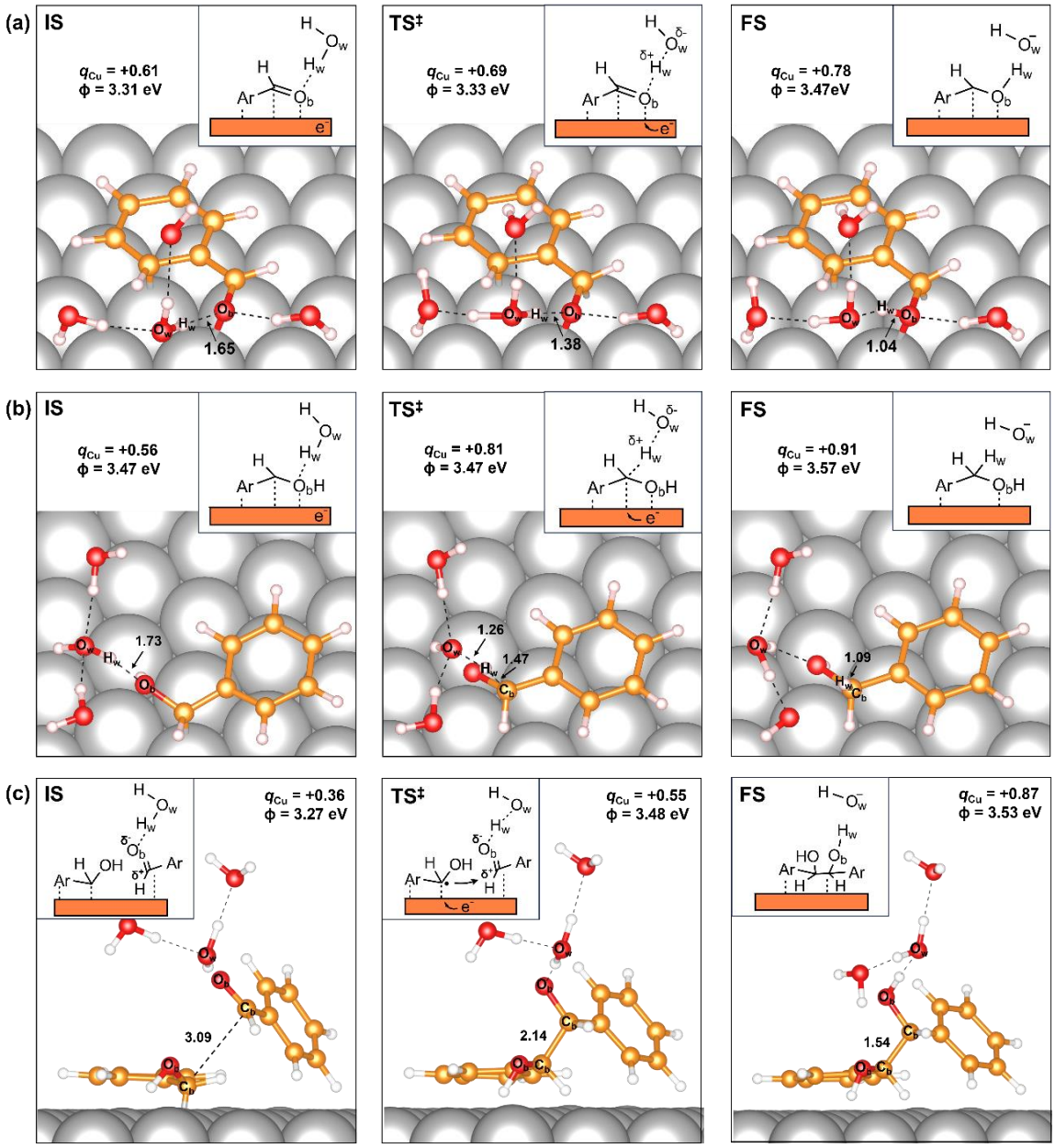

Figure 3-9. Initial state (IS), transition state (TS‡), and final states (FS) of (a) the first H addition, and (b) the second H addition steps, for BA* formation on the Cu(111) surface with net charge = –1. The estimated charges on the Cu surface (q_{Cu}), determined using Bader charge analysis, and the corresponding work-functions (ϕ) are also shown. The reported number are interatomic distances in Å. Cu: grey, C: orange, O: red, H: white. Some H_2O molecules have been removed for clarity.

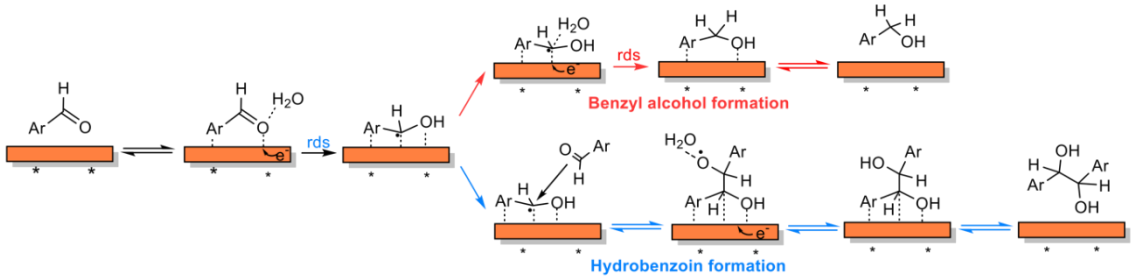

Scheme 3-3. Proposed mechanism for benzyl alcohol and hydrobenzoin formation during benzaldehyde ECH on Cu/C in alkaline media.

Previously, we have described the mechanism for C=O hydrogenation and C–C coupling on Cu/C in acidic media.[16] The key difference between the mechanism in acidic and alkaline media is the shift in the RDS for hydrobenzoin formation from C–C coupling (in acidic media) to the first H addition (in alkaline media). We attribute this difference to the overall slow H addition kinetics in alkaline media because of weaker dissociation ability of H_2O compared to that of H_3O^+. The weaker hydrogenation ability of H_2O (compared to that of H_3O^+) is also evidenced by the fact that HER activity is significantly lower in alkaline media compared to that in acidic media as evidenced by a lower onset potential (**Figure 3-1**). In other words, as the H addition step is more difficult to occur in alkaline conditions, the RDS for hydrobenzoin formation shifted from C–C coupling to the first H addition. We must also mention here that if (i) the first H addition is the RDS for hydrobenzoin formation, and (ii) the second H addition to form benzyl alcohol has a higher energy barrier than the first H addition, we expect only hydrobenzoin to form and the selectivity towards benzyl alcohol must be negligible. However, we observed benzyl alcohol in non-negligible amounts (with a Faradaic selectivity of ~0.16).

The formation of non-negligible quantities of benzyl alcohol can be attributed to the composition of the Helmholtz layer near the electrode's surface. Based on the proposed mechanism (**Scheme 3-3**), the surface hydroxy intermediate either reacts with a H_2O molecule in the Helmholtz layer to form BA* or with a physisorbed benzaldehyde molecule (followed by H addition) to form HB*. Furthermore, based on the bulk electrolyte composition (i.e., $a_{H_2O,bulk} \approx$ 55.5 M and $a_{BZ,bulk} \approx$ 20 mM), we expect H_2O concentration in the Helmholtz layer to be significantly higher than benzaldehyde concentration. We also recall here that the apparent pre-exponential factor for benzyl alcohol formation ($\log A_{app} =$ 8.1; **Figure 3-8**) was significantly higher compared to the apparent pre-exponential factor for hydrobenzoin

formation ($\log A_{app} = 2.0$; **Figure 3-8**).

The apparent pre-exponential factor can be regarded as a qualitative indicator of the frequency of reactive collisions between the reactants and hence the concentration of reactants in the vicinity of the adsorbed hydroxy intermediate. A significantly higher pre-exponential factor for benzyl alcohol formations suggests that the concentration of water molecules in the Helmholtz layer must be higher than the concentration of physisorbed benzaldehyde molecules. The slow expected kinetics towards benzyl alcohol formation is, therefore, compensated by a higher concentration of H_2O molecules in the Helmholtz layer resulting in the formation of benzyl alcohol with non-negligible Faradaic selectivity under the investigated reaction conditions.

3.3.7 Effect of benzaldehyde Concentration on Product Selectivity

Next, we investigated the effects of benzaldehyde concentration (a_{BZ}) on the ECH activity and selectivity during benzaldehyde ECH on Cu/C in alkaline media. **Figure 3-10** shows the initial benzyl alcohol and hydrobenzoin formation rates during benzaldehyde ECH on Cu/C as a function of a_{BZ}. We can clearly see that the hydrobenzoin formation rate increased initially with increasing a_{BZ}. However, at higher a_{BZ} (i.e., above ~20 mM) hydrobenzoin formation rates showed almost a zero-order dependence on benzaldehyde concentration. Contrarily, the benzyl alcohol formation rates remained invariant with increasing a_{BZ} until ~20 mM and then decreased as a_{BZ} increased further.

We attribute this dependence of hydrobenzoin and benzyl alcohol formation rates on a_{BZ} to the change in activity of H_2O and benzaldehyde molecules in the Helmholtz layer. We propose that the activity of H_2O and benzaldehyde in the Helmholtz layer ($a_{H_2O,HL}$ and $a_{BZ,HL}$, respectively) is impacted by $a_{BZ,bulk}$. At very low values of $a_{BZ,bulk}$, the $a_{H_2O,HL}$ must be high while $a_{BZ,HL}$ must be low (as illustrated in **Scheme 3-4a**). The presence of H_2O molecules in the Helmholtz layer in high mole fraction shifts the conversion of surface hydroxy intermediate to benzyl alcohol. However, as $a_{BZ,bulk}$ increases, the $a_{BZ,HL}$ also increases resulting in a positive-order dependence of hydrobenzoin formation rates on a_{BZ}. As $a_{H_2O,HL}$ was still high, the benzyl alcohol formation rates were not significantly affected resulting in almost zero-order dependence of benzyl alcohol formation on $a_{BZ,bulk}$. At $a_{BZ,bulk} \approx 20$ mM,

it is presumed that both H_2O and benzaldehyde are present in a reasonable concentration in the Helmholtz layer. As $a_{BZ,bulk}$ increases further, $a_{BZ,HL}$ increases further, and correspondingly, the $a_{H_2O,HL}$ decreases (as illustrated in **Scheme 3-4b**). A decrease in $a_{H_2O,HL}$ results in low benzyl alcohol formation rate, agreeing with the observed negative reaction order in a_{BZ} for benzyl alcohol formation.

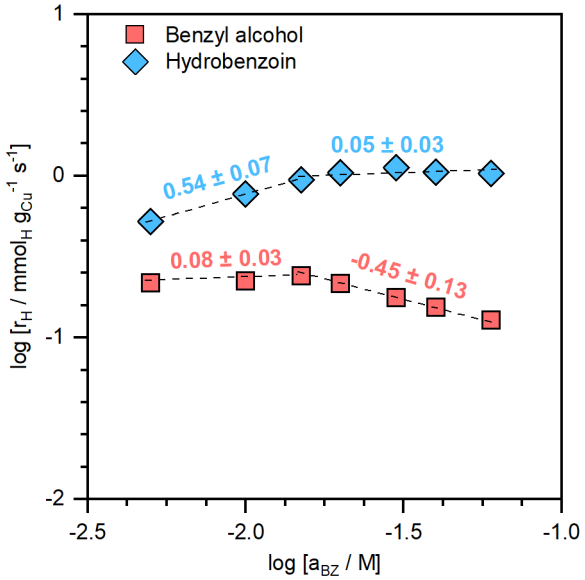

Figure 3-10. Benzyl alcohol and hydrobenzoin formation rates, during benzaldehyde ECH on Cu/C, as a function of initial benzaldehyde concentration. Reaction conditions: 5 - 60 mM benzaldehyde, $\eta =$ –0.5 V vs RHE, 0.01 M NaOH/ 0.99 M NaCl (pH ~11.3), room temperature, ambient pressure. The dashed lines are linear fits, and the reported numbers are the reaction orders.

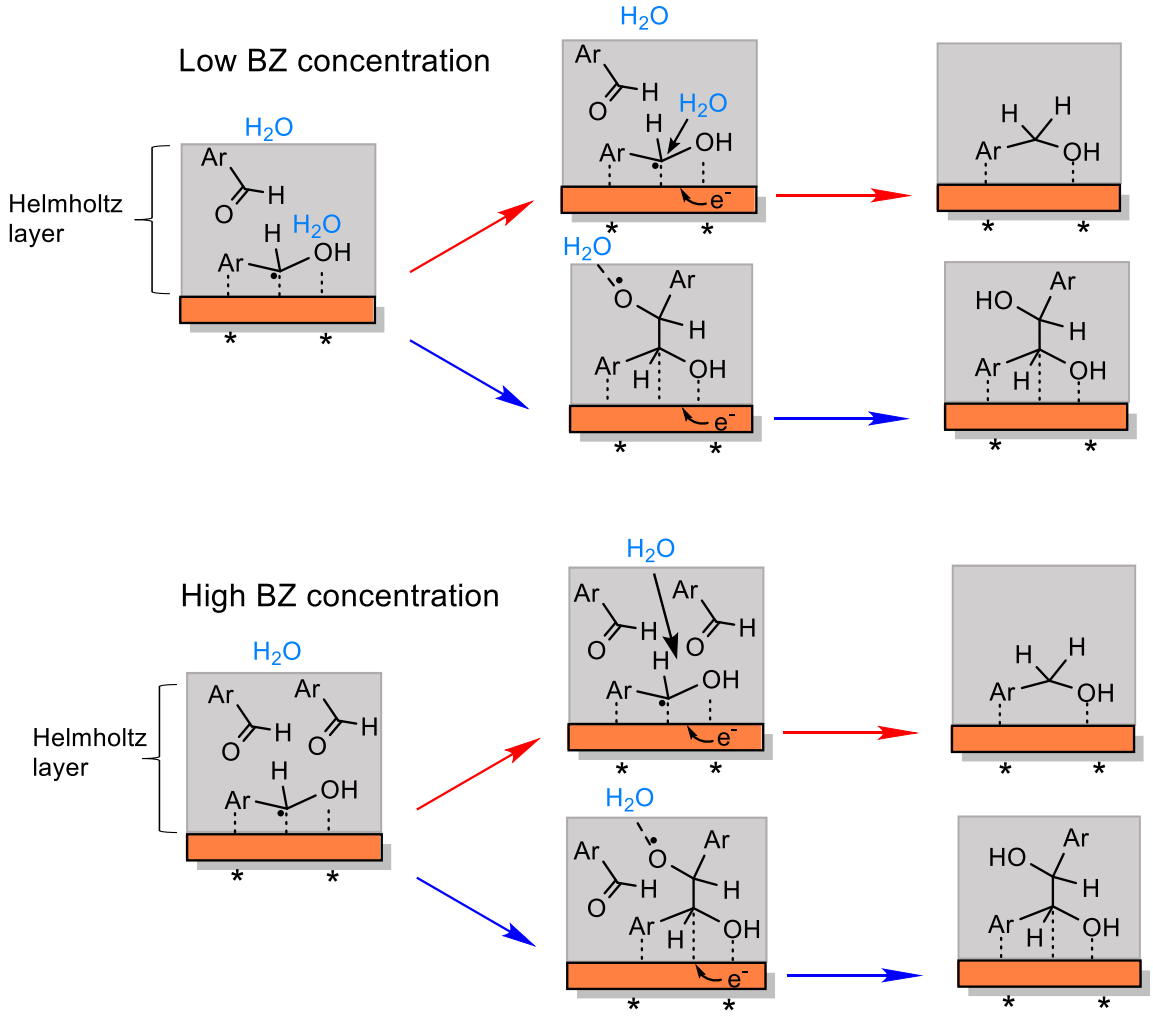

Scheme 3-4. Reaction pathways for benzyl alcohol and hydrobenzoin at low and high benzaldehyde concentrations.

3.3.8 Effect of pH and Na^+ Concentration on benzaldehyde ECH

Figure 3-11a shows the benzyl alcohol and hydrobenzoin formation rates as a function of electrolyte pH. The HER rates were negligible in the investigated pH range and the Faradaic efficiency towards benzaldehyde conversion was ~100% (see Supplementary **Figure S3-5**). We can see that the hydrobenzoin formation rates increased notably from ~0.4 $mmol_H \cdot g_{Cu}^{-1} \cdot s^{-1}$ at $pH = 9.1$ to ~1.75 $mmol_H \cdot g_{Cu}^{-1} \cdot s^{-1}$ at $pH = 12.3$. Similarly, benzyl alcohol formation rate increased with the increasing electrolyte pH; from ~0.05 $mmol_H \cdot g_{Cu}^{-1} \cdot s^{-1}$ at $pH = 9.1$ to ~0.4 $mmol_H \cdot g_{Cu}^{-1} \cdot s^{-1}$ at $pH = 12.3$. The reaction orders in a_{OH^-} for benzyl alcohol and hydrobenzoin formation were estimated to be ~0.30 and ~0.20, respectively. These results indicate that electrolyte pH considerably influences the rate of both benzyl alcohol and hydrobenzoin formation during benzaldehyde ECH on Cu/C.

We recall that the RDS for both benzyl alcohol and hydrobenzoin formation, under the applied reaction conditions, are PCET type steps wherein H_2O acts as the proton source (**Scheme 3-3**). Under these conditions, the benzaldehyde conversion must be independent of pH as neither H_3O^+ nor OH^- are involved in the RDS as reactants (**Scheme 3-2**). Therefore, we propose that similarly to the pH dependence of HER (in pure electrolyte solution) on Cu/C (**Figure 3-3a**), increasing pH increases the near-surface concentration of Na^+ cations, which in turn favorably assists H_2O dissociation, thereby influencing the product formation rates during benzaldehyde ECH.[22, 23]

To investigate the impact of a_{Na^+} on benzyl alcohol and hydrobenzoin formation, we performed benzaldehyde ECH on Cu/C at different a_{Na^+} (250 – 1500 mM) but at a constant electrolyte pH ($pH = 9.1$) and the results are reported in **Figure 3-11b**. The HER rates were negligible in the investigated a_{Na^+} range and the Faradaic efficiency towards benzaldehyde conversion was ~100% (see Supplementary **Figure S3-6**). Both benzyl alcohol and hydrobenzoin formation rates increased monotonically with increasing a_{Na^+}. Furthermore, the reaction order in Na^+ for benzyl alcohol and hydrobenzoin formation were estimated to be ~0.60 and ~0.25, respectively. Overall, these results confirm that Na^+ plays a critical role in the benzaldehyde ECH mechanism by favouring the dissociation of H_2O, thus, increasing the rate of the H addition steps.

Finally, let us look at the effect of pH and a_{Na^+} on benzyl alcohol and hydrobenzoin selectivity during benzaldehyde ECH on Cu/C in alkaline conditions (**Figure 3-12a** and **Figure 3-12b**). The hydrobenzoin selectivity decreased slightly with increasing pH while the Faradaic selectivity towards benzyl alcohol increased with increasing pH (**Figure 3-12a**). We can also see that a_{Na^+} also impacted benzyl alcohol and hydrobenzoin selectivity in a similar fashion. Hydrobenzoin Faradaic selectivity decreased slightly with increasing a_{Na^+} while the Faradaic selectivity towards benzyl alcohol increased with increasing a_{Na^+} (**Figure 3-12b**). These observations, therefore, suggest that in alkaline media, enhancing the H addition rates by favouring H_2O dissociation (either by increasing pH or a_{Na^+}) favours benzyl alcohol formation. This is likely because enhancing H_2O dissociation has a greater impact on the kinetics of the more difficult H addition step (*i.e.*, H addition to the α-C to form benzyl alcohol).

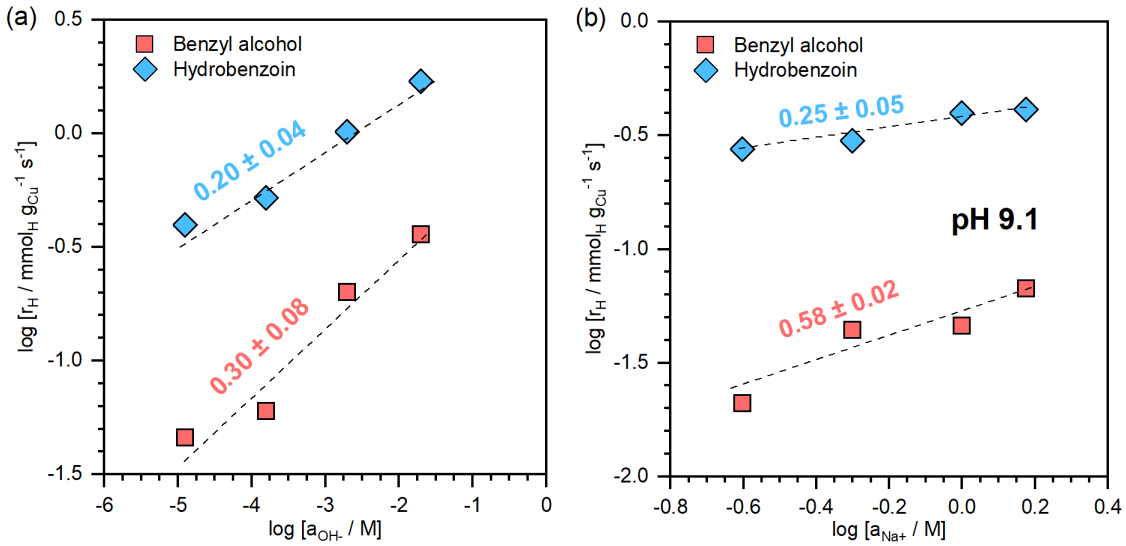

Figure 3-11. Initial benzyl alcohol and hydrobenzoin formation rates at different electrolyte pH (a), and at different Na^+ concentration (b) during benzaldehyde ECH on Cu/C. The pH was varied by changing the concentration of NaCl and NaOH (0.9999 M NaCl + 0.0001 M NaOH (pH ~9.1), 0.999 M NaCl + 0.001 M NaOH (pH ~10.2), 0.99 M NaCl + 0.01 M NaOH (pH ~11.3), and 0.9 M NaCl + 0.1 M NaOH (pH ~12.3)). The Na^+ concentration was varied by changing the concentration of NaCl (0.2499 – 1.4999 M) with 0.0001 M NaOH. Reaction conditions: 20 mM benzaldehyde, $\eta = -0.5$ V vs RHE, room temperature, ambient pressure. The dashed lines are linear fits, and the reported numbers are the reaction orders.

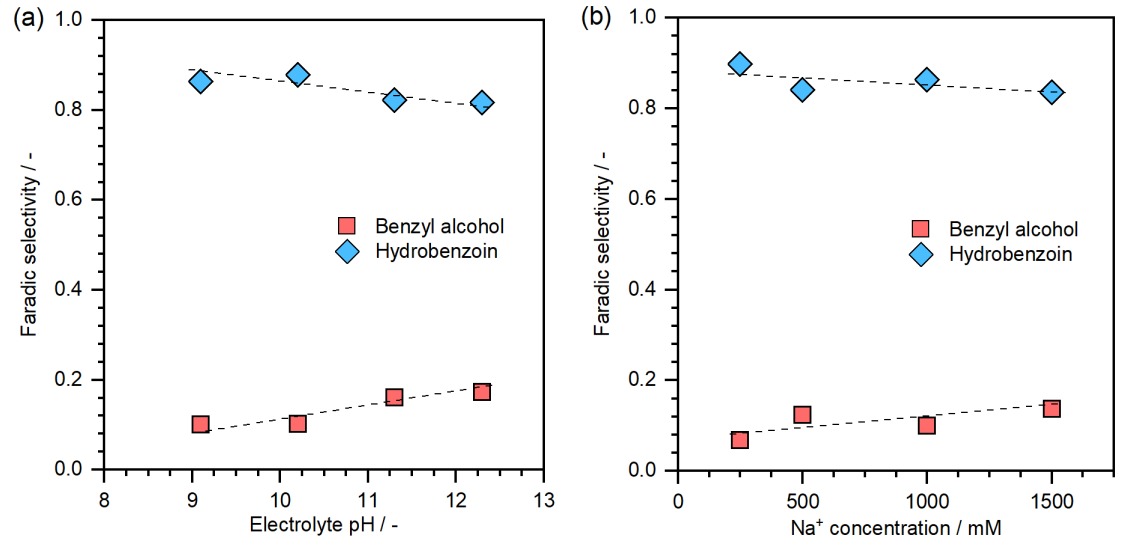

Figure 3-12. Benzyl alcohol and hydrobenzoin Faradic selectivity at different electrolyte pH (a), and at different Na^+ concentration (b) during benzaldehyde ECH on Cu/C. The pH was varied by changing the concentration of NaCl and NaOH (0.9999 M NaCl + 0.0001 M NaOH (pH ~9.1), 0.999 M NaCl + 0.001 M NaOH (pH ~10.2), 0.99 M NaCl + 0.01 M NaOH (pH ~11.3), and 0.9 M NaCl + 0.1 M NaOH (pH ~12.3)). The Na^+ concentration was varied by changing the concentration of NaCl (0.2499 – 1.4999 M) with 0.0001 M NaOH. Reaction conditions: 20 mM benzaldehyde, $\eta = -0.5$ V vs RHE, room temperature, ambient pressure. The dashed lines are linear fits.

3.4 Conclusion

The RDS for H_2 evolution reaction (in pure electrolyte) on Cu/C in alkaline media is the Volmer step (which involves dissociation of H_2O on the surface of Cu to form H*). The HER kinetics in alkaline media, compared to that in acidic media, are slow because dissociation of H_2O is more difficult than H_3O^+ dissociation on the surface of Cu.

benzaldehyde ECH on Cu/C in alkaline electrolyte ($pH = 9.1 - 12.3$) forms two primary products, *i.e.*, benzyl alcohol (the C=O hydrogenation product) and hydrobenzoin (the C–C coupling product). Mechanistically, a benzaldehyde molecule first adsorbs reversibly on a vacant site ($*$). BZ* then undergoes a first H addition to the carbonyl O to form a surface hydroxy intermediate. The hydroxy intermediate then undergoes a second and rate-determining H addition to its radical α-C to form benzyl alcohol. In a parallel reaction, the radical α-C of the hydroxy intermediate is attacked by the electrophilic carbonyl C of a nearby physisorbed benzaldehyde molecule (in the Helmholtz layer) to form an alkoxide intermediate. The C–C bond formation is fast under the applied reaction conditions. The formed alkoxide intermediate undergoes fast and equilibrated protonation to form hydrobenzoin. The first H addition is the RDS for hydrobenzoin formation. The H addition steps occur *via* the PCET type mechanism wherein H_2O molecules act as proton donors (forming OH^- in the process). Alkaline media promotes C–C coupling (with Faradic selectivity toward hydrobenzoin >84%) due to slower H addition kinetics.

Electrolyte pH and concentration of Na^+ cations notably affect the activity of electrocatalytic HER and benzaldehyde ECH on Cu/C. Increasing electrolyte pH indirectly enhances the hydrogenation rates by increasing the near-surface Na^+ concentration, which in turn increase the product formation rates by favoring the dissociation of H_2O. Increasing benzaldehyde concentration in the electrolyte inhibits benzyl alcohol formation by decreasing the H_2O concentration in the Helmholtz layer.

3.5 Supporting information

3.5.1 Supplementary Figures and Tables

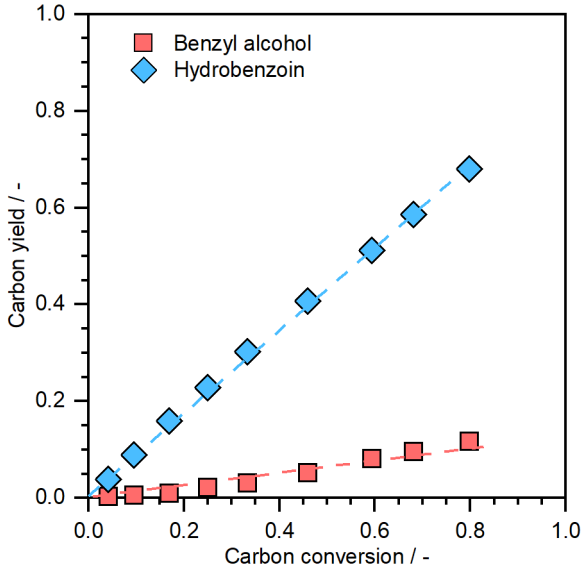

Figure S3-1. Yield vs. conversion (on a carbon basis) plots during benzaldehyde ECH on Cu/C. Reaction conditions: 20 mM benzaldehyde, applied potential –0.5 V vs. RHE, 0.01 M NaOH/ 0.99 M NaCl (pH ~11.3), room temperature, ambient pressure. The dashed lines are linear fits.

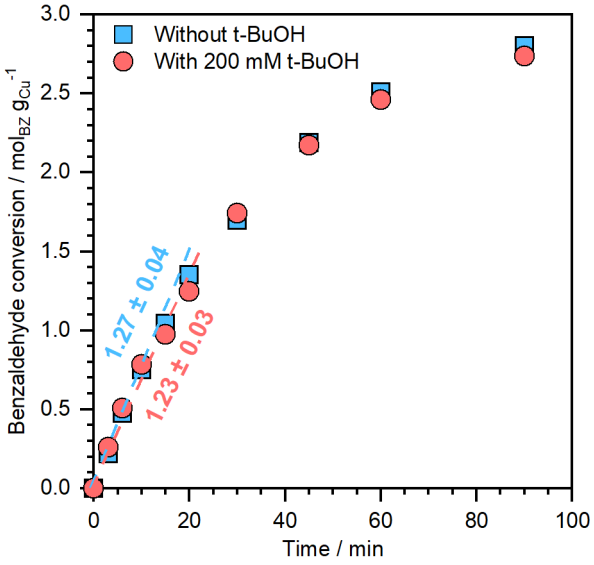

Figure S3-2. benzaldehyde conversion profiles during benzaldehyde ECH with 200 mM t-BuOH or without t-BuOH on Cu/C. Reaction conditions: 20 mM benzaldehyde, applied potential -0.5 V vs RHE, 0.01 M NaOH/ 0.99 M NaCl (pH ~11.3), room temperature, ambient pressure. The dashed lines are guides to the eye and and the reported numbers are the initial rates in $mmol_{BZ} \cdot g_{Cu}^{-1} \cdot s^{-1}$.

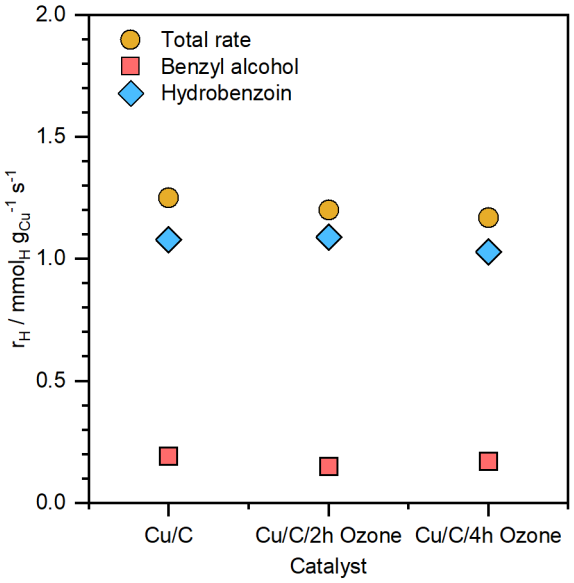

Figure S3-3. Total H consumption rate, benzyl alcohol and hydrobenzoin formation rates during benzaldehyde ECH on Cu/C, Cu/C/O_3-2h, and Cu/C/O_3-4h electrode in alkaline media. Reaction conditions: 20 mM benzaldehyde, applied potential -0.5 V vs RHE, 0.01 M NaOH/ 0.99 M NaCl (pH ~11.3), room temperature, ambient pressure.

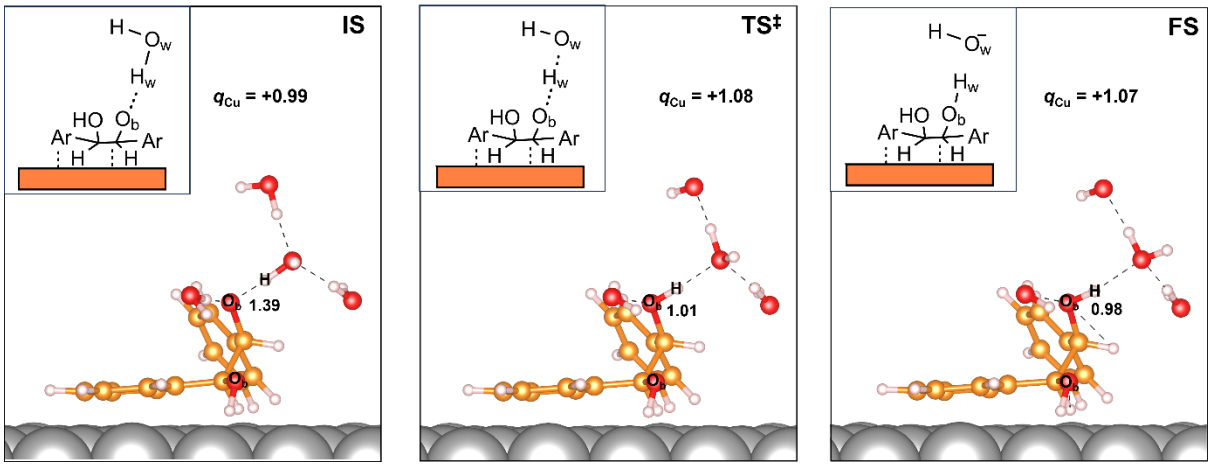

Figure S3-4. Initial state (IS), transition state (TS‡), and final states (FS) obtained during protonation of alkoxide intermediate resulting in HB* formation on the Cu(111) surface with net charge = –1. The estimated charges on the Cu surface (q_{Cu}), determined using Bader charge analysis, are also shown. The reported number are interatomic distances in Å. Cu: grey, C: orange, O: red, H: white. Some H_2O molecules have been removed for clarity.

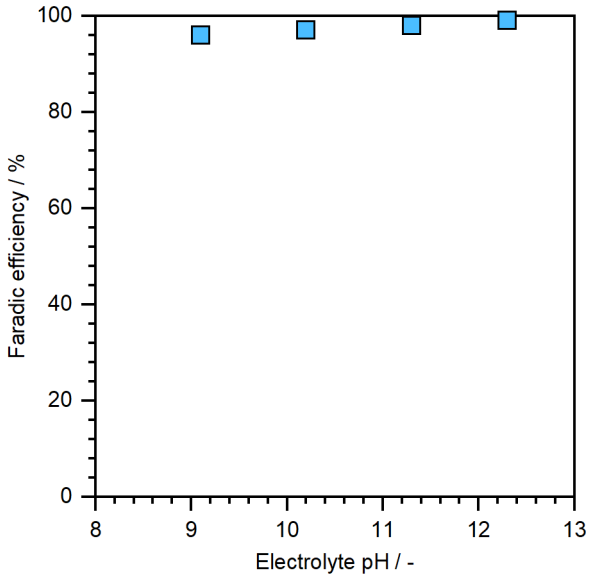

Figure S3-5. Faradic efficiency during benzaldehyde ECH on Cu/C in 0.9999 M NaCl + 0.0001 M NaOH (pH 9.1), 0.999 M NaCl + 0.001 M NaOH (pH 10.2), 0.99 M NaCl + 0.01 M NaOH (pH 11.3), and 0.9 M NaCl + 0.1 M NaOH (pH 12.3), on Cu/C. Reaction conditions: 20 mM benzaldehyde, applied potential -0.5 V vs RHE, NaOH/NaCl (pH 9.1 – 12.3), room temperature, ambient pressure.

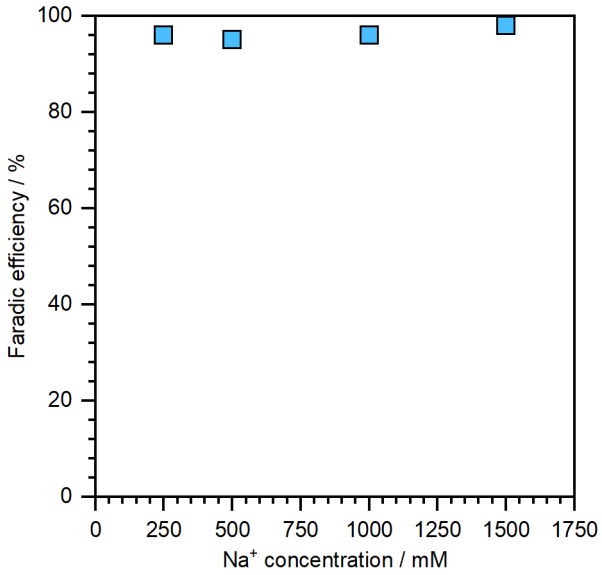

Figure S3-6. Faradic efficiency during benzaldehyde ECH on Cu/C in 0.0001 M NaOH with different concentration of NaCl (249.9999 mM, 499.9999 mM, 999.9999 mM and 1499.9999 mM) on Cu/C. Reaction conditions: 20 mM benzaldehyde, applied potential -0.5 V vs RHE, NaOH/NaCl solution (pH ~9.1), room temperature, ambient pressure.

3.5.2 Additional Calculation Details

The conversion of a reactant i at a given time t was estimated by

$$\chi_i(t) = \frac{n_i(t)}{n_i^0} \quad (3\text{-}4)$$

where $n_i(t)$ is the amount of reactant detected at time t and n_i^0 is the initial amount of reactant in the electrolyte.

Similarly, the yield of a product j with respect to a reactant i at any given time t was estimated by

$$Y_j(t) = \frac{n_j(t)}{n_i^0} \quad (3\text{-}5)$$

where $n_j(t)$ is the amount of reactant j detected at time t and n_i^0 is the initial amount of reactant i in the electrolyte solution.

The initial ECH rate of a product i (in terms of H consumed per gram metal) was calculated from the initial slope (m_i) of the product i formed *vs* time plot using the following equation

$$r_i = \frac{m_i \times \epsilon_i}{w_{cat} \times x_{metal}} \quad (3\text{-}6)$$

where w_{cat} is the amount of catalyst, x_{metal} is the metal loading on the catalyst (as weight fraction), and ϵ_i is the number of H atoms required to form the product i.

The Faradaic efficiency towards the formation of a product i was estimated by

$$FE_i = \frac{q_i}{q_{total}} \quad (3\text{-}7)$$

where q_i is the electrons consumed towards formation of product i, and q_{total} is the total electrons consumed.

3.5.3 Additional Computational Details

All quantum chemical calculations were performed on a periodic electrode-electrolyte interface model using the Vienna *ab initio* simulation package (VASP) with a plane wave basis set.[48-51] The single-electron wavefunctions were estimated using the employed basis set truncated at an energy cut-off of 400 eV. The k-points for these wavefunction calculations were

sampled from a grid size 2 × 2 × 1 in the Brillouin zone. The partial occupancies were set for each orbital using the Methfessel-Paxton scheme to smoothen the wavefunctions.[52] Using projector augmented-wave (PAW) method, the core electrons were treated with the frozen-core approximations, while the valence electron wavefunctions were calculated using the plane wave basis set.[53] Further, to determine electron density from these wavefunctions, the electron self-interaction contribution in the Hartree potential was corrected using generalized gradient approximation (GGA) Perdew-Burke-Ernzerhof (PBE) exchange correlation functional with additional dispersion corrections including using the D3 method with the Becke-Johnson (BJ) damping scheme.[54, 55] The open-source VASPsol package was used to implement implicit solvent in all *ab initio* simulations with spin-polarized calculations.[56] The Bader charge analysis was performed using the code available from Henkelman and co-workers.[57]

All simulations were performed on a 4 × 4 × 4 supercell of the Cu(111) surface, cleaved from bulk Cu with lattice constant of 3.59 Å, and a vacuum of at least 10 Å above the water layer. The top two layers of the Cu(111) slab, representing the surface atoms were not constrained during simulations, while the bottom two layers were fixed representing bulk Cu. The electrode-electrolyte interface was modelled using 20 explicit H_2O molecules and the reaction intermediates above the Cu(111) surface. The system was first relaxed using *ab initio* molecular dynamics (AIMD) simulations. The AIMD simulations were performed using a canonical ensemble at constant temperature (300 K) and volume (NVT). To maintain constant temperature, a Nosé-Hoover thermostat was employed with a time constant of 0.01 ps. AIMD simulation were carried out for at least 5 ps with a time step of 0.5 fs while maintaining the energy and force convergence at 1×10^{-5} eV and 5×10^{-2} eV·Å^{-1}, respectively. The selected configurations from the AIMD simulations were further optimized using density functional theory (DFT). Three different reaction pathways were investigated: first H addition, second H addition, and C–C coupling. The H addition via the PCET-like step (with H_2O molecule as the proton source) was modelled by transferring H^+ from the water layer near the interface and an e^- to the metal surface. The transition states (TS) for each step were identified using the climbing image-nudged elastic band technique (cl-NEB).[58] For this, 8 – 16 frames were developed between the initial state (IS) and the final state (FS) to observe a minimum energy path along the reaction coordinate.

To model the effect of electrode potential, we simulated the IS, TS and FS at different surface potentials. The surface potentials of these states were altered by adding excess electrons to the system. The minimum energy path between IS and FS was estimated by maintaining the same number of electrons. The grand canonical electronic energy (F) for all the states is estimated as below:

$$F = E_{DFT} - q_{electrode} \cdot U \quad (3\text{-}8)$$

where E_{DFT} is the electronic energy from DFT, $q_{electrode}$ is the net charge of the system, and U is the surface potential.

The work function (ϕ_i) at state i can be related to the surface potential of the Cu(111) surface using the following relation:

$$U_{i,SHE} = \frac{\phi_i - \phi_{SHE}}{e} \quad (3\text{-}9)$$

where $U_{i,SHE}$ is the surface potential of Cu(111) relative to SHE at state i, and ϕ_i and ϕ_{SHE} are the work functions of Cu(111) at state i and that of SHE (= 4.44 eV), respectively.

Finally, the calculated surface potential is reported relative to the RHE ($U_{i,RHE}$), as per the Nernst equation:

$$U_{i,RHE} = U_{i,SHE} + 0.0591 \cdot pH \quad (3\text{-}10)$$

Since each state is at different surface potential, the grand canonical energies for IS, TS and FS at the experimental potential were individually extrapolated.

The potential versus grand canonical energy was plotted for IS, TS, and FS separately fitting in the second-order polynomial equation as below:

$$F = aU^2 + bU + c \quad (3\text{-}11)$$

Once fitted, the above equation was used to estimate IS, TS and FS energies at $U_{i,RHE} = -0.5$ V vs RHE.

3.6 Reference

1. Zhang, Qian, et al. "Emerging technologies for green energy conversion and storage." Advanced Sustainable Systems 5.3 (2021): 2000152.
2. Mahlia, T. M. I., et al. "A review of available methods and development on energy storage; technology update." Renewable and sustainable energy reviews 33 (2014): 532-545.

3. Singh, Sandeepa. "Energy crisis and climate change: Global concerns and their solutions." Energy: Crises, Challenges and Solutions (2021): 1-17.
4. Powell, Thomas WR, and Timothy M. Lenton. "Future carbon dioxide removal via biomass energy constrained by agricultural efficiency and dietary trends." Energy & Environmental Science 5.8 (2012): 8116-8133.
5. Li, Kui, and Yujie Sun. "Electrocatalytic upgrading of biomass-derived intermediate compounds to value-added products." Chemistry–A European Journal 24.69 (2018): 18258-18270.
6. Schmitt, Nina, et al. "Thermo-chemical conversion of biomass and upgrading to biofuel: The Thermo-Catalytic Reforming process–A review." Biofuels, Bioproducts and Biorefining 13.3 (2019): 822-837.
7. Baddour, Frederick G., et al. "An exceptionally mild and scalable solution-phase synthesis of molybdenum carbide nanoparticles for thermocatalytic CO_2 hydrogenation." Journal of the American Chemical Society 142.2 (2020): 1010-1019.
8. Nilges, Peter, and Uwe Schröder. "Electrochemistry for biofuel generation: production of furans by electrocatalytic hydrogenation of furfurals." Energy & Environmental Science 6.10 (2013): 2925-2931.
9. Wang, Suheng, et al. "Highly efficient ethylene production via electrocatalytic hydrogenation of acetylene under mild conditions." Nature Communications 12.1 (2021): 7072.
10. Sherbo, Rebecca S., et al. "Efficient electrocatalytic hydrogenation with a palladium membrane reactor." Journal of the American Chemical Society 141.19 (2019): 7815-7821.
11. Akhade, Sneha A., et al. "Electrocatalytic hydrogenation of biomass-derived organics: a review." Chemical reviews 120.20 (2020): 11370-11419.
12. Yuk, Simuck F., et al. "First-principle investigation on catalytic hydrogenation of benzaldehyde over Pt-group metals." Catalysis Today 388 (2022): 208-215.
13. Lopez-Ruiz, Juan A., et al. "Kinetic investigation of the sustainable electrocatalytic hydrogenation of benzaldehyde on Pd/C: effect of electrolyte composition and half-cell potentials." ACS sustainable chemistry & engineering 6.12 (2018): 16073-16085.

14. Yu, Jia, et al. "Electroreductive coupling of benzaldehyde by balancing the formation and dimerization of the ketyl intermediate." Nature Communications 13.1 (2022): 7909.
15. Anibal, Jacob, and Bingjun Xu. "Electroreductive C–C coupling of furfural and benzaldehyde on Cu and Pb surfaces." ACS Catalysis 10.19 (2020): 11643-11653.
16. Chen, Hongwen, et al. "Mechanism of electrocatalytic H2 evolution, carbonyl hydrogenation and carbon – carbon coupling on Cu." Journal of the American Chemical Society, 146.20 (2024): 13949–13961.
17. Zhou, Zheng, et al. "Hydrogen evolution reaction activity of nickel phosphide is highly sensitive to electrolyte pH." Journal of materials chemistry A 5.38 (2017): 20390-20397.
18. Cheng, Tao, et al. "Explanation of dramatic pH-dependence of hydrogen binding on noble metal electrode: Greatly weakened water adsorption at high pH." Journal of the American Chemical Society 140.25 (2018): 7787-7790.
19. Zhang, Mengtian, et al. "Ru-RuO_2/CNT hybrids as high-activity pH-universal electrocatalysts for water splitting within 0.73 V in an asymmetric-electrolyte electrolyzer." Nano Energy 61 (2019): 576-583.
20. Alamillo, Ricardo, et al. "The selective hydrogenation of biomass-derived 5-hydroxymethylfurfural using heterogeneous catalysts." Green Chemistry 14.5 (2012): 1413-1419.
21. Singh, Nirala, et al. "Impact of pH on aqueous-phase phenol hydrogenation catalyzed by carbon-supported Pt and Rh." ACS Catalysis 9.2 (2018): 1120-1128.
22. Goyal, Akansha, and Marc TM Koper. "The interrelated effect of cations and electrolyte pH on the hydrogen evolution reaction on gold electrodes in alkaline media." Angewandte Chemie International Edition 60.24 (2021): 13452-13462.
23. Goyal, Akansha, et al. "Cooperative Effect of Cations and Catalyst Structure in Tuning Alkaline Hydrogen Evolution on Pt Electrodes." Journal of the American Chemical Society 146.11 (2024): 7305-7312.
24. Subbaraman, Ram, et al. "Enhancing hydrogen evolution activity in water splitting by tailoring Li+-Ni (OH) 2-Pt interfaces." Science 334.6060 (2011): 1256-1260.

25. Zheng, Jie, et al. "Universal dependence of hydrogen oxidation and evolution reaction activity of platinum-group metals on pH and hydrogen binding energy." Science advances 2.3 (2016): e1501602.
26. Sheng, Wenchao, et al. "Correlating the hydrogen evolution reaction activity in alkaline electrolytes with the hydrogen binding energy on monometallic surfaces." Energy & Environmental Science 6.5 (2013): 1509-1512.
27. Zuo, Yong, et al. "Ru–Cu nanoheterostructures for efficient hydrogen evolution reaction in alkaline water electrolyzers." Journal of the American Chemical Society 145.39 (2023): 21419-21431.
28. Ledezma-Yanez, Isis, et al. "Interfacial water reorganization as a pH-dependent descriptor of the hydrogen evolution rate on platinum electrodes." Nature Energy 2.4 (2017): 1-7.
29. Zhao, Yige, et al. "Sulfur vacancy-promoted highly selective electrosynthesis of functionalized aminoarenes via transfer hydrogenation of nitroarenes with H2O over a Co3S4− x nanosheet cathode." CCS Chemistry 3.1 (2021): 507-515.
30. Shao, Feng, et al. "Surface water as an initial proton source for the electrochemical CO reduction reaction on copper surfaces." Angewandte Chemie 135.3 (2023): e202214210.
31. Jin, Qiuyan, et al. "In situ promoting water dissociation kinetic of Co based electrocatalyst for unprecedentedly enhanced hydrogen evolution reaction in alkaline media." Nano Energy 49 (2018): 14-22.
32. Chong, Xiaodan, et al. "Potential-tuned selective electrosynthesis of azoxy-, azo-and amino-aromatics over a CoP nanosheet cathode." *National science review* 7.2 (2020): 285-295.
33. Xia, Rong, et al. "Electrochemical reduction of acetonitrile to ethylamine." *Nature Communications* 12.1 (2021): 1-8.
34. Dixit, Ram Ji, et al. "Electrocatalytic hydrogenation of furfural using non-noble-metal electrocatalysts in alkaline medium." *Green Chemistry* 23.11 (2021): 4201-4212.
35. Shang, Xiao, Yang Yang, and Yujie Sun. "Electrohydrodimerization of biomass-derived furfural generates a jet fuel precursor." *Green chemistry* 22.16 (2020): 5395-5401.
36. Lasia, Andrzej. "Mechanism and kinetics of the hydrogen evolution reaction." international journal of hydrogen energy 44.36 (2019): 19484-19518.

37. Shinagawa, Tatsuya, Angel T. Garcia-Esparza, and Kazuhiro Takanabe. "Insight on Tafel slopes from a microkinetic analysis of aqueous electrocatalysis for energy conversion." Scientific reports 5.1 (2015): 13801.
38. Gu, Zhenao, et al. "Simultaneous phenol removal and resource recovery from phenolic wastewater by electrocatalytic hydrogenation." Environmental Science & Technology 56.7 (2022): 4356-4366.
39. Mao, Ran, et al. "Enhanced indirect atomic H* reduction at a hybrid Pd/graphene cathode for electrochemical dechlorination under low negative potentials." Environmental Science: Nano 5.10 (2018): 2282-2292.
40. Buxton, George V., et al. "Critical Review of rate constants for reactions of hydrated electrons, hydrogen atoms and hydroxyl radicals (· OH/· O^- in Aqueous Solution." Journal of physical and chemical reference data 17.2 (1988): 513-886.
41. Anantharaj, Sengeni, et al. "Strategies and perspectives to catch the missing pieces in energy-efficient hydrogen evolution reaction in alkaline media." Angewandte Chemie International Edition 60.35 (2021): 18981-19006.
42. Singh, Nirala, et al. "Aqueous phase catalytic and electrocatalytic hydrogenation of phenol and benzaldehyde over platinum group metals." Journal of Catalysis 382 (2020): 372-384.
43. Song, Yang, et al. "Hydrogenation of benzaldehyde via electrocatalysis and thermal catalysis on carbon-supported metals." Journal of Catalysis 359 (2018): 68-75.
44. Chadderdon, Xiaotong H., et al. "Mechanisms of furfural reduction on metal electrodes: Distinguishing pathways for selective hydrogenation of bioderived oxygenates." Journal of the American Chemical Society 139.40 (2017): 14120-14128.
45. Love, J. Christopher, et al. "Self-assembled monolayers of thiolates on metals as a form of nanotechnology." Chemical reviews 105.4 (2005): 1103-1170.
46. Liu, Cuibo, et al. "Designed Nanomaterials for Electrocatalytic Organic Hydrogenation Using Water as the Hydrogen Source." Accounts of Chemical Research 56.13 (2023): 1872-1883.
47. Koh, Katherine, et al. "Electrochemically tunable proton-coupled electron transfer in Pd-catalyzed benzaldehyde hydrogenation." *Angewandte Chemie* 132.4 (2020): 1517-1521.

48. Kresse, Georg, and Jürgen Furthmüller. "Efficiency of ab-initio total energy calculations for metals and semiconductors using a plane-wave basis set." Computational materials science 6.1 (1996): 15-50.
49. Kresse, Georg, and Jürgen Furthmüller. "Efficient iterative schemes for ab initio total-energy calculations using a plane-wave basis set." Physical review B 54.16 (1996): 11169.
50. Kresse, Georg, and Jürgen Hafner. "Ab initio molecular-dynamics simulation of the liquid-metal–amorphous-semiconductor transition in germanium." Physical Review B 49.20 (1994): 14251.
51. Kresse, Georg, and Jürgen Hafner. "Ab initio molecular dynamics for liquid metals." Physical review B 47.1 (1993): 558.
52. Methfessel, M. P. A. T., and A. T. Paxton. "High-precision sampling for Brillouin-zone integration in metals." *physical review B* 40.6 (1989): 3616.
53. Blöchl, Peter E. "Projector augmented-wave method." *Physical review B* 50.24 (1994): 17953.
54. Grimme, Stefan, Stephan Ehrlich, and Lars Goerigk. "Effect of the damping function in dispersion corrected density functional theory." *Journal of computational chemistry* 32.7 (2011): 1456-1465.
55. Hammer, B. H. L. B., Lars Bruno Hansen, and Jens Kehlet Nørskov. "Improved adsorption energetics within density-functional theory using revised Perdew-Burke-Ernzerhof functionals." *Physical review B* 59.11 (1999): 7413.
56. Mathew, Kiran, et al. "Implicit solvation model for density-functional study of nanocrystal surfaces and reaction pathways." *The Journal of chemical physics* 140.8 (2014).
57. Tang, W., E. Sanville, and G. Henkelman. "A grid-based Bader analysis algorithm without lattice bias." *Journal of Physics: Condensed Matter* 21.8 (2009): 084204.
58. Henkelman, Graeme, Blas P. Uberuaga, and Hannes Jónsson. "A climbing image nudged elastic band method for finding saddle points and minimum energy paths." *The Journal of chemical physics* 113.22 (2000): 9901-9904.

Chapter 4

Conjugated Aromatic Aldehydes Uniquely Undergo Electroreductive Carbon–Carbon Coupling on Cu

Cu catalyzes carbon-carbon coupling during the electrochemical hydrogenation (ECH) of conjugated aromatic aldehydes, like benzaldehyde. Contrarily, C–C coupling was not observed during the ECH of (i) aliphatic aldehydes, like pentanal, (ii) cyclic aldehydes, like cyclohexanal, or (iii) non-conjugated aromatic aldehydes like hydrocinnamaldehyde. Mechanistically, on the surface of Cu, an adsorbed aldehyde molecule first undergoes H addition to the carbonyl O to form a surface-bound hydroxy intermediate. Subsequently, the radical α-C of the hydroxy intermediate is attacked by the electrophilic carbonyl C of a physisorbed aldehyde, accompanied by a fast second H addition to the radical alkoxy O to form the C–C coupling product. The conjugated aldehyde molecules like benzaldehyde are planar and, therefore, adsorb strongly on the surface of Cu. The strong binding of the aldehyde with the metal surface and the conjugation between the aromatic ring and the C=O stabilizes the surface hydroxy intermediate, thus facilitating C–C coupling. Conversely, preferential first H addition to the carbonyl C (*via* the alkoxy pathway) or a fast second H addition to the α-C (resulting in the formation of the alcohol product) inhibits C–C coupling.

This chapter is based on the article: Hongwen Chen et al. Conjugated Aromatic Aldehydes Uniquely Undergo Electroreductive Carbon–Carbon Coupling on Cu (prepared for submission). Hongwen Chen performed the experiments, did the data analysis and wrote the manuscript.

4.1 Introduction

Upgrading lignocellulosic biomass to fuels, fine chemicals, and other high-value products has recently attracted attention.[1-6] Biomass is highly oxygenated and functionalized;[7-9] therefore, upgrading it typically involves hydrogenation and carbon-carbon bond formation to improve its stability and energy density.[7,10-15] Electrochemical hydrogenation (ECH) and electroreductive C-C coupling are, therefore, promising strategies that operate under milder reaction conditions than thermocatalytic alternatives that typically require elevated H_2 pressures and higher temperatures.[16-18]

Hydrogenation of the carbonyl (C=O) functional group and formation of C-C bonds in biomass-derived platform molecules are generally desired to stabilize the molecular structure and increase the molecular weight, respectively.[19-21] ECH of the C=O group to the corresponding alcohol has been extensively studied experimentally and computationally on different base and noble metal catalysts.[22-24] On the other hand, limited studies have focused on the electroreductive C-C coupling. A reason for this is that C-C coupling has only been observed on a limited number of catalysts (*e.g.*, Cu and Pb) under typically studied reaction conditions.[25,26]

Xiaotong *et al.* proposed that furfural reduction on Cu follows two distinct mechanisms: hydrogenation to furfuryl alcohol and C–C coupling to hydrofuroin.[27] Like furfural, benzaldehyde derivatives have also been suggested as a potential fuel source following C–C coupling and hydrogenation reactions. Song *et al.* observed that the ECH of benzaldehyde on Ni produced small quantities of hydrobenzoin (its C–C coupling product) at an applied external potential (η) of –1.1 V *vs* Ag/AgCl reference.[28] Yu *et al.* also observed hydrobenzoin during benzaldehyde ECH on bimetallic Pd-Cu catalysts with a Faradaic efficiency of ~63% at η = –0.4 V *vs* RHE.[26] We have recently reported on the unique property of Cu to catalyze both C=O hydrogenation to benzyl alcohol and C–C coupling to hydrobenzoin during benzaldehyde ECH in both acidic and alkaline conditions.[29]

The C–C coupling between two different aldehyde molecules, referred to as cross C–C coupling, is also a promising strategy for synthesizing high-value products and fine chemicals.[30-33] Cu has been proposed as a viable catalyst for cross C–C coupling reactions.

Villalobos *et al.* reported on the unique attributes of a Cu-catalyzed aerobic reaction system for the formation of ketones by coupling thiol esters with boronic acids at neutral pH.[34] Anibal *et al.* reported that Cu shows high selectivity toward the cross C–C coupling products in the co-reactant system of benzaldehyde and furfural.[25]

Electroreductive C–C coupling in aldehydes has been suggested to proceed *via* a Langmuir-Hinshelwood (LH)-type reaction of surface-bound intermediates.[35, 36] However, based on experimental results and first-principle molecular simulations, we have recently proposed an Eley-Rideal (ER)-type mechanism wherein a surface hydroxy intermediate reacts with a solvated physisorbed benzaldehyde molecule.[29] Combining kinetic measurements and isotope-labelling studies, we showed that the second H addition is the rate-determining step for benzyl alcohol formation, while the C–C bond formation is the rate-determining step for hydrobenzoin formation.

In this work, we present a detailed investigation of the ECH of various aliphatic, cyclic, and aromatic aldehydes on base (Cu and Ni) and noble metal (Pt, Pd, Ru and Rh) catalysts. We show that Cu uniquely catalyzes C–C coupling during the ECH of conjugated aromatic aldehydes. We discuss the mechanistic reasons that facilitate C–C bond formation uniquely on Cu.

4.2 Materials and methods

4.2.1 Chemicals

All chemicals, *viz.*, benzaldehyde (≥99.5%), propanal (97%), pentanal (≥98.0%), butanal (≥99.5%), heptanal (≥97.0%), *trans*-cinnamaldehyde (99%), hydrocinnamaldehyde (≥95.0%), 1,2,3,6-tetrahydrobenzaldehyde (cyclohexenal; 97%), cyclohexanal (anhydrous, 99.5%), furfural (99%), 4-methylbenzaldehyde (≥97%), 4-methoxybenzaldehyde (≥98.0%), copper (II) acetate (99.99%), palladium (II) acetate (97%), ruthenium (III) chloride hydrate (≥99.9%), rhodium (III) nitrate hydrate (~36% Rh basis), tetraammineplatinum (II) chloride (99.99%), nickel (II) nitrate (99.999%), acetic acid (≥99.7%), sodium acetate (≥99.0%), sodium hydroxide (≥98%), sodium chloride (≥99.0%), 2-propanol (anhydrous, 99.5%), acetone (≥99.9%), diphenyl ether (≥99%), and ethyl acetate (≥99.5%), were all purchased from Sigma-Aldrich and

used without further purification. Deionized (DI) water (18.2 MΩ·cm) was used to prepare all aqueous solutions.

4.2.2 Catalysts synthesis

All catalysts were prepared *via* the incipient wetness impregnation method, maintaining the same loading of different metals (~5 wt.-%) on a Vulcan XC-72R carbon black (QUINTECH) support. The metal precursors were dissolved in DI water or acetone. After impregnation, the slurries were dried at 383 K overnight. The dried powder was heated to temperatures ranging between 453 – 673 K (ramp: 5 $K \cdot min^{-1}$) for 2 – 4 h under ~100 $mL \cdot min^{-1}$ N_2 followed by reduction at 473 – 673 K (ramp: 5 $K \cdot min^{-1}$) for 2 – 4 h under 100 $mL \cdot min^{-1}$ H_2. The specific conditions employed for the synthesis of different carbon-supported metal catalysts are reported in Supplementary **Table S3-1**.

4.2.3 Carbon felt pretreatment

Carbon felt (Sigma-Aldrich, 3.0 cm × 1.5 cm) was immersed sequentially in acetone, DI water, and acetone again for at least 30 min each under ultrasonication treatment at ambient temperature. Finally, the treated carbon felt was dried in an oven at 333 K for 12 h.

4.2.4 Electrode preparation

The synthesized Cu/C (~10 mg) was dispersed in a 1:1 solution of 1 mL 2-propanol and 1 mL DI water for 30 min under ultrasonication treatment at room temperature. The catalyst ink was then deposited on both sides of the pretreated carbon felt. The carbon felt electrode (containing Cu/C catalyst) was finally dried overnight in an oven at 333 K.

4.2.5 Nafion membrane pretreatment

The Nafion-117 proton exchange membrane (Ion Power) was first immersed in a 3% H_2O_2 solution for 1 h at 353 K. The Nafion membrane was then immersed in DI water at 353 K for 2 h. Subsequently, the membrane was immersed in 1 $mol \cdot L^{-1}$ H_2SO_4 at 353 K for 1 h. Finally, the Nafion membrane was washed several times with DI water and stored in DI water under ambient conditions.

4.2.6 Electrochemical measurements

All electrochemical measurements were performed on a BioLogic VSP-300 workstation. A two-compartment batch electrocatalysis cell was used to perform the electrochemical experiments. A carbon felt coated with the metal catalyst was used as the working electrode. A double-junction Ag/AgCl electrode (eDAQ) and a Pt wire (Sigma-Aldrich) were used as the reference and counter electrodes, respectively. The cathode and anode compartments were separated by the Nafion proton exchange membrane. The reference electrode was calibrated against a reversible hydrogen electrode (RHE) and all potentials herein are reported with respect to the RHE reference electrode, per the following equation:

$$E_{RHE} = E_{Ag/AgCl} + 0.197 + 0.059 \cdot pH \quad (4\text{-}1)$$

where E_{RHE} and $E_{Ag/AgCl}$ are electrode potentials relative to RHE and Ag/AgCl, respectively. All electrochemical experiments were performed under ambient conditions. A constant flow of pure N_2 (~25 mL·min^{-1}) was bubbled through the catholyte during the entire course of reaction to remove dissolved gases. The electrolyte solution was continuously stirred at a speed of 500 rpm. The solution resistance between the working and the reference electrodes was measured by potentiostatic electrochemical impedance spectroscopy (PEIS) and compensated (~85%) by the electrochemical workstation. Prior to the reaction, the catalysts were polarized at –40 mA for at least 20 min to ensure complete reduction of the metal.

4.2.7 Product Analysis

The course of the electrochemical experiment was followed by periodically withdrawing ~1 mL aliquots from the catholyte. The organics in the aqueous catholyte were extracted with 0.5 mL ethyl acetate. The extract was mixed with 0.5 mL ethyl acetate containing 20 mM diphenyl ether as an external standard. The extracted organic compounds were analyzed by an offline gas chromatograph coupled with a mass spectrometer (Agilent Technologies 7890B GC/5977A MSD).

The electron consumption towards H_2 formation was indirectly estimated from the difference in total electron consumption and electron consumption towards the formation of organic products. The amount of H_2 formed was then calculated using the following equation:

$$n_{H2} = \frac{e_{H2}}{2 \cdot F} \quad (4\text{-}2)$$

where n_{H_2} is the amount of H_2 formed (in mol), e_{H_2} is the electron consumption towards H_2 formation (in C), and F is the Faraday's constant (= 96485 C·mol^{-1})

4.2.8 Calorimetry measurements

Aqueous-phase heat of the adsorption of the organic substrates on carbon-supported metal catalysts was determined at room temperature using a Setaram C80 calorimeter. An aqueous solution (~1 mL) with specific concentration of the organic substrate was added to the calorimetry cell together with the catalyst (~20 mg). Another aqueous solution with the same concentration of the organic substrate but without the catalyst was used as the reference.

4.2.9 Computational details.

All quantum chemical simulations were performed on a periodic model using the CP2K electronic structure and molecular dynamics software package (v2022.2).[37] The simulations were performed on Cu(111) and Ru(0001) surfaces composed of four atomic layers. The bottom two layers were constrained while the top two layers were allowed to relax during the electronic structure calculations The model electrodes containing 100 atoms were solvated using 48 explicit water molecules, a proton and the organic substrate.

Electronic structure optimizations were carried out employing the hybrid Gaussian and plane waves (GPW) method implemented in the Quickstep module of the CP2K software package.[38] The expanded electron density in the auxiliary plane wave basis set were moderated with the energy cutoff of 400 Ry. The 4d5s electrons of Ru, 3d4s electrons of Cu, 2s2p electrons of O and C, and the 1s electrons of H were considered as the valence states expanded using the optimized double-ζ plus polarization quality Gaussian basis sets (MOLOPT-SR DZVP)[39] while the ionic cores were represented by norm-conserving Goedecker−Teter−Hutter (GTH) pseudopotentials.[40-42] The Perdew−Burke−Ernzerhof (PBE)[43] density functional approximation was applied in conjunction with DFT-D3 dispersion corrections described by Grimme *et al.*[44] to treat the exchange correlation effects with the Generalized Gradient Approximation (GGA). Matrix diagonalization was used to solve the Kohn−Sham equations and the electronic structure convergence criteria was set to 1.0×10^{-6} a.u. for the electronic Self-Consistent Field (SCF) loops. The SCF convergence was further accelerated by applying Fermi−Dirac smearing at an electronic temperature of 300 K.

4.3 Results and discussion

The carbon-supported metal catalysts (with ~5 wt.-% metal loading) were synthesized *via* a previously described incipient-wetness impregnation method using Vulcan carbon black as the support. Detailed characterization of the synthesized Cu/C catalyst has been reported elsewhere.[29]

4.3.1 ECH of Aldehydes on Different Base and Noble Metals

First, let us focus on the ECH of benzaldehyde (an aromatic aldehyde) on different carbon-supported base metal (Cu and Ni) and noble metal (Pd, Pt, Ru and Rh) catalysts. **Figure 4-1a** shows the initial product formation rates and Faradaic efficiencies towards benzaldehyde conversion (FE_{BZ}) during benzaldehyde ECH on different metal catalysts. Notably, Pd exhibited the highest ECH rate (~14.7 $mmol_H \cdot g_{Pd}^{-1} \cdot s^{-1}$) amongst the investigated metals. However, the FE_{BZ} on Pd was only ~58%. Other noble metals, *i.e.*, Pt, Ru and Rh, also showed relatively high ECH rates (5.6 – 11.6 $mmol_H \cdot g_{metal}^{-1} \cdot s^{-1}$) but low FE_{BZ} (less than 30 %). The low Faradaic efficiency on noble metals is likely due to the high applied overpotential (η = –0.5 V *vs* RHE), which typically results in high H_2 formation rates. Interestingly, benzyl alcohol was the only product detected on all investigated noble metal catalysts except Rh/C, which, in addition to the hydrogenation of the C=O group, also catalyzed complete hydrogenation of the aromatic ring, resulting in the formation of small amounts of cyclohexanemethanol (~1.4% Faradaic selectivity).

The base metals, *viz.*, Ni and Cu, exhibited relatively low ECH rates (~2.39 $mmol_H \cdot g_{metal}^{-1} \cdot s^{-1}$ on Cu/C and ~2.45 $mmol_H \cdot g_{metal}^{-1} \cdot s^{-1}$ on Ni/C) than the noble metals for the benzaldehyde ECH reaction; however, the FE_{BZ} was significantly higher, especially on Cu (almost 94%), under the investigated reaction conditions (**Figure 4-1a**). A high Faradaic efficiency indicates high coverage of the organic substrate (and consequentially low H* coverage resulting in low HER rates) under the investigated reaction conditions. Remarkably, in addition to the hydrogenation of C=O, Cu also catalyzed the C–C coupling reaction, resulting in the formation of hydrobenzoin with significant Faradaic selectivity (~46%). Both hydrobenzoin and benzyl alcohol were detected as the kinetically primary products of benzaldehyde ECH on Cu. Again, we emphasize that the formation of hydrobenzoin, and thus the electroreductive C–C coupling,

was not observed on any other base or noble metal catalysts (except Cu/C) that were investigated in this work under the applied reaction conditions.

Next, we investigated the ECH of pentanal, an aliphatic aldehyde, on the different base and noble metal catalysts under the same reaction conditions. **Figure 4-1b** shows the initial product formation rates and the Faradaic efficiencies towards pentanal conversion (FE_{PA}) during the ECH of pentanal on different metals. The noble metals again exhibited high total ECH rates (6.4 – 7.9 $mmol_H \cdot g_{metal}^{-1} \cdot s^{-1}$) but low FE_{PA} (less than 19%). The low FE_{PA} on noble metals can be attributed to the high applied overpotential. Again, the total pentanal ECH rates on the base metals were much lower (*e.g.*, ~1.95 $mmol_H \cdot g_{metal}^{-1} \cdot s^{-1}$ on Cu/C and ~2.44 $mmol_H \cdot g_{metal}^{-1} \cdot s^{-1}$ on Ni/C). However, the FE_{PA} was relatively high, especially on Cu (almost 54%), under the investigated reaction conditions. Pentanol (C=O hydrogenation product) was the only product observed in all cases. Interestingly, we did not observe the C–C coupling product, even on Cu, during pentanal ECH under these reaction conditions.

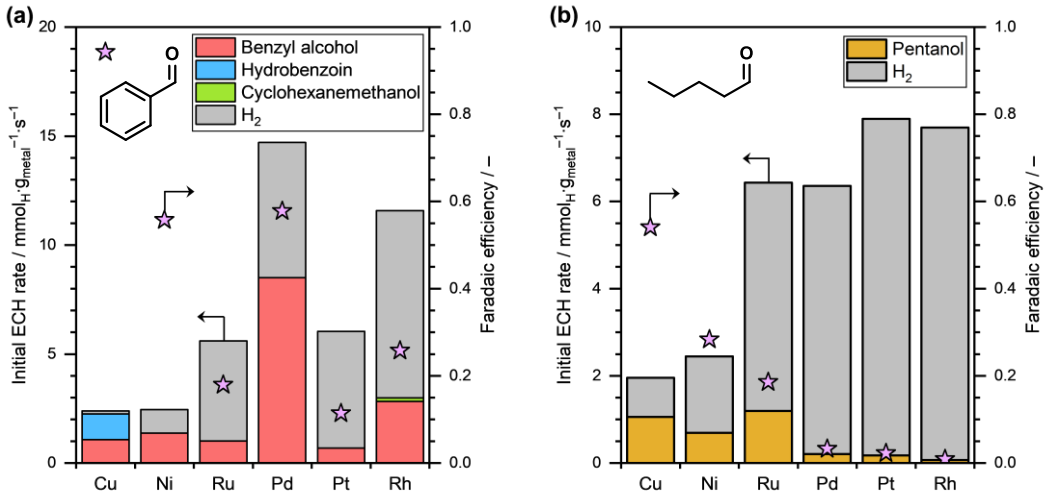

Figure 4-1. Initial rates of formation of different products, and FE towards aldehyde conversion, during the ECH of (a) benzaldehyde and (b) pentanal on different carbon-supported base and noble metal catalysts. Reaction conditions: ~10 mg catalyst, ~20 mM organic substrate, η = – 0.5 V *vs* RHE, 1.5 M acetate buffer solution (pH ~4.6), ambient temperature and pressure.

To further understand the difference in product selectivity on Cu for benzaldehyde and pentanal ECH, we performed the ECH of several aliphatic and aromatic aldehydes on Cu/C under similar reaction conditions. **Figure 4-2a** shows the ECH rates of four linear aliphatic aldehydes with varying carbon chain lengths, *viz.*, propanal (C_3), butanal (C_4), pentanal (C_5) and heptanal (C_7). Although the total ECH rates were comparable in all cases (varying between

1.8 and 2.8 $mmol_H \cdot g_{Cu}^{-1} \cdot s^{-1}$), the FE towards aldehyde conversion increased systematically with increasing carbon chain length – from ~9.6% during propanal ECH to ~90% during heptanal ECH. The monotonous increase in the FE suggests that the surface coverage of the organic substrate increased with increasing chain length of the aliphatic aldehydes. This is likely due to the stronger interaction of longer chain aldehydes with the electrode's surface. Notably, no C–C coupling products were detected during the ECH of any of the aliphatic aldehydes we investigated. Overall, these experimental results strongly suggest that C–C coupling does not occur during the ECH of aliphatic aldehydes, even on Cu.

Next, we performed the ECH of several cyclic aldehydes on Cu/C under similar reaction conditions. **Figure 4-2b** shows the ECH product distribution during the ECH of hydrocinnamaldehyde, cyclohexenal and cyclohexanal on Cu/C. The product distribution during benzaldehyde ECH on Cu/C is also shown for comparison. Again, the total ECH rates were similar for all cyclic aldehydes (varying between 1.3 and 2.4 $mmol_H \cdot g_{Cu}^{-1} \cdot s^{-1}$). The Faradaic efficiency towards aldehyde conversion was also relatively high (≥87%) in all cases, suggesting high organic coverage (and consequentially low H* coverage) on the electrode's surface. However, C–C coupling products were not observed during the ECH of cyclic aldehydes (other than benzaldehyde) that we investigated. The absence of C–C coupling during the ECH of cyclohexenal or cyclohexanal suggests that the aromatic ring in aldehydes facilitates C–C bond formation on Cu/C. Furthermore, the absence of any C–C coupling products during the ECH of hydrocinnamaldehyde suggests that the aromatic ring in the aldehyde must be in conjugation with the C=O group for the C–C coupling to occur.

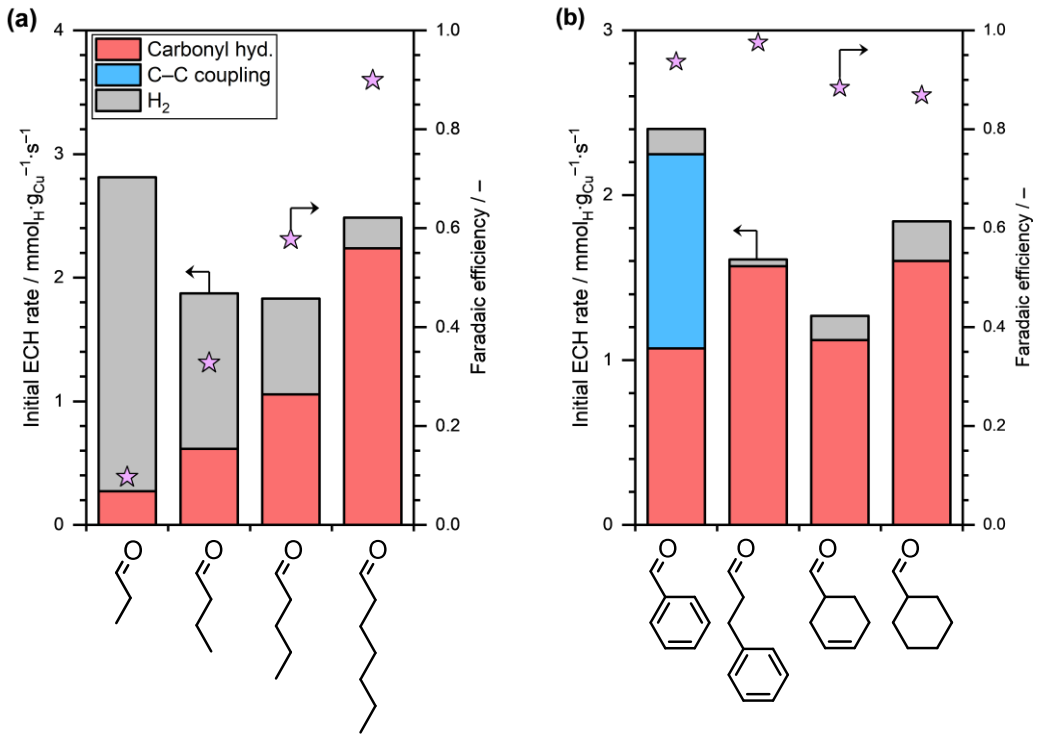

Figure 4-2. Initial rates of C=O hydrogenation, C-C coupling, and H_2 evolution, and FE towards aldehyde conversion, during the ECH of (a) propanal, butanal, pentanal, and heptanal, and (b) benzaldehyde, hydrocinnamaldehyde, cyclohexenal, and cyclohexanal, on Cu/C. Reaction conditions: ~10 mg catalyst, ~20 mM organic substrate, η = –0.5 V *vs* RHE, 1.5 M acetate buffer solution (pH ~4.6), ambient temperature and pressure.

To investigate further, we performed the ECH of several aromatic aldehydes with a conjugated aromatic ring and C=O group. **Figure 4-3** shows the selectivity (on a carbon basis) towards C=O hydrogenation and C–C coupling products during the ECH of 4-methylbenzaldehyde, 4-methoxybenzaldehyde, and furfural on Cu/C. The product selectivity during benzaldehyde ECH on Cu/C is also shown for comparison. Remarkably, we observed the formation of both C=O hydrogenation and C–C coupling products during the ECH of all conjugated aromatic aldehydes. We note that in some cases (*e.g.*, during the ECH of furfural or 4-methoxybenzaldehyde), the carbon balance between the reactant converted and products formed during the reaction was not complete; the difference is denoted as "Others" in **Figure 4-3**. These byproducts are likely to be either (i) high molecular weight compounds that are adsorbed on the carbon felt electrode or (ii) light hydrocarbons that escaped to the gas phase due to constant bubbling of N_2 through the electrolyte solution. For example, methylfuran has been observed as a byproduct during furfural ECH on Cu.[27] The formation of C–C coupling

products during the ECH of conjugated aromatic aldehydes allows us to conclude that a conjugated system of an aromatic ring and a C=O group facilitates C–C coupling on Cu.

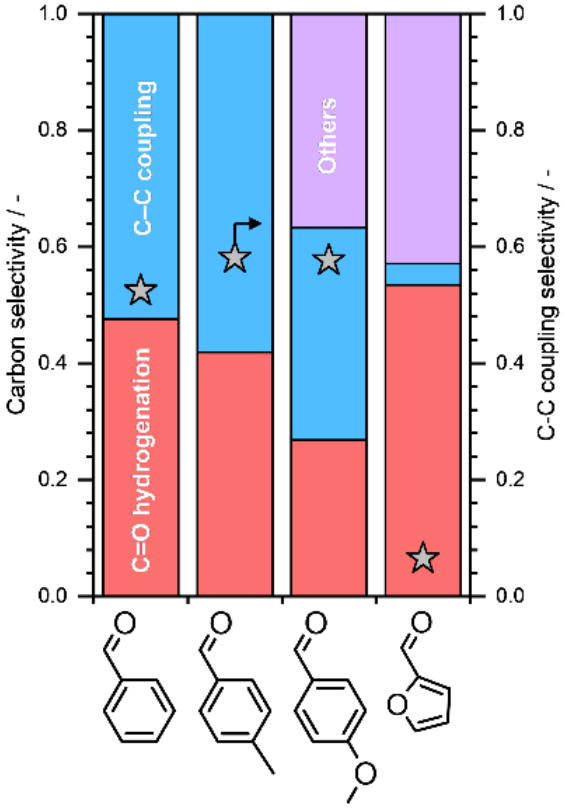

Figure 4-3. Selectivity (on a carbon basis) towards C=O hydrogenation products (red), C–C coupling products (blue), and "others" (purple) during the ECH of several aromatic aldehydes on Cu/C. The selectivity towards C–C coupling product (without considering "Others") is also shown. Reaction conditions: ~10 mg catalyst, ~20 mM organic substrate, η= –0.5 V vs RHE, 1.5 M acetate buffer solution (pH= 4.6), ambient temperature and pressure.

Alkaline electrolytes have been suggested to provide a good platform for C–C coupling reactions with high Faradaic selectivity.[45, 46] Therefore, we performed the ECH of conjugated aromatic aldehydes on Cu/C in alkaline media ($pH = 11.3$). **Figure 4-4** shows the product selectivity (on a carbon basis) during the ECH of benzaldehyde, 4-methylbenzaldehyde and 4-methoxybenzaldehyde on Cu/C in an alkaline electrolyte with $pH = 11.3$. The product selectivities during the ECH of pentanal and cyclohexanal in alkaline media are also shown. First of all, like in acidic media, we observed the formation of both C=O hydrogenation and C–C coupling products during the ECH of conjugated aromatic aldehydes. On the other hand, we did not observe C–C coupling products during the ECH of aliphatic (pentanal) or cyclic (cyclohexanal) aldehydes. These results clearly illustrate that only conjugated aromatic

aldehydes (like benzaldehyde) undergo C–C coupling during their ECH on Cu/C, even in alkaline conditions.

Furthermore, we noted that the selectivity towards C–C coupling products was generally higher in alkaline conditions. For example, the hydrobenzoin selectivity during benzaldehyde ECH was significantly higher in alkaline media (~84%) than in acidic media (~46%). These results, therefore, clearly show that alkaline media facilitates C–C coupling during ECH of conjugated aromatic aldehydes.

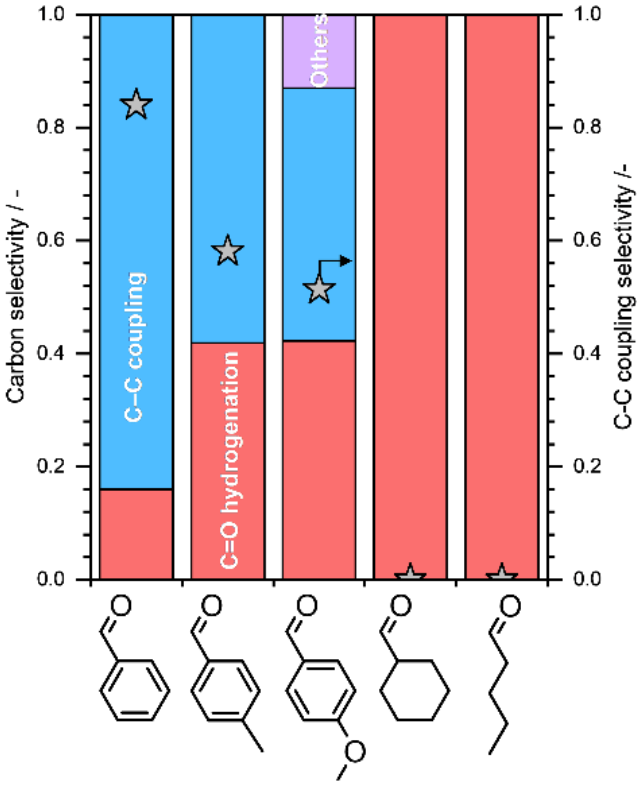

Figure 4-4. Selectivity (on a carbon basis) towards C=O hydrogenation products (red), C–C coupling products (blue), and others (purple) during the ECH of several aldehydes on Cu/C under alkaline conditions. The selectivity towards C–C coupling product (without considering "Others") is also shown. Reaction conditions: ~10 mg catalyst, ~20 mM organic substrate, $\eta =$ –0.5 V *vs* RHE, NaOH/NaCl electrolyte ($pH =$ 11.3), room temperature and pressure.

4.3.2 Aqueous-phase Heat of Adsorption of Aldehydes on Metals

We performed calorimetry measurements to investigate the adsorption of aldehydes on Cu/C. The experimentally obtained aqueous-phase heat of adsorptions (Q_{ads}) of several aldehydes on Cu/C are reported in **Figure 4-5**. We can see that the Q_{ads} of conjugated aromatic aldehydes (*i.e.*, benzaldehyde, furfural or cinnamaldehyde) on Cu/C was very high (>145 kJ·mol^{-1}). Note

that conjugated aromatic aldehydes are planar. These planar molecules likely adsorb flat on the surface of Cu with strong interaction between the surface and the (unsaturated electron-rich) aromatic ring, resulting in high values of Q_{ads}. On the other hand, saturated aliphatic aldehydes are not planar. Therefore, the Q_{ads} of aliphatic (pentanal) and cyclic (cyclohexanal) aldehydes on Cu/C were relatively low (<50 kJ·mol^{-1}; **Figure 4-5**). Interestingly, non-conjugated aromatic aldehydes showed intermediate Q_{ads} values. For example, the Q_{ads} of hydrocinnamaldehyde was estimated to be ~85 kJ·mol^{-1}.

We also performed calorimetry measurements to investigate the adsorption of benzaldehyde on Pd/C and Ru/C (*i.e.*, metals that did not promote C–C coupling). The obtained Q_{ads} values are also presented in **Figure 4-5**. Interestingly, the Q_{ads} of benzaldehyde was very low on both metals (*i.e.*, ~25 kJ·mol^{-1} on Pd/C and ~21 kJ·mol^{-1} on Ru/C). These results clearly suggest that a strong interaction of the conjugated aromatic ring of planar aldehydes with the surface of Cu promotes the C–C coupling reaction.

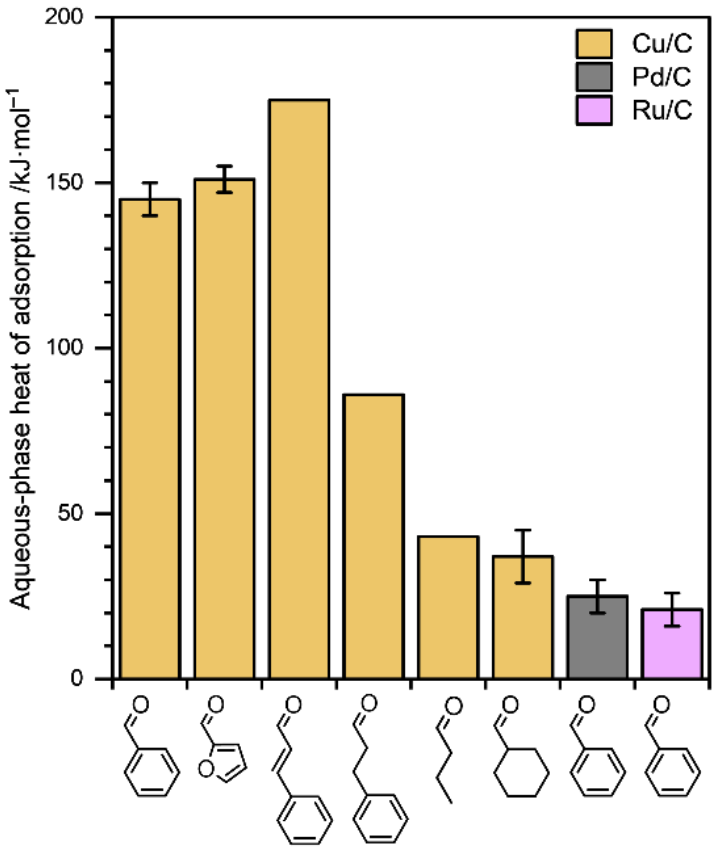

Figure 4-5. Aqueous-phase heat of adsorptions of various aldehydes on Cu/C, Pd/C or Ru/C under ambient conditions.

4.3.3 Mechanism of Aldehyde ECH on Metal Surfaces

We have previously described the mechanism for electrochemical C=O hydrogenation and C–C coupling during benzaldehyde ECH on Cu/C in acidic media (**illustrated in Scheme 4-1a**).[29] First, a benzaldehyde molecule (RCHO) reversibly adsorbs on a vacant site (*). The adsorbed benzaldehyde (RCHO*) undergoes a first H addition to the carbonyl O atom to form a surface hydroxy intermediate (RCHOH*). The hydroxy intermediate then undergoes a second H addition to its α-C to form BA*. The second H addition is the rate-determining step for benzyl alcohol formation. In a parallel reaction, the electrophilic carbonyl C of a nearby physisorbed benzaldehyde molecule ($RC^{\delta+}HO^{\delta-}$) attacks the radical α-C of the hydroxy intermediate to form the C–C bond. The C–C bond formation is followed by a fast H addition to the radical O to form HB*. The C–C bond formation is the rate-determining step for hydrobenzoin formation during benzaldehyde ECH. We have also described the mechanism of benzaldehyde ECH on Cu/C in alkaline media.[47] The key difference between the mechanisms in acidic media and alkaline media is the shift in the RDS for hydrobenzoin formation from C–C coupling (in acidic media) to the first H addition (in alkaline media).[29, 47]

Note that C=O hydrogenation of an aldehyde (to form the corresponding alcohol) requires two H addition steps, each to the aldehyde's carbonyl C and O atoms, respectively. Therefore, C=O hydrogenation could proceed *via* two distinct pathways: the hydroxy pathway (illustrated in **Scheme 4-1a**) or the alkoxy pathway (illustrated in **Scheme 4-1b**). In the hydroxy pathway, the first H addition occurs on the carbonyl O atom of the adsorbed benzaldehyde (ArCHO*) to form a surface hydroxy intermediate (ArCHOH*), followed by a second H addition to its α-C to form BA*. In the alkoxy pathway, on the other hand, the first H addition occurs on the carbonyl C atom of benzaldehyde to form a surface alkoxy intermediate ($ArCH_2O$*), followed by H addition to the O radical to form BA*. Through isotopic labelling studies, we have shown that benzaldehyde hydrogenation on Cu/C proceeds primarily *via* the hydroxy pathway.[29]

Based on kinetic measurements aided by first-principle molecular simulations, we have also shown that C–C coupling, during benzaldehyde ECH on Cu/C, occurs via an Eley-Rideal (ER)-type reaction between a surface hydroxy intermediate and a physisorbed benzaldehyde molecule.[29] In the proposed mechanism, the radical α-C of the surface hydroxy intermediate (RCHOH*) is attacked by the electrophilic carbonyl C of a physisorbed aldehyde molecule

($RC^{\delta+}HO^{\delta-}$). We note that such a C–C coupling reaction requires C–C bond formation between the carbonyl C atoms of the two aldehyde molecules in addition to hydrogenation of the carbonyl O atoms of each aldehyde. The formation of the C–C coupling product, therefore, necessitates that the H addition proceeds *via* the hydroxy pathway. A preferential first H addition to the carbonyl C (*via* the alkoxy pathway) will saturate the C atom and, therefore, hinder C–C bond formation (as illustrated in **Scheme 4-1b**).

Finally, based on kinetic measurements and first-principle molecular simulations, we also showed that the second H addition is the rate-determining step for benzyl alcohol formation during benzaldehyde ECH. In other words, the second H addition is slower than the first H addition. A slow second H addition step (like in the case of benzaldehyde ECH), therefore, results in a high concentration of the hydroxy intermediate on the surface. Contrarily, a fast second H addition would consume the surface hydroxy intermediate, which is a reactant in the C–C coupling reaction, and thus only form the C=O hydrogenation product (as illustrated in **Scheme 4-1c**). In other words, a fast second H addition step (compared to the first H addition step) will inhibit the C–C coupling reaction during aldehyde ECH.

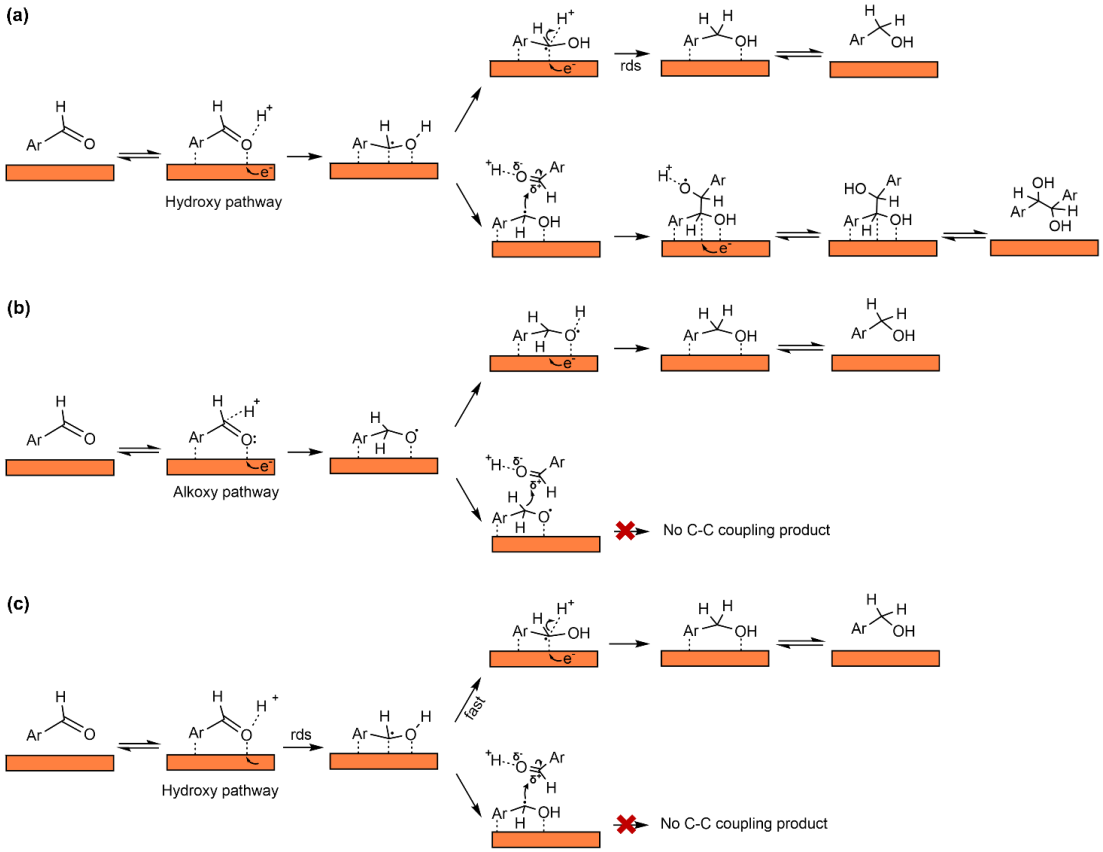

Scheme 4-1. Mechanism of C=O hydrogenation and C–C coupling during aldehyde ECH on a metal surface.

4.3.4 First-principle Molecular Simulations

We performed first-principle periodic density functional theory simulations to understand further the H addition to benzaldehyde (a conjugated aromatic aldehyde that undergoes C–C coupling) and cyclohexanal (an aldehyde that does not undergo C–C coupling) on Cu(111) and Ru(0001) surfaces. The simulations were performed on a system comprising an aldehyde (benzaldehyde or cyclohexanal) molecule adsorbed flat on a 5×5×4 metal surface. The aqueous-phase acidic environment was simulated by adding 47 explicit water molecules and one H_3O^+ ion to the system. Charges were estimated using the Bader charge analysis.

First of all, let us focus on the adsorption configurations of saturated and unsaturated aldehydes on the Cu surface. **Figure 4-6** shows the optimized geometry of benzaldehyde and cyclohexanal adsorbed on the Cu(111) surface in an aqueous environment (with an H_3O^+ ion). We can clearly see that the (planar) benzaldehyde molecule is adsorbed flat at a distance of ~2.15 Å from the surface of Cu. The cyclohexanal molecule, on the other hand, is adsorbed at a significantly larger distance (~2.65 Å) from the surface of Cu. These DFT calculations clearly indicate that the benzaldehyde adsorbs more strongly on the surface of Cu compared to cyclohexanal, which agrees with the experimental observations ($Q_{ads} \approx$ 145 kJ·mol^{-1} for benzaldehyde and $Q_{ads} \approx$ 40 kJ·mol^{-1} for cyclohexanal on Cu/C; **Figure 4-5**).

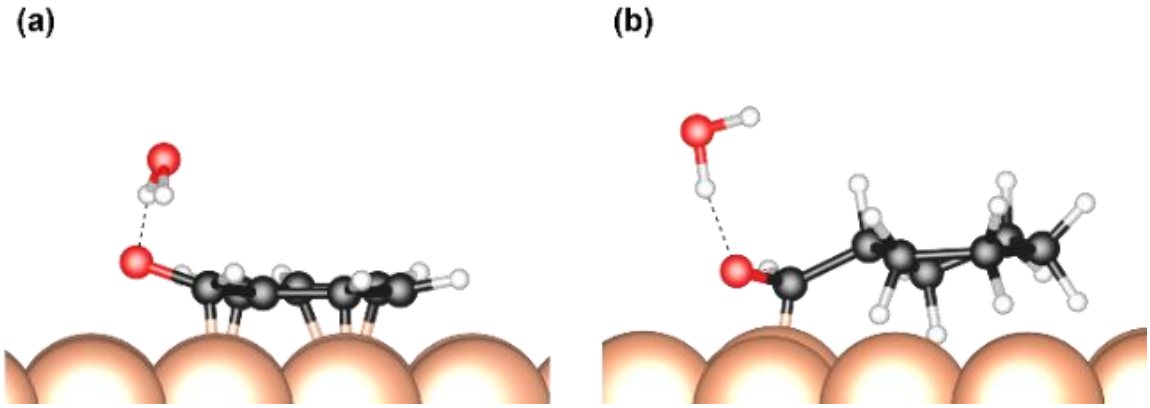

Figure 4-6. Adsorption configurations of (a) B benzaldehyde* and (b) cyclohexanal* on Cu(111) surface. Cu: orange, C: black, O: red, H: gray. Some H_2O molecules have been removed for clarity.

Next, let us look at the hydroxy and alkoxy pathways for H addition on a benzaldehyde benzaldehyde molecule adsorbed flat on the Cu(111) surface. For this, we added an H atom to either the carbonyl C atom or the carbonyl O atom (O_b) and relaxed the system to obtain the

optimized structure of the corresponding hydroxy (RCHOH*) and alkoxy (RCH_2O*) intermediates. The optimized geometry of BZ*, BA*, RCHOH*, and RCH_2O* are presented in **Figure 4-7a**. From these optimized configurations, we estimated the difference in the electronic energy (at 0 K) of the hydroxy and alkoxy intermediates (referred to as ΔE_{OH-CH}). In the case of benzaldehyde adsorbed on Cu(111) surface, ΔE_{OH-CH} was estimated to be –25 kJ·mol^{-1}, *i.e.*, the hydroxy intermediate was found to be thermodynamically more stable than the alkoxy intermediate. This result agrees with the experimental evidence, which suggested that benzaldehyde ECH on Cu/C proceeds *via* the hydroxy pathway.[29]

We also investigated the relative stability of hydroxy and alkoxy intermediates for cyclohexanal ECH on the Cu(111). Interestingly, in this system, we were not able to stabilize either the alkoxy or the hydroxy intermediate on the Cu(111) surface. The formed intermediates underwent the second H addition during the geometry optimization, resulting in the formation of cyclohexanol in both cases. These results clearly suggest that the second H addition, in the case of cyclohexanal ECH on Cu, must be facile under these reaction conditions (*i.e.*, the presence of hydronium ions). As discussed above, a fast second H addition will consume the hydroxy or the alkoxy intermediate (formed after the first H addition) and hence suppress the C–C coupling reaction. This result agrees with the experimental evidence, which showed that no C–C coupling products are formed during cyclohexanal ECH on Cu/C.

Next, we simulated the relative stability of the hydroxy and alkoxy intermediates formed during benzaldehyde ECH on the Ru(0001) surface. The optimized configurations of BZ*, BA*, RCHOH* and RCH_2O* are presented in **Figure 4-7b**. Again, based on the optimized configurations, we estimated the ΔE_{OH-CH} in this case to be +46 kJ·mol^{-1}. In other words, in the case of benzaldehyde ECH on Ru, the alkoxy intermediate is thermodynamically more stable than the hydroxy intermediate. Therefore, H addition to benzaldehyde on Ru likely proceeds *via* the alkoxy pathway, and the preferential first hydrogenation of the carbonyl C atom prevents the C–C coupling pathway on Ru/C. This prediction agrees with the experimental evidence where we observed no C–C coupling products during benzaldehyde ECH on Ru/C.

Based on the experimental evidence and molecular simulation results, we postulate the conditions that facilitate C–C coupling during the ECH of aldehydes on metals. Firstly, planar (conjugated) aromatic aldehydes adsorb flat on the surface of the metal. This flat adsorption is

facilitated by the strong interaction of the aromatic ring with the metal surface resulting in a high adsorption heat. We postulate that a strong interaction of the aromatic ring with the metal surface and a conjugation between the aromatic ring and the C=O group results in a stable hydroxy intermediate. Secondly, the hydroxy pathway (*i.e.*, preferential first H addition to the carbonyl O) must be the preferred pathway for H addition. A preferential first H addition to the carbonyl C via the alkoxy pathway will saturate the C atom and thus hinder C–C bond formation. Lastly, the second H addition must be slower than the first H addition. A relatively fast second H addition (to the hydroxy or the alkoxy intermediate) will consume the surface intermediate (that is required for C–C coupling) and thus only form the C=O hydrogenation product.

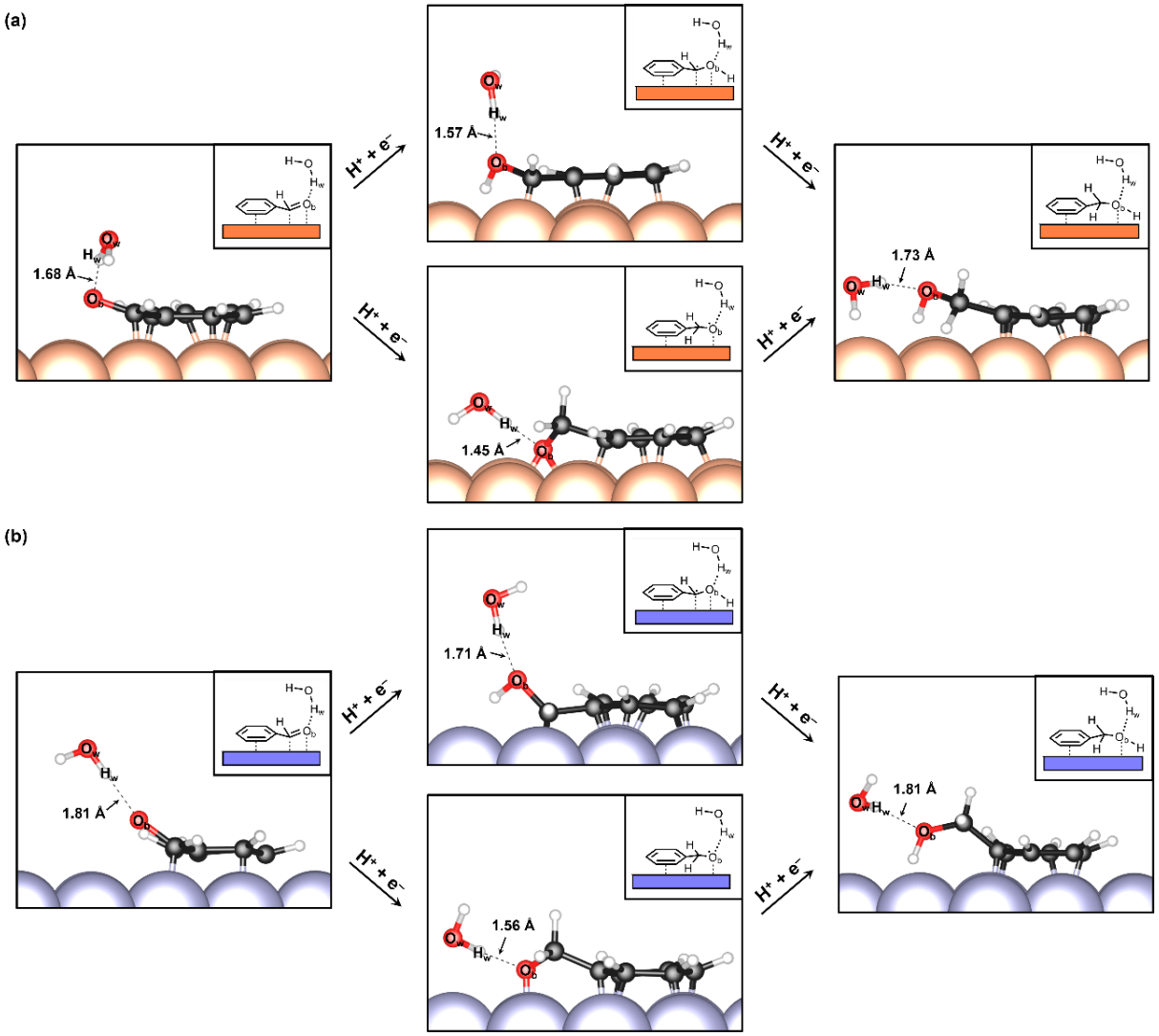

Figure 4-7. Optimized configurations of the adsorbed aldehyde, hydroxy intermediate, alkoxy intermediate, and the alcohol on the Cu(111) and Ru(0001) surfaces. The reported number are interatomic distances. Cu: orange, Ru: blue, C: black, O: red, H: gray. Some H_2O molecules have been removed for clarity.

4.3.5 Co-reaction between Aldehydes on Metal Surfaces

We also investigated the simultaneous ECH of two different aldehydes on metal surfaces. First, let us focus on the co-reaction of benzaldehyde and pentanal on Cu. **Figure 4-8a** shows the concentration profiles of reactants and products as a function of reaction time during the co-reaction of benzaldehyde and pentanal on Cu/C. The concentration profiles during the individual reactions (*i.e.*, without the co-reactant) of benzaldehyde and pentanal under the same reaction conditions are also shown for comparison. Interestingly, in this co-reaction experiment, in addition to the formation of the respective C=O hydrogenation products (*i.e.*, benzyl alcohol and pentanol), we only observed the C–C coupling product of benzaldehyde (*i.e.*, hydrobenzoin) but not the C–C coupling product of pentanal. These results further corroborate that the C–C coupling reactions only occur in the case of conjugated aromatic aldehydes on Cu/C.

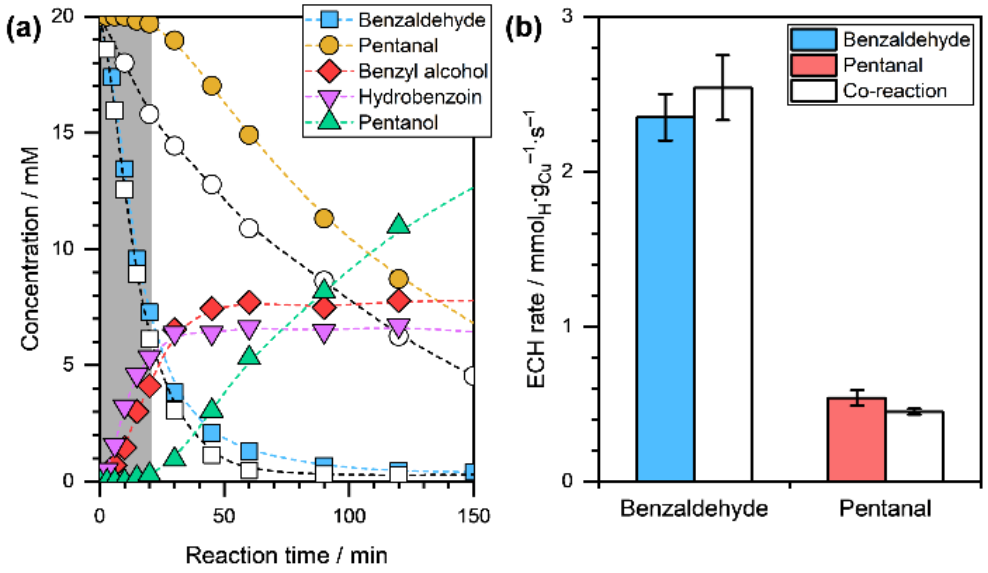

Figure 4-8. (a) Concentration profile of reactants and products, as a function of reaction time, during the co-reaction (closed symbols) of benzaldehyde with pentanal. The concentration profiles during the individual reactions are shown (open symbols). (b) Initial ECH rates during the individual and co-reaction of benzaldehyde and pentanal on Cu/C. Reaction conditions: ~10 mg catalyst, ~20 mM organic substrate, $\eta = -0.5$ V *vs* RHE, 1.5 M acetate buffer solution ($pH = 4.6$), ambient temperature and pressure. The dashed lines are guides to the eye.

Interestingly, we noticed an unusual phenomenon during the co-reaction of benzaldehyde and pentanal. Although benzaldehyde conversion started immediately at the start of the reaction, pentanal conversion was suppressed at initial reaction times (indicated by the grey zone in **Figure 4-8a**). Pentanal conversion started only after ~20 min of reaction when a substantial amount of benzaldehyde had been converted, and as a result, benzaldehyde concentration in the

electrolyte became low. We also observed similar behavior during the co-reaction of benzaldehyde with butanal and heptanal (see Supplementary **Figure S4-2**). In both cases, the conversion of butanal or heptanal was suppressed initially and only started once the benzaldehyde concentration was low. This behavior during the co-reaction of benzaldehyde with aliphatic aldehydes suggests that the surface of Cu is initially saturated with benzaldehyde (or its hydrogenated derivatives), and the surface coverage of pentanal is negligible. As the reaction proceeds, the surface coverage of benzaldehyde decreases due to a decrease in its concentration, which allows pentanal to adsorb on the surface and be subsequently hydrogenated to pentanol. The relative surface coverages of benzaldehyde and pentanal agree well with the measured Q_{ads} of benzaldehyde (~145 kJ·mol^{-1}) and pentanal (~40 kJ·mol^{-1}) on Cu/C. We note that this difference in the surface coverages of benzaldehyde and pentanal (on Cu) is further evidenced by the different FEs observed during their ECH reactions (~54% during pentanal ECH and ~94% during benzaldehyde ECH; **Figure 4-2**). A high FE during benzaldehyde ECH indicates high organic coverage, while a low FE in the case of pentanal ECH suggests low organic coverage.

In order to further investigate this phenomenon, we performed a co-reaction experiment (with benzaldehyde and pentanal) on Cu/C, in which we reintroduced benzaldehyde to the electrolyte after ~90 min reaction time. The concentration profiles of benzaldehyde and pentanal during this experiment, as a function of reaction time, are presented in **Figure 4-9**. We can again see that, like in the previous case (*i.e.*, **Figure 4-8a**), pentanal conversion was suppressed initially (indicated by the grey zone in **Figure 4-9**) and only began after benzaldehyde concentration was substantially reduced. However, remarkably, upon the introduction of ~20 mM equivalent benzaldehyde to the electrolyte solution at ~90 min, benzaldehyde conversion started immediately. More interestingly, pentanal conversion was suppressed again when benzaldehyde was being converted (*i.e.*, between 90 and 110 min, indicated by the yellow zone in **Figure 4-9**). Pentanal started converting again only when the benzaldehyde concentration was low again (*i.e.*, after ~110 min). These results suggest that upon its reintroduction to the electrolyte, benzaldehyde replaced pentanal from the surface of the catalyst, thus suppressing its conversion.

Based on the observed results, we can now describe the co-reaction of benzaldehyde and pentanal (and other aliphatic aldehydes) on Cu/C in terms of two phases: (i) an initial phase

(corresponding to the first 20 min under these reaction conditions) when only benzaldehyde conversion takes place, and (ii) a second phase (that starts after ~20 min) when primarily pentanal conversion takes place. The surface of the catalyst is saturated with benzaldehyde in the first phase due to its significantly higher Q_{ads} (~145 kJ·mol^{-1}) compared to that of pentanal (~40 kJ·mol^{-1}). In the second phase, the benzaldehyde concentration becomes low; the lower concentration decreases the surface coverage of benzaldehyde, thus allowing pentanal to adsorb on the surface and be subsequently converted to pentanol. Furthermore, upon its reintroduction, benzaldehyde would again saturate the surface due to its significantly high Q_{ads}, thus again suppressing pentanal conversion, as observed in **Figure 4-9**.

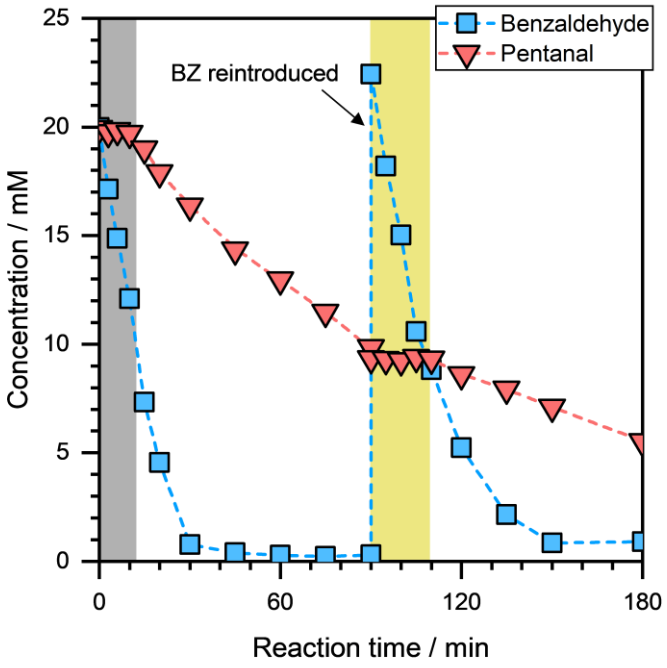

Figure 4-9. Concentration profiles of benzaldehyde and pentanal, as a function of reaction time, during the ECH of benzaldehyde and pentanal on Cu/C. 20 mM benzaldehyde was reintroduced into the electrolyte solution at ~90 min reaction time. Reaction conditions: ~10 mg catalyst, ~20 mM organic substrate, η = –0.5 V *vs* RHE, 1.5 M acetate buffer solution (pH ~4.6), ambient temperature and pressure. Dashed lines are guides to the eye.

We also investigated if the presence of the co-reactant had any effect on the individual reactivity of benzaldehyde or pentanal on Cu/C. **Figure 4-8b** shows a comparison between the (initial) aldehyde conversion rates during the individual and co-reactions of benzaldehyde and pentanal on Cu/C. Note that the rate of pentanal conversion was estimated after ~20 min reaction time in the case of co-reaction. We can see that the initial conversion rates of benzaldehyde and pentanal were comparable in both cases, *i.e.*, with and without the co-reactant.

Similar rates indicate that the individual aldehyde reactivity was not affected by the presence of the additional co-reactant. Interestingly, the estimated reaction orders (in initial aldehyde concentration) were also similar in both individual and co-reaction experiments, again indicating that the presence of the co-reactant did not influence individual aldehyde reactivity (Supplementary **Figure S4-3**). Moreover, a reaction order of approximately zero in benzaldehyde concentration for benzyl alcohol formation also indicates that the surface of Cu is saturated with benzaldehyde. On the other hand, a reaction order of less than one (~0.6) in pentanal concentration for pentanol formation indicates partial coverage of the pentanal on the surface of Cu. The observed reaction orders (and the deduced surface coverages) also agree with the Q_{ads} of benzaldehyde and pentanal on Cu/C.

Next, we performed the co-reaction of benzaldehyde and pentanal on metals that did not promote the C–C coupling reaction, *viz.*, Pd and Ru. The corresponding concentration profiles of reactants and products, as a function of reaction time, are shown in **Figure 4-10a** and **Figure 4-10b**. Interestingly, during the co-reactions of benzaldehyde and pentanal on Pd/C and Ru/C, we did not observe any suppression of pentanal conversion at the beginning of the reaction. The conversion of both co-reactants started immediately at the beginning of the reaction. This concurrent conversion indicates that both aldehydes (benzaldehyde and pentanal) are co-adsorbed on the metal surface. We also estimated the initial aldehyde conversion rates during the individual reaction and co-reaction, and the results are reported in **Figure 4-10c** and **Figure 4-10d**. We can clearly see that on Ru/C, unlike Cu/C, ECH rates decreased significantly when the two aldehydes were co-reacted. This decrease in activity further indicates that both aldehydes were co-adsorbed on the surface of Ru; lower individual coverage due to co-adsorption results in lower individual conversion rates.

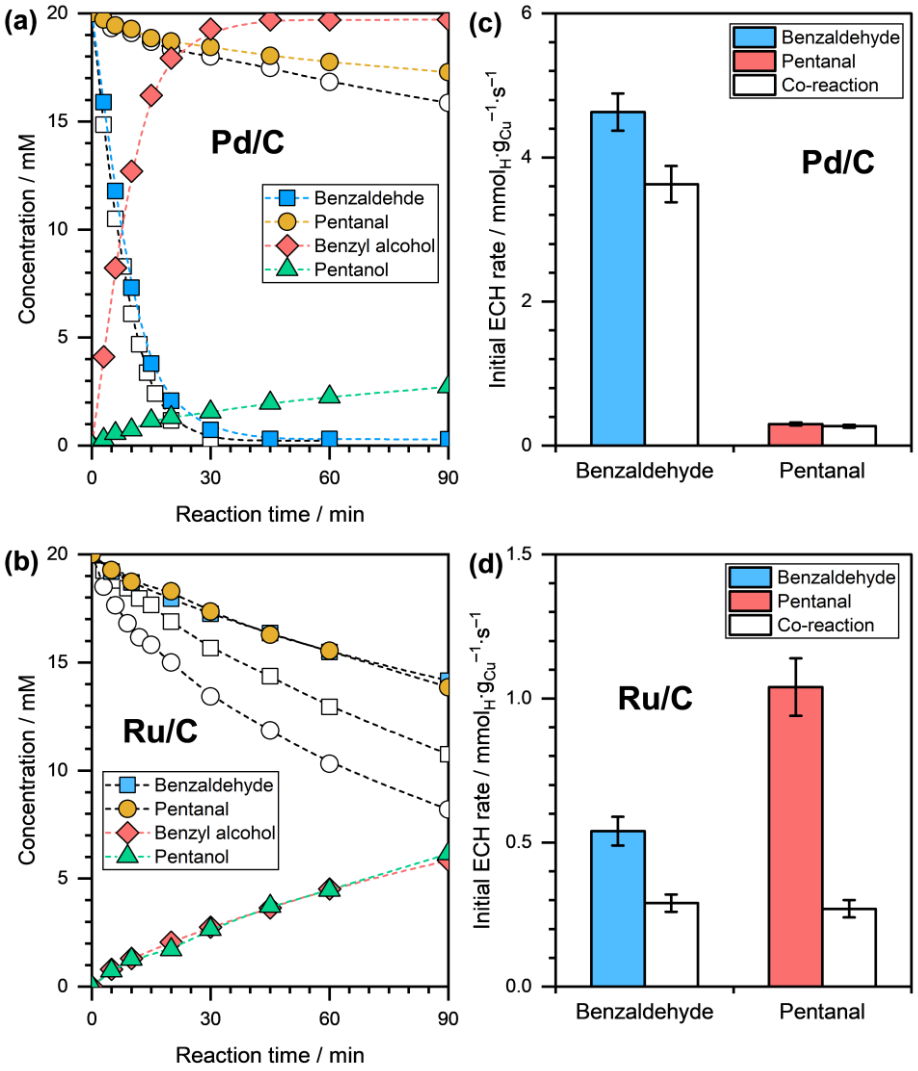

Figure 4-10. (a, b) Concentration profiles of reactants and products, as a function of reaction time, during the ECH of benzaldehyde and pentanal on (a) Pd/C and (b) Ru/C. The concentration profiles during individual reactions of benzaldehyde and pentanal are also shown (as open symbols) for comparison. (c, d) Initial aldehyde conversion rates during the individual and co-reaction of benzaldehyde and pentanal on (c) Pd/C. and (d) Ru/C. Reaction conditions: ~10 mg catalyst, ~20 mM organic substrate, η = –0.5 V *vs* RHE, 1.5 M acetate buffer solution (pH ~4.6), ambient temperature and pressure. Dashed lines are guides to the eye.

Like in the case of Ru/C, ECH rates also decreased during the co-reaction of benzaldehyde and pentanal on Pd/C, however, to a much lesser extent. This is likely due to relatively high benzaldehyde coverage and low pentanal coverage on Pd/C under the applied reaction conditions. We recall that on Pd/C, the observed FEs towards aldehyde conversion during benzaldehyde and pentanal ECH were significantly different, *i.e.*, ~54% and ~5%, respectively (**Figure 4-1**). In comparison, on Ru/C, the FEs during benzaldehyde and pentanal ECH were comparable (~20% in both cases). We also note that the Q_{ads} of benzaldehyde on Pd/C and

Ru/C was relatively low (~25 kJ·mol^{-1} on Pd/C and ~21 kJ·mol^{-1} on Ru/C, respectively; **Figure 4-5**), suggesting that benzaldehyde adsorbs weakly on Pd and Ru surfaces. The low Q_{ads} explains the co-adsorption of both benzaldehyde and pentanal on Pd/C and Ru/C, resulting in their concurrent conversion during the co-reaction experiments.

Next, we investigated the co-reaction of pentanal with cyclic aldehydes that did not undergo C–C coupling, *i.e.*, cyclohexenal and cyclohexanal, on Cu/C. The corresponding concentration profiles of reactants and products are shown in **Figure 4-11**. During the co-reaction of these non-conjugated aldehydes with pentanal, we observed that the conversion of both co-reactants started immediately. The concurrent conversion again indicates the co-adsorption of both aldehydes on the surface of Cu. It is noteworthy that the Q_{ads} of cyclohexanal on Cu/C (~37 kJ·mol^{-1}; see **Figure 4-5**) was similar to that of pentanal on Cu/C (~43 kJ·mol^{-1}), and much lower than that of benzaldehyde on Cu/C (~145 kJ·mol^{-1}). Due to similar Q_{ads} of cyclohexanal and pentanal, we expect cyclohexanal and pentanal to compete for the available sites, resulting in their co-adsorption and, therefore, concurrent conversion on Cu/C.

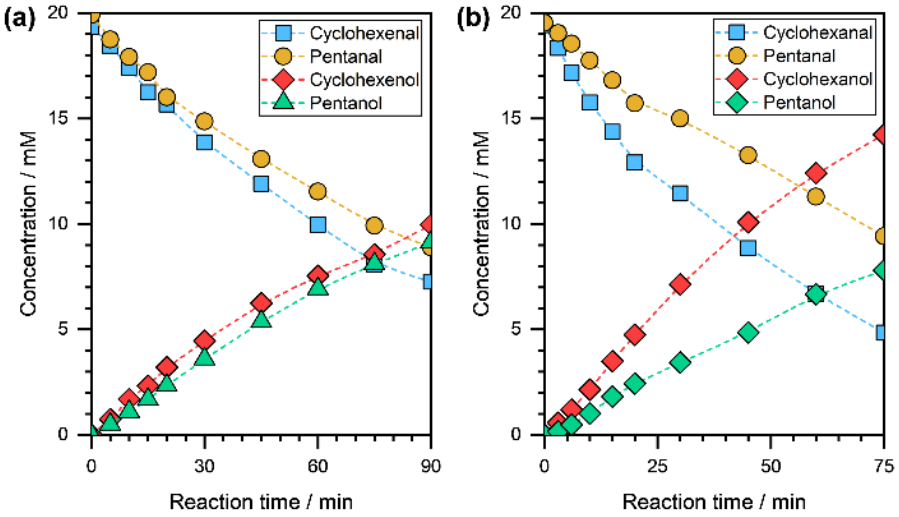

Figure 4-11. Concentration profiles of reactants and products, as a function of reaction time, during the co-reaction of (a) cyclohexenal and pentanal and (b) cyclohexanal and pentanal on Cu/C. Reaction conditions: ~10 mg catalyst, ~20 mM organic substrate, η = –0.5 V *vs* RHE, 1.5 M acetate buffer solution (pH ~4.6), ambient temperature and pressure. The dashed lines are guides to the eye.

Lastly, we investigated the co-reaction of benzaldehyde with a conjugated aromatic aldehyde (*i.e.*, furfural) on Cu/C (see Supplementary **Figure S4-4**). Interestingly, in addition to the respective C=O hydrogenation and self C–C coupling products, we observed cross C–C

coupling between the two aldehydes in both co-reaction experiments (**Figure S4-4**). We also noticed concurrent conversion of both conjugated aromatic aldehydes during their co-reaction, again indicating the co-adsorption of both aldehydes on the surface of Cu. Notably, the Q_{ads} of furfural on Cu/C was estimated to be ~151 kJ·mol^{-1}, which is similar to that of benzaldehyde on Cu/C (~145 kJ·mol^{-1}). Again, similar Q_{ads} of benzaldehyde and furfural on Cu explains their co-adsorption and thus concurrent conversion during this experiment. Finally, these experimental results clearly highlight the remarkable property of Cu to catalyze not only self but also cross C–C coupling reaction during ECH of conjugated aromatic aldehydes.

Overall, through individual and co-reaction experiments on different metals, we have shown that a conjugated system of an aromatic ring and a C=O functional group (in aldehydes like benzaldehyde and furfural) undergoes electroreductive C–C coupling, uniquely, on Cu/C. The experimental results also indicate a correlation between the strong adsorption of the aldehyde on the metal surface (facilitated by the conjugation between the aromatic ring and C=O functional group) and the occurrence of the C–C coupling reaction.

4.4 Conclusion

ECH of several aliphatic and cyclic aldehydes on different carbon-supported base (Cu and Ni) and noble metal (Pd, Pt, Ru and Rh) catalysts highlights the unique property of Cu to promote electroreductive C–C coupling during the ECH of conjugated aromatic aldehydes (like benzaldehyde and furfural). Other metals primarily catalyzed hydrogenation of the C=O functional group to form corresponding alcohols. C–C coupling products were also not observed, even on Cu, during the ECH of (i) aliphatic aldehydes, like pentanal, (ii) cyclic aldehydes, like cyclohexanal, or (iii) non-conjugated aromatic aldehydes like hydrocinnamaldehyde. The C–C coupling during aldehyde ECH is facilitated by (i) flat adsorption of the planar organic substrate on the surface of metal which stabilizes the surface hydroxy intermediate, (ii) the preferential hydrogenation of the carbonyl O (*i.e.*, hydroxy pathway) over the alkoxy pathway, and (iii) a slow (rate-determining) second H addition step for alcohol formation.

4.5 Supporting information

4.5.1 Supplementary Figures and Tables

Table S4-1. Metal precursors and conditions (temperature and duration) for N_2 and H_2 treatment for the synthesis of different carbon-supported metal catalysts.

Catalysts	Precursors	Conditions for N_2 treatment	Conditions for H_2 treatment
Cu/C	$Cu(CH_3COO)_2$	673 K, 4 h	623 K, 4 h
Ni/C	$Ni(NO_3)_2$	673 K, 4 h	673 K, 4 h
Ru/C	$RuCl_3 \cdot xH_2O$	673 K, 4 h	523 K, 3 h
Pd/C	$Pd(CH_3COO)_2$	453 K, 2 h	523 K, 2 h
Pt/C	$Pt(NH_3)_4Cl_2$	523 K, 2 h	523 K, 2 h
Rh/C	$Rh(NO_3)_3 \cdot xH_2O$	673 K, 3 h	473 K, 1 h

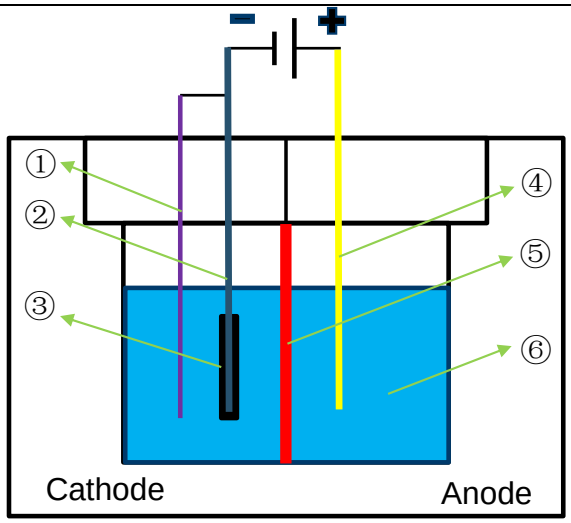

Figure S4-1. Schematic of the electrochemical cell. (1) Ag/AgCl reference electrode; (2) Titanium rod; (3) Catalyst on a carbon felt (working electrode); (4) Counter electrode (Pt wire); (5) Nafion membrane; (6) Electrolyte solution.

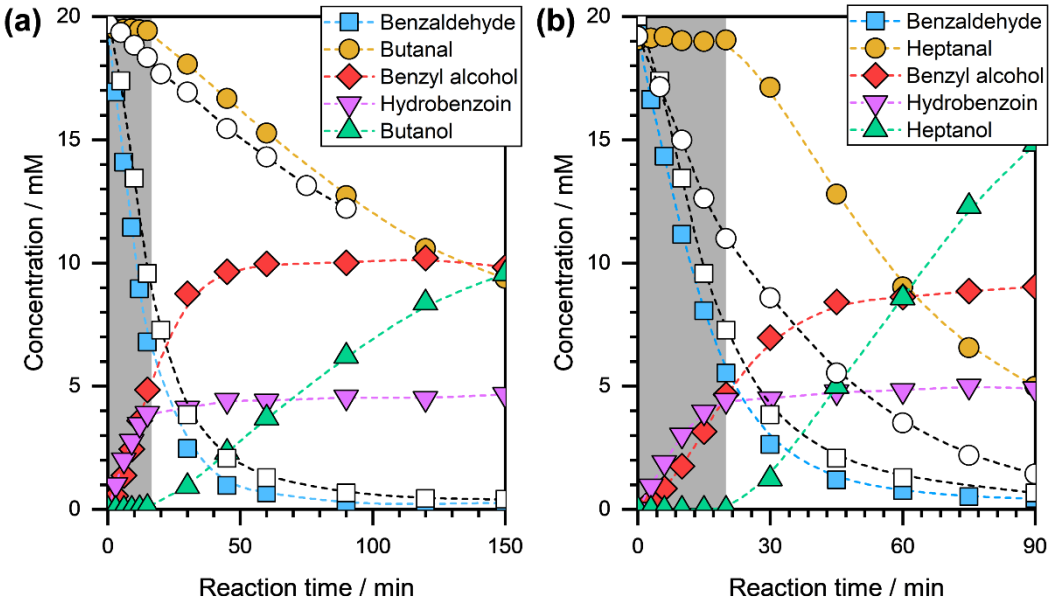

Figure S4-2. Concentration profile of reactants and products as a function of reaction time during the co-reaction (closed symbols) of (a) benzaldehyde with butanal, and (b) benzaldehyde with heptanal. The concentration profiles during the individual reactions are shown as open symbols. Reaction conditions: ~10 mg catalyst, ~20 mM organic substrate, $\eta = -0.5$ V vs RHE, 1.5 M acetate buffer solution (pH ~4.6), ambient tempera-ture and pressure. The dashed lines are guides to the eye.

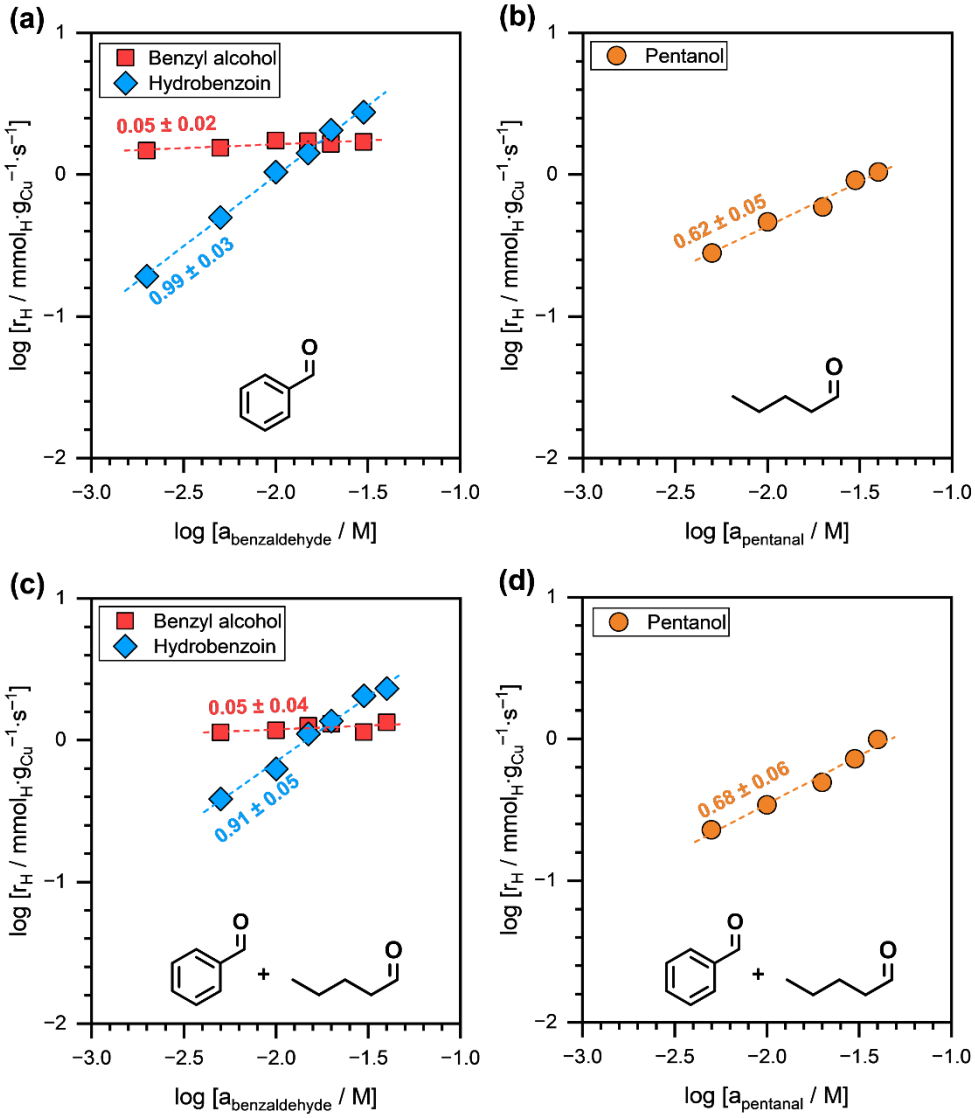

Figure S4-3. ECH rates towards product formation, as a function of reactant concentration, during the individual reactions of benzaldehyde (a) and pentanal (b) and during the co-reaction of benzaldehyde and pentanal (c,d). Reaction conditions: ~10 mg catalyst, ~20 mM organic substrate, η = –0.5 V vs RHE, 1.5 M acetate buffer solution (pH ~4.6), ambient temperature and pressure. Dashed lines are linear fits and reported numbers are estimated reaction orders.

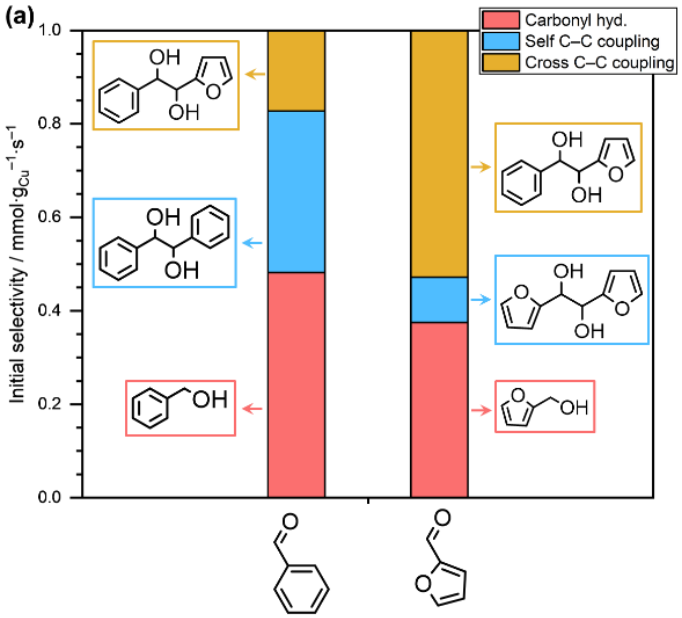

Figure S4-4. Initial selectivity towards C=O hydrogenation (hyd.), self C-C coupling, and cross C-C coupling during the ECH of benzaldehyde and FAL on Cu/C. Reaction conditions: ~10 mg catalyst, ~20 mM organic substrate, η = –0.5 V *vs* RHE, 1.5 M acetate buffer solution (pH ~4.6), ambient temperature and pressure.

4.5.2 Additional Calculation Details

The conversion of a reactant i at a given time t was estimated by

$$\chi_i(t) = \frac{n_i(t)}{n_i^0} \tag{4-3}$$

where $n_i(t)$ is the amount of reactant detected at time t and n_i^0 is the initial amount of reactant in the electrolyte.

Similarly, the yield of a product j with respect to a reactant i at any given time t was estimated by

$$Y_j(t) = \frac{n_j(t)}{n_i^0} \tag{4-4}$$

where $n_j(t)$ is the amount of reactant j detected at time t and n_i^0 is the initial amount of reactant i in the electrolyte solution.

The initial ECH rate of a product i (in terms of H consumed per gram metal) was calculated from the initial slope (m_i) of the product i formed *vs* time plot using the following equation

$$r_i = \frac{m_i \times \epsilon_i}{w_{cat} \times x_{metal}} \tag{4-5}$$

where w_{cat} is the amount of catalyst, x_{metal} is the metal loading on the catalyst (as weight

fraction), and ϵ_i is the number of H atoms required to form the product i.

The Faradaic efficiency towards the formation of a product i was estimated by

$$FE_i = \frac{q_i}{q_{total}} \quad (4\text{-}6)$$

where q_i is the electrons consumed towards formation of product i, and q_{total} is the total electrons consumed.

4.6 Reference

1. Luterbacher, J. S., D. Martin Alonso, and J. A. Dumesic. "Targeted chemical upgrading of lignocellulosic biomass to platform molecules." Green Chemistry 16.12 (2014): 4816-4838.
2. Gilkey, Matthew J., and Bingjun Xu. "Heterogeneous catalytic transfer hydrogenation as an effective pathway in biomass upgrading." ACS catalysis 6.3 (2016): 1420-1436.
3. Garedew, Mahlet, et al. "Electrochemical upgrading of depolymerized lignin: a review of model compound studies." Green Chemistry 23.8 (2021): 2868-2899.
4. Stöcker, Michael. "Biofuels and biomass-to-liquid fuels in the biorefinery: Catalytic conversion of lignocellulosic biomass using porous materials." Angewandte Chemie International Edition 47.48 (2008): 9200-9211.
5. Alonso, David Martin, Jesse Q. Bond, and James A. Dumesic. "Catalytic conversion of biomass to biofuels." Green chemistry 12.9 (2010): 1493-1513.
6. Nanda, Sonil, et al. "Pathways of lignocellulosic biomass conversion to renewable fuels." Biomass Conversion and Biorefinery 4 (2014): 157-191.
7. Alonso, David Martin, Stephanie G. Wettstein, and James A. Dumesic. "Bimetallic catalysts for upgrading of biomass to fuels and chemicals." Chemical Society Reviews 41.24 (2012): 8075-8098.
8. Chheda, Juben N., George W. Huber, and James A. Dumesic. "Liquid-phase catalytic processing of biomass-derived oxygenated hydrocarbons to fuels and chemicals." Angewandte Chemie International Edition 46.38 (2007): 7164-7183.
9. Questell-Santiago, Ydna M., et al. "Stabilization strategies in biomass depolymerization using chemical functionalization." Nature Reviews Chemistry 4.6 (2020): 311-330.
10. Sutton, Andrew D., et al. "The hydrodeoxygenation of bioderived furans into alkanes." Nature chemistry 5.5 (2013): 428-432.

11. Chen, Henan, et al. "Efficient electrocatalytic hydrogenation of cinnamaldehyde to value-added chemicals." Green Chemistry 24.9 (2022): 3655-3661.
12. Bender, Michael T., et al. "Electrochemical hydrogenation, hydrogenolysis, and dehydrogenation for reductive and oxidative biomass upgrading using 5-hydroxymethylfurfural as a model system." ACS Catalysis 12.19 (2022): 12349-12368.
13. Zhao, Chen, et al. "Aqueous-phase hydrodeoxygenation of bio-derived phenols to cycloalkanes." Journal of Catalysis 280.1 (2011): 8-16.
14. Serrano-Ruiz, Juan Carlos, and James A. Dumesic. "Catalytic routes for the conversion of biomass into liquid hydrocarbon transportation fuels." Energy & Environmental Science 4.1 (2011): 83-99.
15. Vlachos, Dionisios G., et al. "Catalysis center for energy innovation for biomass processing: research strategies and goals." Catalysis letters 140 (2010): 77-84.
16. Zhang, Lijuan, et al. "A review of thermal catalytic and electrochemical hydrogenation approaches for converting biomass-derived compounds to high-value chemicals and fuels." Fuel Processing Technology 226 (2022): 107097.
17. Zhang, Jingfang, et al. "Single-atom catalysts for thermal- and electro-catalytic hydrogenation reactions." Journal of Materials Chemistry A 10.11 (2022): 5743-5757.
18. Singh, Nirala, et al. "Aqueous phase catalytic and electrocatalytic hydrogenation of phenol and benzaldehyde over platinum group metals." Journal of catalysis 382 (2020): 372-384.
19. Shigeno, Masanori, Taiga Yamamoto, and Masahiro Murakami. "Stereoselective restructuring of 3-arylcyclobutanols into 1-indanols by sequential breaking and formation of carbon-carbon bonds." Chemistry-A European Journal 15.47 (2009): 12929-12931.
20. West, Ryan M., et al. "Carbon–carbon bond formation for biomass-derived furfurals and ketones by aldol condensation in a biphasic system." Journal of Molecular Catalysis A: Chemical 296.1-2 (2008): 18-27.
21. Idriss, Hicham, K. S. Kim, and M. A. Barteau. "Carbon–Carbon Bond Formation via Aldolization of Acetaldehyde on Single Crystal and Polycrystalline TiO_2 Surfaces." Journal of Catalysis 139.1 (1993): 119-133.

22. Song, Yang, et al. "Aqueous phase electrocatalysis and thermal catalysis for the hydrogenation of phenol at mild conditions." Applied Catalysis B: Environmental 182 (2016): 236-246.
23. Yang, Jianjing, et al. "Advances in electrochemical hydrogenation since 2010." Advanced Synthesis & Catalysis 363.24 (2021): 5407-5416.
24. Carneiro, Juliana, and Eranda Nikolla. "Electrochemical conversion of biomass-based oxygenated compounds." Annual Review of Chemical and Biomolecular Engineering 10 (2019): 85-104.
25. Anibal, Jacob, and Bingjun Xu. "Electroreductive C–C coupling of furfural and benzaldehyde on Cu and Pb surfaces." ACS Catalysis 10.19 (2020): 11643-11653.
26. Yu, Jia, et al. "Electroreductive coupling of benzaldehyde by balancing the formation and dimerization of the ketyl intermediate." Nature Communications 13.1 (2022): 7909.
27. Chadderdon, Xiaotong H., et al. "Mechanisms of furfural reduction on metal electrodes: Distinguishing pathways for selective hydrogenation of bioderived oxygenates." Journal of the American Chemical Society 139.40 (2017): 14120-14128.
28. Song, Yang, et al. "Hydrogenation of benzaldehyde via electrocatalysis and thermal catalysis on carbon-supported metals." Journal of Catalysis 359 (2018): 68-75.
29. Chen, Hongwen, et al. "Mechanism of electrocatalytic H_2 evolution, carbonyl hydrogenation and carbon – carbon coupling on Cu." Journal of the American Chemical Society, 146.20 (2024): 13949–13961.
30. Korch, Katerina M., and Donald A. Watson. "Cross-coupling of heteroatomic electrophiles." Chemical reviews 119.13 (2019): 8192-8228.
31. Thapa, Surendra, et al. "Copper-catalysed cross-coupling: an untapped potential." Organic & biomolecular chemistry 13.17 (2015): 4816-4827.
32. Taylor, Buck LH, Michael R. Harris, and Elizabeth R. Jarvo. "Synthesis of Enantioenriched Triarylmethanes by Stereospecific Cross-Coupling Reactions." Angewandte Chemie International Edition 51.31 (2012): 7790-7793.
33. Beletskaya, Irina P., and Andrei V. Cheprakov. "Copper in cross-coupling reactions: The post-Ullmann chemistry." Coordination Chemistry Reviews 248.21-24 (2004): 2337-2364.

34. Villalobos, Janette M., Jiri Srogl, and Lanny S. Liebeskind. "A new paradigm for carbon− carbon bond formation: aerobic, copper-templated cross-coupling." Journal of the American Chemical Society 129.51 (2007): 15734-15735.
35. Liang, Yongxiang, et al. "Stabilizing copper sites in coordination polymers toward efficient electrochemical CC coupling." Nature Communications 14.1 (2023): 474.
36. Tomboc, Gracita M., et al. "Potential link between Cu surface and selective CO2 electroreduction: perspective on future electrocatalyst designs." Advanced Materials 32.17 (2020): 1908398.
37. Kühne, Thomas D., et al. "CP2K: An electronic structure and molecular dynamics software package-Quickstep: Efficient and accurate electronic structure calculations." The Journal of Chemical Physics 152.19 (2020).
38. Lippert, By Gerald, and JURG HUTTER and MICHELE PARRINELLO. "A hybrid Gaussian and plane wave density functional scheme." Molecular Physics 92.3 (1997): 477-488.
39. VandeVondele, Joost, and Jürg Hutter. "Gaussian basis sets for accurate calculations on molecular systems in gas and condensed phases." The Journal of chemical physics 127.11 (2007).
40. Goedecker, Stefan, Michael Teter, and Jürg Hutter. "Separable dual-space Gaussian pseudopotentials." Physical Review B 54.3 (1996): 1703.
41. Hartwigsen, Christian, Sephen Gœdecker, and Jürg Hutter. "Relativistic separable dual-space Gaussian pseudopotentials from H to Rn." Physical Review B 58.7 (1998): 3641.
42. Krack, Matthias. "Pseudopotentials for H to Kr optimized for gradient-corrected exchange-correlation functionals." Theoretical Chemistry Accounts 114 (2005): 145-152.
43. Perdew, John P., Kieron Burke, and Matthias Ernzerhof. "Generalized gradient approximation made simple." Physical review letters 77.18 (1996): 3865.
44. Grimme, Stefan, et al. "A consistent and accurate ab initio parametrization of density functional dispersion correction (DFT-D) for the 94 elements H-Pu." The Journal of chemical physics 132.15 (2010).
45. Dixit, Ram Ji, et al. "Electrocatalytic hydrogenation of furfural using non-noble-metal electrocatalysts in alkaline medium." Green Chemistry 23.11 (2021): 4201-4212.

46. Shang, Xiao, Yang Yang, and Yujie Sun. "Electrohydrodimerization of biomass-derived furfural generates a jet fuel precursor." Green Chemistry 22.16 (2020): 5395-5401.
47. Chen, Hongwen, et al. Electrocatalytic Conversion of Benzaldehyde on Cu in Alkaline Media. 2024 (submitted).

Chapter 5

Tuning product selectivity in electrocatalytic hydrogenation of benzaldehyde on Cu/C+MoS_2

Aqueous-phase electrocatalytic hydrogenation of benzaldehyde on Cu/C leads not only to benzyl alcohol but also catalyzes C–C coupling to hydrobenzoin in both acidic and alkaline media. Acidic media is more suitable for hydrogenation pathway with a high selectivity toward benzyl alcohol, while alkaline media conduct better C-C coupling pathway for a high selectivity toward hydrobenzoin. Co-catalyst MoS_2 with high H adsorption ability can significantly increase benzyl alcohol selectivity on Cu/C+MoS_2 electrode by accelerating the second H addition step for benzyl alcohol formation, thus increase hydrogenation of the hydroxyl intermediate to alcohol product, and prevent C-C coupling pathway on Cu in acidic media. However, MoS_2 oppositely increases hydrobenzoin (C-C coupling) selectivity on Cu/C+MoS_2 electrode by accelerating the first H addition step (rate-determining for hydrobenzoin in alkaline media) during hydroxyl intermediate formation in alkaline media. The accumulated hydroxyl intermediate is more likely to follow the lower energy barrier pathway toward C-C bond formation.

This chapter is based on the article: Hongwen Chen et al. Tuning product selectivity in electrocatalytic hydrogenation of benzaldehyde on Cu/MoS_2 catalysts (prepared for submission). Hongwen Chen performed the experiments, did the data analysis and wrote the manuscript.

5.1 Introduction

The conversion of biomass-derived feedstocks into value-added chemicals and fuels through electrocatalytic hydrogenation (ECH) offers numerous advantages over traditional thermal-catalytic strategies.[1-4] Hydrogen sources from water solutions during the ECH process eliminate the problems related to H_2 gas storage and transport and reduce costs. Mild operating reaction conditions (ambient temperature and air pressure) for ECH can also reduce the additional cost and keep the catalytic activity longer. Electricity can be supplied by renewable energy (solar, wind, and hydro), and electrocatalytic equipment can easily integrate with renewable power harvesting. Lastly, controlling the hydrogenation rate by potential or current density adjustments is easy during the ECH process.[5-8]

Some efforts have been devoted to studying the electrocatalytic hydrogenation of biomass-derived carbonyls, including furfural,[9,10] cinnamaldehyde,[11,12] and 5-hydroxymethylfurfural.[13,14] As the simplest biomass aldehyde molecule, benzaldehyde has also been reported in detail for electrocatalytic hydrogenation.[15-17] Two main products can be found during benzaldehyde ECH: hydrogenation for benzyl alcohol formation (increasing the molecular stability) and C-C coupling for hydrobenzoin formation (increasing the molecular weight).[18-20] Interesting, Cu can uniquely catalyze the electroreductive C-C coupling reaction for benzaldehyde ECH, while other catalysts (Ni, Pd, Pt, Ru, and Rh) only get alcohol products.[21,22]

Both value-added products from benzaldehyde ECH are beneficial and essential to our society. Benzyl alcohol is an important industrial chemical generally used as a solvent for paints, lacquers, and inks. It is also an effective precursor for preparing esters in the cosmetics and flavoring industries.[23,24] Hydrobenzoin is a structural motif in antiepileptic drugs (e.g., Phenytoin Sodium) and photo-initiators. At the same time, Owing to the rigid chiral structure of the diphenylethylene group, multifunctional diol groups, and excellent availability, hydrobenzoin and the derivatives have recently been applied to various areas of chiral chemistry and further broadened application area to synthetic chemistry.[25,26] So, selective hydrogenation of unsaturated benzaldehyde molecules to different aimed products has recently received a growing interest.

Product generation (benzyl alcohol and hydrobenzoin) during benzaldehyde ECH on Cu has been confirmed to use the same intermediate (hydroxyl intermediate).[21,22] Hydroxyl intermediate, whether undergoing further hydrogenation to get alcohol or the C-C coupling, is crucial in determining the product selectivity for benzaldehyde ECH. During the reaction process, the second hydrogenation step for alcohol formation is rate-determining and slower than the first hydrogenation step on Cu in acidic media.[21,22] A faster second hydrogenation would primarily make the hydroxyl intermediate format benzyl alcohol and prevent C-C bond formation (rate-determining for hydrobenzoin formation). Based on this, a new strategy like introducing a co-catalyst that can affect activity for the H addition step and thus can expectantly change the product selectivity during benzaldehyde ECH.

Molybdenum(IV) sulfide (MoS_2) is a typical transition metal dichalcogenide (TMD) compound with a two-dimensional S−Mo−S triatomic layer structure, acting as a stable and non-toxic material, exhibiting great potential in catalysis, sensing, electrochemical operations, and environmentally related fields.[27-29] MoS_2 has been recently reported as a promising and efficient non-precise metal catalyst for hydrogen evolution reaction (HER) since it can catalyze HER with near zero free energy of H adsorption analogous to Pt-like catalyst.[30-32] With such excellent hydrogen adsorption (high H coverage) and hydrogen reaction ability, MoS_2 is a promising co-catalyst that may accelerate the hydrogen addition step for benzaldehyde ECH on the co-catalyst system of MoS_2 and Cu/C.

In the present work, we have investigated the ECH of benzaldehyde on Cu/C+MoS_2 electrode in both acidic and alkaline media. We found that co-catalyst MoS_2 can significantly increase benzyl alcohol selectivity on Cu/C+MoS_2 electrodes in acidic media but oppositely increase C-C coupling selectivity on Cu/C+MoS_2 electrodes in alkaline media. We also provide mechanistic insight into how MoS_2 affects product selectivity during benzaldehyde ECH on Cu/C+MoS_2 electrodes.

5.2 Materials and methods

5.2.1 Chemicals

All chemicals, *viz.* benzaldehyde (99.5%), copper (II) acetate (99.9%), N,N-Dimethylformamide (99.0%), sodium molybdate dehydrate (99.5%), thiourea (99.0%), acetic acid (99.8%), sodium acetate (99.0%), sodium hydroxide (99.5%), sodium chloride (99.9%), isopropanol (99.5%), acetone (99.9%), diphenyl ether (99.0%), and ethyl acetate (99.5%) were purchased from Sigma-Aldrich and used without further purification. Deionized (DI) water (18.2 $M\Omega \cdot cm^{-1}$) was used to prepare all aqueous solutions.

5.2.2 Catalysts synthesis

Cu/C were prepared by incipient-wetness impregnation method maintaining the mass loading of metal (~5 wt.-%) on a Vulcan XC-72 carbon support. An aqueous solution of copper (II) acetate was dropped onto carbon black support, mixed thoroughly, and dried overnight at 333 K. The resulting dried material was first treated in 100 $mL \cdot min^{-1}$ N_2 at 673 K (temperature ramp: 10 $K \cdot min^{-1}$) for 4 h, followed by reduction in 100 $mL \cdot min^{-1}$ H_2 at 623 K (temperature ramp: 10 $K \cdot min^{-1}$) for 4 h.

MoS_2 were prepared by one-step hydrothermal method. 242 mg (1 mmol) of $Na_2MoO_4 \cdot 2H_2O$ were dissolved in 70 mL DMF in 100 mL hydrothermal reactor vessel for 30 min sonication treatment at room temperature. After the addition of 456 mg (6 mmol) of thiourea, the reactor vessel was put into a stainless steel autoclave. The autoclave was heated to 493 K for 24 h and naturally cooled down to room temperature. After reaction, the MoS_2 were collected by centrifugation, washed successively with ethanol and ultrapure water, and then dried at 333 K for 12 h.

Cu/C+MoS_2 were prepared by physical stirring method. Synthesized 5 wt% Cu/C was dissolved in acetone for 30 min sonication treatment at room temperature. Different quantities of MoS_2 synthesized by hydrothermal method (to get different loading MoS_2 on Cu/C) were then added to the solution for another 30 min sonication treatment. The solution containing Cu/C and MoS_2 was finally put into oven for drying at 333 K for 12 h.

5.2.3 Carbon felt pretreatment

Carbon felt (Sigma-Aldrich, 3.0 cm × 1.5 cm) was immersed sequentially in acetone, DI water, and acetone again for at least 30 min each under ultrasonication treatment at ambient temperature. Finally, the treated carbon felt was dried in an oven at 333 K for 12 h.

5.2.4 Electrode preparation

The synthesized catalyst (~10 mg) was dispersed in a 1:1 solution of 1 mL 2-propanol and 1 mL DI water for 30 min under ultrasonication treatment at room temperature. The catalyst ink was then deposited on both sides of the pretreated carbon felt. The carbon felt electrode (containing Cu/C catalyst) was finally dried overnight in an oven at 333 K.

5.2.5 Nafion membrane pretreatment

The Nafion-117 proton exchange membrane (Ion Power) was first immersed in a 3% H_2O_2 solution for 1 h at 353 K. The Nafion membrane was then immersed in DI water at 353 K for 2 h. Subsequently, the membrane was immersed in 1 mol·L^{-1} H_2SO_4 at 353 K for 1 h. Finally, the Nafion membrane was washed several times with DI water and stored in DI water under ambient conditions.

5.2.6 Electrochemical measurements

Electrochemical measurements were performed on a BioLogic VSP-300 workstation. A two-compartment batch electrocatalysis cell was used to perform all ECH experiments. A carbon felt coated with the metal catalyst was used as the working electrode. A double-junction Ag/AgCl (eDAQ) and a Pt wire (Sigma-Aldrich) were used as the reference and counter electrodes, respectively. The cathode and anode compartments were separated by a Nafion™ N-117 proton exchange membrane (Ion Power). The reference electrode was calibrated against a reversible hydrogen electrode (RHE) according to the following equation and all potentials herein are reported with respect to the RHE reference.

$$E(vs.RHE) = E(vs.Ag/AgCl) + 0.197\ V + 0.0591 \times pH \quad (5\text{-}1)$$

All electrochemical experiments were performed under ambient conditions (room temperature and atmospheric pressure). A constant flow of N_2 was bubbled through the catholyte during the entire course of reaction to remove any dissolved gases and the evolved H_2. The electrolyte solutions were continuously stirred at a speed of 500 rpm. The solution resistance between the working and the reference electrodes was measured by potentiostatic electrochemical impedance spectroscopy (PEIS) and compensated (85%) by the

electrochemical workstation. Prior to the electrochemical reaction, the catalysts were polarized at –40 mA for ~20 min to ensure complete reduction of the metal.

The linear sweep voltammetry (LSV) measurements were performed in either pure electrolyte or 20 mM benzaldehyde solution at a scan rate of 1 $mV \cdot s^{-1}$.

5.2.7 Product Analysis

The course of an ECH experiment was followed by periodically withdrawing aliquots of 1 mL from the cathode compartment. The organic reactants and products in the aqueous electrolyte were extracted with 0.5 mL ethyl acetate. The extracted organics were analysed by an offline gas chromatograph coupled with a mass spectrometer (Agilent Technologies 7890B GC/5977A MSD).

5.3 Results and discussion

Molybdenum(IV) sulfide (MoS_2) has been confirmed to be a good catalyst for H adsorption and high-performance hydrogen evolution reactions (HER). Our previous work[21,22] concluded that the H adsorption ability and H addition mechanism play vital roles in determining reaction activity and product selectivity during benzaldehyde ECH on Cu/C. In this work, we combined MoS_2 and Cu/C catalysts to research whether the high H activity on MoS_2 can affect benzaldehyde ECH on Cu/C+MoS_2 electrodes toward H consumption activity, Faradic efficiency, or product selectivity.

5.3.1 Hydrogen evolution reaction for Cu/C and MoS_2

We first conducted linear sweep voltammetry (LSV) in both acidic (NaOAc/AcOH, pH=4.6) and alkaline media (NaOH/NaCl, pH=11.3) in the absence of organic substrate (pure electrolyte) to compare the activity of hydrogen evolution reaction between MoS_2 (synthesized by hydrothermal method, materials and methods section) and Cu/C (incipient-wetness impregnation method, materials and methods section), the result was shown in **Figure 5-1**. In acidic media (**Figure 5-1a**), The current density on MoS_2 was significantly higher than that on Cu/C. Additionally, the onset potential for HER on MoS_2 was estimated to be –0.3 V vs RHE (compared to –0.4 V vs RHE for HER on Cu/C). Therefore, based on the higher current density

and positively shift onset potential, we conclude that the overall H consumption activity on MoS_2 is superior to Cu/C in acidic media.

Figure 5-1b shows the LSV curves on Cu/C and MoS_2 electrode in pure electrolyte in alkaline media. The current density on MoS_2 was significantly higher than that on Cu/C. The onset potential for HER on MoS_2 (-0.57 V vs RHE) was significant higher than that on Cu/C (-0.74 V vs RHE). These results also suggest that overall H consumption activity on MoS_2 is superior to Cu/C in alkaline media.

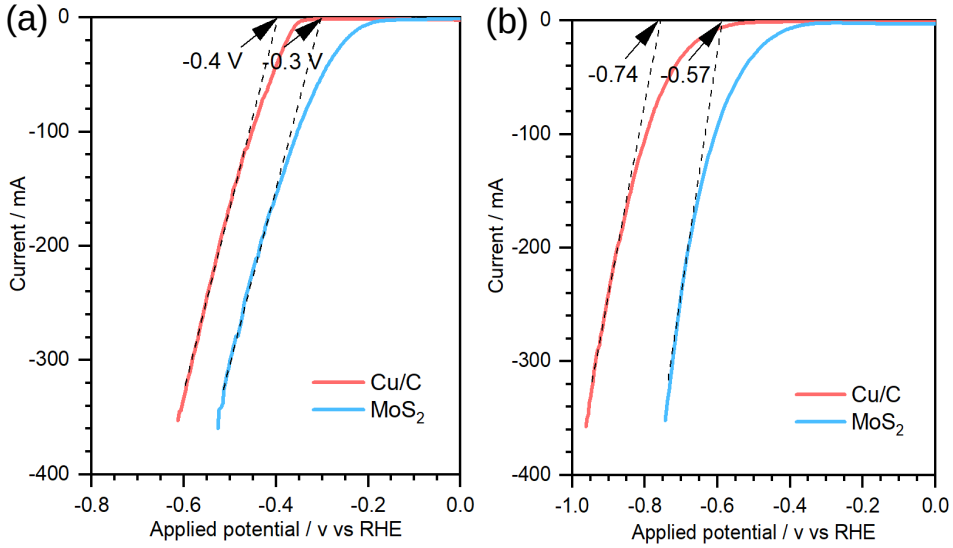

Figure 5-1. LSV curves on Cu/C and MoS_2 electrode in pure electrolyte in acidic media (a) and alkaline media (b). Reaction conditions: NaOAc/AcOH media (pH ~4.6), NaOH/NaCl media (pH ~11.3), room temperature, ambient pressure.

5.3.2 Benzaldehyde ECH on MoS_2

In order to further compare the H consumption ability between hydrogen evolution and benzaldehyde ECH, we added 20 mM benzaldehyde into the electrolyte and conducted the LSV experiments. **Figure 5-2** shows the LSV curves with or without 20 mM benzaldehyde on MoS_2 electrode in both acidic and alkaline media. The LSV curves on the MoS_2 electrode were almost overlapped in acidic media (**Figure 5-2a**), suggesting that the activity of hydrogen evolution was not affected by benzaldehyde molecule. The surface of MoS_2 was fully covered by adsorbed hydrogen (H*) in acidic media, even in the presence of benzaldehyde. The coverage of benzaldehyde was negligible on MoS_2. In other words, benzaldehyde ECH was inactive on MoS_2 in acidic media.

Unlike the overlapped LSV curves on MoS_2 in acidic media, the LSV curve on MoS_2 in the presence of benzaldehyde in alkaline media (**Figure 5-2b**) has a lower onset potential and higher current density compared with that in the absence of benzaldehyde. This suggests that benzaldehyde ECH is active on MoS_2 in alkaline media.

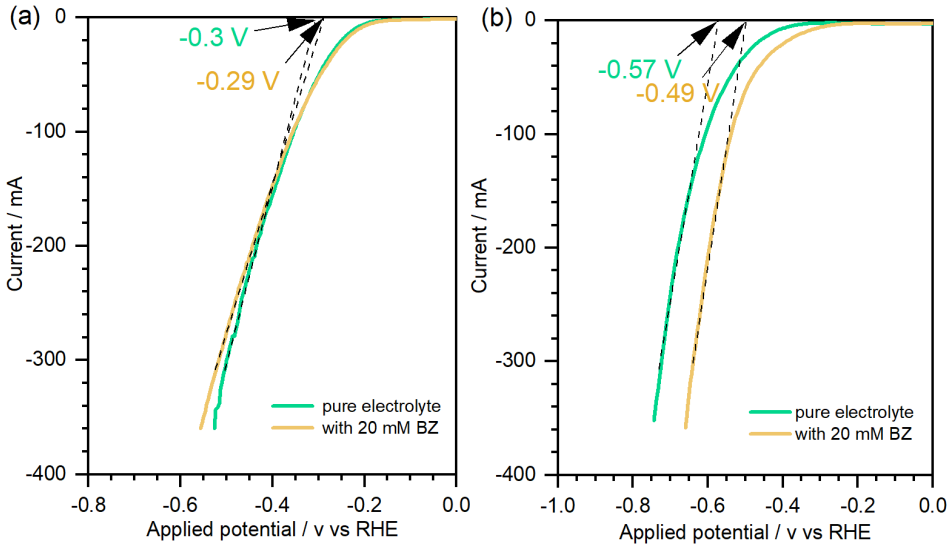

Figure 5-2. LSV curves on MoS_2 electrode in acidic media (a) and alkaline media (b) with or without benzaldehyde. Reaction conditions: 20 mM benzaldehyde, NaOAc/AcOH media (pH ~4.6), NaOH/NaCl media (pH ~11.3), room temperature, ambient pressure.

Next, we conducted benzaldehyde ECH experiments on MoS_2 electrode to further reveal the inactive benzaldehyde ECH on MoS_2 in acidic media and the active benzaldehyde ECH on MoS_2 in alkaline media. **Figure 5-3** shows the concentration profiles during benzaldehyde ECH on MoS_2 electrode. In acidic media (**Figure 5-3a**), the benzaldehyde ECH activity (~10% conversion, 60 min duration) on MoS_2 electrode was much lower than that on Cu/C in **Figure S5-1** (~80% conversion, 60 min duration), agree with the former conclusion that the HER is the dominate reaction on MoS_2 electrode in electrolyte with 20 mM benzaldehyde addition (the overlapped LSV curves in **Figure 5-2a**). On the other hand, Cu, in addition to hydrogenation of the C=O group to benzyl alcohol, significantly promoted C-C coupling to hydrobenzoin (**Figure S5-1**). However, MoS_2 only slightly catalyzes C=O hydrogenation to generate benzyl alcohol. No C-C coupling product was observed on MoS_2 electrode in acidic media.

Figure 5-3b shows the concentration profiles during benzaldehyde ECH on MoS_2 electrode in alkaline media. The benzaldehyde ECH activity (~25% conversion, 60 min duration) on MoS_2 electrode in alkaline media is higher than that on MoS_2 electrode in acidic media

in **Figure 5-3a** but still much lower compared with the benzaldehyde ECH activity on Cu/C electrode in alkaline media (~60% conversion, 60 min duration, in **Figure S5-2**). On the other hand, our former work concluded that alkaline perform better C-C coupling than acidic media during benzaldehyde ECH on Cu/C. **Figure S5-2** also shows that the Faradic selectivity towards hydrobenzoin can reach to 80%. However, as shown in **Figure 5-3b**, MoS_2 only promotes hydrogenation of the C=O group to benzyl alcohol in alkaline media, suggesting that MoS_2 cannot form a new C-C bond to generate hydrobenzoin, even in alkaline media.

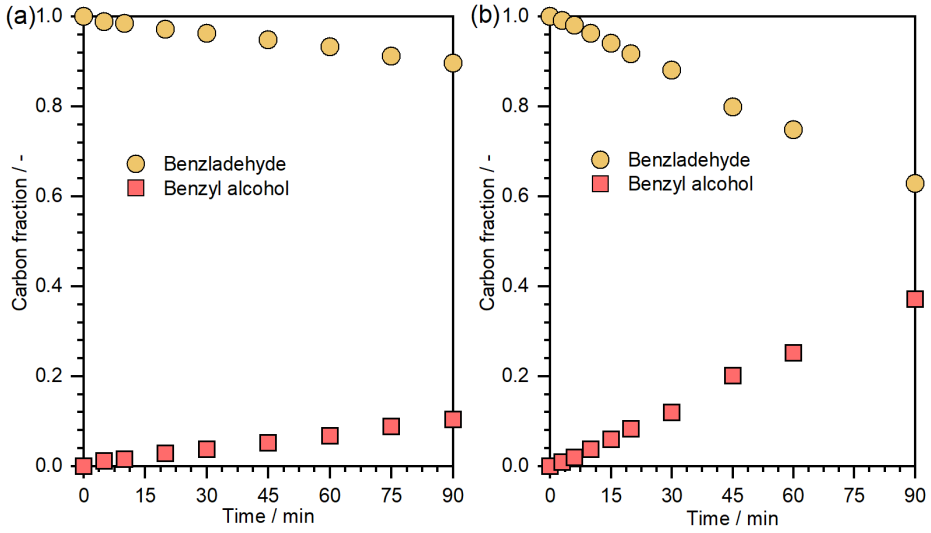

Figure 5-3. Concentration profiles of reactants and products during benzaldehyde ECH on MoS_2 electrode in (a) acidic media, and (b) alkaline media. Reaction conditions: 20 mM benzaldehyde, applied potential = -0.5 V vs. RHE, NaOAc/AcOH media (pH ~4.6), NaOH/NaCl media (pH ~11.3), room temperature, ambient pressure.

5.3.3 Hydrogen evolution reaction on Cu/C+2.5wt% MoS_2 electrode

Considering the high activity and unique performance (both hydrogenation and C-C coupling) of benzaldehyde ECH on Cu/C, as well as the outstanding performance of hydrogen evolution but relatively inactive benzaldehyde ECH on MoS_2 in acidic media, we combined Cu/C and MoS_2 by very simple physical stirring method (Materials and Methods section), and to study whether the co-catalyst MoS_2 with high H adsorption ability can affect activity for the H addition step and thus change the product selectivity during benzaldehyde ECH on co-catalyst electrode. We synthesized 2.5 wt% loading MoS_2 on 5wt% Cu/C, referred to Cu/C+2.5wt% MoS_2. Only Cu and amorphous MoS_2 peaks were detected from the Cu/C+2.5wt% MoS_2 XRD pattern in **Figure S5-3**, illustrating that the Cu/C is just physically combined with MoS_2. We

can not get any chemical interaction or new chemical bond between Cu/C and MoS_2 by the physical stirring method. The BET result for Cu/C and Cu/C + 2.5 wt% MoS_2 catalysts in **Figure S5-4** suggests that the surface area (~220 m^2 s^{-1}) of catalysts did not change as well.

We conducted LSV experiments on Cu/C+2.5wt% MoS_2 electrode in the presence or absence of benzaldehyde. **Figure 5-4a** shows the LSV curves on Cu/C+2.5wt% MoS_2 electrode in acidic media. Compared with the LSV curves on Cu/C electrode in the absence of benzaldehyde in **Figure 5-1a**, the onset potential (-0.44 V vs. RHE) on Cu/C+2.5wt% MoS_2 electrode increased. However, the current density on Cu/C+2.5wt% MoS_2 electrode increased compared with that on Cu/C electrode. For example, in the absence of benzaldehyde, at an external potential of -0.5 V vs. RHE, the current on Cu/C and Cu/C+2.5wt% MoS_2 are ~150 mA and ~200 mA, respectively, suggesting that the co-catalyst MoS_2 can increase the total H consumption rate. On the other hand, in **Figure 5-4a**, the LSV curve for Cu/C+2.5wt% MoS_2 in the presence of benzaldehyde has same onset potential compared with that in the absence of benzaldehyde, but higher current density.

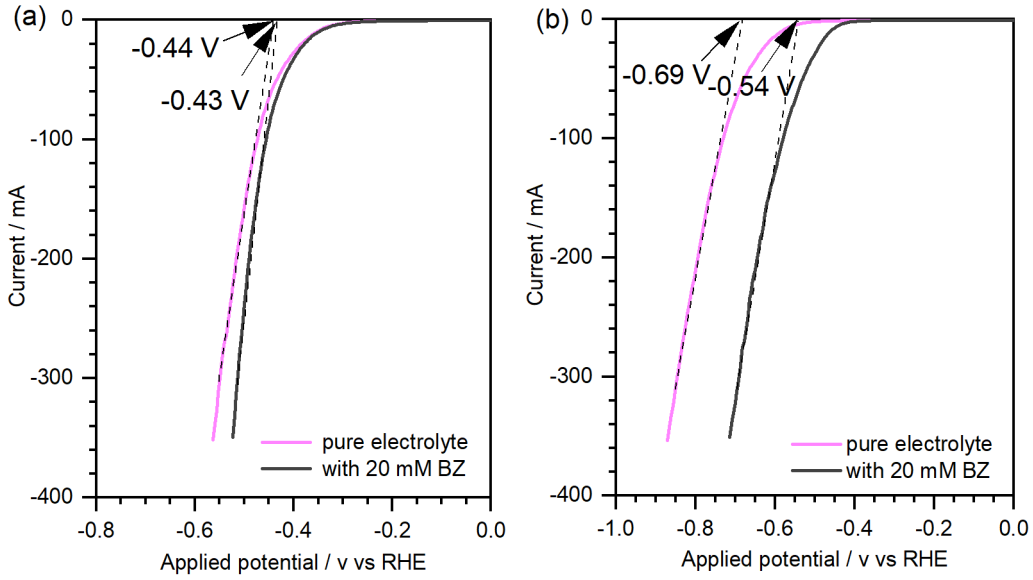

Figure 5-4. LSV curves on Cu/C + 2.5wt% MoS_2 electrode with or without 20 mM benzaldehyde in acidic media (a) and alkaline media (b). Reaction conditions: NaOAc/AcOH media (pH ~4.6), NaOH/NaCl media (pH ~11.3), room temperature, ambient pressure.

Figure 5-4b shows the LSV curves on Cu/C+2.5wt% MoS_2 electrode in alkaline media. Obviously, in the absence of benzaldehyde, the onset potentials moved to positive direction on Cu/C+2.5wt% MoS_2 electrode (-0.69 V vs. RHE) compared with that on Cu/C electrode (-0.74

V vs. RHE, **Figure 5-1b**). At the same time, the current density for Cu/C+2.5wt% MoS_2 electrode also significantly increased compared with that for Cu/C electrode (**Figure 5-1b**). These results suggest that the co-catalyst MoS_2 can increase the total H addition activity on Cu/C+MoS_2 system compared with that on Cu/C electrode in the alkaline media. **Figure 5-4b** also compared the LSV curves on Cu/C+2.5wt% MoS_2 electrode in the presence or absence of benzaldehyde. Clearly, the onset potential and the current density improved after adding 20 mM benzaldehyde compared with that in pure electrolyte.

5.3.4 Benzaldehyde ECH on Cu/C + MoS_2 electrode

Benzaldehyde ECH experiments were conducted on Cu/C+2.5wt% MoS_2 electrode in both acidic and alkaline media. **Figure 5-5** shows the concentration profile during benzaldehyde ECH on Cu/C+2.5wt% MoS_2 electrode. Unlike a significant fraction of hydrobenzoin formation on Cu/C electrode in acidic media in **Figure S5-1**, Cu/C+2.5wt% MoS_2 only promotes hydrogenation of the C=O group to benzyl alcohol in acidic media (**Figure 5-5a**). Because MoS_2 has very low activity towards benzaldehyde ECH compared with Cu/C, we initially concluded that the C-C coupling reaction pathway on Cu/C in acidic media was entirely hindered by adding co-catalyst MoS_2. MoS_2 significantly changed the product selectivity during benzaldehyde ECH on Cu/C in acidic media.

Figure 5-5b shows the concentration profile during benzaldehyde ECH on Cu/C+2.5wt% MoS_2 electrode in alkaline media. Cu/C+2.5wt% MoS_2 largely promotes C-C coupling to generate hydrobenzoin, the selectivity towards benzyl alcohol was extremely low (~3%). However, Cu/C can get a relatively higher selectivity towards benzyl alcohol (~20%) during benzaldehyde ECH in alkaline media (**Figure S5-2**). Although MoS_2 also catalyzes benzaldehyde ECH in alkaline media (**Figure 5-3b**), it only catalyzes carbonyl hydrogenation to benzyl alcohol. No hydrobenzoin was observed on pure MoS_2 electrode. So, the C-C coupling reaction pathway was only promoted on the Cu surface even we added MoS_2. We can initially conclude that the C-C coupling reaction pathway on Cu/C in alkaline media significantly increased by adding co-catalyst MoS_2.

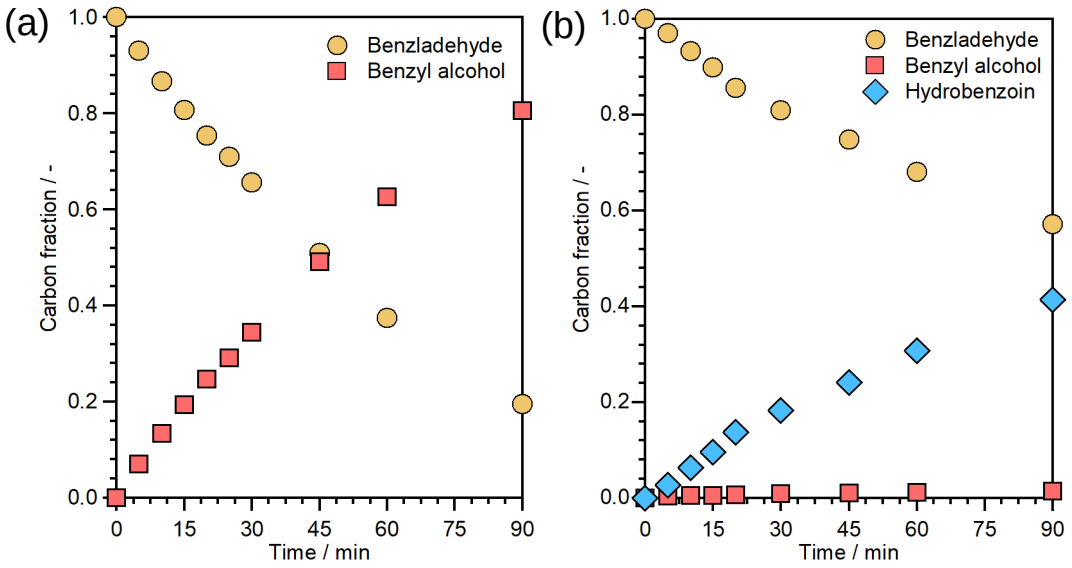

Figure 5-5. Concentration profiles of reactants and products during benzaldehyde ECH on Cu/C+2.5wt% MoS_2 electrode in (a) acidic media, and (b) alkaline media. Reaction conditions: 20 mM benzaldehyde, applied potential = -0.5 V vs. RHE, NaOAc/AcOH media (pH ~4.6), NaOH/NaCl media (pH ~11.3), room temperature, ambient pressure.

MoS_2 (with 2.5wt% loading) can entirely hinder C-C coupling during benzaldehyde ECH on Cu/C+MoS_2 electrode in acidic media; however, it significantly increases C-C coupling on Cu/C + MoS_2 electrode in alkaline media. The opposite effects toward product selectivity during benzaldehyde ECH on Cu/C+ MoS_2 highlight the MoS_2 role among Cu/C + MoS_2 co-catalyst system. We then synthesis different loading of MoS_2 on 5wt% Cu/C, referred to Cu/C+1wt% MoS_2, Cu/C+2.5wt% MoS_2, Cu/C+5wt% MoS_2, and Cu/C+10wt% MoS_2. We investigated the activity and product selectivity towards benzaldehyde ECH on Cu/C+MoS_2 catalysts in both acidic (**Figure 5-6**) and alkaline media (**Figure 5-7**). In **Figure 5-6a**, the benzaldehyde conversion in acidic media slightly decreased compared with Cu/C when we added a small amount of MoS_2 (1 wt% and 2.5 wt%). Further increasing MoS_2 loading to 5 wt% and 10 wt% would noticeably hinder benzaldehyde conversion. This would be caused by the relatively higher content of MoS_2 covering the active site on the surface of Cu. On the other hand, benzyl alcohol selectivity significantly increased when we introduced MoS_2 into Cu/C (**Figure 5-6b**). The C-C coupling was entirely hindered when introducing more than 2.5 wt% MoS_2 as the hydrobenzoin selectivity comes to 0. At the same time, the Faradic efficiency (**Figure S5-5**) on Cu/C + MoS_2 co-catalyst electrodes gradually decreased by increasing the loading of MoS_2.

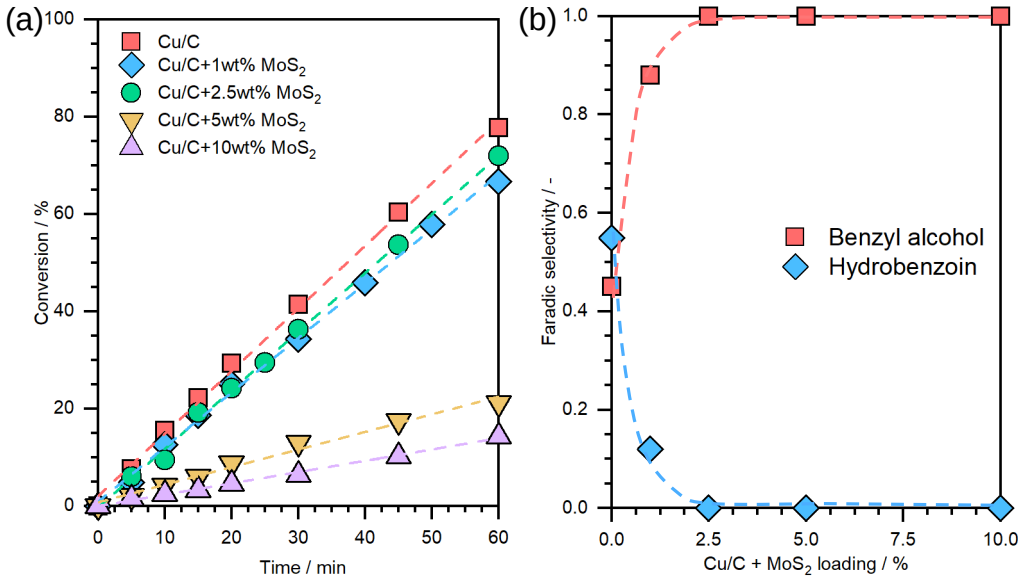

Figure 5-6. (a) Benzaldehyde conversion as a function of reaction time on Cu/C+MoS_2 catalysts. (b) Product selectivity toward benzyl alcohol and hydrobenzoin formation during 20 mM benzaldehyde ECH on Cu/C and Cu/C+MoS_2 electrodes. 20 mM benzaldehyde, applied potential -0.5 V vs RHE, NaOAc/AcOH media (pH ~4.6), room temperature, ambient pressure.

Benzaldehyde conversion of Cu/C+MoS_2 catalysts also decreased to different degrees in alkaline media compared with Cu/C (**Figure 5-7a**). This may also be caused by MoS_2 covering the active site on the surface of Cu. However, unlike the product selectivity trend in acidic solution, C-C coupling selectivity in alkaline media significantly increased after introducing MoS_2 (**Figure 5-7b**). The highest selectivity towards hydrobenzoin comes to 0.97 on Cu/C+2.5wt% MoS_2 electrode (compared with 0.8 for hydrobenzoin selectivity on Cu/C). Cu/C+MoS_2 catalysts performed oppositely toward product selectivity during benzaldehyde ECH in acidic or alkaline media. **Figure S5-6** provides details of the corresponding Faradic efficiency for Cu/C+MoS_2 electrodes in alkaline media. Faradic efficiency on Cu/C + MoS_2 co-catalyst electrodes gradually decreased by increasing the loading of MoS_2.

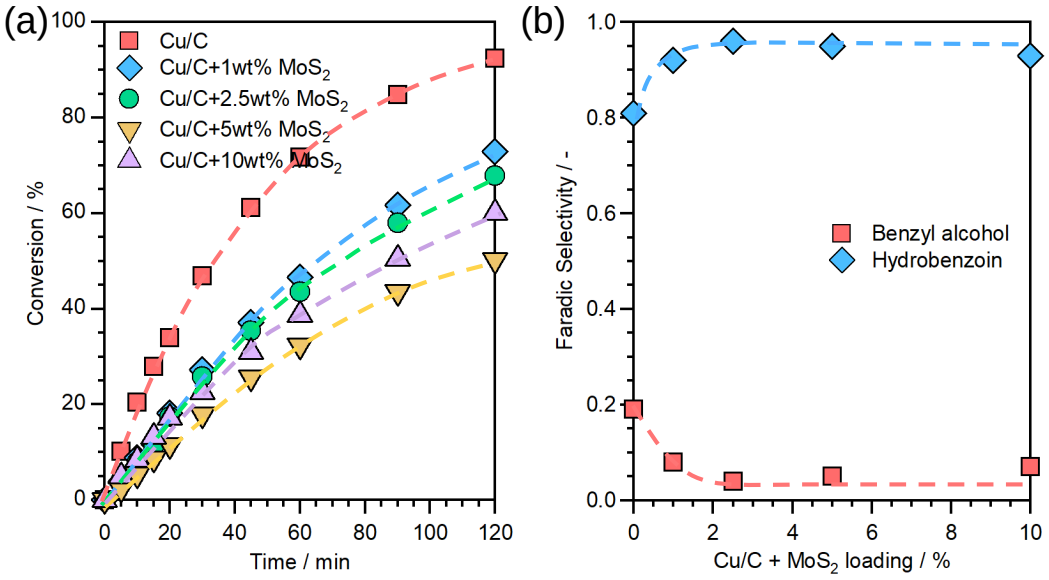

Figure 5-7. (a) Benzaldehyde conversion as a function of reaction time on Cu/C+MoS_2 catalysts. (b) Product selectivity toward benzyl alcohol and hydrobenzoin formation during 20 mM benzaldehyde ECH on Cu/C and Cu/C+MoS_2 electrodes. 20 mM benzaldehyde, applied potential -0.5 V vs RHE, NaOH/NaCl media (pH ~11.3), room temperature, ambient pressure.

5.3.5 Mechanistic insight towards product selectivity during benzaldehyde ECH on Cu/C+MoS_2 co-catalysts

MoS_2 can significantly increase benzyl alcohol selectivity on Cu/C+MoS_2 electrode in acidic media but oppositely increase C-C coupling selectivity in alkaline media. One hypothesis for this phenomenon could be that Cu and MoS_2 generate a new phase during the synthesis process. XRD result excludes this hypothesis because we do not detect new peaks for other species except Cu and MoS_2 (**Figure S5-3**). Considering that MoS_2 is much more inactive for benzaldehyde ECH in acidic media compared with Cu, and MoS_2 cannot promote C-C coupling to generate hydrobenzoin in alkaline media (it can not increase hydrobenzoin selectivity by adding MoS_2 if the active site for hydrobenzoin formation exists on the surface of MoS_2), we put our emphasis on the reaction mechanism for benzaldehyde ECH on Cu phase to investigate mechanistic insight towards product selectivity changes during benzaldehyde ECH on Cu/C+MoS_2 electrodes.

Scheme 5-1 shows the reaction mechanism of benzaldehyde ECH to both benzyl alcohol and hydrobenzoin on Cu/C in acidic media or alkaline media.[21,22] In the proposed mechanism for acidic media,[21] benzaldehyde initially adsorbs on an active site (*) to get adsorbed species. The

adsorbed benzaldehyde undergoes fast first hydrogen addition following the PCET mechanism to form the hydroxyl intermediate. Under the reaction conditions, the surface is predominantly covered with the adsorbed benzaldehyde and/or hydroxyl intermediate, and hydrogen coverage is low. The hydroxyl intermediate then follows two parallel reaction pathways. In the first pathway, the hydroxyl intermediate undergoes a second and rate-determining proton coupled electron transfer (PCET) mechanism on its α-C to form adsorbed benzyl alcohol. In a parallel reaction, the electrophilic carbonyl C of a nearby physisorbed benzaldehyde molecule is attacked by the radical α-C of the hydroxyl intermediate to form the C-C bond. The C-C coupling is followed by a fast barrier-less PCET to the radical O of the formed alkoxy radical intermediate to form adsorbed hydrobenzoin. The C-C bond formation is the rate-determining step for benzaldehyde ECH to hydrobenzoin.

The overall mechanism for benzaldehyde ECH to benzyl alcohol and hydrobenzoin formation on Cu/C in alkaline media was also illustrated in **Scheme 5-1**.[22] In alkaline media, the catalyst surface is also predominantly covered with the organic substrate. The adsorbed benzaldehyde undergoes the first H addition to the carbonyl O atom to form a surface hydroxyl intermediate. The hydroxyl intermediate undergoes two parallel reactions. In the first case, the hydroxyl intermediate undergoes a second and rate-determining H addition on the carbonyl C to form an adsorbed benzyl alcohol species. In the parallel reaction, the radical α-C of the hydroxy intermediate is attacked by the electrophilic carbonyl C of a nearby physisorbed benzaldehyde molecule to form an alkoxy radical intermediate. The C–C bond formation is fast and equilibrated. The formed alkoxy radical finally undergoes a second and fast H addition to its radical O to form HB*, which finally desorbs to form hydrobenzoin. The first H addition is the kinetically rate-determining step for hydrobenzoin formation. During the reaction, the H addition steps occur via the PCET-like mechanism wherein H_2O molecules act as proton donors (forming OH^- in the process).

Compared with Cu/C, the mechanism for benzaldehyde ECH on Cu phase may be different after adding MoS_2 which would contribute to the product selectivity changes during benzaldehyde ECH on Cu/C+MoS_2 electrode. The H addition mechanism for benzaldehyde ECH on Cu/C+MoS_2 electrode should be figured out firstly because MoS_2 with strong H activity may have some impact towards H addition mechanism for benzaldehyde hydrogenation.

To conclusively distinguish between PCET and LH pathways for H addition, we performed benzaldehyde ECH on Cu/C+2.5wt% MoS_2 in the presence of t-butanol (t-BuOH), a specific quenching agent toward surface H*. The obtained results are presented in **Figure S5-7** (in acidic media) and **Figure S5-8** (in alkaline media). It can be clearly see that, in acidic media, benzaldehyde conversion profiles are overlapped. The benzaldehyde conversion rate just slightly decreased from 1.5 $mmol_{BZ}\cdot g_{Cu+MoS2}^{-1}\cdot s^{-1}$ to 1.47 $mmol_{BZ}\cdot g_{Cu+MoS2}^{-1}\cdot s^{-1}$. This strongly suggests that PCET mechanism dominate H addition for benzaldehyde ECH on Cu/C+2.5wt% MoS_2. In alkaline media, benzaldehyde conversion rate decreased a lot in the presence of t-BuOH. The benzaldehyde conversion rate decreased from 0.43 $mmol_{BZ}\cdot g_{Cu+MoS2}^{-1}\cdot s^{-1}$ to 0.23 $mmol_{BZ}\cdot g_{Cu+MoS2}^{-1}\cdot s^{-1}$. This clearly suggests that the LH pathway also contributes to the H addition. So, in alkaline media, both PCET and LH mechanism promote the H addition during benzaldehyde ECH on Cu/C+2.5wt% MoS_2.

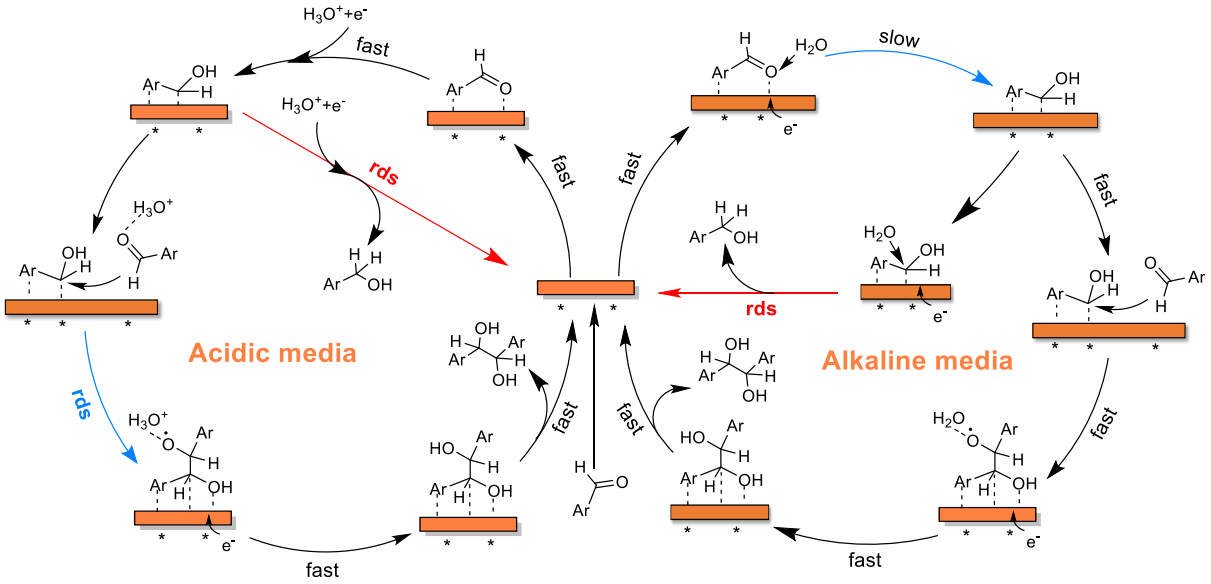

Scheme 5-1. Proposed mechanism for benzyl alcohol and benzyl alcohol formation during benzaldehyde ECH on Cu/C in acidic and alkaline media.

We have to mention here that PCET is the dominating pathway for H addition on Cu/C in acidic media, contributing ~82% toward H addition.[21] While PCET contributes ~100% toward H addition on Cu/C in alkaline media.[22] MoS_2 do not change the H addition mechanism towards benzaldehyde ECH in acidic media. This is mainly due to the fact that MoS_2 has negligible activity towards benzaldehyde ECH in acidic media, the active site for benzaldehyde ECH is located in the Cu surface. So the H addition mechanism for benzaldehyde ECH on Cu/C+ MoS_2

electrode did not change. However, MoS_2 significantly impacts the H addition mechanism in alkaline media. MoS_2 phase can promote benzaldehyde conversion to benzyl alcohol. So, the contribution of LH H addition mechanism mainly derived from MoS_2. The PCET still dominate the H addition on Cu surface. This is why benzaldehyde conversion rate decreased in half after adding t-BuOH to the solvent on Cu/C+ 2.5wt% MoS_2 electrode.

Next, we conduct isotopic labelling experiments to elucidate the kinetically relevant step for benzyl alcohol and hydrobenzoin formation during benzaldehyde ECH on Cu/C+ 2.5wt% MoS_2 electrode. Our former work shows that benzyl alcohol has strong primary kinetic isotope effect (KIE) on Cu/C in acidic media as the second H addition step is the rate-determining step, while hydrobenzoin shows very weak KIE on Cu/C as C-C coupling is the rate-determining step.[21] Benzyl alcohol also shows strong KIE on Cu/C+ 2.5wt% MoS_2 electrode in acidic media (left panel, **Figure 5-8a**), which suggests that the H addition step still control overall rate for benzyl alcohol formation. However, hydrobenzoin shows reverse strong KIE on Cu/C+MoS_2 electrode in acidic media (right panel, **Figure 5-8a**). Such strong KIE can not conclude the rate-determining step for hydrobenzoin formation change from C-C coupling to H addition because the MoS_2 phase do not promote hydrobenzoin formation (**Figure 5-3a**). So the rate-determining step for hydrobenzoin formation can not change by adding MoS_2. When changing the solvent from H_2O to D_2O, the H addition ability significant decreased as the dissociation of D_2O is much difficult than H_2O. The weak H addition ability make Cu/C+2.5wt% MoS_2 electrode generate hydrobenzoin again in D_2O based solvent.

In alkaline media, we previously reported the second H addition step is the rate-determining step for benzyl alcohol formation while the first H addition (for hydroxyl intermediate formation) is the kinetically rate-determining step for hydrobenzoin formation on Cu/C due to the strong primary KIE and the energy barrier of fundamental steps from DFT calculation during benzyl alcohol and hydrobenzoin formation process.[22] On Cu/C+2.5wt% MoS_2 electrode, benzyl alcohol formation rates were negligible in both H_2O and D_2O based solvents (left panel, **Figure 5-8b**). While hydrobenzoin formation rate on Cu/C+2.5 MoS_2 electrode has a strong reverse KIE (right panel, **Figure 5-8b**). Such strong reverse KIE for hydrobenzoin formation can also be explained by the weak H addition ability in D_2O based solvent.

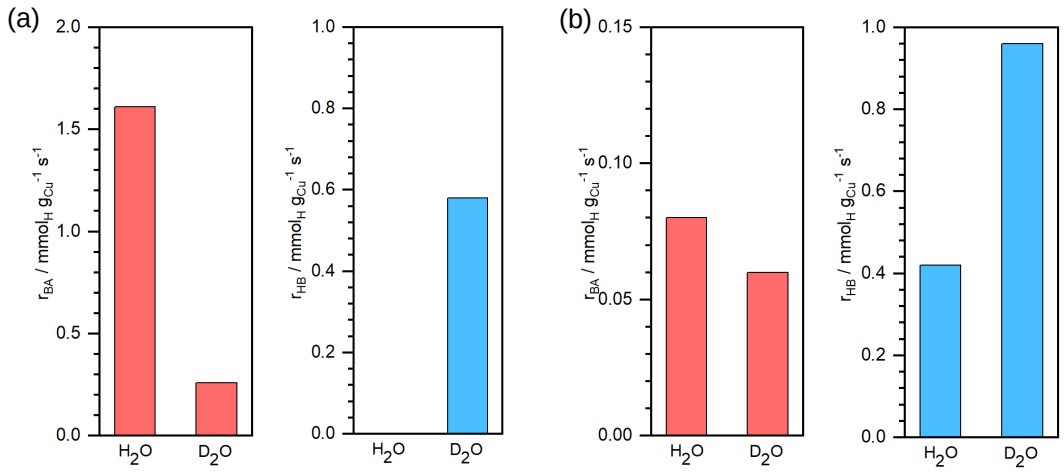

Figure 5-8. Benzyl alcohol and hydrobenzoin formation rates, during benzaldehyde ECH on Cu/C+2.5 MoS_2 in H_2O or D_2O solvents in acidic media (a) or alkaline media (b). Reaction conditions: 20 mM benzaldehyde, applied potential -0.5 V vs RHE, NaOAc/AcOH media (pH ~4.6), NaOH/NaCl media (pH ~11.3), room temperature, ambient pressure

Based on the t-BuOH and isotopic labelling experiments, we can conclude that benzaldehyde ECH on Cu/C+MoS_2 follow the same mechanism (e.g. H addition mechanism and rate-determining step) with Cu/C. The only difference should be that the MoS_2 can promote benzaldehyde hydrogenation to benzyl alcohol by LH mechanism in alkaline media. However, MoS_2 can not promote C-C coupling towards benzaldehyde ECH in alkaline media, the above mechanism difference can not be used to explain the increased C-C coupling selectivity on Cu/C+ MoS_2 electrode in alkaline media. So the mechanism change by adding MoS_2 can not explain why MoS_2 can significantly increase benzyl alcohol selectivity on Cu/C+MoS_2 electrode in acidic media and oppositely increase C-C coupling selectivity in alkaline media.

As illustrated before, H addition steps play vital role during the benzaldehyde ECH process in acidic and alkaline media. It can control the product formation rate as the H addition step is the rate-determining step for benzyl alcohol formation in both media and for hydrobenzoin formation in alkaline media. So changing the H addition activity could be a possible way to change the product selectivity during benzaldehyde ECH.

In acidic media, the PCET is the dominating pathway for H addition on Cu, and the contribution of LH-pathway towards H addition is <20%.[21] This is mainly due to the very low H coverage on Cu in the presence of benzaldehyde because the Cu surface is predominantly covered with the adsorbed organic substrate. This conclusion was also confirmed by the zero-

order for benzyl alcohol formation during benzaldehyde ECH on Cu.[21] However, due to the high H adsorption ability for MoS_2, the H coverage in the presence of benzaldehyde on Cu/C+MoS_2 electrode may be different compared with Cu. **Figure 5-9a** shows the effects of initial benzaldehyde concentration on benzaldehyde ECH on Cu/C+2.5wt% MoS_2 electrode in acidic media. The reaction order in benzaldehyde for benzyl alcohol formation was estimated to be ~0.5. This suggests that the benzaldehyde coverage was insufficient for benzaldehyde ECH on Cu/C+2.5wt% MoS_2. The positive order for benzyl alcohol formation further confirmed that MoS_2 can increase surface H coverage or near electrode surface hydronium ions concentration on Cu/C+2.5wt% MoS_2 electrode in acidic media.

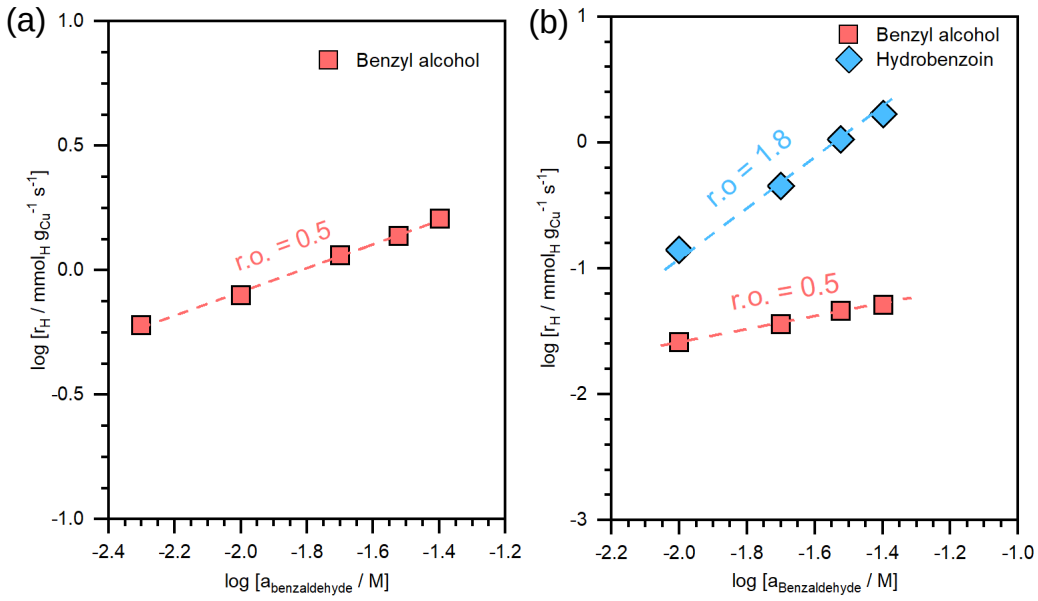

Figure 5-9. Benzyl alcohol and hydrobenzoin formation rates, during benzaldehyde ECH on Cu/C+2.5 MoS_2, as a function of initial benzaldehyde concentration in acidic media (a) and alkaline media (b). Reaction conditions: 5 - 40 mM benzaldehyde, applied potential -0.5 V vs RHE, NaOAc/AcOH media (pH ~4.6), NaOH/NaCl media (pH ~11.3), room temperature, ambient pressure. The dashed lines are linear fits.

In alkaline media, water molecules is the proton donors and joined in the H addition steps following PCET mechanism during benzaldehyde ECH on Cu/C.[22] In this case, the reaction orders in benzaldehyde for benzyl alcohol and hydrobenzoin formation during benzaldehyde ECH on Cu/C were estimated to be ~ -0.45 (negative order) and ~0.05 (approx-imately zero-order), respectively.[22] Zero order for hydrobenzoin suggests that the benzaldehyde coverage was sufficient for benzaldehyde ECH. However, the reaction orders changed after adding MoS_2.

Figure 5-9b shows the reaction order for benzyl alcohol and hydrobenzoin formation on Cu/C+2.5wt% MoS_2 electrode in alkaline media. Compared with Cu/C, the reaction orders for benzyl alcohol and hydrobenzoin formation on Cu/C+2.5wt% MoS_2 electrode increased from -0.45 to 0.5 and from 0 to 1.8, respectively. The increased and positive reaction orders suggest that water coverage or physisbored water molecule (in Helmholtz layer) increased and the benzaldehyde coverage was not enough for benzaldehyde ECH process. So, MoS_2 can increase H addition ability by increasing water coverage on Cu/C+2.5wt% MoS_2 electrode or near surface physisbored water molecule in alkaline media.

In order to further confirm the higher H addition ability on Cu/C+MoS_2 electrode, we performed the cyclohexanal ECH experiment. Unlike benzaldehyde ECH, carbonyl hydrogenation for cyclohexanol formation was the only product during cyclohexanal ECH. We do not detect any C-C coupling during cyclohexanal ECH. So the H addition ability can be directly indicated from the alcohol formation rate. **Figure S5-9** shows the cyclohexanol formation rate during cyclohexanal ECH on Cu/C and Cu/C+2.5wt% MoS_2 electrode in acidic or alkaline media. The increased cyclohexanol formation rate on Cu/C+MoS_2 electrode in both acidic and alkaline media further suggest the H addition ability on Cu/C+MoS_2 electrode was higher than that on Cu/C, which will contribute to the product selectivity changes during benzaldehyde ECH on Cu/C+MoS_2 electrode.

The H addition ability has been confirmed to be a vital role for tuning product selectivity during benzaldehyde ECH. The protonation and electron transfer processes during H addition have been described as either inner-sphere or outer-sphere processes. The inner-sphere reactions occur on the electrode surface while outer-sphere reactions occur in the solvent layer and do not require a strong interaction between the reactants or intermediates and the electrode surface. Self-assembled monolayers of organothiols (e.g. 2-mercaptobenzothiazole (MBT)) have been shown to inhibit the inner-sphere reactions but not the outer-sphere reactions. We have also confirmed the formation of benzyl alcohol and hydrobenzoin during benzaldehyde ECH are inner-sphere processes and occur on the surface of Cu in both acidic and alkaline media by performing benzaldehyde ECH in the presence of 10 mM MBT.[21,22] We also performed benzaldehyde ECH on MoS_2 and Cu/C+2.5wt% MoS_2 electrode in the presence of 10 mM MBT to further confirm the protonation process. The result was shown in **Figure S5-10** (in acidic

media) **and Figure S5-11** (in alkaline media). It can be clearly seen that benzyl alcohol formation rate on MoS_2 in acidic media kept constant after adding 10 mM MBT (**Figure S5-10a**), indicating that the protonation process on MoS_2 in acidic media are an out-sphere reaction. On Cu/C+2.5wt% MoS_2 electrode (**Figure S5-10b**), benzyl alcohol formation decreased significantly in the presence of MBT, clearly indicating that the reactions involved in the formation of benzyl alcohol during benzaldehyde ECH on Cu/C+2.5wt% MoS_2 electrode is inner-sphere process. This also suggests that the active sites for benzaldehyde ECH are mainly located on Cu surface on Cu/C+ MoS_2 electrode, which consist with the former viewpoint that MoS_2 only slightly catalyzes C=O hydrogenation to generate benzyl alcohol (**Figure 5-3a**).

Figure S5-11 shows benzaldehyde ECH on MoS_2 or Cu/C+2.5wt% MoS_2 electrode in the presence of 10 mM MBT in alkaline media. It can be clearly see that the protonation process (promoted by H_2O molecule) on MoS_2 electrode in alkaline media was an out-sphere reaction. On Cu/C+2.5wt% MoS_2 electrode, the benzyl alcohol formation rates were negligible in the presence or absence of MBT (**Figure S5-11b**). The hydrobenzoin formation rate, on the other hand, decreased from 0.42 $mmol_H \cdot g_{Cu+MoS2}^{-1} \cdot s^{-1}$ to 0.32 $mmol_H \cdot g_{Cu+MoS2}^{-1} \cdot s^{-1}$, indicating that the formation of hydrobenzoin during benzaldehyde ECH on Cu/C+2.5wt% MoS_2 electrode is mixed processes, including both inner-sphere and outer-sphere process. We have reported that the hydrobenzoin formation reaction was an inner-sphere process on Cu/C electrode in alkaline media.[22] The MoS_2 phase can not promote hydrobenzoin formation in alkaline media (**Figure 5-3b**). So MoS_2 may help the hydrobenzoin formation on Cu also from an outer-sphere pathway.

From the reaction pathways (**Scheme 5-1**), the hydroxyl intermediate is the common surface species used for benzyl alcohol and hydrobenzoin generation in both acidic and alkaline media. The hydroxyl intermediate will go to two different reaction pathways. The second hydrogen addition to hydroxyl intermediate is always the rate-determining step for benzyl alcohol formation in both media. The C-C coupling is the rate-determining step for hydrobenzoin formation in acidic media, while it changes to the first hydrogen addition for hydroxyl intermediate formation in alkaline media. So, the hydrogen addition step plays a vital role in controlling the product formation rate. Controlling the hydrogen addition activity during benzaldehyde ECH can determine the product's generation direction. For example, a faster second hydrogen addition rate (rate-determining) for benzyl alcohol formation in acidic media

will inevitably decrease C-C coupling formation by consuming the hydroxyl intermediate species (for further H addition) faster. On the other hand, a faster first hydrogen addition rate for hydroxyl intermediate formation (rate-determining for hydrobenzoin formation) in alkaline media will increase surface hydroxyl intermediate concentration, thus affecting the following two reaction pathways.

Both LH and PCET mechanisms contribute to the hydrogen addition for benzaldehyde ECH on Cu/C in acidic media under our reaction conditions,[21] and the second hydrogen addition is the rate-determining for benzyl alcohol formation. Consequently, the rate of benzyl alcohol formation can be described by **Equation 5-2** in acidic media, in which α is the proportion that LH mechanism contributes to the hydrogen addition for benzyl alcohol formation in acidic media; k_{LH} and k_{LH}' are the rate constant for the first and second hydrogen addition for benzyl alcohol formation by LH mechanism; θ_{RCHO} is the surface coverage of benzaldehyde; θ_H is the surface coverage of hydrogen; k_{PCET} and k_{PCET}' are the rate constant for the first and second hydrogen addition for benzyl alcohol formation by PCET mechanism; $a_{H_3O^+}$ is the activity of hydronium ions in **Equation 5-2**.

On the other hand, the H addition steps in alkaline media occur primarily via a proton-coupled electron-transfer (PCET)-like mechanism wherein H_2O molecules act as the proton donors (forming OH^- in the process). The first H addition step is the rate-determining step for hydrobenzoin formation during benzaldehyde ECH in alkaline media. Consequently, the rate of hydrobenzoin formation can be described by **Equation 5-3** in alkaline media, in which $k_{alkaline}$ is the rate constant for the first hydrogen addition for hydroxyl intermediate formation in alkaline media; a_{H_2O} is the H_2O activity in Helmholtz layer in alkaline media.

$$r_{BA} = \alpha \cdot k_{LH} \cdot k'_{LH} \cdot \theta_{RCHO} \cdot (\theta_H)^2 + (1-\alpha) \cdot k_{PCET} \cdot k'_{PCET} \cdot \theta_{RCHO} \cdot (a_{H_3O^+})^2 \qquad (5\text{-}2)$$

$$r_{HB} = k_{alkaline} \cdot \theta_{RCHO} \cdot a_{H2O} \qquad (5\text{-}3)$$

In acidic media, co-catalyst MoS_2 with higher hydrogen coverage compared with Cu/C and almost no benzaldehyde coverage (inactive benzaldehyde ECH, which does not affect benzaldehyde coverage on the surface of Cu, θ_{RCHO}) can significantly increase θ_H on Cu/C+MoS_2 electrode. MoS_2 can also increase the local availability of hydronium ions for proton transfer to benzaldehyde, typically increasing the concentration of hydronium ions

($a_{H_3O^+}$) near the surface of Cu/C+MoS_2 electrode. Thus, the second hydrogen addition rate (**Equation 5-2**) increased on Cu/C+MoS_2 electrode compared with Cu/C electrode.

In alkaline media, co-catalyst MoS_2 with higher hydrogen adsorption ability can increase H_2O activity (a_{H_2O}) in the Helmholtz layer (near the electrode surface). Thus, the hydroxyl intermediate formation rate increased according to **Equation 5-3**. So, the hydroxyl intermediate accumulated on the surface of the catalyst. The second hydrogen addition is the rate-determining step for benzyl alcohol formation, so the second H addition rate must be lower than the first H addition rate. The first H addition step at the same time is the rate-determining step for hydrobenzoin, this suggests that the following C-C coupling has lowest energy barrier compared with the first H addition. So, the accumulated surface hydroxyl intermediate can push the following reaction to the C-C coupling reaction pathway due to the lowest energy barrier. Thus, the selectivity toward hydrobenzoin obviously increased on Cu/C+MoS_2 electrode in alkaline media.

Based on the experimental results (LSV result in **Figure 5-1** and the reaction order in **Figure 5-9**) and kinetic analysis (**Equation 5-2** and **Equation 5-3**), we concluded that MoS_2 can increase the rate of the second hydrogen addition for benzyl alcohol formation in acidic media and the rate of the first hydrogen addition for hydroxyl intermediate formation in alkaline media during benzaldehyde ECH on Cu/C+MoS_2 electrode. Thus, MoS_2 can tune the product selectivity during benzaldehyde ECH on Cu/C+MoS_2 electrode by faster hydrogenating the hydroxyl intermediate to alcohol product on Cu in acidic media or accumulating the hydroxyl intermediate on the surface of Cu and pushing it to the C-C coupling formation pathway (less energy barrier than the second hydrogen addition on hydroxyl intermediate) in alkaline media.

5.4 Conclusion

We present a detailed kinetic and mechanistic study of MoS_2 tuning product selectivity during electrochemical hydrogenation of benzaldehyde on Cu/C in both acidic and alkaline media. MoS_2 can significantly increase benzyl alcohol selectivity on Cu/C+MoS_2 electrodes in acidic media but oppositely increase hydrobenzoin selectivity on Cu/C+MoS_2 electrodes in alkaline media.

Due to the high H adsorption ability, MoS_2 can increase benzyl alcohol selectivity on Cu/C+MoS_2 electrode by accelerating the second H addition step during benzyl alcohol formation, thus faster hydrogenating the hydroxyl intermediate to alcohol product on Cu in acidic media. However, MoS_2 will oppositely increase hydrobenzoin selectivity on Cu/C+MoS_2 electrode by accelerating the first H addition step during hydroxyl intermediate formation in alkaline media. The accumulated hydroxyl intermediate is more likely to follow the lower energy barrier pathway for C-C bond formation.

5.5 Supporting information

5.5.1 Supplementary Figures

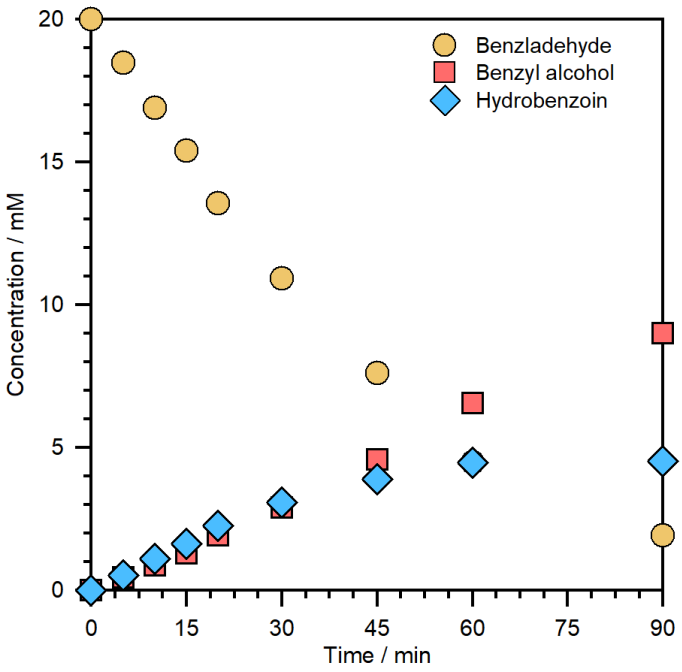

Figure S5-1. Concentration profiles of reactants and products during benzaldehyde ECH on Cu/C electrode in acidic media, Reaction conditions: 20 mM benzaldehyde, applied potential = -0.5 V vs. RHE, NaOAc/AcOH media (pH ~4.6), room temperature, ambient pressure.

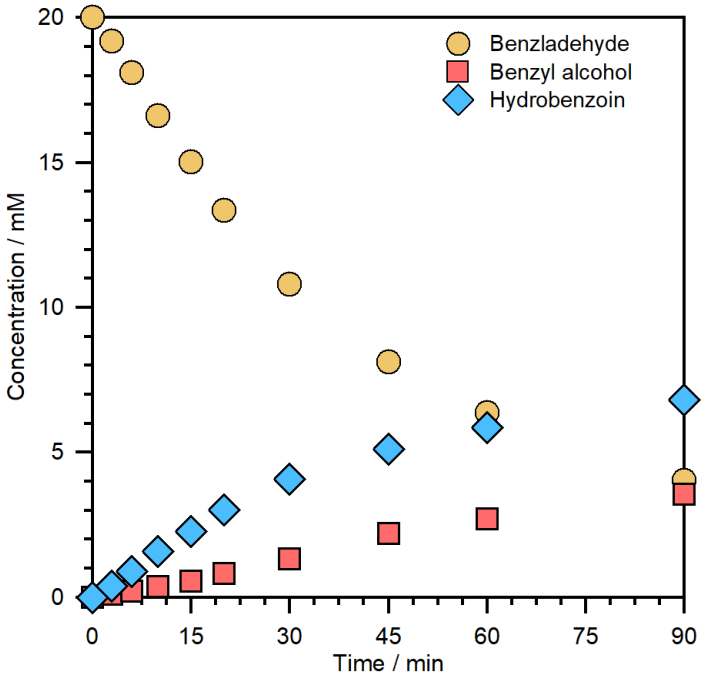

Figure S5-2. Concentration profiles of reactants and products during benzaldehyde ECH on Cu/C electrode in alkaline media, Reaction conditions: 20 mM benzaldehyde, applied potential = -0.5 V vs. RHE, NaOH/NaCl media (pH ~11.3), room temperature, ambient pressure.

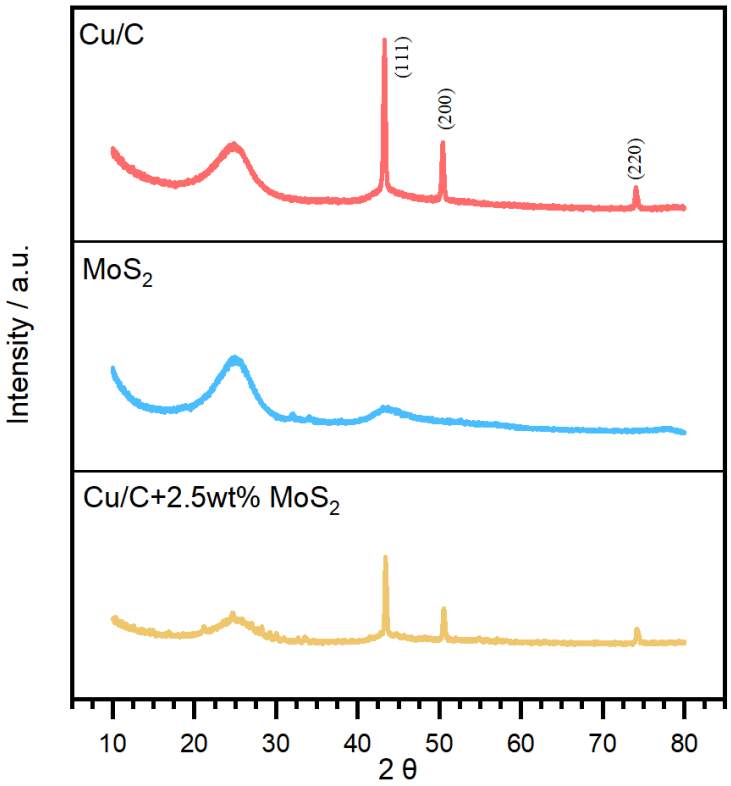

Figure S5-3. XRD patterns for Cu/C, MoS_2 and Cu/C+2.5wt% MoS_2 catalysts.

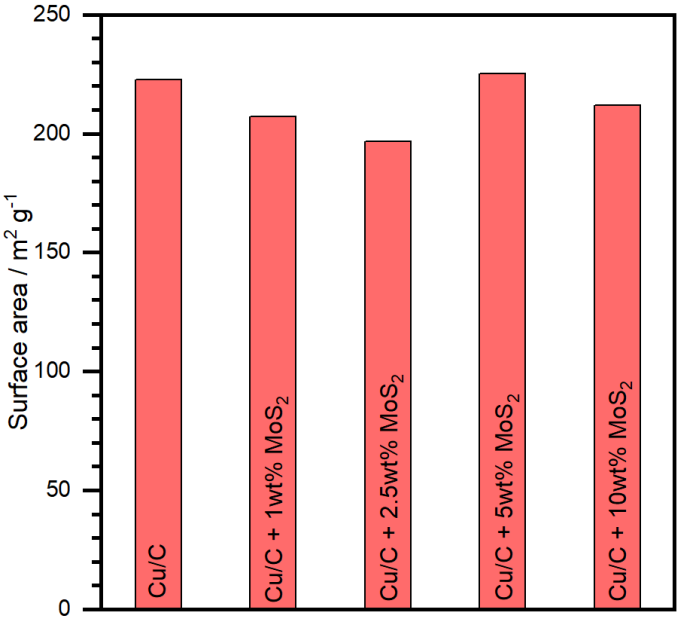

Figure S5-4. BET results for Cu/C, Cu/C+1wt% MoS_2, Cu/C+2.5wt% MoS_2, Cu/C+5wt% MoS_2 and Cu/C+10wt% MoS_2 catalysts.

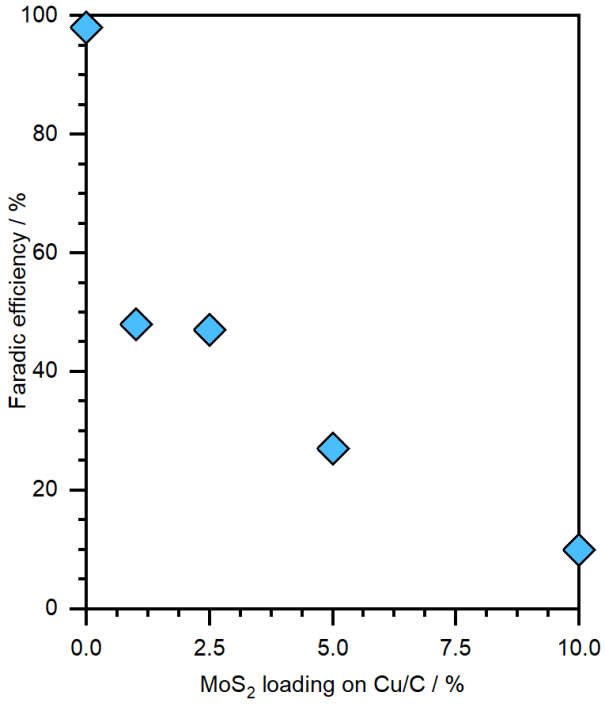

Figure S5-5. Corresponding Faradic efficiency during 20 mM benzaldehyde ECH on Cu/C and Cu/C+MoS_2 electrodes. Reaction conditions: 20 mM benzaldehyde, applied potential -0.5 V vs RHE, NaOAc/AcOH media (pH ~4.6), room temperature.

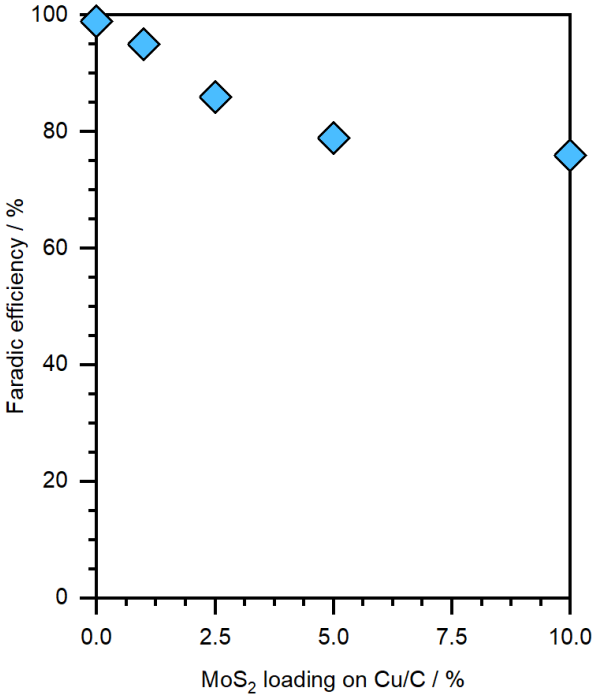

Figure S5-6. Corresponding Faradic efficiency during 20 mM benzaldehyde ECH on Cu/C and Cu/C+MoS_2 electrodes. Reaction conditions: 20 mM benzaldehyde, applied potential -0.5 V vs RHE, NaOH/NaCl media (pH ~11.3), room temperature.

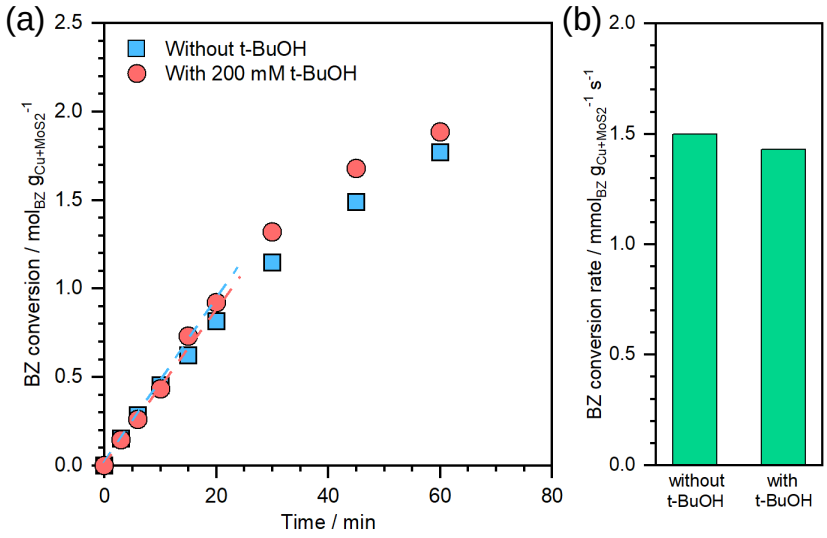

Figure S5-7. (a) Benzaldehyde conversion as a function of reaction time during benzaldehyde ECH with or without t-butanol (t-BuOH) on Cu/C+2.5wt% MoS_2. (b) Initial benzaldehyde conversion rates during benzaldehyde ECH with or without t-butanol (t-BuOH) on Cu/C+2.5 MoS_2. Reaction conditions: 20 mM benzaldehyde, applied potential -0.5 V vs RHE, NaOAc/AcOH media (pH ~4.6), room temperature, ambient pressure.

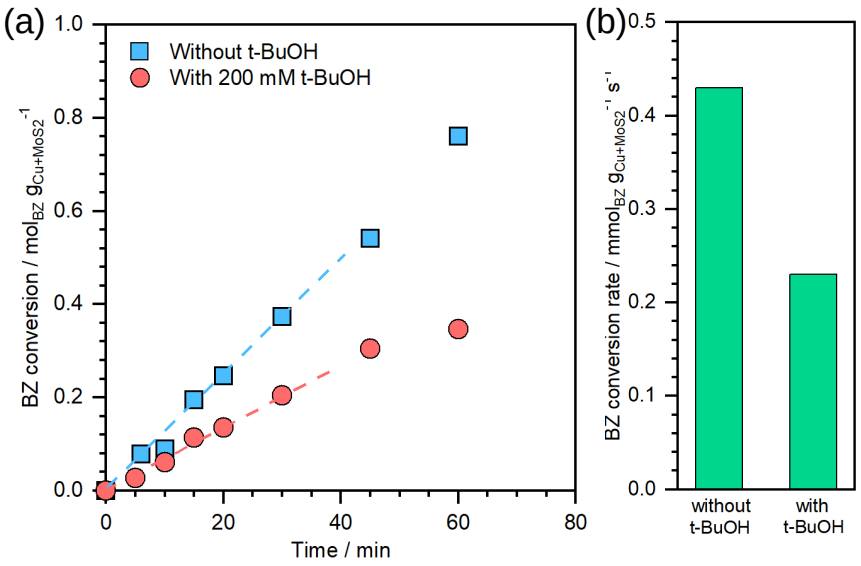

Figure S5-8. (a) Benzaldehyde conversion as a function of reaction time during benzaldehyde ECH with or without t-butanol (t-BuOH) on Cu/C+2.5wt% MoS_2. (b) Initial benzaldehyde conversion rates during benzaldehyde ECH with or without t-butanol (t-BuOH) on Cu/C+2.5 MoS_2. Reaction conditions: 20 mM benzaldehyde, applied potential -0.5 V vs RHE, NaOH/NaCl media (pH ~11.3), room temperature, ambient pressure.

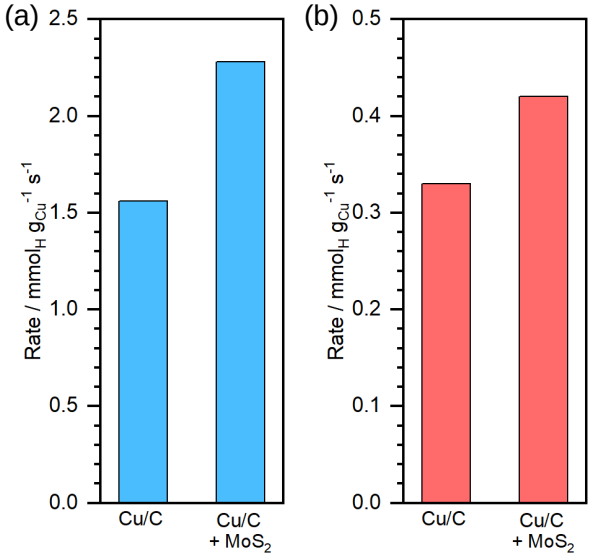

Figure S5-9. Cyclohexanol formation rate during electrocatalytic hydrogenation of cyclohexanal on Cu/C and Cu/C+2.5wt% MoS_2 electrode in acidic (a) or alkaline media (b). Reaction conditions: 20 mM cyclohexanal, applied potential -0.5 V vs RHE, NaOAc/AcOH media (pH ~4.6), NaOH/NaCl media (pH ~11.3), room temperature, ambient pressure.

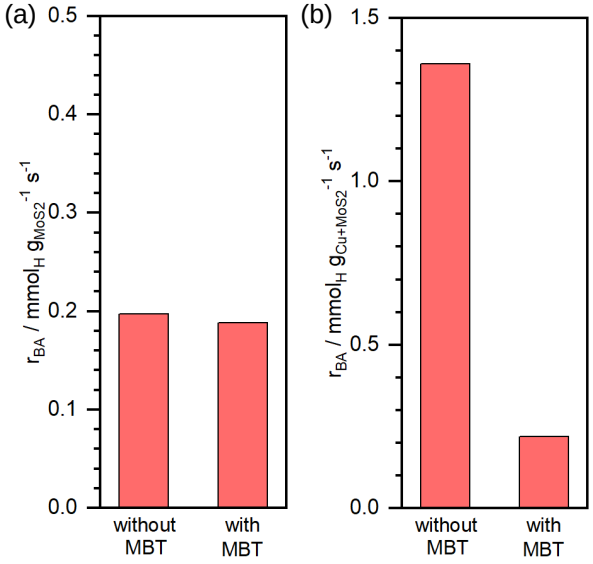

Figure S5-10. Initial benzyl alcohol formation rates during benzaldehyde ECH on MoS_2 (a) or Cu/C+2.5wt% MoS_2 (b) with and without 10 mM 2-mercaptobenzothiazole (MBT). Reaction conditions: 20 mM benzaldehyde, 0 mM or 10 mM MBT, η = –0.5 V vs RHE, NaOAc/AcOH media (pH ~4.6), room temperature, ambient pressure.

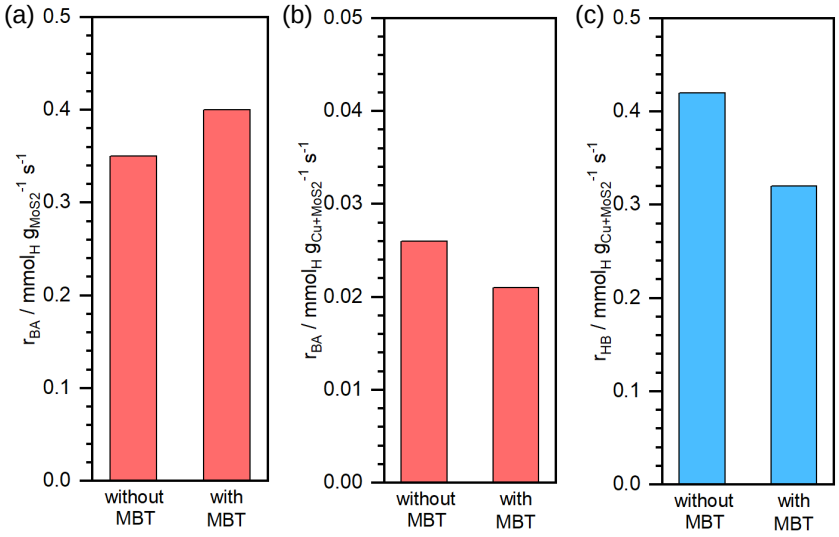

Figure S5-11. (a) Initial benzyl alcohol formation rate during benzaldehyde ECH on MoS_2 with and without 10 mM MBT. Initial benzyl alcohol (b) and hydrobenzoin (c) formation rates during benzaldehyde ECH on Cu/C+2.5wt% MoS_2 with and without 10 mM MBT Reaction conditions: 20 mM benzaldehyde, 0 mM or 10 mM MBT, η = –0.5 V vs RHE, NaOH/NaCl media (pH ~11.3), room temperature, ambient pressure.

5.5.2 Additional Calculation Details

Calculations of Conversion, Selectivity, ECH rate, Product formation rate, HER rate, and Faradic efficiency

$$\text{Conversion} = \frac{\text{Moles of reactant consumed}}{\text{Initial moles of reactant}} \quad (5\text{-}4)$$

$$\text{Selectivity}_{\text{Benzyl alcohol}} = \frac{\text{Moles of benzyl alcohol generated}}{\text{Moles of benzyl alcohol generated+Moles of hydrobenzoin generated}} \quad (5\text{-}5)$$

$$\text{Selectivity}_{\text{Hydrobenzoin}} = \frac{\text{Moles of hydrobenzoin generated}}{\text{Moles of benzyl alcohol generated+Moles of hydrobenzoin generated}} \quad (5\text{-}6)$$

$$\text{ECH rate} = \frac{\text{Moles of reactant consumed via ECH} \times \text{number of H required}}{\text{Time} \times \text{mass of catalyst} \times \text{metal loading}} \quad (5\text{-}7)$$

$$\text{Formation rate}_{\text{Benzyl alcohol}} = \frac{\text{Moles of benzyl alcohol generated} \times \text{number of H required}}{\text{Time} \times \text{mass of catalyst} \times \text{metal loading}} \quad (5\text{-}8)$$

$$\text{Formation rate}_{\text{Hydrobenzoin}} = \frac{\text{Moles of hydrobenzoin generated} \times \text{number of H required}}{\text{Time} \times \text{mass of catalyst} \times \text{metal loading}} \quad (5\text{-}9)$$

$$\text{HER rate} = \frac{\text{Moles of hydrogen generated} \times \text{number of H required}}{\text{Time} \times \text{mass of catalyst} \times \text{metal loading}} \quad (5\text{-}10)$$

$$\text{Faradic efficiency} = \frac{\text{Electrons consumed } \textit{via} \text{ Electrocatalytic hydrogenation}}{\text{Total electrons consumed}} \quad (5\text{-}11)$$

5.6 Reference

1. Zhang, Lijuan, et al. "A review of thermal catalytic and electrochemical hydrogenation approaches for converting biomass-derived compounds to high-value chemicals and fuels." Fuel Processing Technology 226 (2022): 107097.

2. Akhade, Sneha A., et al. "Electrocatalytic hydrogenation of biomass-derived organics: a review." Chemical reviews 120.20 (2020): 11370-11419.
3. Wijaya, Yanuar Philip, et al. "Electrocatalytic hydrogenation and depolymerization pathways for lignin valorization: toward mild synthesis of chemicals and fuels from biomass." Green Chemistry 22.21 (2020): 7233-7264.
4. Han, Guanqun, Guodong Li, and Yujie Sun. "Electrocatalytic Hydrogenation Using Palladium Membrane Reactors." JACS Au (2024).
5. Zhang, Jingfang, et al. "Single-atom catalysts for thermal- and electro-catalytic hydrogenation reactions." Journal of Materials Chemistry A 10.11 (2022): 5743-5757.
6. Han, Chenhui, et al. "Electrocatalytic hydrogenation of alkenes with Pd/carbon nanotubes at an oil–water interface." Nature Catalysis 5.12 (2022): 1110-1119.
7. Tang, Jianfei, et al. "Emerging energy harvesting technology for electro/photo-catalytic water splitting application." Catalysts 11.1 (2021): 142.
8. Zhang, Peili, and Licheng Sun. "Electrocatalytic hydrogenation and oxidation in aqueous conditions." Chinese Journal of Chemistry 38.9 (2020): 996-1004.
9. Liu, Lichao, et al. "Mechanism and kinetics of the electrocatalytic hydrogenation of furfural to furfuryl alcohol." Journal of electroanalytical chemistry 804 (2017): 248-253.
10. Dixit, Ram Ji, et al. "Electrocatalytic hydrogenation of furfural using non-noble-metal electrocatalysts in alkaline medium." Green Chemistry 23.11 (2021): 4201-4212.
11. Huang, Xun, et al. "High selective electrochemical hydrogenation of cinnamaldehyde to cinnamyl alcohol on RuO_2–SnO_2–TiO_2/Ti electrode." ACS Catalysis 9.12 (2019): 11307-11316.
12. Torres, María José, et al. "Electrocatalytic hydrogenation of cinnamaldehyde in a PEM cell: The role of sodium hydroxide and platinum loading." Molecular Catalysis 492 (2020): 110936.
13. Ji, Kaiyue, et al. "Electrocatalytic hydrogenation of 5‐hydroxymethylfurfural promoted by a Ru1Cu single‐atom alloy catalyst." Angewandte Chemie International Edition 61.37 (2022): e202209849.

14. Guo, Xinyue, et al. "Promoting Electrocatalytic Hydrogenation of 5-Hydroxymethylfurfural over a Cooperative Ag/SnO_2 Catalyst in a Wide Potential Window." ACS Catalysis 13.20 (2023): 13528-13539.
15. Song, Yang, et al. "Hydrogenation of benzaldehyde via electrocatalysis and thermal catalysis on carbon-supported metals." Journal of Catalysis 359 (2018): 68-75.
16. Koh, Katherine, et al. "Electrochemically tunable proton‐coupled electron transfer in Pd‐catalyzed benzaldehyde hydrogenation." Angewandte Chemie 132.4 (2020): 1517-1521.
17. Sanyal, Udishnu, et al. "Hydrogen bonding enhances the electrochemical hydrogenation of benzaldehyde in the aqueous phase." Angewandte Chemie 133.1 (2021): 294-300.
18. Lopez-Ruiz, Juan A., et al. "Understanding the role of metal and molecular structure on the electrocatalytic hydrogenation of oxygenated organic compounds." ACS Catalysis 9.11 (2019): 9964-9972.
19. Anibal, Jacob, Arnav Malkani, and Bingjun Xu. "Stability of the ketyl radical as a descriptor in the electrochemical coupling of benzaldehyde." Catalysis Science & Technology 10.10 (2020): 3181-3194.
20. Anibal, Jacob, and Bingjun Xu. "Electroreductive C–C coupling of furfural and benzaldehyde on Cu and Pb surfaces." ACS Catalysis 10.19 (2020): 11643-11653.
21. Chen, Hongwen, et al. "Mechanism of electrocatalytic H_2 evolution, carbonyl hydrogenation and carbon – carbon coupling on Cu." Journal of the American Chemical Society, 146.20 (2024): 13949–13961.
22. Chen, Hongwen et al. "Mechanistic insights into electrocatalytic H2 evolution and electroreduction of benzaldehyde on Cu in alkaline media." Technical University of Munich: 2024 (Submitted for publication).
23. Bhanushali, Jayesh T., et al. "Catalytic hydrogenation of benzaldehyde for selective synthesis of benzyl alcohol: a review." ChemistrySelect 1.13 (2016): 3839-3853.
24. Jayesh, T. B., et al. "Vapour phase selective hydrogenation of benzaldehyde to benzyl alcohol using Cu supported Mg-Al hydrotalicite catalyst." Catalysis Communications 106 (2018): 73-77.

25. Yu, Jia, et al. "Electroreductive coupling of benzaldehyde by balancing the formation and dimerization of the ketyl intermediate." Nature Communications 13.1 (2022): 7909.
26. Gong, Li, et al. "Semiconductor nanosheets for electrocatalytic self-coupling of benzaldehyde to hydrobenzoin." Chemical Engineering Journal 479 (2024): 147612.
27. Singh, Eric, et al. "Atomically thin-layered molybdenum disulfide (MoS2) for bulk-heterojunction solar cells." ACS applied materials & interfaces 9.4 (2017): 3223-3245.
28. Cao, Yang. "Roadmap and direction toward high-performance MoS_2 hydrogen evolution catalysts." ACS nano 15.7 (2021): 11014-11039.
29. Thomas, Nishanth, et al. "2D MoS_2: structure, mechanisms, and photocatalytic applications." Materials Today Sustainability 13 (2021): 100073.
30. Shi, Yi, et al. "Energy level engineering of MoS_2 by transition-metal doping for accelerating hydrogen evolution reaction." Journal of the American Chemical Society 139.43 (2017): 15479-15485.
31. Yu, Yifei, et al. "Layer-dependent electrocatalysis of MoS_2 for hydrogen evolution." Nano letters 14.2 (2014): 553-558.
32. Li, Yanguang, et al. "MoS_2 nanoparticles grown on graphene: an advanced catalyst for the hydrogen evolution reaction." Journal of the American Chemical Society 133.19 (2011): 7296-7299.

Chapter 6

Summary

The incentive of this dissertation is to figure out the detailed mechanism (e.g., H addition mechanism, reaction pathway, and rate-determining step) toward H_2 evolution reaction, benzyl alcohol (hydrogenation product) and hydrobenzoin (C-C coupling product) formation during benzaldehyde ECH on Cu in both acidic and alkaline media. This dissertation also presents a mechanistic basis for cross C-C coupling between aldehydes on Cu. The conversions were conducted under mild operating conditions, i.e., room temperature and ambient pressure in aqueous phase. The reaction conditions (e.g., external potential, electrolyte pH) were controlled. The kinetic measurements (e.g., reaction order, kinetic isotopic experiments) and the first-principle periodic DFT calculations were used to analyze the mechanism.

The coverage of the Cu catalyst surface species was initially analyzed. In acidic media (**Chapter 2**), the HER rates on Cu/C in the presence of benzaldehyde (~0.2 $mmol_H \cdot g_{Cu}^{-1} \cdot s^{-1}$) were much lower compared to that in its absence (~3.7 $mmol_H \cdot g_{Cu}^{-1} \cdot s^{-1}$) at an external potential of -0.5 V vs RHE. This suggests that the H* coverage on the Cu surface was very low in the presence of benzaldehyde. At the same time, the zero-order for benzyl alcohol formation during benzaldehyde ECH strongly suggests that the surface of Cu is predominantly covered with the organic substrate. The adsorption heat value can further confirm the strong benzaldehyde adsorption ability on Cu by conducting calorimetric experiments (**Chapter 4**). The aqueous-phase heat of adsorption of benzaldehyde on Cu/C was estimated to be ~145 $kJ \cdot mol^{-1}$. This high value also suggests the strong adsorption ability of benzaldehyde on Cu. In alkaline media (**Chapter 3**), the inactive hydrogen evolution reactions at -0.5 V vs. RHE in the presence or absence of benzaldehyde suggest the negligible adsorbed hydrogen species coverage on Cu. The zero-order of hydrobenzoin formation during benzaldehyde ECH strongly suggests that the surface of Cu is also predominantly covered with the organic substrate in alkaline media.

The C-C coupling for hydrobenzoin formation can proceed via two different mechanisms: the Langmuir-Hinshelwood (LH) mechanism involving the reaction between two surface radicals or the Eley-Rideal (ER) mechanism wherein a surface hydroxy intermediate reacts with a solvated physisorbed benzaldehyde molecule via nucleophilic addition to form the C-C bond. The full benzaldehyde species coverage on Cu in both acidic and alkaline media suggests that the reaction order for C-C coupling (hydrobenzoin formation) should be zero if it follows the LH mechanism or first if it follows the ER mechanism. From the experimental results, the first

order for hydrobenzoin formation (**Chapter 2**) reveals that C-C bond formation follows the ER mechanism in acidic media. On the other hand, the hydrobenzoin formation shows zero order during benzaldehyde ECH in alkaline media (**Chapter 3**). Based on the revealed mechanism for hydrobenzoin formation on Cu, the zero order for hydrobenzoin formation in alkaline media initially suggests that the rate-determining step (RDS) for hydrobenzoin in alkaline media should be different compared with that in acidic media.

By conducting the kinetic isotopic experiments (H/D exchange), the rate-determining step for product formation was figured out. In acidic media (**Chapter 2**), benzyl alcohol formation has a strong primary kinetic isotope effect (KIE) of r_H/r_D = 2.4/1. The strong primary KIE suggests that H addition (either the first or the second) is the RDS for benzyl alcohol formation. The energy barriers for these two H addition steps were also calculated (DFT calculation, **Chapter 2**). The energy barrier for the second H addition is much higher than that for the first H addition, suggesting that the second H addition step is the RDS for benzyl alcohol. In contrast, hydrobenzoin formation has a very weak KIE of r_H/r_D = 1/1.08. The weak (secondary) KIE suggests that H is not directly involved in the kinetically relevant step for hydrobenzoin formation. Instead, the C-C bond formation is the RDS for hydrobenzoin formation. In alkaline media (**Chapter 3**), both benzyl alcohol and hydrobenzoin have strong KIE. This suggests that the H addition step determines benzyl alcohol and hydrobenzoin formation. Based on the calculated energy barrier for each step (DFT calculation), the first H addition is the RDS for hydrobenzoin formation while the corresponding second H addition is the RDS for benzyl alcohol formation. The first and rate-determining H addition for hydrobenzoin formation also consist with the former conclusion (the zero-order for hydrobenzoin formation in alkaline media).

H addition can also proceed via two different mechanisms: the Langmuir-Hinshelwood (LH) mechanism or the proton-coupled electron transfer (PCET) mechanism. The H addition mechanism during benzaldehyde ECH on Cu was figured out by introducing the H* quenching agent, tert-butanol (t-BuOH), into the electrolyte. In acidic media (**Chapter 2**), the benzaldehyde conversion rate decreased from ~1.6 $mmol_{BZ}\cdot g_{Cu}^{-1}\cdot s^{-1}$ without t-BuOH to ~1.2 $mmol_{BZ}\cdot g_{Cu}^{-1}\cdot s^{-1}$ in the presence of ~200 mM t-BuOH. This suggests the PCET is the dominating pathway for H addition on Cu/C. In alkaline media (**Chapter 3**), the benzaldehyde

conversion rate kept almost constant (1.27 $mmol_{BZ}{\cdot}g_{Cu}^{-1}{\cdot}s^{-1}$ without t-BuOH and 1.23 $mmol_{BZ}{\cdot}g_{Cu}^{-1}{\cdot}s^{-1}$ with 200 mM t-BuOH), suggesting that the surface H* did not joined in the benzaldehyde ECH process in alkaline media. The experiments conducted on ozone-treated catalysts (**Chapter 3**) suggest that the H did not come from hydronium ions. The water molecule, acting as the proton donor, took the role of taking part in the H addition during the benzaldehyde ECH and generated OH^- dissolving into solution in alkaline media.

The mechanistic requirements that facilitate the C–C coupling on Cu in acidic media were also elucidated by conducting kinetic measurements, calorimetry measurements for aqueous-phase heat of the adsorption of the organic substrates and DFT calculations (**Chapter 4**). The conjugated aromatic aldehydes like benzaldehyde and furfural are planar and adsorb strongly on the surface of Cu (evidenced by their high heat of adsorption). The strong binding of the aromatic aldehyde with Cu and the conjugated carbonyl group facilitate C-C coupling. Furthermore, the flat orientation allows (sterically) an ER-type attack by the physisorbed aldehyde molecule. Conversely, weak adsorption of non-conjugated aldehydes, preferential first H addition to the carbonyl C, or a fast second H addition inhibits C-C coupling.

The product selectivity can be tuned by introducing co-catalyst MoS_2 to the Cu/C catalyst (**Chapter 5**). The MoS_2 phase has better H adsorption ability and hydrogen evolution activity compared with Cu/C by comparing LSV curves. MoS_2 can significantly increase benzyl alcohol selectivity on Cu/C+MoS_2 electrodes during benzaldehyde ECH in acidic media but oppositely increase C-C coupling selectivity on Cu/C+MoS_2 electrodes in alkaline media. By analyzing the mechanism for benzaldehyde ECH on Cu in acidic media (**Chapter 2**) and alkaline media (**Chapter 3**), we illustrated that MoS_2, with its high H adsorption ability can accelerate the second H addition step during benzyl alcohol formation, then accelerate hydrogen addition of the hydroxyl intermediate to alcohol product on Cu in acidic media. However, MoS_2 can accelerate the first H addition step (rate-determining for hydrobenzoin in alkaline media) during hydroxyl intermediate formation in alkaline media. The accumulated hydroxyl intermediate is more likely to follow the lower energy barrier pathway toward C-C bond formation. Thus, MoS_2 increases C-C coupling selectivity on Cu/C+MoS_2 electrodes in alkaline media.

Curriculum Vitae

Hongwen Chen was born on 18th May 1995 in Yiyang, Hunan, P. R. China. He started his study in the Department of Materials Science and Engineering at Hebei University of Technology (Tianjin, China) and received his bachelor degree in June 2017. He entered Zhejiang University (Hangzhou, Zhejiang, China) as a master student for further studying in the same year, and obtained his master degree after defending the thesis titled “Synthesis of tin-based composites for anodes in lithium-ion batteries” under the supervision of Prof. Jianguo Lu in June 2020. In October 2020, he started the research as a Ph.D. student under the supervision of Prof. Dr. Johannes A. Lercher in Chair II of Chemical Technology at Technical University of Munich (Munich, Germany). His research mainly focuses on the mechanistic insights into electrocatalytic H_2 evolution and electroreduction of benzaldehyde on Cu. Some representative results of the work were summarized in the present thesis.

List of publications

1. Mechanism of electrocatalytic H_2 evolution, carbonyl hydrogenation and carbon-carbon coupling on Cu, **Hongwen Chen**, Jayendran Iyer, Yue Liu, Simon Krebs, Fuli Deng, Andreas Jentys, Debra J. Searles, M. Ali Haider, Rachit Khare, Johannes A. Lercher, ***Journal of the American Chemical Society***, 2024, 146, 20, 13949–13961.
2. Electrocatalytic conversion of benzaldehyde on Cu in alkaline media, **Hongwen Chen**, Jayendran Iyer, Debra J. Searles, M. Ali Haider, Rachit Khare, Johannes A. Lercher, ***Journal of the American Chemical Society,*** (under review).
3. Conjugated Aromatic Aldehydes Uniquely Undergo Electroreductive Carbon–Carbon Coupling on Cu, **Hongwen Chen**, Rachit Khare, Johannes A. Lercher, to be submitted.
4. Tuning product selectivity in electrocatalytic hydrogenation of benzaldehyde on Cu/MoS_2 catalysts, **Hongwen Chen**, Rachit Khare, Johannes A. Lercher, to be submitted.
5. Intercalation Pseudocapacitance in 2D VS_2/Ti_3C_2Tx MXene Hybrids for All-Climate and Long-Cycle Sodium-Ion Batteries, Zhenyun Zhao, Yang Wu, Rui Hu, Jianguo Lu, Dongliang Chen, Tongtong Li, Yunna Guo, Liqiang Zhang, **Hongwen Chen**, Zhizhen Ye, Chuanfang (John) Zhang, ***Advanced Functional Materials***, 2023, 2307794.
6. Self-Propelled Micro-/Nanomotors of ZnO Nanoshuttles Induced by Surface Defects, Rumin Liu, Liyan Zhao, Shikuan Yang, Jingwen Lin, Xu Wang, Dongliang Chen, Guanjin Lu, **Hongwen Chen**, Zhaoying Wang, Zhizhen Ye, and Jianguo Lu, ***The Journal of Physical Chemistry C***, 2023, 127, 12026–12034.
7. Carbonized Waste Milk Powders as Cathodes for Long-Term Stable Lithium-Sulfur Batteries with Ultra-Large Capacity and High Initial Coulombic Efficiency, Rabia Khatoon, Sanam Attique, Rumin Liu, Sajid Rauf, Nasir Ali, Luhong Zhang, Yu-Jia Zeng, Yichuan Guo, Yusuf Valentino Kaneti, Jongbeom Na, Haichao Tang, **Hongwen Chen**, Yang Tian, Jianguo Lu, ***Green Energy & Environment***, 2022, 7, 1071-1083.
8. $NiTe_2$-based electrochemical capacitors with high-capacitance AC line filtering for regulating TENGs to steadily drive LEDs, Haichao Tang, Kequan Xia, Jianguo Lu, Jiangming Fu, Zhiyuan Zhu, Yang Tian, Yang Wang, Meiqin Liu, Jian Chen, Zhiwei Xu, Yichuan Guo, Rabia Khatoon, **Hongwen Chen**, Zhizhen Ye, ***Nano Energy***, 2021, 84,

105931.

9. Interface coupling 2D/2D $SnSe_2$/graphene heterostructure as long-cycle anode for all-climate lithium-ion battery, **Hongwen Chen**, Rumin Liu, Yang Wu, Junhui Cao, Jian Chen, Yang Hou, Yichuan Guo, Rabia Khatoon, Lingxiang Chen, Qinghua Zhang, Qinggang He, Jianguo Lu, ***Chemical Engineering Journal***, 2021, 407, 126973.
10. Design of highly sensitive and selective ethanol sensor based on α-Fe_2O_3/Nb_2O_5 heterostructure, Rabia Khatoon, Sajid Rauf, Mahmood Ul Haq, Sanam Attique, Salah Ud Din, Nasir Ali, Yichuan Guo, **Hongwen Chen**, Yang Tian, Jianguo Lu, ***Nanotechnology***, 2021, 32, 195503.
11. Facile synthesis of α-Fe_2O_3/Nb_2O_5 heterostructure for advanced Li-Ion batteries, Rabia Khatoon, Yichuan Guo, Sanam Attique, Karim Khan, Ayesha Khan Treen, Mahmood Ul Haq, Haichao Tang, **Hongwen Chen**, Yang Tian, Mohammad Nisar, Salah Ud Din, Jianguo Lu, ***Journal of Alloys and Compounds***, 2020, 837, 155294.
12. Core-shell ZnO@C:N hybrids derived from MOFs as long-cycling anodes for lithium ion batteries, Yichuan Guo, Zhaoying Wang, Xinsheng Lu, Jianguo Lu, Khatoon Rabia, **Hongwen Chen**, Rui Hu, Haichao Tang, Qinghua Zhang, Zhoupeng Li, ***Chemical Communications***, 2020, 56, 1980-1983.
13. Hydrothermal synthesis of Cu-doped $SnSe_2$ nanostructure for efficient lithium storage, **Hongwen Chen**, Yichuan Guo, Peihong Ma, Rui Hu, Rabia Khatoon, Yangdan Lu, Hangjian Zhu, Jianguo Lu, ***Journal of Electroanalytical Chemistry***, 2019, 847, 113205
14. Two-Dimensional $SnSe_2$/CNTs Hybrid Nanostructures as Anode Materials for High-Performance Lithium-Ion Batteries, **Hongwen Chen**, Bei-Er Jia, Xinsheng Lu, Yichuan Guo, Rui Hu, Rabia Khatoon, Lei Jiao, Jianxing Leng, Liqiang Zhang, Jianguo Lu, ***Chemistry–A European Journal***, 2019, 25, 9973-9983.
15. Crystalline SnO_2@ amorphous TiO_2 core-shell nanostructures for high-performance lithium ion batteries, **Hongwen Chen**, Yangdan Lu, Hangjian Zhu, Yichuan Guo, Rui Hu, Rabia Khatoon, Lingxiang Chen, Yu-Jia Zeng, Lei Jiao, Jianxing Leng, Jianguo Lu, ***Electrochimica Acta***, 2019, 310, 203-212.
16. $FeSe_2$/carbon nanotube hybrid lithium-ion battery for harvesting energy from triboelectric nanogenerators, Yang Tian, Zhaoying Wang, Jiangming Fu, Kequan Xia, Jianguo Lu,

Haichao Tang, Khatoon Rabia, **Hongwen Chen**, Zhiyuan Zhu, Qinghua Zhang, Yu-Jia Zeng, Zhizhen Ye, ***Chemical Communications***, 2019, 55, 10960-10963.

17. Nanostructured Nb_2O_5 cathode for high-performance lithium-ion battery with Super-P and graphene compound conductive agents, **Hongwen Chen**, Haixin Zhang, Yuhao Wu, Tian Zhang, Yichuan Guo, Qinghua Zhang, Yujia Zeng, Jianguo Lu, ***Journal of Electroanalytical Chemistry***, 2018, 827, 112-119.

List of presentations

1. Carbon – carbon coupling during electrocatalytic hydrogenation of aldehydes on Cu/C (talk), **Hongwen Chen**, Rachit Khare, Johannes A. Lercher, 57. Jahrestreffen Deutscher Katalytiker, 2024, Weimar, Germany.
2. Carbon – carbon coupling during electrocatalytic hydrogenation of aldehydes on Cu/C (poster), **Hongwen Chen**, Rachit Khare, Johannes A. Lercher, The Netherlands' Catalysis and Chemistry Conference, 2024, Noordwijkerhout, The Netherlands.
3. Mechanistic insight into electrocatalytic H_2 evolution and electroreduction of benzaldehyde on Cu (talk), **Hongwen Chen**, Rachit Khare, Johannes A. Lercher, International Congress on Catalysis, 2024, Lyon, France.